U.PORTO

DOUTORAMENTO

CIÊNCIAS BIOMÉDICAS

Myosin Function During Cytokinesis in the *C. elegans* One-cell Embryo

Joana Saramago

D

2021

U.PORTO

Joana Saramago. Myosin Function During Cytokinesis in the *C. elegans* One-cell Embryo

Myosin Function During Cytokinesis in the *C. elegans* One-cell Embryo

Joana Saramago

D.ICBAS **2021**

INSTITUTO DE CIÊNCIAS BIOMÉDICAS ABEL SALAZAR

JOANA FILIPA SILVA SARAMAGO

MYOSIN FUNCTION DURING CYTOKINESIS IN THE *C. ELEGANS* ONE-CELL EMBRYO

Tese de Candidatura ao grau de Doutor em Ciências Biomédicas;

Programa Doutoral da Universidade do Porto (Instituto de Ciências Biomédicas de Abel Salazar)

Orientador – Doutora Ana Carvalho

Categoria – Investigador Principal

Afiliação – Instituto de Biologia Molecular e Celular, Instituto de Investigação e Inovação em Saúde, Universidade do Porto

Co-orientador – Doutor Daniel Osório

Categoria – Investigador Júnior

Afiliação – Instituto de Biologia Molecular e Celular, Instituto de Investigação e Inovação em Saúde, Universidade do Porto

The work presented in this thesis was developed at:

IBMC – Instituto de Biologia Molecular e Celular,
i3S - Instituto de Investigação e Inovação em Saúde,
Universidade do Porto, Porto, Portugal.
Cytoskeletal Dynamics
Rua Alfredo Allen Nº204
4200-135 Porto, Portugal

www.i3s.up.pt

FUNDING

The research leading to these results has received funding from the European Research Council under the European Union's Horizon 2020 research and innovation program to A.X.C. (640553 - ACTOMYO); This work is also funded by Fundação para a Ciência e Tecnologia (FCT) and the European Regional Development Fund (FEDER) (F-COMP-01-0124-FEDER-028255, grant PTDC/BEX-BCM/0654/2012); and from Norte Portugal Regional Operational Programme - NORTE 2020 (Norte-01-0145-FEDER-000029).

European Research Council

Established by the European Commission

UNIÃO EUROPEIA

Fundo Europeu de Desenvolvimento Regional

ACKNOWLEDGEMENTS/AGRADECIMENTOS

Quero agradecer à minha orientadora Ana Carvalho por todo o suporte e ajuda durante a produção desta tese e do meu tempo no lab. Agradeço toda a disponibilidade e conhecimento transmitido.

De igual forma agradeço ao meu co-orientador por toda a ajuda e conhecimento que me transmitiu. Obrigada pelo tempo que me foi dedicado.

Aos restantes membros do meu lab que me ajudaram sempre que necessitei. Em especial às restantes phD, Joana Leite, Filipa e Inês. Sem vocês teria sido uma luta bem mais dificil e agradeço por terem estado sempre lá quando necessitei. Fico tão contente por nos ajudarmos umas às outras independentemente do que se passe. Love you, Cobritxas.

Aos membros de todo o GCPlab, que lá continuam ou que já partiram em novas aventuras, agradeço toda a ajuda e apoio que me deram nestes anos. Dos que lá continuam, não podi deixar de agradecer especialmente ao Daniel Barbosa e ao Benny que sempre se disponibilizaram prontamente para me ajudar e aturar. Aos que já passaram, à Marisa, à Inês Loureiro e à Taninha. Vocês ajudaram me muito, muito mesmo e levo a vossa amizade no meu coração. Das melhores pessoas que conheci. Também à Patricia, que desde que nos pegavamos pelos equipamentos evoluimos tanto juntas, pessoal e profissionalmente. Estás sempre presente e preocupada comigo, mesmo eu sendo uma desnaturada. Capa dura e coração mole. Obrigada pela tua amizade, sempre.

Quero agradecer ainda à Cristina e à Marta Reis por aturarem os meus desvaneios e me apoiarem sempre. Duas queridas.

Fora de ciência, quero agradecer primeiro aos meus pais, o meu porto seguro. Estes ultimos anos foram tão dificieis e mesmo assim nunca, mas nunca me deixaram de amar ou de se preocupar. Sabem o orgulho que tenho em vós, meus guerreiros.

À minha filha, minha fonte de motivação diária, a minha luz que me guia. Se nunca desisti de nada foi por ti. Meu amor.

Ao resto da minha familia que levou com todas as minhas crises e sempre me apoiaram e orgulham se do que sou.

Aos Shennenigans por todas as risadas e por tornarem tudo bem mais leve quando necessitei. Amizades para a vida.

Finalmente, a mim. Sabes o que passaste e de onde vieste. Sabes o quanto te esforças e o quanto te dás. Não duvides de ti, nunca, és capaz de tudo.

Para finalizar aqui deixo uma frase de um grande Senhor, que me fez refletir muitas vezes, talvez demasiadas, enquanto ouvia seminários no auditório: «Só os valores humanos da ciência podem motivar e permear a cultura das novas gerações» Mariano Gago.

DECLARAÇÃO DE HONRA

Declaro que a presente tese é de minha autoria e não foi utilizada previamente noutro curso ou unidade curricular, desta ou de outra instituição. As referências a outros autores (afirmações, ideias, pensamentos) respeitam escrupulosamente as regras da atribuição, e encontram-se devidamente indicadas no texto e nas referências bibliográficas, de acordo com as normas de referenciação. Tenho consciência de que a prática de plágio e auto-plágio constitui um ilícito cadémico.

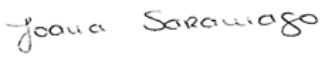

PUBLICATIONS

Na preparação desta tese foram incluídos os dados das publicações abaixo indicadas. A autora declara ter participado ativamente na concepção e execução das experiências que estiveram na origem dos mesmos, assim como na sua interpretação, discussão e redação. Fazem parte integrante desta tese os seguintes artigos já publicados:

In the preparation of this thesis data from the publications listed below were included. The author declares that she participated actively in the execution of the experiments that produced that data, as well as in their interpretation, discussion, and writing.
The following published articles have been included in this thesis:

Publication 1 (co-author in Chapter 5): The work presented here includes a full and adapted copy from the article published in *Development* (2019 146: dev179150 doi: 10.1242/dev.179150). In this publication, I share first authorship with two other authors, and I contributed to the overall methodology, formal analysis, investigation, data curation and writing - review & editing. Specifically, I contributed to the experimental data in figures 5.3, 5.4, 5.5 E-H, 5.6A, 5.7A-C, 5.E-F, S3A-F, and 5.S5H-G.

Osório, D. S., Chan, F. Y., **Saramago, J.,** Leite, J., Silva, A. M., Sobral, A. F., Gassman, R., & Carvalho, A. X. (2019). Crosslinking activity of non-muscle myosin II is not sufficient for embryonic cytokinesis in *C. elegans*. *Development*, *146*(21).

Publication 2 (third author part of Chapter 6): In this publication, I contributed to methodology, formal analysis, investigation, and data curation. Specifically, I contributed to the experimental data in the figure 2 of the paper. Only the Figure 2 of this publication is inserted in this thesis.

Chan, F. Y., Silva, A. M., **Saramago, J.,** Pereira-Sousa, J., Brighton, H. E., Pereira, M., Oegema, K., Gassmann, R., & Carvalho, A. X. (2019). The ARP2/3 complex prevents excessive formin activity during cytokinesis. *Molecular Biology of the Cell*, *30*(1), 96-107.

SUMMARY

Myosins are a superfamily of motor proteins involved in many cell events including cytokinesis. Many myosin classes are expressed in a single organism, suggesting function specificity or complementary/redundant roles. Here I describe that during cytokinesis in *C. elegans* one-cell embryo NMY-2 one of the three NMIIs expressed in *C. elegans* is the only myosin essential for cytokinesis is NMY-2. Here, I show that MYO-1, a class II muscle myosin, is important for contractile ring constriction. To my knowledge it is the first that a class II muscle myosin is reported in such a role. Therefore, NMY-2 together with MYO-1 regulate contractile ring constriction in *C. elegans* one-cell embryos. The use of NMY-2 motor-impaired or motor-dead mutants which bind normally to F-actin shows that this NMII function, and not F-actin crosslinking, is essential for embryonic cytokinesis in *C. elegans*. The motor-dead mutants failed cytokinesis and were not able to compact and align a F-actin equatorial band. In addition, the use of these mutants shows that NMII motor activity is required throughout cytokinesis. The motor-impaired mutants had prolonged cytokinesis and were more sensitive to the amount of NMII present in the contractile ring. I also described the existence of a NMII membrane-bound pool during cytokinesis. In agreement, both *in vitro* and in vivo results indicate that NMII is bound to the plasma membrane during cytokinesis and that this binding is likely dependent on NMII activation status.

Altogether my results show that despite all the myosin diversity, in *C. elegans* embryonic cytokinesis only NMY-2, one of the NMIIs that are expressed, is essential for cytokinesis. Surprisingly, I described that, in addition to NMII, a muscle class II myosin may be involved during cytokinesis.

Keywords: *C. elegans*, one-cell embryo, cytokinesis, myosins, non-muscle myosin II, motor activity, membrane-bound.

SUMÁRIO

As miosinas são uma superfamília de proteínas motoras envolvidas em vários eventos celulares, incluindo citocinese. Um único organismo pode expressar várias classes de miosinas o que sugere que estas podem ter uma função especifica ou papéis complementares/redundantes. Nesta tese, descrevo que, durante a citocinese do embrião unicelular de *C. elegans* a NMY-2, uma das três NMIIs expressas em *C. elegans*, é a única miosina essencial para a citocinese. Demonstro também que a MYO-1, uma miosina muscular de classe II, é importante para a constrição do anel contrátil. No meu conhecimento, é a primeira vez que uma miosina muscular de classe II é descrita como importante nesse contexto. Assim sendo, a NMY-2 juntamente com a MYO-1 parecem regular a constrição do anel contrátil em embriões unicelulares de *C. elegans*. O uso de mutantes de NMY-2 com capacidade motora diminuída ou nula mas que se ligam normalmente à F-actina mostra que a translocação da F-actina, não é suficiente para a citocinese embrionária em *C. elegans*. Os mutantes sem capacidade motora falharam citocinese e não foram capazes de compactar e alinhar uma banda de F-actina no equador da célula. Além disso, o uso destes mutantes mostra que a atividade motora da NMII é necessária durante toda a citocinese. Os mutantes com capacidade motora reduzida completaram citocinese mais lentamente e foram mais sensíveis à redução de NMII presente no anel contrátil. Também descrevi a existência de uma população de NMY-2 ligada à membrana durante a citocinese. Em concordância, os resultados *in vitro* e *in vivo* indicam que a NMII está ligada à membrana plasmática durante a citocinese e que essa ligação provavelmente depende do seu estado de ativação.

Em conjunto, os meus resultados mostram que, apesar de toda a diversidade de miosinas existente, apenas a NMY-2, uma das NMIIs expressas, é essencial para a citocinese embrionária de *C. elegans*. Surpreendentemente, eu demonstrei que, além da NMY-2, uma miosina muscular de classe II pode estar envolvida durante a citocinese.

Palavras-chave: *C. elegans*, embrião unicelular, citocinese, miosinas, miosina II não muscular, atividade motora, ligação à membrana.

TABLE OF CONTENTS

LIST OF FIGURES

Chapter 1

Chapter 4

Chapter 5

LIST OF TABLES

Chapter 1

Chapter 3

Chapter 4

LIST OF ABBREVIATIONS

ADF	Actin depolymerizing factors
ALLO-1	Allophagy-defective 1
ANI-1	Anillin 1
ARP-2/3	Actin-Related Proteins 2/3 complex
ARPE-19	Retinal pigment epithelial
ATP	Adenosine Triphosphate
ATPase	Adenosine triphosphate hydrolase
ATZ-1	Abnormal transition zone 1
CAM	Calmodulin
CDC-42	Cell division control protein 42
CIT-K	Citron Rho-interacting kinase
CK2	Casein kinase 2
CPC	Chromosomal passenger complex
CRISPR-CAS9	Clustered regularly interspaced short palindromic repeats CRISPR associated protein 9
CYK-1	Cytokinesis defect 1
CYK4	Rac GTPase-activating protein 1
DsRNA	Double-stranded RNAs
EB1	Microtubule-associated protein RP/EB family member 1
ECT2	Epithelial Cell Transforming 2
ELC	Myosin essential light chain
F-actin	Filamentous actin
FERM	Ezrin, Radixin, Moesin
FH2	Formin-homology domain 2

G-actin	Globular actin
GAP	GTPase-activating proteins
GDP	Guanosine diphosphate
GEF	Guanine nucleotide exchange factor
Gex	Gut on the exterior
GLUT4	Glucose transporter type 4
GOLG-4	Golgi associated coiled-coil protein homolog 4
gRNA	Guide RNA
GST	Glutathione S-transferase
GTD	Globular tail domain
GTP	Guanosine triphosphate
HC	Myosin heavy chain
HCM	Hypertrophic cardiomyopathy
HMM	Heavy meromyosin
HMR-1	Hammerhead embryonic lethal
HR	Homologous Repair
HUM-1	Heavy chain unconventional myosin 1
HUM-10	Heavy chain unconventional myosin 10
HUM-2	Heavy chain unconventional myosin 2
HUM-4	Heavy chain unconventional myosin 4
HUM-5	Heavy chain Unconventional Myosin 5
HUM-6	Heavy chain unconventional myosin 6
HUM-7	Heavy chain unconventional myosin 7
HUM-8	Heavy chain unconventional myosin 8
INCENP	Inner centromere protein
KEAP1	Kelch-like ECH-associated protein

KIF4	Kinesin superfamily protein member 4
LC	Myosin light chain
MAP	Microtubule-associated protein
MDCK	Madin-Darby Canine Kidney
MhcA	Myosin 2 heavy chain
MIHCK	Myosin I HC kinase
MKLP1	Mitotic kinesin-like protein
MLC-4	Myosin light chain 4
MLC-5	Myosin light chain 5
MLCK	Myosin light-chain kinase
MRCK	Myotonic dystrophy protein kinase-related Cdc42-binding kinase
MTS1	Metastasis-associated protein
MYH10	Myosin Heavy Chain 10
MYH14	Myosin Heavy Chain 14
MYH9	Myosin Heavy Chain 9
MYO-1	Myosin Heavy Chain 1
MYO18A	Myosin XVIIIA
MYO18B	Myosin XVIIIB
MYO1A	Myosin IA
MYO1B	Myosin IB
MYO1C	Myosin IC
MYO1D	Myosin ID
MYO1E	Myosin IE
MYO1G	Myosin IG
MYO-2	Myosin heavy chain 2

MYO-3	Myosin heavy chain 3
Myo31DF	Unconventional myosin ID
MYO-5	Myosin heavy chain 5
MYO5A	Myosin VA
MYO5B	Myosin VB
MYO-6	Myosin heavy chain 6
MYO7A	Myosin VIIA
MYO7B	Myosin VIIB
MYO9A	Myosin IXA
MYO9B	Myosin IXB
MYPT	Myosin phosphatase targeting protein
MyTH4	Myosin Tail Homology 4 domain
NHEJ	Non-Homologous End-Joining
NMII	Non-muscle myosin II
NMY-1	Non muscle myosin 1
NMY-2	Non muscle myosin 2
NMY-3	Non muscle myosin 3
P, PI, PII	Pellet
PA	Phosphatidic acid
PAK	P21-activated protein kinase
PAM	Protospacer Adjacent Motif
PCDH15	Protocadherin 15
PE	Phosphatidylethanolamine
PH	Pleckstrin homology
Pi	Inorganic phosphate
PI(4)P	Phosphatidylinositol 4-phosphate

PIP2	Phosphatidylinositol 4,5-bisphosphate
PKC	Protein kinase C
PLC1	Phospholipase C
PLK1	Polo-like kinase
PLST-1	Plastin
PRC1	Protein Regulator of Cytokinesis 1
PS	Phosphatidylserine
PtdIns(3)P	Phosphatidylinositol 3- phosphate
PtdIns(3,4)P2	Phosphatidylinositol 3,4-bisphosphate
PtdIns(3,4,5)P3	Phosphatidylinositol 3,4,5-trisphosphate
PtdIns(3,5)P2	Phosphatidylinositol 3,5- bisphosphate
PtdIns(4)P	Phosphatidylinositol 4-phosphate
PtdIns(4,5)P2	Phosphatidylinositol 4,5- bisphosphate
PtdIns(5)P	Phosphatidylinositol 5-phosphate
RAC1	Ras-related C3 botulinum toxin substrate 1
RHOA	Ras homolog family member A
RLC	Myosin regulatory light chain
RNAi	RNA interference
ROCK	Rho-associated protein kinase
RPE	Retinal pigment epithelium
S, SI, SII	Supernatant
SAX-3	Sensory axon guidance 3
SAX-7	Sensory axon guidance 7
SH1-SH2	Src homology domain 1- Src homology domain 2
SH3	Src-homology domain
SHROOM2	Shroom Family Member 2

SPE-15	Defective spermatogenesis 15
ssRNA	Single-stranded RNA
TEDS	Threonine, glutamate, aspartate or serine
TH1	Tail homology domain 1
TH2	Tail homology domain 2
TH3	Tail homology domain 3
THs	Tail homology domains
TIRF	Total internal reflection fluorescence
TRPM6	Transient receptor potential ion channel kinase 6
TRPM7	Transient receptor potential ion channel kinase 7
ts	Temperature-sensitive
UNC-54	Uncoordinated 54
USH1C	Harmonin
USH1G	Sans
USH2A	Usherin
USH2D	Whirlin
Vlgr1/USH2C	Very Large G-protein coupled receptor 1
WT	Wild-type
ZIP	Zipper-interacting protein kinase

CHAPTER 1

GENERAL INTRODUCTION

1. GENERAL INTRODUCTION

Myosin, dynein, and kinesin are the three classes of motor proteins expressed in organisms. This thesis focuses on the myosin class. Myosin was first described almost two centuries ago (Kühne, 1859), and it is crucial for muscle contraction, intracellular motility, cytokinesis, and contractile processes in all cells. Myosins form a superfamily of proteins, which bind actin, hydrolyse ATP and generate force. The work presented in this thesis is focused mostly on Non-muscle myosin II (NMII); a conventional myosin ubiquitously expressed in cells. NMII is critical throughout development and cell division and its deregulation has been implicated in several diseases, including cancer (Hernandez et al., 2007; Ouderkirk & Krendel, 2014; Newell-Litwa et al., 2015).

1.1. Actin filaments

Actin is a highly conserved and abundant protein with adenosine triphosphate hydrolase (ATPase) activity. Globular actin monomers (G-actin) polymerize into double helical filamentous actin (F-actin) with the concomitant hydrolysis of adenosine triphosphate (ATP) (Fujii et al., 2010; Holmes et al., 1990; Oda et al., 2009). Actin constantly polymerizes and depolymerizes, and the assembly and disassembly of F-actin is a very dynamic process. The assembly occurs at the barbed end (also known as plus end) while the disassembly happens at the pointed-end (also termed minus-end). Actin nucleation, elongation, branching, capping, or severing of filaments are essential to maintain actin dynamics within the cells. These processes are regulated by different actin-binding proteins. F-actin nucleation and elongation largely depend on formins (Bement et al., 2006; Goode & Eck, 2007; Matsumura et al., 2011; Piekny et al., 2005; Figure 1.2). Formins are highly conserved multidomain proteins that form a doughnut-shaped conformation upon dimerization of their formin-homology domain 2 (FH2). This structure initiates F-actin filament assembly and remains associated with the barbed end of the actin filament to facilitate rapid elongation. Formins are the specific nucleators/elongators of linear F-actin in the contractile ring (Chan et al., 2019; Severson et al., 2002; Coffman et al., 2013; Davies et al., 2014). The Actin-Related Proteins 2/3 complex (ARP2/3) is responsible for the formation of branched actin filament networks and is thought to be inhibited in the cleavage furrow (Canman et al., 2008; Chan et al., 2019). Profilin promotes F-actin disassembly because it binds and sequesters actin monomers that are normally used for filament elongation (Carlsson et al., 1977). While profilin favours the nucleation/elongation of formin-mediated non-branched F-actin, it also

antagonizes the polymerization of ARP2/3-mediated branched F-actin (Suarez et al., 2015). The actin depolymerizing factors (ADF)/cofilin are essential for F-actin severing and depolymerization (Lappalainen & Drubin, 1997). Capping proteins bind to the F-actin barbed ends and regulate the addition or removal of G-actin monomers to the filament (Cooper & Sept, 2008).

1.2 Myosins

Dyneins, kinesins, and myosins are super families of cytoskeletal motors which transport material and maintain the correct organelle organization within the cell (Cross & Dodding, 2019). Myosins are a large family of actin-based motors that are essential for several cellular processes including cytokinesis, organelle transport, trafficking, cell polarization, and signal transduction (Figure 1.1; Sellers, 2000; Yin et al., 2000; Bähler, 2000).

Myosins convert chemical energy, in the form of ATP, into mechanical force. Myosins are composed of three functional subdomains: (1) the motor or head domain, which interacts with actin and has ATPase activity, (2) the lever arm, or neck domain, which binds to the light chains (LCs) or Calmodulin (CAM), and (3) the tail domain which allows myosin dimerization through the coiled-coil domain and bipolar filament formation. The motor domains are well conserved, but the number of IQ motifs present in the neck domains can vary between zero and six. The IQ motifs correspond to an amino acid sequence motif in which LCs or CAM bind in order to regulate myosins. The tail region is the most diverse. Src-homology (SH3) domain, GTPase-activating proteins (GAP) domains, Ezrin, Radixin, Moesin (FERM) domains, and Pleckstrin homology (PH) domains are found in the myosins tails.

The number of myosin classes reported varies between 14 and 37 depending on the number of sequences analyzed, statistics parameters and alignment methods (Hodge & Cope, 2000; Furusawa et al., 2000; Richards & Cavalier-Smith, 2005; Foth et al., 2006; Odronitz & Kollmar, 2007). Traditionally, myosins are grouped based on the amino acid sequence of their head domains, as the high degree of conservation allows for phylogenetic comparison.

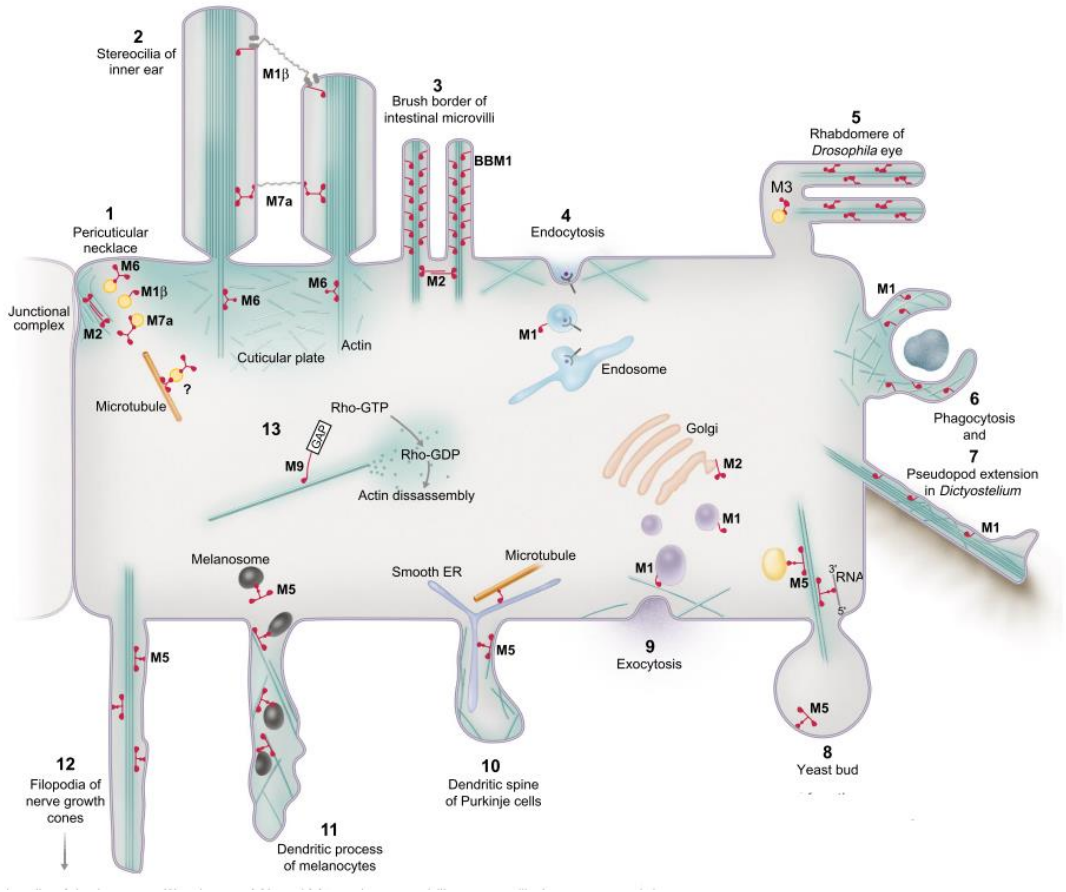

Figure 1.1 Illustration of myosin functions. Myosin I, myosin VI, and myosin VII (M1, M6, and M7, respectively) exist at the base of the stereocilia, between the actin-rich cuticular plate and the circumferential actin band associated with the junctional complex **(1)**. M1 is the motor of stereocilia in the hair cells of the inner ear **(2)**, while M6 and M7 anchor or stabilize stereocilia. myosin II (M2) localizes in the terminal base of intestine microvilli, where it cross-links actin core bundles **(3)** M1 is involved in endocytosis **(4)**. myosin III (M3) is required for rhabdomere integrity **(5)** and phototransduction in the fly eye. M1 may play a role in phagocytosis **(6)** and regulates pseudopod extension **(7)**. Myosin V (M5) is involved in organelle and RNA transport **(8)** M2 is required for vesicle budding from the trans-Golgi and M1 participates in yeast secretion and *D. discoideum* exocytosis **(9)**. M5 is responsible for transporting smooth ER through dendritic spines of Purkinje cells **(10)**, melanosomes through the dendritic processes of melanocytes **(11)**, and acts in the filopodia extension of nerve growth cones **(12)**. Myosin IX (M9) is a RHOA GAP that inactivates RHOA and possibly regulates actin organization **(13)**. These structures are not drawn to scale. (Figure adapted from (Mermall et al., 1998); used under permission).

Conventional myosins or class II myosins are very similar in structure and can be divided into muscle, and non-muscle myosins. The first ones are specific to muscle while the second function in all cells, including muscle cells. Both dimerize, form bipolar filaments, and translocate actin. The unconventional myosins, are a very diverse group that comprise many myosin classes. Some form dimers, others function as monomers. Different isoforms from the same class and myosins from different classes can form heterotypic filaments and function together in the same cellular process (Beach & Hammer, 2015; Billington et al., 2015; Taneja et al., 2020). Even if not forming heterotypic filaments, myosins are able to

cooperate (Ono & Ono, 2016; Hu et al., 2019). Which myosins cooperate, functionally compensate for one another, or regulate one another *in vivo* remains to be explored. Given the relevance of myosins function in health and disease, it is important to investigate their mechanisms of action as they might be interesting therapeutic targets to consider in the future.

1.3 Actomyosin Contractility

The primordial knowledge of how actin and myosin interact and generate contractility came from studying muscle contraction, a process essential for diverse functions such as pumping blood through vessels, running and lifting objects. Myosin was discovered in 1859 (Kühne, 1859) but it was only described as an actin-activated ATPase around 80 years later (Engelhardt & Ljubimowa, 1939; Straub, 1942). In muscle sarcomeres, conventional myosin II and actin are organized into thick and thin filaments, respectively, that are anchored in different regions of the sarcomere. While thin filaments have their plus-ends anchored to the Z-lines at both ends of the sarcomere, thick filaments are attached to the M-line at the center of the sarcomere. During muscle contraction, thin and thick filaments slide past one another due to myosin movement towards the plus ends of actin filaments, leading to muscle contraction (Huxley & Hanson, 1954; Huxley & Niedergerke, 1954). Actomyosin processes in non-muscle cells were initially evaluated considering knowledge coming from muscle sarcomeres since these also involve actin and myosin based contractilility (Clarke & Spudich, 1977). However, unlike muscle cells, in which actin and myosin organize in ordered sarcomeres, actomyosin networks in non-muscle cells have more versatile arrangements (Henson et al., 2017). The wide variety of processes that involve actomyosin contractility in non-muscle include: retraction of plasma membrane blebs (Jiao et al., 2018), clathrin-mediated endocytosis (Chandrasekaran et al., 2016), cortical polarization (Wang et al., 2017), cytokinesis (Schroeder, 1968; Schroeder, 1972), amoeboid cell migration (Ruprecht et al., 2015; Liu et al., 2015), gastrulation (Heer & Martin, 2017; Anlaş & Nelson, 2018) and syncytial germline architecture (Agarwal & Zaidel-Bar, 2019) are examples in which actomyosin contractility is essential.

1.4 Cytokinesis

Cytokinesis was described more than 100 years ago (Flemming, 1882; Whitman, 1887), and the role of actin and myosin in the cleavage furrow was first described more than 50 years ago (Schroeder, 1968; Schroeder, 1972). This essential process has been studied in many biological models such as plants, budding and fission yeast, slime mold, marine invertebrates, nematodes, fruit flies and vertebrate cells (review in Guertin et al., 2002). Cytokinesis is the last step of cell division that starts at anaphase onset, when the sister chromatids separate, and components of the cytokinesis machinery, such as myosin and actin, are recruited to the cell equator. Together these form an actomyosin ring that contracts and pulls the plasma membrane behind it, creating a cleavage furrow that ingresses until the mother cell is divided into two daughter cells (Raich et al., 1998; Field et al., 1999; Jantsch-Plunger et al., 2000; Robinson & Spudich, 2000; Glotzer, 2001). At the end of cytokinesis, abscission occurs resulting in the complete physical separation of two daughter cells (Figure 1.2; Glotzer, 2001).

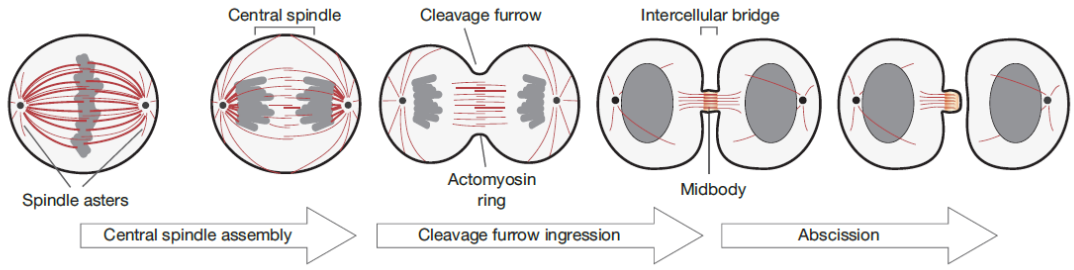

Figure 1.2 Schematic of cytokinesis in animal cells. Signals from the central spindle lead to the assembly of an actomyosin contractile ring beneath the plasma membrane at the cell equator, between the two masses of chromosomes. The cleavage furrow compacts the spindle midzone into a dense structure called the midbody. Then abscission occurs, leading to the complete separation of the two daughter cells (Figure Reprinted from (Fededa & Gerlich, 2012) and used under permission).

Cytokinesis defects have been associated with tetraploidy and chromosomal instability, promoting tumorigenesis (Fujiwara et al., 2005; Ganem et al., 2007; Steigemann et al., 2009), which further highlights the importance of understanding the mechanisms of cytokinesis.

1.4.1. Division site specification

Cytokinesis initiates with the specification of the cleavage site, which requires signalling from the central spindle. The central spindle consists of a set of bundled antiparallel microtubules that forms between the separating chromosomes and accumulates several cytokinesis regulators ensuring cleavage site specification (Figure 1.3). Protein Regulator of Cytokinesis 1 (PRC1) is a microtubule-associated protein (MAP) that bundles the central spindle microtubules and is essential for cytokinesis in most animal cells (Mollinari et al., 2002; Vernì et al., 2004; Verbrugghe & White, 2004). Kinesin superfamily protein member 4 (KIF4), binds to PRC1 and moves to the microtubule plus end where it stabilizes microtubules (Kurasawa et al., 2004, Zhu & Jiang, 2005). Two protein complexes, centralspindlin and the chromosomal passenger complex (CPC), are also crucial for central spindle assembly (Ruchaud et al., 2007; Glotzer, 2009; Carmena et al., 2012).

Centralspindlin is a heterotetrameric complex (Pavicic-Kaltenbrunner et al., 2007) consisting of two molecules of the mitotic kinesin-like protein 6 (MKLP1), and two molecules of Rac GTPase-activating protein 1 (CYK4), which is a GTPase activating protein (GAP) for the Rho family of small GTPases. Small GTPases like Ras homolog family member A (RHOA) act as molecular switches that are active when bound to GTP and inactive when bound to GDP. Guanine nucleotide exchange factors (GEFs) and GAPs regulate small GTPases. GEFs activate GTPases by stimulating guanosine diphosphate (GDP) release and therefore allowing guanosine triphosphate (GTP) to bind. GAPs enhance GTP hydrolysis rate and therefore reduce or inhibit their activation (Rossman et al., 2005; Tcherkezian & Lamarche-Vane, 2007). Epithelial Cell Transforming 2 (ECT2) is the essential RHOA GEF during cytokinesis (Kimura et al., 2000). Confining active RHOA to the equator requires rapid inactivation by GAPs. In the RHOA flux model, RHOA global inactivation by GAPs counteracts the localized activation by GEFs. This model predicts that when GAP-inactivated RHOA levels decrease, equatorial GEF-activated RHOA increases and diffuses throughout the plasma membrane, generating a broader RHOA zone (Bement et al., 2006). The function of CYK4 as a RHOA GAP has been questioned because some reports suggest that its GAP domain promotes RHOA activation (Loria et al., 2012; Zhang & Glotzer, 2015), whereas others suggest that it functions as a GAP for the GTPase Ras-related C3 botulinum toxin substrate 1 (RAC1) (Zhuravlev et al., 2017). RAC1 triggers ARP2/3 activation which is responsible for the formation of branched F-actin. During cytokinesis RAC1 is inhibited at the cell equator in order to avoid branched F-actin in this location (Bastos et al., 2012). In human cells, CYK4 interacts and recruits ECT2 to the midzone (Yüce et al., 2005, Zhao &

Manser, 2005). The Polo-like kinase 1 (PLK1) also promotes ECT2 recruitment by phosphorylating CYK4 and consequently generating a binding site for ECT2 (Brennan et al., 2007; Burkard et al., 2007; Petronczki et al., 2007). In addition to phosphorylating CYK4, PLK1 binds to ECT2 and relieves its autoinhibited state (Niiya et al., 2006). Then, ECT2 binds to the equatorial plasma membrane through its pleckstrin homology domain (PH domain) and adjacent polybasic region in the C-terminus (Figure 1.3; Su et al., 2011).

The CPC is composed of Aurora B kinase, the scaffold protein INner CEntromere Protein (INCENP), and two other non-enzymatic proteins Survivin and Borealin (Carvalho et al., 2003; Pereira & Schiebel, 2003; Honda et al., 2003; Gassmann et al., 2004). Aurora B promotes the recruitment of centralspindlin to the midzone and phosphorylates the mitotic kinesin-like protein 1 (MKLP1), which is essential for cytokinesis to happen (Zhu & Jiang, 2005; Douglas et al., 2010).

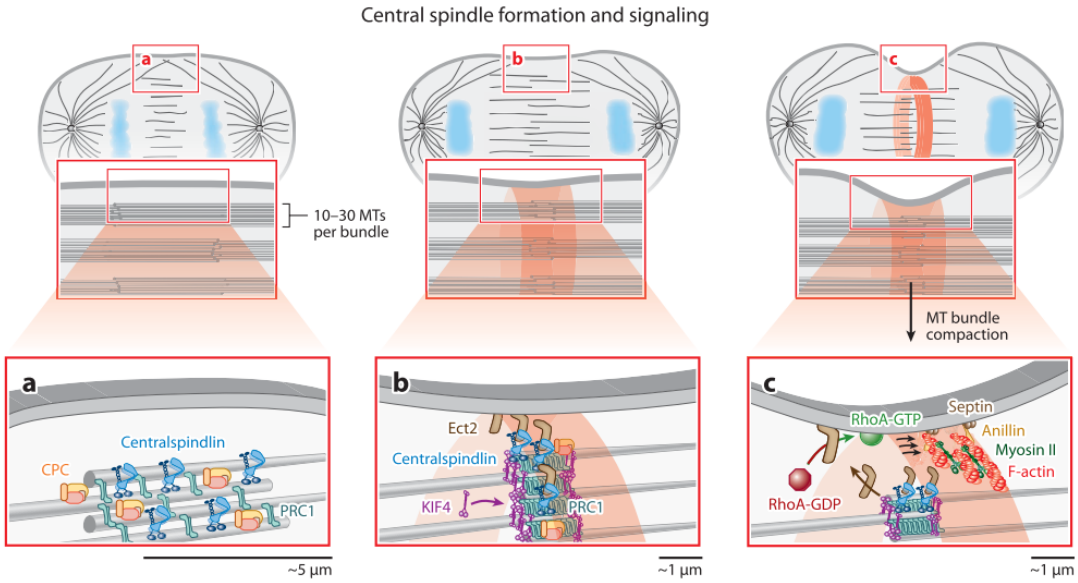

Figure 1.3 Division site specification requires correct central spindle formation and signalling. (a) In early anaphase, PRC1, centralspindlin, and the CPC localize at the spindle midzone, where they bundle the overlapping microtubules. (b) PRC1 recruits KIF4 to MT plus ends to stop their growth, limiting the length of the overlap zone. ECT2 binds centralspindlin and goes to the plasma membrane. (c) ECT2 promotes the conversion of inactive RHOA-GDP to active RHOA-GTP, leading to contractile ring assembly. (Reprinted from (Green et al., 2012); used under permission).

The furrow formation is additionally regulated by astral microtubules. In a classic study summarized in Figure 1.4, Rappaport pressed *D. excentricus* (sand dollar) eggs with a glass bead altering their form to a donut shape. At the second mitosis, these eggs contained two

spindles that were bisected by a cleavage furrow, resulting in three cells: two with a single aster, and one in the middle with two asters without a central spindle or chromosomes. A furrow formed and ingressed completely between the two asters, which indicated that a contractile ring can form and constrict between two asters that are not connected (Rappaport, 1961).

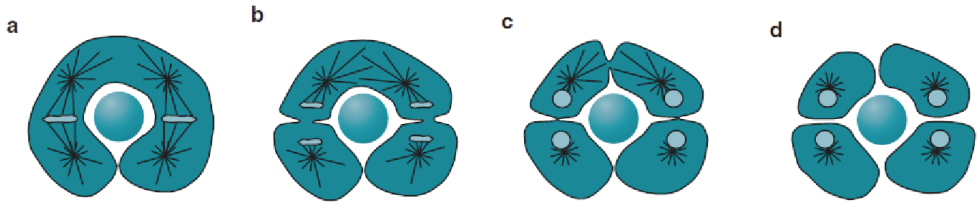

Figure 1.4 Astral microtubules regulate the formation of the contractile ring furrow. The experiment carried out by Rappaport involved a *D. excentricus* egg in the form of a doughnut shape generated by pressing a glass bead in the center of the egg. (a) The first cell cleavage leads to a doughnut-shaped cell with two spindles. (b) During the second cell division, cleavage furrows are formed in the middle of the two spindles and start to constrict. (c-d) A third cleavage furrow is formed and constrict between the two asters that were not connected by a spindle or chromosomes (Adapted from (Maddox & Oegema, 2003) used under permission)

In the *C. elegans* embryo, signals from both midzone and the asters contribute to furrow positioning (Bringmann & Hyman, 2005). The asters prevent the accumulation of contractile ring proteins at the poles, restricting them to the equatorial region (Werner et al., 2007; Mangal et al., 2018). Local inhibition of contractile ring protein accumulation at the cell poles by the asters also occurs in grasshopper spermatocytes and vertebrate cells (Chen et al., 2008; Zhou & Wang, 2008). A cleavage furrow can also form and constrict in the absence of signals from the midzone (Dechant & Glotzer, 2003; Lewellyn, 2010; Verbrugghe & White, 2007; von Dassow et al., 2009). However, furrow constriction does not happen if the asters are too close to one another (Lewellyn, 2010). In sea urchin eggs, eliminating dynamic astral microtubules leads to a broader zone of active RHOA and contractile ring proteins at the cell equator (Bement et al., 2005; Foe & von Dassow, 2008; von Dassow et al., 2009), which suggests that the asters prevent active RHOA from spreading outside the cell equator (von Dassow et al., 2009).

1.4.2 Contractile Ring Assembly and Constriction

Early studies reveal that the contractile ring is a thin (0.1–0.2 μm) filamentous structure that assembles beneath the plasma membrane at the cell equator (Schroeder, 1972). Cytokinesis inhibition by actin-depolymerizing drugs demonstrated that F-actin is crucial for contractile ring formation (Carter, 1967). F-actin in the contractile ring is nucleated and elongated by formins and organizes circumferentially around the cell equator. F-actin in the ring is associated with the motor protein NMII (Fujiwara et al., 1978). NMII is organized in bipolar filaments parallel to the cleavage plane, within the equatorial F-actin band (Fenix et al., 2016; Henson et al., 2017). This type of filament organization suggests that like what happens in the muscle sarcomere, a sliding-filament mechanism of contraction may occur during cytokinesis.

NMII is essential during cytokinesis since genetic perturbation, specific inhibition and injection of anti-NMII antibodies block furrow ingression (Mabuchi & Okuno, 1977; Guo & Kemphues, 1996; Karess et al., 1991; Shelton et al., 1999; Young et al., 1993; Straight et al., 2003). For NMII filaments to be able to exert force on F-actin filaments, NMII needs to be activated. NMII activation occurs by active RHOA that recruits Rho-associated protein kinase (ROCK) and Citron Rho-interacting kinase (CIT-K). These phosphorylate the myosin regulatory light chain (RLC) promoting NMII activation (see section 1.5.2). Additionally, ROCK can also phosphorylate myosin phosphatase (MYPT) inactivating it and thus increasing RLC phosphorylation. Active RHOA also activates cytokinesis formins at the cell equator leading to nucleation of F-actin (Figure 1.5).

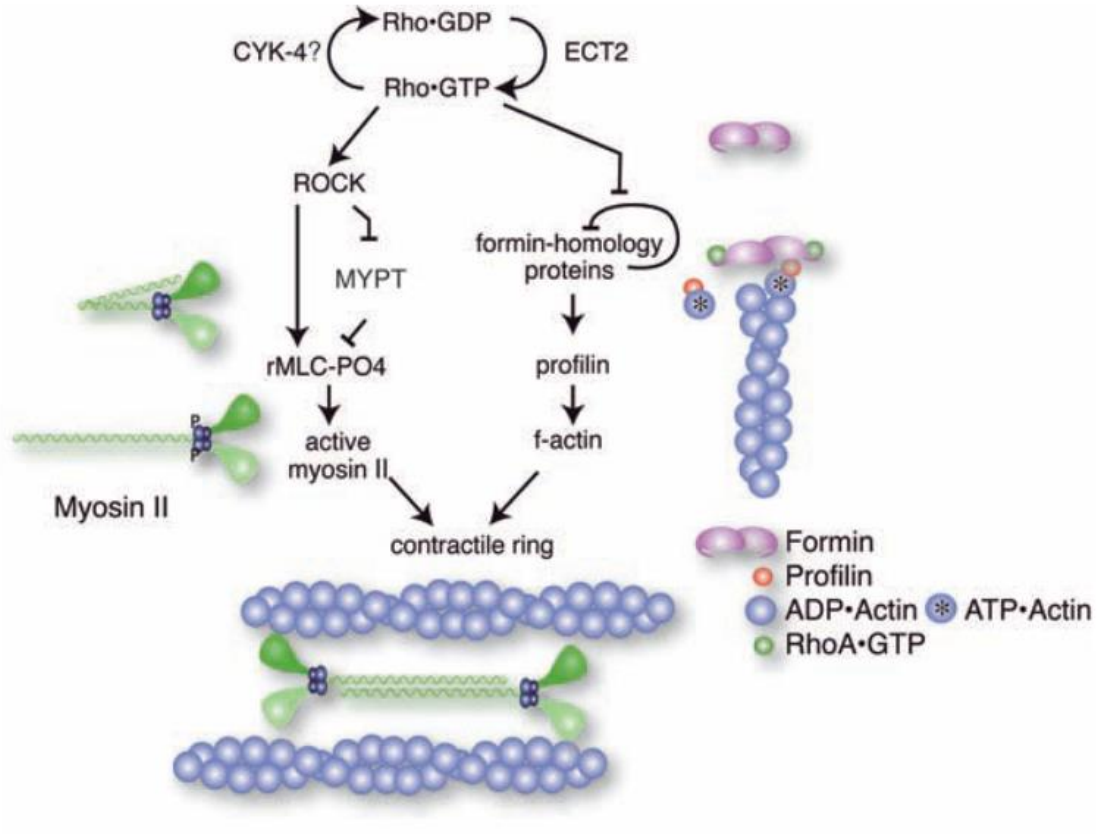

Figure 1.5 The RHOA GTPase activates NMII and F-Actin. RHOA activates ROCK, which phosphorylates the RLC (dark blue). This leads to a change of conformation in NMII that allows the formation of myosin bipolar filaments. RHOA indirectly modulates Myosin Phosphatase Targeting Protein (MYPT) through ROCK. Active RHOA, RHOA-GTP, relieves formin autoinhibition allowing the nucleation and elongation of F-actin (From Glotzer, 2005. Reprinted with permission from AAAS).

Formins are locally activated by active RHOA at the cell equator (Figure 1.6; Motegi & Sugimoto, 2006; Watanabe et al., 2010). Active RHOA releases formins from its autoinhibited state (Watanabe et al., 1997). There are several formins, but the ones involved in cytokinesis localize at the cleavage furrow and in their absence, cleavage furrow ingression does not occur (Castrillon & Wasserman, 1994; Chang, 1999; Kovar et al., 2003; Watanabe et al., 2008). Partial depletion of *C. elegans* Cytokinesis defect 1 (CYK-1), the only formin implicated in cytokinesis in this system, leads to slow contractile ring constriction (Chan et al., 2019). CYK-1 inactivation specifically during cleavage furrow initiation also slows ring constriction, revealing that formin is also involved in the constriction step of cytokinesis (Davies et al., 2014). The role of CYK-1 during late cytokinesis is unclear as there are contradictory results. In a study CYK-1 is described to be required for complete abscission while in another, abscission occurs even when CYK-1 is perturbed (Swan et al., 1998; Davies et al., 2014).

Anillin is a conserved multidomain protein that interacts with several contractile ring components, acting as a scaffold protein. Anillin localizes to the cleavage furrow (Figure 1.6; Field & Alberts, 1995) and it is responsible for recruiting septins to the contractile ring (D'Avino et al., 2008; Goldbach et al., 2010; Hickson & O'Farrell, 2008; Maddox et al., 2005). Besides septins, anillin binds to F-actin, NMII, RHOA, and its regulators, ECT2, and RacGAP50C, among others (Piekny & Maddox, 2010). Anillin binds to the plasma membrane through its PH domain and anillin mutants lacking the PH domain do not localize at the cleavage furrow and, consequently, are not able to recruit septins to this location (Field et al., 2005; Liu et al., 2012). Anillin also binds to the plasma membrane via the C2 domain localized next to the PH domain (Sun et al., 2015). Anillin is thought to act as an anchor of the contractile ring to the plasma membrane because it can bind both the plasma membrane and several contractile ring components. Anillin depletion in mammalian cells and *D. melanogaster* S2 cells leads to cytokinesis failure and abnormal furrow cleavage oscillations occur indicating incorrect attachment to the plasma membrane (Straight et al., 2005; Piekny & Glotzer, 2008; Hickson & O'Farrell, 2008; Kechad et al., 2012). In *C. elegans* zygotes, anillin regulates the asymmetric closure of the cleavage furrow and promotes polar body extrusion during meiosis, which relies in a specialized asymmetric division but is not essential for cytokinesis to happen (Maddox et al., 2005; Dorn et al., 2016).

Septins are highly conserved GTP-binding proteins that form hetero-oligomeric complexes and higher-order structures like filaments or rings (Kinoshita et al., 2002). All mammalian septins have a core domain that directly binds to the plasma membrane, a GTP-binding domain, and a highly conserved series of amino acids of unknown function called the unique septin element (Cao et al., 2007; Pan et al., 2007). Septins perform diverse functions by serving as scaffolds, diffusion barriers between different membrane compartments, and cross-linking F-actin (Caudron & Barral, 2009; Mavrakis et al., 2014). The requirement of septins during cytokinesis seems to differ between organisms and tissues. In *C. elegans* one-cell embryos*,* septin mutant versions mutants in *unc61(n3169)* and *unc59(e1005)* embryos do not localize in the contractile ring but cytokinesis completes (Nguyen et al., 2000). However, like anillin, septins are required for asymmetric furrow ingression (Maddox et al., 2007; Dorn et al., 2016). In *D. melanogaster*, cytokinesis failure is observed upon septin depletion in the follicular epithelium during oogenesis, during cellularization in embryos and in several larval tissues including the brain and lymph glands (Neufeld & Rubin, 1994; Fares et al., 1995; Adam et al., 2000; O'Neill & Clark, 2016). Cytokinesis failure also occurs in mammalian cells when septins are depleted or inhibited with a specific antibody (Kinoshita et al., 1997; Nagata et al., 2003; Estey et al., 2010).

Other proteins can regulate contractile ring assembly. For example, actin-binding proteins, such as cofilin, the ARP2/3 complex, and profilin (see section 1.1).

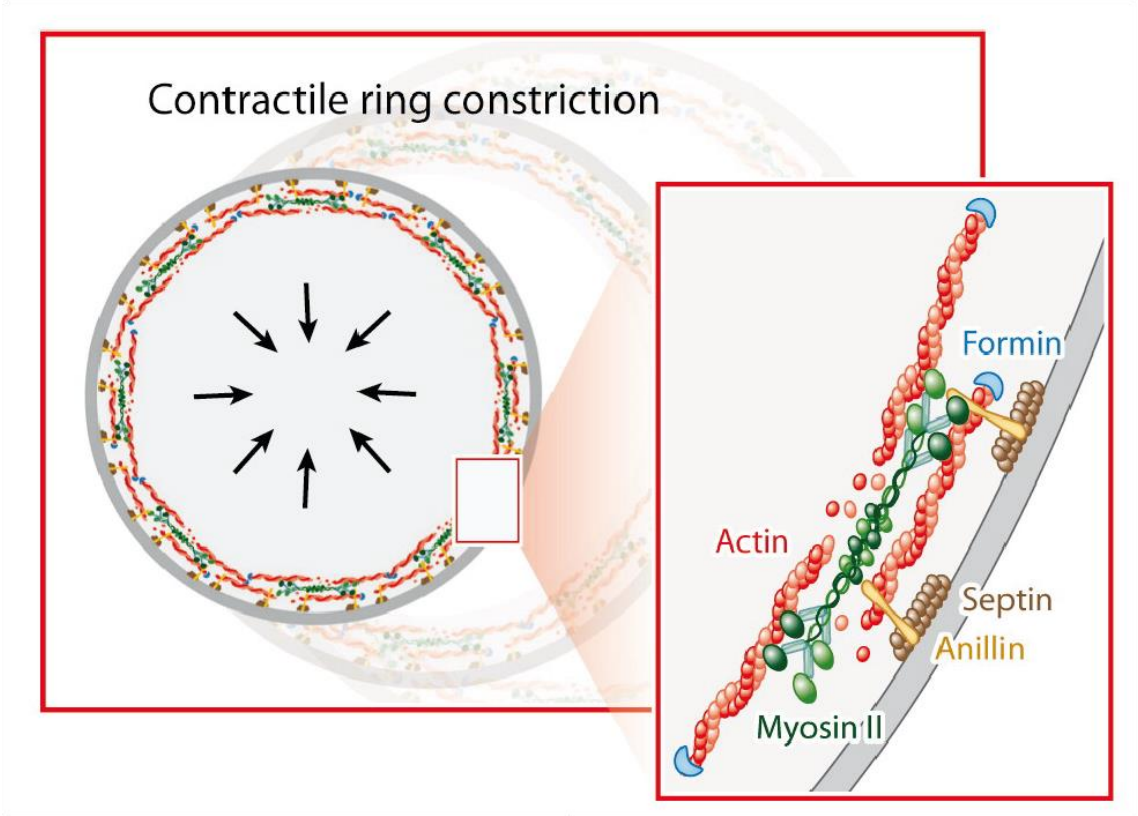

Figure 1.6 The contractile ring is an actomyosin filamentous network. The contractile ring is mostly composed by actin and myosin filaments, but other proteins are required for the formation of a normal contractile ring. Formins, septins, and anillin are all proteins required for a functional contractile ring. While formins nucleate and elongate F-actin, anillin and septins are thought to act as anchors of the contractile ring to the plasma membrane (Reprinted from (Green et al., 2012); used under permission).

1.5. Conventional myosins

1.5.1 Non-muscle myosin II structure and ATPase cycle

Conventional myosins or class II myosins are ubiquitous myosins required for many cellular processes such as cell migration, cell adhesion, cell shape, and cytokinesis. Class II myosins are hexameric proteins composed of two myosin heavy chains (HCs) and two pairs of LCs. The myosin II motor domain comprises four subdomains connected by flexible linkers (Houdusse et al., 1999; Figure 1.7). The amino-terminal subdomain includes an SH3-like motif (Kodera & Ando, 2014). The SH3 domain is usually found in proteins implicated in

signal transduction, actin dynamics and membrane trafficking (Lynch et al., 1986; Jung & Hammer, 1994; Doberstein & Pollard, 1992; Lee et al., 1999; Mayer, 2001). This is linked to the upper 50 kDa subdomain that, in turn, is connected to the lower 50 kDa subdomain. The latter subdomains are separated by a cleft that constitutes the conserved actin-binding region (Houdusse et al., 1999). This cleft closes slightly upon nucleotide binding to the ATPase site and then closes completely upon actin binding. The nucleotide-binding pocket is formed by at the edge of a beta-sheet with seven strands connected by loops that is surrounded by alpha-helices (Rayment et al., 1993). Purine-binding A-loop, phosphate-binding P-loop, Switch I and the Switch II are four well-conserved sequence motifs in the nucleotide-binding pocket that mediate nucleotide binding. The converter subdomain connects the lever arm where the LCs bind to the catalytic domain (Ruppel & Spudich, 1996; Friedman et al., 1998; Furch et al., 1999). The converter is connected to the motor domain by the relay helix and the Src homology domain 1- Src homology domain 2 (SH1-SH2) helix. These are important for mechanically driving the angular change of the lever arm during the cross-bridge cycle (Dominguez et al., 1998). The myosin essential light chain (ELC) binds closer to the converter than the RLC. This elongated region of the neck acts as a lever arm to generate the movement of the actin filament (Rayment et al., 1993). In agreement, there is a correlation between the neck size and the speed of myosin II motility on F-actin *in vitro* (Uyeda et al., 1996). This myosin movement was mapped and reconstructed based on electron micrographs of actin-myosin complexes in the presence and absence of ADP (Whittaker et al., 1995).

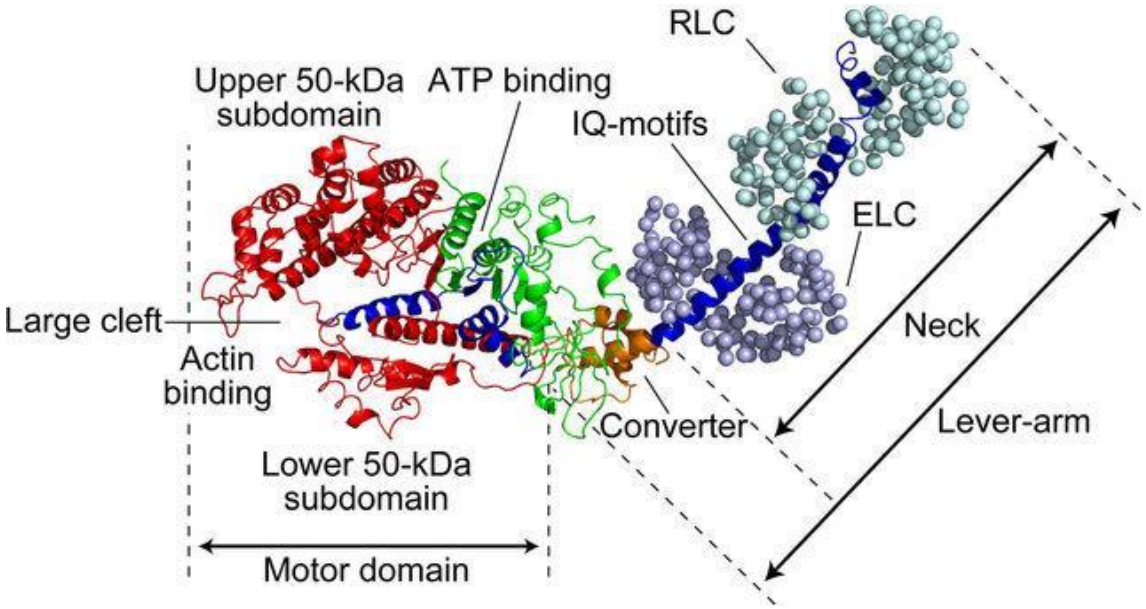

Figure 1.7 Crystal structure of skeletal myosin II S-1. The HC of myosin II and the LCs are shown as a ribbon and a sphere diagram, respectively. The 50-kDa regions are colored red. The converter domain is colored in orange and the IQ motifs in dark blue. Crystal structure from (Rayment et al., 1993). (Figure reprinted from (Kodera & Ando, 2014) used under permission).

The actin translocation by myosin is described in a model for force transduction. In this model, the motion is due to the movement of the myosin neck while the N-terminus, the upper and lower 50 kDa subdomains remain fixed. The converter subdomain acts as a joint, and conformational changes in structural domains near the Switch II of the nucleotide-binding pocket control the movement (Rayment et al., 1993).

Actin translocation occurs by cyclic attachment and detachment of myosin from F-actin, the cross-bridge cycle (Figure 1.8; Huxley, 1969). First, in the rigor state, myosin is tightly bound to F-actin. Then, ATP binds to the nucleotide-binding site on the myosin head, causing the detachment of the myosin head from F-actin. The myosin head converts the bound ATP to ADP and inorganic phosphate (Pi) through its ATPase activity. Both ADP and Pi remain bound to the myosin head. The energy released from ATP hydrolysis causes a change in the conformation of the myosin head. The lower 50 kDa subdomain re-attaches to the actin cleft. The cleft closes and both upper and lower 50 kDa subdomains strongly bind to actin triggering Pi release, which induces the power stroke. The power stroke corresponds to the movement of the myosin lever arm that generates force and movement of F-actin. The myosin head changes its conformation and ADP is released. The myosin head remains bound to F-actin in a new position. If ATP is present, this cycle keeps occurring resulting in

the sliding of actin filaments, which will lead to contractility of the network, depending on the biological context.

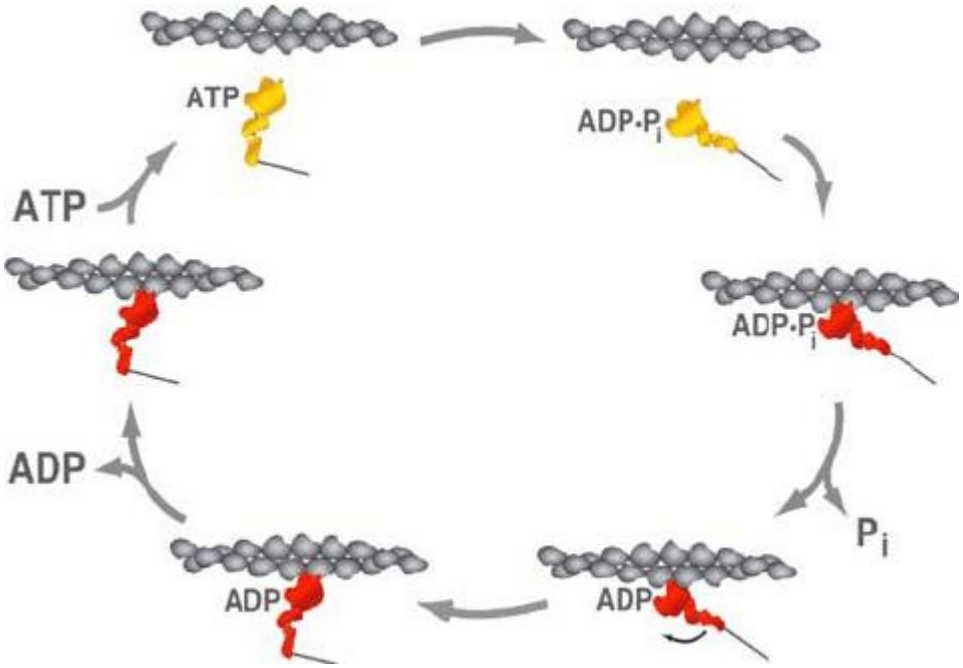

Figure 1.8 Myosin cross-bridge cycle. Myosin head binds and hydrolyses ATP into ADP and Pi (yellow myosin heads in the top). A conformational change occurs in the myosin head which results in a stronger bind to F-actin (red myosin heads). The Pi is released, and a stroke of the lever arm follows. When ADP is released, ATP can bind to the myosin head, which releases the myosin head from F-actin (Figure reprinted from (Sivaramakrishnan et al., 2009); used under permission).

1.5.2 Non-muscle myosin II activation during cytokinesis

NMII HC (~230 kDa) dimerizes and binds two pairs of LCs, the RLC (20 kDa) and the ELC (17 kDa; Figure 1.9). NMII is described as a slow motor with a step size along F-actin between 10 nm and 28 nm (Uyeda et al., 1990), which are small distances when compared to those of myosins from other classes.

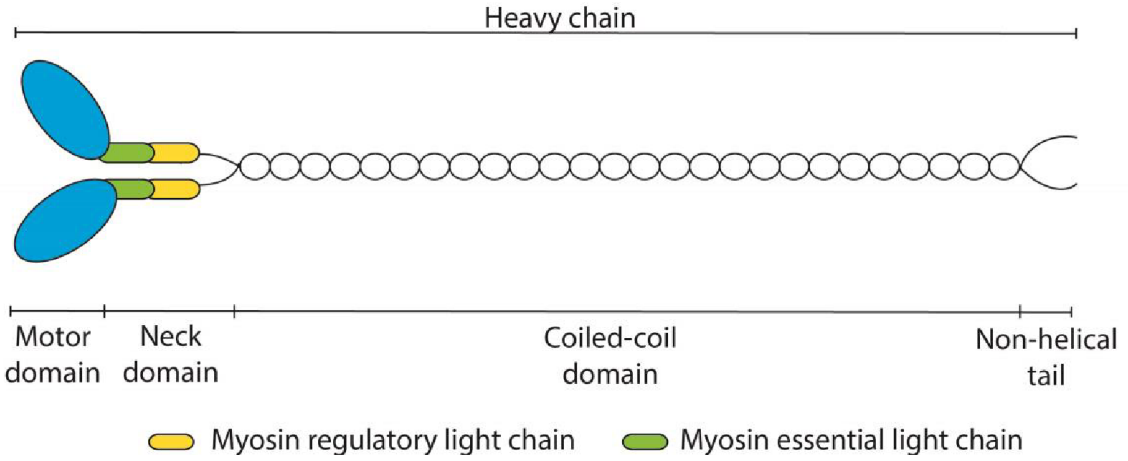

Figure 1.9 Schematic of Non-Muscle myosin II (NMII) structure. NMII is composed of a dimer of HCs. Each HC binds one ELC for stabilization and one RLC for regulation. The HC comprises three regions: a motor domain that has ATPase activity and binds F-actin, a neck domain where the LCs bind, a coiled-coil domain that enables dimerization, and bipolar filament formation and a tail domain. Image reprinted from Saramago (2014). Phospho-regulation of Myosin Regulatory Light Chain in *Caenorhabditis elegans* embryos during cytokinesis (Master's thesis, University of Porto (FCUP), Porto, Portugal). Retrieved from https://repositorio-aberto.up.pt/handle/10216/80077

NMII molecules are regulated by several mechanisms that control the ATPase activity and the formation of bipolar filaments. In vertebrates, the critical step for NMII to form bipolar filaments is the phosphorylation of RLC on serine 19 (Adelstein & Conti, 1975). This induces conformational changes in NMII molecules from a folded form into an open and competent form (Figure 1.10; Trybus & Lowey, 1984; Vicente-Manzanares et al., 2009). The serine 19 phosphorylation primarily controls ATPase activity, bipolar filament assembly, and myosin motility. An additional phosphorylation on threonine 18 increases the ATPase activity and filament assembly, but not the motility (Ikebe, 1989; Umemoto et al., 1989).

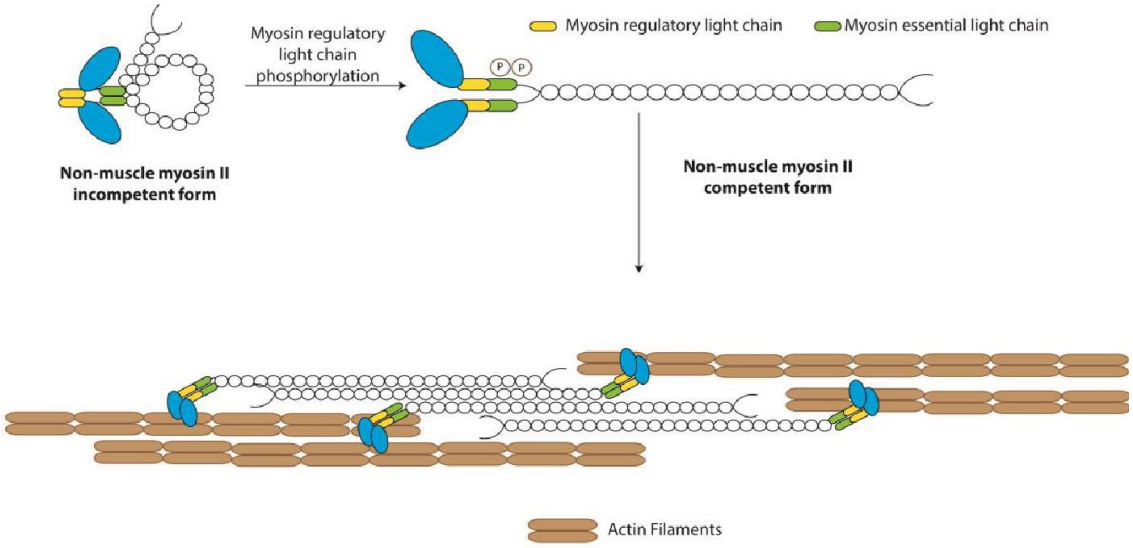

Figure 1.10 RLC phosphorylation changes NMII conformation in order to promote bipolar filament formation. RLC phosphorylation in the residues serine 19 and threonine 18 leads to NMII dimer unfolding. The unfolded dimer is competent to establish interactions with other unfolded dimers through their coiled-coil regions. Bipolar filaments arise and can slide actin filaments past one another. Image reprinted from Saramago (2014). Phospho-regulation of Myosin Regulatory Light Chain in *Caenorhabditis elegans* embryos during cytokinesis (Master's thesis, University of Porto (FCUP), Porto, Portugal). Retrieved from https://repositorio-aberto.up.pt/handle/10216/80077

Myosin activation by RLC phosphorylation is key for cytokinesis. RLC phosphorylation at these Serine/Threonine activation sites initiates at anaphase and remains increased in the cleavage furrow throughout cytokinesis. At the cell poles, phosphorylation levels are decreased (DeBiasio et al., 1996; Matsumura et al., 1998; Yamashiro et al., 2003). NMII with a non-phosphorylatable RLC is unable to localize at the cleavage furrow in *D. melanogaster* S2 cells (Dean & Spudich, 2006). In contrast, NMII with a phosphomimetic RLC, a constitutively active NMII, localizes at the cleavage furrow in *D. melanogaster* S2 cells (Dean & Spudich, 2006). In human cells, RLC phosphorylation at serine 19 is detected at the equatorial region at the same time as NMII (Yamakita et al., 1994). Altogether, these suggest that NMII is activated at the cell equator. NMII activation by RLC phosphorylation also seems to be involved in regulating actin turnover in the contractile ring, since actin turnover is slower when RLC phosphorylation is inhibited (Murthy & Wadsworth, 2005). In agreement, actin turnover is slower when NMII is perturbed, suggesting that NMII can modulate actin turnover likely by functioning during F-actin disassembly (Guha et al., 2005; Mendes Pinto et al., 2012; Wilson et al., 2010).

Several kinases, including Myosin light-chain kinase (MLCK) and ROCK, can phosphorylate the RLC at the activation sites (Matsumura, 2005; Zhao & Manser, 2005). While ROCK can

phosphorylate other proteins, MLCK is RLC specific (Kimura et al., 1996). CIT-K, p21-activated protein kinase (PAK), myotonic dystrophy protein kinase-related Cdc42-binding kinase (MRCK), and Zipper-interacting protein kinase (ZIP) can also phosphorylate the RLC (Leal et al., 2003; Wilkinson et al., 2005).

During cytokinesis, ROCK phosphorylates and inactivates myosin phosphatase targeting protein (MYPT), which when active can dephosphorylate RLC leading to NMII inactivation. MYPT is composed of a type 1 phosphatase catalytic subunit (MBS) and a regulatory subunit. MBS is a target of active RHOA and ROCK. MBS binding to active RHOA translocates MYPT to the equatorial membrane where it is phosphorylated by ROCK, turning the phosphatase off (Kawano et al., 1999). ROCK phosphorylates the RLC *in vitro,* suggesting a possible role *in vivo* (Amano et al., 1996; Osório et al., 2019) and ROCK inhibition reduces phosphorylated RLC levels (Kosako et al., 2000). ROCK contributes to cytokinesis, because its perturbation leads to cytokinesis slowdown in cultured human cells and *C. elegans* (Kosako et al., 2000; Piekny & Mains, 2002). Additional kinases may play a role, since most *C. elegans* one-cell embryos, expressing a temperature sensitive ROCK mutant, *let-502(sb106),* complete cytokinesis (Piekny & Mains, 2002).

CIT-K, which is activated by active RHOA, localizes at the cleavage furrow (Madaule et al., 1998; Eda et al., 2001) and at the midbody during cytokinesis (Watanabe et al., 2013; D'Avino & Capalbo, 2016). Initial studies using CIT-K overexpression in cells and *in vitro* assays suggested that CIT-K was responsible for NMII regulation, since it was able to phosphorylate the RLC (Madaule et al., 1998; Madaule et al., 2000; Yamashiro et al., 2003). However, studies in *D. melanogaster* and human cells suggest that CIT-K is only required during late stages of cytokinesis (D'Avino et al., 2004; Watanabe et al., 2013). CIT-K is thought to organize and correctly maintain the midbody proteins (Bassi et al., 2011; Bassi et al., 2013; McKenzie et al., 2016). Therefore, instead of contributing to cleavage furrow ingression, CIT-K may act as an organizing centre for the midbody. In *C. elegans,* CIT-K homologues do not seem to play a role during cytokinesis (Piekny & Mains, 2002; Sönnichsen et al., 2005).

RLC phosphorylation by MLCK occurs via the Ca^{2+} pathway when the kinase binds to the Ca^{2+}/CAM complex and is therefore activated. In vertebrates, two MLCKs exist, a short and a long version. The short MLCK is expressed in all smooth muscle and non-muscle cells while the long MLCK is expressed in only some of these tissues. In non-muscle cells the long isoform is the most expressed MLCK (Gallagher et al., 1995). In HeLa cells, the short MLCK is diffusely distributed throughout the cell during the entire cell cycle and the long

MLCK is enriched at the cell cortex from metaphase until cytokinesis (Poperechnaya et al., 2000). The short version is responsible for targeting the long MLCK to the cleavage furrow. MLCK is maximally activated just before cleavage furrow formation and during cleavage furrow ingression (Chew et al., 2002). After furrow ingression, MLCK localizes to the poles of the daughter cells (Chew et al., 2002). In the case of large eggs, such as those of zebrafish, sea urchins and frogs, a local increase in Ca^{2+} correlates with cell cycle events such as anaphase onset and cytokinesis (Ciapa et al., 1994; Chang & Meng, 1995; Webb et al., 1997). During cytokinesis of mammalian cells, there are no measurements of local changes in intracellular Ca^{2+} levels. However, global Ca^{2+} levels seem to increase in anaphase, indicating that global activation of MLCK could occur at this point (Ratan et al., 1988). Other kinases, including PAK, phosphorylate MLCK, inhibiting its activity (Sanders et al., 1999). The small GTPase RAC1, which can activate PAK, is activated at the polar cortex at late anaphase. This may inhibit MLCK at the poles, causing it to remain active only at the cell equator (Yoshizaki et al., 2003).

NMII HC phosphorylation also regulates NMII function. *In vitro*, protein kinase C (PKC), casein kinase 2 (CK2), and the transient receptor potential ion channel kinases 6 and 7 (TRPM6 and TRPM7) can phosphorylate the HC at the coiled coil domain or at the non-helical tailpiece (Even-Faitelson & Ravid, 2006; Clark et al., 2008; Ronen et al., 2010).

In mammalian cells, phosphorylation of the HC at Serine 1943 inhibits the formation of NMII filaments by reducing the stability of the coiled coil (Dulyaninova et al., 2005). In NMII-A, HC phosphorylation by CK2 inhibits binding of the metastasis-associated protein (MTS1). MTS1 is responsible for inducing filament disassembly and inhibition of assembly (Dulyaninova et al., 2005; Mitsuhashi et al., 2011). How HC phosphorylation regulates NMII *in vivo* is not well understood, but in *D. discoideum,* phosphorylation of Threonine 1823, Threonine 1833, and Threonine 2029 is essential for NMII accumulation at the cleavage furrow (Sabry et al., 1997).

1.5.3 Non-muscle myosin II functions

Different animals express several isoforms of NMII with different properties and expression patterns. There are three human NMII HC isoforms: NMII-A, NMII-B, and NMII-C, encoded by three genes Myosin Heavy Chain 9, Myosin Heavy Chain 10, Myosin Heavy Chain 14 (MYH9, MYH10, and MYH14), respectively (Simons et al., 1991; Golomb et al., 2004). NMII-B has a higher duty-ratio than NMII-A and NMII-C, meaning that it spends more time bound

to actin than the other NMIIs. NMII-A has the lowest duty ratio from the three isoforms (Kovács et al., 2003). *In vitro,* homotypic filaments of NMII-A cannot move processively on F-actin while filaments solely composed by NMII-B can. The addition of NMII-B to NMII-A filaments allows these to move processively in the F-actin, suggesting that the regulation of NMII filaments composition can ensure the different NMII functions within the cell (Melli et al., 2018). During cytokinesis in HeLa cells, NMII-A and NMII-B co-localize and form stacks of heterotypic filaments to maintain cell contractility and shape (Taneja et al., 2020). While both NMII-A and NMII-B are required for normal cortical tension and correct cell shape, NMII-A maintains the contractile ring constriction rate and NMII-B is essential for cytokinesis due to its important role during abscission (Taneja et al., 2020). In COS-7 cells, NMII-A and NMII-B filaments co-assemble and form heterotypical filaments in the cleavage furrow (Beach et al., 2014). During mouse embryo development, all the isoforms are ubiquitously expressed. While cardiac cardiomyocytes express NMII-B and NMII-C but not NMII-A, the non-myocyte cells in the heart contain NMII-A. NMII-A is enriched in blood cells, spleen, thymus, and lymph nodes. NMII-B and NMII-C are enriched in the brain. Both NMII-A and NMII-C are present in the colon and stomach, while NMII-B is not (Golomb et al., 2004). In chicken, NMII-B is highly expressed in cardiomyocytes (Rhee et al., 1994; Du et al., 2003). In vertebrates, the distribution of the isoforms also changes during development (Takeda et al., 2000; Golomb et al., 2004; Jana et al., 2006).

In *D. melanogaster* there is a single gene encoding for NMII, *zipper* (Kiehart et al., 1989; Young et al., 1991), which is regulated by the phosphorylation of its RLC, *Spaghetti Squash* (Karess et al., 1991; Jordan & Karess, 1997). Zipper function is important for several processes during development such as cell division, cellularization, cell migration, and dorsal closure (Young et al., 1993; Edwards & Kiehart, 1996; Field & Alberts, 1995; Royou et al., 2004; Liu et al., 2008).

C. elegans expresses three NMIIs: Non-muscle myosin 1, Non-muscle myosin 2, Non-muscle myosin 3 (NMY-1, NMY-2 and NMY-3). NMY-1 is the major NMII expressed in the spermatheca (Wirshing & Cram, 2017). It is expressed in all cells at the beginning of embryonic elongation and in the adherens junctions of the pharynx (Piekny, 2003). NMY-1 is also expressed in the sheath cells, cells that outline the gonads and contract to ensure correct oocyte maturation and ovulation (Mccarter et al., 1999; Priti et al., 2018). Contractility of the sheath cells was shown to depend on NMY-2 and the muscle myosin heavy chain 3 (MYO-3) (Ono & Ono, 2016), but the localization of NMY-1 in these cells indicates that this might also play a role. Depletion of NMY-1 leads to reduced contraction in the spermatheca,

which leads to embryo entrapment inside this structure (Kovacevic et al., 2013; Wirshing & Cram, 2017). The *C. elegans* germ cells of the gonads are partially cellularized and connected to a common cytoplasm, by the ring canals. The rings in the canals maintain a constant diameter until oogenesis. Cytoplasmic flow through the canals allows the delivery of material required for the germ cells to cellularize and mature into oocytes (Wolke et al., 2007; Kim et al., 2013). NMY-1 was described to antagonize NMY-2 function in these ring canals. While NMY-1 depletion led to early ring canal constriction and cellularization, NMY-2 depletion led to open rings and did not allow for cellularization (Coffman et al., 2017). However, in a more recent study, NMY-1 depletion was found not to affect this process and NMY-1 was shown not to localize in the germ cells (Priti et al., 2018). NMY-2 is essential in *C. elegans* gonads: its depletion leads to germ cell multinucleation, incomplete cellularization and sterility (Green et al., 2011), and results in reduced tension within the gonad, which decreases the cytoplasmic flow required for proper oocyte formation (Priti et al., 2018). NMY-2 is essential for embryonic cytokinesis as its depletion leads to cytokinesis failure (Shelton et al., 1999; Guo & Kemphues, 1996). NMY-2 localizes at the embryo cortex and at the cleavage furrow. The regulation and localization of NMY-2 is dependent on its RLC, MLC-4 (Shelton et al., 1999; Chapter 4 of this thesis). NMY-2 is required throughout cytokinesis and its inactivation at different stages of cytokinesis always results in cytokinesis failure (Davies et al., 2014; Chapter 4 of this thesis). Embryonic cytokinesis failure is also observed when NMY-2 motor activity is strongly impaired (Osório et al., 2019; Chapter 5 of this thesis). Additionally, NMY-2 is required for correct embryo polarization (Guo & Kemphues, 1996), and embryonic elongation (Piekny, 2003). In spermatids, NMY-2 localizes at the cortex and pseudo-cleavage furrow and is responsible for driving an incomplete cytokinesis that is important for sperm differentiation (Hu et al., 2019). NMY-2 localizes in the division site of the seam cells, pluripotent cells distributed along the animal, where it maintains the correct cell fate without impairing the polarity of the asymmetric division (Ding & Woollard, 2017). To date, no function has been attributed to NMY-3 and large RNAi screens revealed that NMY-3 depletion was not associated with animal sterility or embryonic lethality (Kamath, 2003; Sönnichsen et al., 2005)

In *D. discoideum* a single NMII is expressed, Myosin 2 heavy chain (MhcA), and its knockout does not allow cells to grow in suspension, although they are able to grow when adhered to a substrate (Manstein et al., 1989). Cells expressing a mutant of MhcA in which the tail was partially deleted and cannot form filaments become multinucleated due to cytokinesis failure (Lozanne & Spudich, 1987). MhcA knockout cells are not polarized, and their pseudopodia,

lamellipodia, and filopodia that normally extend in a single direction, extend in random directions (Fukui et al., 1990).

S. pombe expresses two NMIIs, Myo2p and Myp2p. Myo2p is required for cytokinesis and cell growth (Kitayama et al., 1997; May et al., 1997; Balasubramanian et al., 1998). Myp2p is only essential for growth at high temperature or high salt concentration (Bezanilla et al., 1997; Motegi et al., 1997). In the contractile ring, Myo2p and Myp2p localize in different regions. Myo2p localizes in an outer region of the ring while Myp2p localizes in an inner part of the structure. They are described to have different functions during cytokinesis. While Myo2p is mainly required for ring assembly, Myp2p functions during ring constriction. In addition, Myo51p, a myosin from class V, cooperates with Myo2p and Myp2p during contractile ring assembly and constriction (Laplante et al., 2015). Another study proposed that the three myosins function during cytokinesis, but Myo2p and not Myp2 is the major myosin for both contractile ring assembly and constriction (Zambon et al., 2017).

In *S. cerevisiae,* Fission yeast myosin 1 (Myo1p), the single NMII is required for yeast growth and localizes in the contractile ring (Bi et al., 1998). The level of cytokinesis failure depends on the type of genomic background used (Bi et al., 1998). Mutants of Myo1p are not able to form a contractile ring (Schmidt et al., 2002), however most cells can divide due to the growth of the dividing septum. Nevertheless, in *S. cerevisiae,* only a percentage of cells fail cytokinesis in the absence of actin (Ayscough et al., 1997; Bi et al., 1998), suggesting a different mechanism of ring assembly and constriction in this system.

1.6. Unconventional myosins

After the discovery of conventional myosis, other molecular motors that walk on F-actin were identified. Unconventional myosins are composed of one or two HCs which have a highly conserved motor domain and bind to a variable number of LCs and/or CAMs. Different myosins have different sizes, which allows for different step sizes while moving on F-actin. They are designated unconventional myosins because they do not form filaments (Figure 1.11). Multiple myosins from different classes can be found within one single cell, suggesting that these can act in different processes that require movement along F-actin, and/or that they cooperate. Indeed, unconventional myosins from classes I, VI, VII and XV cooperate for example in the trafficking of molecules at the stereocilia of hair cells in the inner ear in vertebrates (Hasson et al., 1997; Belyantseva et al., 2005). Due to the high number of

classes existing in different organisms, in this section, I will only mention those represented in *C. elegans* since it was the experimental model I used.

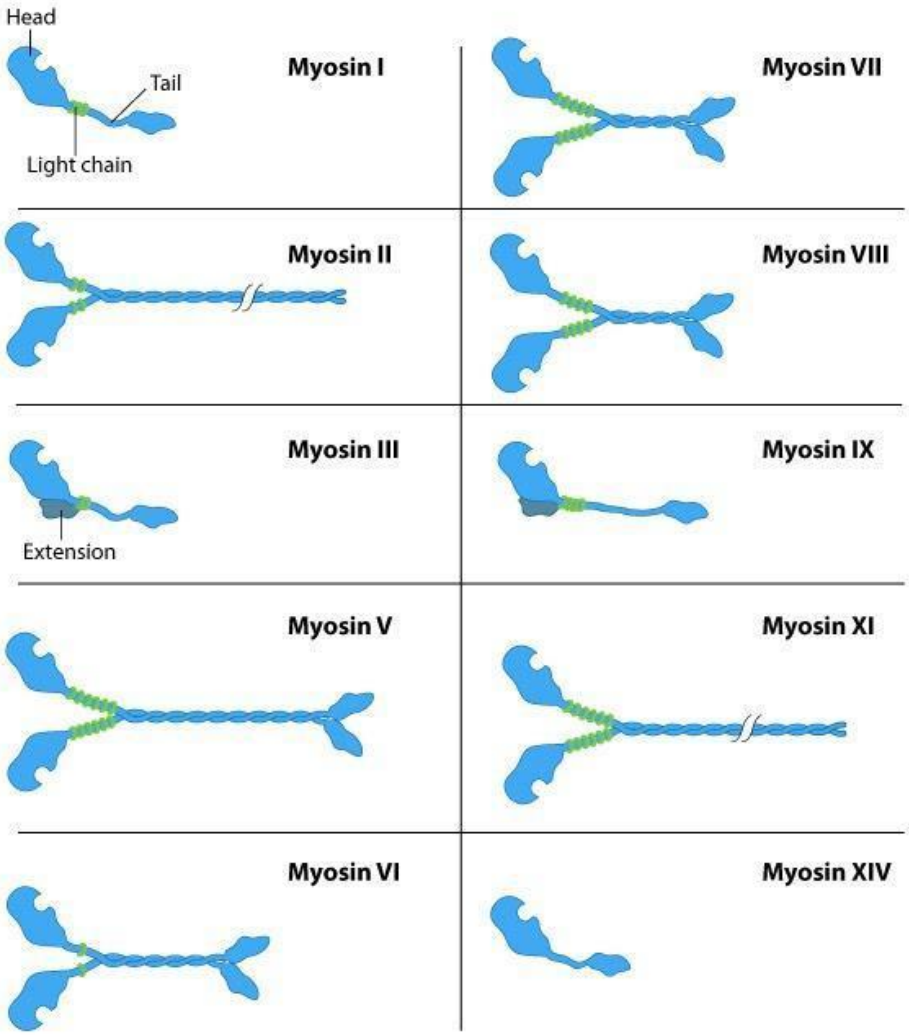

Figure 1.11 Schematics showing some members of the myosin superfamily. All myosins have a conserved motor domain, but they are substantially different at the tail. Myosins from classes III and IX also have an -terminal extension. The number of LCs that bind to the HC changes between myosin classes. While some myosins can act as a dimer, other myosins act as a monomer. https://www.mechanobio.info/cytoskeleton-dynamics/what-are-motor-proteins/what-is-myosin/

1.6.1 Class I

Myosins I are expressed in many organisms as monomeric myosins, meaning that they are composed and function as a single HC. These myosins are involved in many different cellular contexts which mainly associated with its ability to bind actin and to the plasma

membrane. They regulate the structure and function of inner hear hair cells, neurons and intestinal microvillar, maintain the normal membrane tension of the cells, regulate the cell-cell adhesion and act as anchors to other proteins at the plasma membrane.

The HC can be divided into head, neck, and tail domains (Figure 1.12; Albanesi et al., 1985; Stafford et al., 2005). The tail can be further divided into three tail homology domains (THs) (Hammer, 1991). TH1 is involved in membrane binding, TH2 contains an ATP-insensitive actin-binding site, and TH3 is an SH3 domain. Myosins I that possess all the THs are designated long-tailed, whereas those containing only TH1 are designated short-tailed. Both short-tailed and long-tailed class I myosins exist in higher organisms. Vertebrate myosin IC (MYO1C) is known to interact with hair cell receptors via its IQ domain (Cyr et al., 2002; Lin et al., 2005) and with acidic phospholipids via its basic tail domain (Adams & Pollard, 1989; Doberstein & Pollard, 1992; Tang et al., 2002). A MYO1C fragment composed by the IQ and the tail domains has a higher affinity for Phosphatidylinositol 4,5-bisphosphate (PIP2) when compared to other phospholipids and a MYO1C tagged tail localizes to cell regions enriched in PIP2 (Hokanson & Ostap, 2006). PIP2 concentrates in actin-rich structures and it is known to regulate cytoskeletal proteins such as profilin (Yin & Janmey, 2003; Scholze et al., 2018). In addition, MYO1C binding to PIP2 indicates that MYO1C can participate in processes like endocytosis or cytokinesis (Hokanson & Ostap, 2006; Scholze et al., 2018). During cytokinesis PIP2 is enriched at the cleavage furrow in mammalian cells, where it promotes the anchoring of cytoskeleton components to the plasma membrane maintaining the actomyosin ring structure (Emoto et al., 2005; Field et al., 2005). In *C. elegans* one-cell embryos, PIP2 forms structures at the cortex that colocalize with ECT-2, Cell division control protein 42 (CDC-42) and RHO-A, and partially with actin. The formation of these PIP2 structures depends on actin, and dysregulation of PIP2 levels creates a disorganized F-actin cytoskeleton, indicating that PIP2 and F-actin cortical organizations are co-dependent (Scholze et al., 2018).

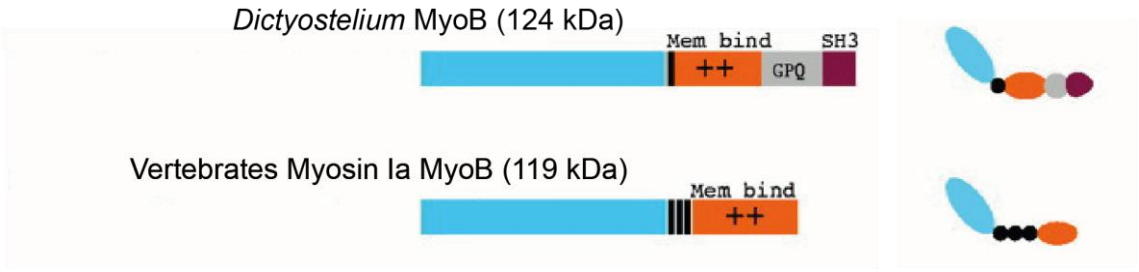

Figure 1.12 Schematic showing myosin I structure in *D. discoideum* and vertebrates. The motor domains are in blue, IQ domains are in black, membrane-binding domains are in orange. Other regions in the tail are: GPQ, a glycine-, proline-, and glutamine-rich region (grey); ++, positively charged regions; SH3 domain (purple) (Figure adapted from (Krendel & Mooseker, 2005); used under permission)

Studies using optical-tweezers on class I myosins showed that these bind to F-actin 20–50 times more strongly than a single-headed motor produced by proteolytic cleavage of muscle myosin II (Batters et al., 2004; Veigel et al., 1999). In contrast to the slower myosins IA (MYO1A), IB (MYO1B), and IC (MYO1C), myosin ID (MYO1D) has a larger step size (9 to 14 nm vs 6 nm), probably due to the fact that the position of the pivot point in its head domain is similar to that of NMII allowing for significant rotation of the lever arm (Veigel et al., 1999; Köhler et al., 2003).

The number of class I myosins expressed is variable between organisms and tissues (Table 1.1). Additionally, the number of IQ motifs is variable between myosin I isoforms (parentheses in Table 1.1). Some myosins I bind to CAM while others bind to LCs. CAM-binding does not require Ca^{2+}, and the binding affinity to the myosin neck varies among IQ sequences (Cyr et al., 2002; Lin et al., 2005).

Organism	myosin I proteins (number of IQ domains)	LCs/proteins binding to IQ domains	References
Acanthamoeba	myosin-IA (3), IB (1), and IC (1)	CAM	(Hammer et al., 1986; Jung et al., 1987; Jung et al., 1989; Brzeska et al., 1989; Lee et al., 1999; Brzeska et al., 2001)

Dictyostelium discoideum	MyoA to MyoC (1), MyoD (2), MyoE to MyoF (3) and MyoK(3)	CAM (MyoA) LCs (others)	(Côté et al., 1985; De la Roche et al., 2002; Crawley et al., 2006; Soldati, 2003)
Saccharomyces cerevisiae	Myo3p and Myo5p	CAM	(Goodson & Spudich, 1995; Goodson et al., 1996;)
Aspergillus nidulans	myoA	CAM	(McGoldrick et al., 1995; Joseph & Means, 2002)
Caenorhabditis elegans	HUM-1 and HUM-5	N/I	(Shaye & Greenwald, 2011; Kim et al., 2018)
Drosophila melanogaster	Myo31DF or myosin1-A(2), Myo61F or myosin1-B (3) and myosin-1C (2)	N/I	(Morgan et al., 1994; Morgan et al., 1995; Tzolovsky et al., 2002)
Homo Sapiens	MYO1A(3), MYO1B (6), MYO1C (3, MYO1D(2), MYO1E-F(1), MYO1G (3) and MYO1H (2)	CAM	(Halsall & Hammer, 1990; Ruppert et al., 1993; Gillespie et al., 2001; Navinés-Ferrer & Martín, 2020)

Table 1.1 Myosins I expressed in several organisms. Table indicates the organism in which myosin I is found (first column), the protein names and the number of IQ-domains in each myosin (second column), the type of protein that binds to the IQ domains (third column) and the references in which this information can be found (fourth column). N/I: non-identified.

Myosins from class I are regulated by phosphorylation and Ca^{2+}. *In vitro*, the ATPase activity and motility of the *Acanthamoeba* myosin I and *D. discoideum* MyoA, MyoD and MyoE depends on the phosphorylation of a single serine or threonine residue in the HC (Albanesi et al., 1985; Brzeska et al., 1989; Brzeska et al., 1996; Zot et al., 1992). Vertebrate myosins

I, like other myosins, follow the TEDS rule. meaning that around 16 amino acids upstream of a highly conserved DALAK amino acid sequence in the head domains they have either a threonine, a glutamate, an aspartate or a serine (TEDS site). Phosphorylation at the TEDS site regulates different myosins and regulates the phosphate-release step, which is the limiting step of the ATPase cycle (Albanesi et al., 1983; Albanesi et al., 1985; Côté et al., 1985; Lee & Côté, 1993; Ostap & Pollard, 1996; Attanapola et al., 2009; Figure 1.8). Phosphorylation by myosin I HC kinase (MIHCK) at the TEDS site leads to maximal ATPase activity (Brzeska et al., 1989; Lynch et al., 1989; Brzeska et al., 1999; Fujita-Becker et al., 2005). MIHCK is a PAK, which is activated by RAC and CDC42 in the presence of acidic lipids at the cellular membranes (Brzeska et al., 1999). Not all class I myosins are phosphorylated, for example *D. discoideum,* MyoA and MyoC are not phosphorylated by PAK (Crawley et al., 2006). In contrast to the lower eukaryotic myosins I, vertebrate class I myosins are regulated by Ca^{2+} binding (Williams & Coluccio, 1994; Zhu et al., 1998; Cyr et al., 2002). In the presence of Ca^{2+}, myosin I does not translocate F-actin *in vitro*, but the addition of exogenous CAM restores the motility, suggesting that Ca^{2+} dissociates CAM from the HC (Williams & Coluccio, 1994; Zhu et al., 1996). In the presence of Ca^{2+}, when motility is inhibited, the ATPase activity increases (Williams & Coluccio, 1994; Zhu et al., 1996) due to an increase in ADP release (Coluccio & Geeves, 1999). Electron micrographs of purified MYO1A suggest a substantial reorganization of the tail region of MYO1A in the presence of Ca^{2+} (Whittaker & Milligan, 1997), indicating that, similar to myosin II (Rayment et al., 1993), CAM stabilizes the neck so that it can act as a lever arm (Whittaker & Milligan, 1997).

Vertebrate myosins I are localized in microvillar membranes, membrane-bound vesicles in the cytoplasm, and leading edge of cells (Matsudaira & Burgess, 1979; Fath et al., 1994). The first myosin I found in higher eukaryotic cells was MYO1A, which localizes at the intestinal epithelial microvilli (Mukherjee & Staehelin, 1971; Mooseker & Tilney, 1975). Vertebrate myosins from class I are thought to regulate plasma membrane tension due to their role in maintaining adhesion between the plasma membrane and the cytoskeleton. MYO1C, specifically, is localized to the stereocilia membrane in the hair cells of the inner ear (Gillespie et al., 1993; Garcia et al., 1998). Studies with optical tweezers in fibroblasts showed that MYO1A, MYO1B, MYO1C, MYO1D, or myosin IE (MYO1E) overexpression causes an increase in the force required to pull an artificial tether from the plasma membrane (Nambiar et al., 2009). In MYO1A knockout mice the intestinal epithelial cells display a decreased attachment between the plasma membrane and the actin cytoskeleton that results in membrane herniation (Tyska et al., 2005). In lymphatic cells, myosin IG (MYO1G) depletion results in decreased membrane tension which impairs cell migration, cell

adhesion, phagocytosis and endocytosis (Gérard et al., 2014; López-Ortega et al., 2016). MYO1C, MYO1D and MYO1E maintain cell-cell adhesion at adherens junctions (Spéder et al., 2006; Petzoldt et al., 2012; Oh et al., 2013; Tokuo & Coluccio, 2013; Hegan et al., 2015). In addition, MYO1E is important for normal structure and function of the focal adhesions (Bi et al., 2013). In kidney epithelial cells, MYO1C co-localizes with E-cadherin at cell–cell contacts where it regulates the stability of cell junctions (Tokuo & Coluccio, 2013). MYO1E localizes and regulates the specialized junctions of kidney podocyte cells (Mele et al., 2011; Bi et al., 2013). In lamellipodia, MYO1E localizes at actin polymerization and adhesion sites, where it regulates adhesion and actin dynamics through localization of actin binding partners, like formins (Stöffler et al., 1998; Gupta et al., 2013). MYO1A, MYO1C, MYO1D and MYO1E also regulate F-actin architecture: intestinal microvilli length depends on actin filaments and MYO1A knockdown mice show microvilli of irregular length (Tyska et al., 2005); in the neuronal growth cone and in lymphocytes B, MYO1C directly regulates F-actin architecture (Wang et al., 2003; Maravillas-Montero et al., 2011) and in migrating epithelial cells it facilitates G-actin transport to the leading edge (Fan et al., 2012). MYO1D localizes to tips of intestinal microvilli where it influences the length of actin filaments (Benesh et al., 2010). In clathrin-mediated endocytosis MYO1E recruits actin polymerization and the endocytosis machinery (Cheng et al., 2012; Krendel et al., 2007).

In addition, MYO1A, MYO1B, MYO1C, and MYO1G are important for exocytosis, endocytosis, intracellular membrane trafficking and nuclear organization. MYO1C is required for the exocitosis of several proteins (Nakamori et al., 2006; Arif et al., 2011; Tiwari et al., 2013), and it is involved in the recycling of lipid raft cargo towards the plasma membrane (Brandstaetter et al., 2012). MYO1C isoforms have been described to localize to the nucleus where they interact with RNA polymerase I and II and regulate the signalling to enhance long-range chromosomal movement or it is specifically involved in transcription initiation (Pestic-Dragovich et al., 2000; Philimonenko et al., 2004; Kyselá et al., 2005; Percipalle & Farrants, 2006; Chuang et al., 2006). MYO1B localizes to endosomes and lysosomes (Salas-Cortes et al., 2005; Almeida et al., 2011). In rat alveolar type II cells, MYO1B and MYO1C are important for the compression of the actin coat of secretory granules in order to extrude surfactant secretions (Kittelberger et al., 2016). Depletion of MYO1B in these cells increases actin compression rates, while MYO1C depletion decreases the compression rate, indicating opposite roles during compression. MYO1E and MYO1G, but not MYO1F have been described to be important for phagocytosis and phagosome closure (Swanson et al., 1999; Kim et al., 2006; Dart et al., 2012)

MYO1B and MYO1C also act as molecular anchors. In response to insulin stimulation, MYO1C facilitates the anchoring of vesicles containing glucose transporter type 4 (GLUT4) at the plasma membrane. GLUT4 is an insulin-regulated glucose transporter that is responsible for glucose uptake into adipocytes and muscle cells (Bose et al., 2002; Boguslavsky et al., 2012). In kidney cells, MYO1B anchors amino acid transporters to the plasma membrane to facilitate neutral amino acid transport across the membrane (Komaba & Coluccio, 2015).

In *D. melanogaster,* unconventional myosin ID (Myo31DF), the MYO1D homologue, localizes at the adherens junctions, where it binds to both armadillo/β-catenin and DE-cadherin (Spéder et al., 2006; Petzoldt et al., 2012). Myo31DF antagonizes Myo61F, the MYO1C homologue, in order to maintain visceral asymmetry (Spéder et al., 2006; Petzoldt et al., 2012).

During *C. elegans* embryonic development, axons travel considerable distances to reach their final targets. A screen in *C. elegans* which aimed to find genes involved in axon guidance revealed that animals depleted of Heavy chain Unconventional Myosin 5 (HUM-5), had fewer motor neurons reaching the dorsal cord (Schmitz et al., 2007). Other defects like embryonic lethality or animal sterility were not detected (Kamath, 2003; Sönnichsen et al., 2005)

In both *Acanthamoeba* and *D. discoideum*, myosin I localizes at the leading edge of cells and in phagocytic cups (Fukui et al., 1989; Yonemura & Pollard, 1992; Baines et al., 1992).

Myosin I mutations are associated with deafness in humans. Mutations in MYO1A were found in patients with non-syndromic hearing loss (Donaudy et al., 2003; Kwon et al., 2014). Mutations in MYO1C and MYO1F that are likely to affect ATPase activity were found in patients with bilateral sensorineural hearing loss (Zadro et al., 2009).

1.6.2 Class V

Class V myosins were first purified in the 1990s (Larson et al., 1990; Espindola et al., 1992; Espreafico et al., 1992) and are responsible for transporting organelles and cellular cargos along F-actin. While myosin V drives the long-range actin-based movement of cargo to the plasma membrane, myosin VI moves vesicles for short distances (reviewed in Sweeney & Houdusse, 2007). Myosin V is mainly associated with actin and the plasma membrane which

reflects its functions in many cellular processes such as translocation and anchorage of vacuoles, Golgi, peroxisomes, mitochondria and vesicle transport in many different cells, spindle pole alignment though indirect association with the microtubules, and gene regulation and transcription.

The myosin V has a motor domain, a neck with six IQ motifs that bind CAM or LCs (Table 1.2), and a tail comprising an extended coiled-coil region that allows for dimerization. A globular tail domain (GTD), at the end of the tail is involved in cargo transport (Figure 1.13). The myosin V motor domain structure is similar to that in other myosin classes but the cleft between the upper and lower 50-kDa domains (Figure 1.7) is narrower, which favors strong actin binding (Coureux et al., 2003; Coureux et al., 2004).

Figure 1.13 Schematic showing myosin V structure. Motor domains are in blue, IQ domains are in black. Several regions in the tail domains include: Five coiled-coil domains, CC; a DLC, presumptive dynein LC binding domain, and a GTD at the end of the C-terminus (Figure adapted from (Krendel & Mooseker, 2005); used under permission)

Myosin V is a high duty-ratio motor, meaning that it spends a long time in the actin-bound state (Yengo et al., 2002; Yengo & Sweeney, 2004). Vertebrate myosin Va is a processive motor and single fluorescently-labelled molecules of myosin Va can be observed moving processively on F-actin using total internal reflection fluorescence (TIRF) microscopy (Yildiz et al., 2003; Warshaw et al., 2005; Lu et al., 2006). Conversely, *D. melanogaster* myosin V (Toth et al., 2005), and the two myosins V from *S. cerevisiae* are not able to move on F-actin in a processive manner (Reck-Peterson et al., 2001). It has been suggested that myosin V moves in a “hand-over-hand” manner. By tracking the two heads with different dyes, the myosin heads can switch positions while taking 72-nm steps (Churchman et al., 2005; Warshaw et al., 2005). While many cargoes and cargo-receptors have been identified, the mechanism of how myosin V attaches and detaches from cargoes is poorly understood.

Organism	myosin V proteins (number of IQ domains)	LCs/proteins binding to IQ domains	References
Dictyostelium discoideum	Myo5A(former MyoH, 6), Myo5B (former MyoJ, 6)	CAM LCs	(Zhu & Clarke, 1992; Cheney & Mooseker, 1992; Peterson et al., 1996; Kollmar, 2006; Jung et al., 2009)
Saccharomyces cerevisiae	Myo2p(6) and Myo4p(6)	CAM LCs	(Brockerhoff et al., 1994; Schott et al., 2002; Lipatova et al., 2008; Altmann et al., 2008)
Aspergillus nidulans	myoE (6)	CAM	(Taheri-Talesh et al., 2012);
Caenorhabditis elegans	HUM-2 (6)	N/I	(Baker & Titus, 1997)
Drosophila melanogaster	DmV or Didum(6)	CAM LCs	(Bonafé & Sellers, 1998; Tóth et al., 2005)
Homo Sapiens	MYO5A, MYO5B and MYO5C (6)	CAM LCs	(Coelho & Larson, 1993; Hasson & Mooseker, 1996; Rodriguez & Cheney, 2002; Trybus, 2008)

Table 1.2 Myosins V expressed in several organisms. Table indicates the organisms in which myosin V is found (first column), the protein names and the number of IQ domains in each myosin (second column), the type of protein that binds to the IQ domains (third column) and the references in which the information was obtained (fourth column). N/I: non-identified.

Myosin V can be regulated by Ca^{2+} and by binding-cargo. Increased Ca^{2+} levels modulate myosin Va conformation and regulate the ATPase activity (Li & Cui, 2004; Wang & Pesacreta, 2004). Electron microscopy shows that in the presence of high levels of Ca^{2+}, myosin Va has an open conformation and, when Ca^{2+} levels are low, myosin Va has a folded and inactive conformation. Interestingly, Ca^{2+} inhibits myosin Va motility on actin, leading to

shorter runs, probably due to the dissociation of the CAMs from the neck, which compromises the ability of the neck to remain stiff (Lu et al., 2006; Nguyen & Higuchi, 2005).

Cargo receptor binding to the GTD activates myosin Va by disrupting the head-tail interaction (Li et al., 2005). In order to transport different types of cargos in the same cell, there are cargo-specific receptors that link a specific cargo to a specific myosin V. In addition, regulation may be achieved by cargo-binding to its GTD (Cheney et al., 1993). Point mutations in this domain in the yeast Myo2p disrupt vacuole movement, but not secretory-vesicle movement (Catlett & Weisman, 1998; Schott et al., 1999; Catlett et al., 2000). Fluorescently tagged GTD colocalizes with centrosomes and melanosomes, suggesting that this domain could be the only region required to bind myosin V to cargoes (Espreafico et al., 1998).

In *S. cerevisiae*, cells expressing mutated Myo2p fail to bud and are abnormally large (Johnston et al., 1991) due to defects in the polarized movement of secretory vesicles to the bud (Govindan et al., 1995). Myo2p cargos include vacuoles, Golgi, peroxisomes, and mitochondria (Catlett & Weisman, 1998; Rossanese et al., 2001; Itoh et al., 2002; Fagarasanu et al., 2006). Myosins V can also interact with microtubules. In yeast, mitotic spindle positioning is achieved through binding of Myo2p in the cell cortex to the plus ends of microtubules via Bim1p, and Kar9p (Yin et al., 2000).

D. melanogaster myosin V, Didum, is expressed in most tissues and is essential for normal larvae development and spermatid differentiation (Mermall et al., 2005). Mutants lacking Didum do not display problems during embryogenesis and larvae do not show major cytologic defects, but their development is delayed. Few animals reach adulthood and males are infertile. During spermatogenesis, Didum is associated with membranes, microtubules, and actin structures required for spermatid maturation. In Didum mutants, the late steps of spermatogenesis are abnormal, actin levels in the spermatids are low, and their structure is disrupted (Mermall et al., 2005).

Mouse knockouts of myosin Va display neurological defects and die within a few weeks of birth because the distribution of the endoplasmic reticulum in the cerebellar Purkinje cells is disrupted. In these neuron cells, the endoplasmic reticulum stores Ca^{2+} that is essential for proper synaptic transmission (Takagishi et al., 2005). Mammalian myosin Va transport melanosomes, smooth endoplasmic reticulum, centrosomes and vesicles (Lalli et al., 2003; Rosé et al., 2003Varadi et al., 2005; Ivarsson et al., 2005). Myosin Vb recycles proteins from the plasma membrane and endosomal compartments (Wakabayashi et al., 2005; Nedvetsky et al., 2007; Swiatecka-Urban et al., 2007). Myosin Va and Vb can transport the same type

of cargos in different cellular contexts (Lapierre et al., 2001; Takagishi et al., 2005). Myosin Vc is mostly expressed in epithelial cells where it transports transferrin receptors (Rodriguez & Cheney, 2002). Myosin Va binds and targets the microtubule-associated protein RP/EB family member 1 (EB1- the human orthologue of Bim1p) to the plus ends of microtubules (Wu et al., 2005).

Interestingly, myosin Va is found in nuclear speckles (Pranchevicius et al., 2008), which are nuclear domains enriched in pre-mRNA splicing factors that facilitate integrated regulation of gene expression (Galganski et al., 2017), indicating that myosin Va can be involved in gene expression regulation. Myosin Va is described to interact with viral capsid proteins (Roberts & Baines, 2011) and It has been proposed that myosin V moves viruses along nuclear actin filaments (Roberts & Baines, 2011). Myosin Vb localizes at the cell nucleoli where it interacts with actin and RNA polymerase I, suggesting a role during transcription (Lindsay & McCaffrey, 2009).

To this date, the function or localization of the *C. elegans* Heavy chain Unconventional Myosin 2 (HUM-2), the myosin V homologue, is not known. HUM-2 depletion does not lead to embryonic lethality, worm sterility or other major defects in the animal (Kamath, 2003; Sönnichsen et al., 2005)

In *S. cerevisiae*, myosin V Myo4p, is required for the correct localization of several mRNAs (Shepard et al., 2003)

Mutations in myosin V are associated with disease. Mutations in myosin VA (MYO5A) are found in humans with the Griscelli syndrome, which is a rare autosomal recessive disorder characterized by the loss of hair and skin pigmentation. Mutated MYO5A does not correctly transport melanosomes that produce melanin, the pigment of skin and hair (Van Gele et al., 2009). Mutations in myosin VB (MYO5B) are associated with microvillus inclusion disease, which affects the intestine enterocytes. These cells usually have microvilli on the surface that are important for food absorption. Patients with mutations on MYO5B do not have microvilli and instead present intracellular vacuolar structures containing microvilli. Mutated MYO5B is not able to transport transferrin receptors in intestinal enterocytes suggesting that the trafficking of apical and basolateral proteins by MYO5B is impaired (Müller et al., 2008).

1.6.3 Class VI

Myosin VI was first identified in *D. melanogaster* and it is ubiquitously expressed in multicellular organisms. It is not expressed in unicellular species such as yeast (Brown, 1997). This is the only class of myosins described so far that moves towards the minus end of F-actin (Kellerman & Miller, 1992; Hasson & Mooseker, 1994; Wells et al., 1999; Kelleher et al., 2000). Myosin VI functions involve the maintenance of the stereocilia in the inner, regulation of spermatogenesis, oogenesis, cell division and cell motility. It is also involved in endocytosis, and membrane trafficking.

Myosin VI comprises a motor domain, a short neck with a single CAM-binding IQ domain, and a tail with a C-terminal cargo-binding region (Hasson & Mooseker, 1994, Figure 1.14).

Figure 1.14 Schematic showing myosin VI structure as a monomer or dimer. The motor domains are in blue with an insert in light blue, IQ domains are in black. Colored boxes in the second half of the protein (tail) represent different regions: a single coiled-coil (CC) domain in green, and a cargo-binding domain in grey (Figure adapted from ((Krendel & Mooseker, 2005); used under permission).

The minus-end directed movement of myosin VI motors is determined by a unique insert in the converter subdomain that contains a CAM-binding motif (Bahloul et al., 2004; Park et al., 2007; Bryant et al., 2007). The removal of this insert causes myosin VI to move towards the plus end of F-actin (Park et al., 2007; Bryant et al., 2007), indicating that the movement direction solely depends on the insert. In the actin-binding domain, myosin VI contains a hypertrophic cardiomyopathy (HCM) loop that obeys the TEDS rule for phosphorylation sites (Bement & Mooseker, 1995), suggesting that myosin VI is phosphorylated in the head domain. The cargo-binding region is composed of two domains, a site for the binding of cargo-partners and a region that binds PIP2 (Spudich et al., 2007). The binding to lipids contributes to the recruitment of myosin VI to clathrin-coated vesicles (Spudich et al., 2007).

Kinetic studies on myosin VI have used artificially induced dimerization through specific inserts on myosin sequence, like leucine zippers (Morris et al., 2003; Robblee et al., 2004). These artificial dimers have a high duty ratio and move processively along F-actin (Rock et al., 2001; Yildiz et al., 2004). Like myosin V, dimerized myosin VI moves along F-actin in a

hand-over-hand fashion with a step size of 30 nm (Yildiz et al., 2004; Ökten et al., 2004). Monomeric myosin VI coupled to polystyrene beads can also walk on F-actin (Iwaki et al., 2006), but only for short distances. However, longer distances are achieved when multiple monomers move a single bead (Sweeney & Houdusse, 2007; O'Connell et al., 2007).

The number of myosins VI expressed differ between species (Table 1.3), and within the same organism myosin VI expression is tissue-specific.

Organism	myosin VI proteins (number of IQ domains)	LCs/proteins binding to IQ domains	References
Caenorhabditis elegans	SPE-15 or HUM-3, HUM-8 (1)	N/I	(Baker & Titus, 1997)
Drosophila melanogaster	Jaguar or 95F (1)	CAM LCs	(Kellerman & Miller, 1992; Frank et al., 2006)
Homo Sapiens	MYO6 (1)	CAM LCs	(Bahloul et al., 2004; Ménétrey et al., 2005)

Table 1.3 Myosins VI expressed in several organisms. Table indicates the organisms in which myosin VI is found (first column), the protein names and the number of IQ domains in each myosin (second column), the type of protein that binds to the IQ- domains (third column) and the references in which the information can be found(fourth column). N/I: non-identified.

Myosin VI can be regulated by phosphorylation in both motor and tail domains. The phosphorylation by PAK kinases occurs at the TEDS site in the head domain (Bement & Mooseker, 1995). The phosphorylation does not alter the ATPase activity or the F-actin sliding rate *in vitro* (De La Cruz et al., 2001; Yoshimura et al., 2001; Morris et al., 2003) but *in vivo* it may regulate the interaction with F-actin (Buss et al., 1998; Naccache & Hasson, 2006). In this sense, expression of a myosin VI phosphomimetic mutant, in which threonine 406 was substituted by a glutamate, leads to the accumulation of vesicle clusters at distinct peripheral sites of retinal pigment epithelial (ARPE-19) cells. Increased levels of F-actin at the vesicle cluster sites due to reduced actin depolymerization are also observed (Naccache & Hasson, 2006). Phosphorylation in the tail by PAK modulates optineurin binding to myosin

VI tail, which is important for exocytosis and Golgi organization (Sahlender et al., 2005). The binding of myosin VI to other known partners also requires phosphorylation at this site. The myosin VI binding to the other partners occur via specific motifs to the cargo-binding domain (Morris, 2002; Arden et al., 2007). Myosin VI function is also regulated by Ca^{2+} levels. CAM can bind to the single IQ domain and to the insert in the converter region. Increased levels in Ca^{2+} reduce both the rate of ADP release and F-actin translocation. Myosin VI dimer processive movement also decreases in the presence of higher levels of Ca^{2+} (Morris et al., 2003). The myosin VI tail changes its conformation in the presence of $Ca^{2+}$and binds to liposomes containing PIP2 (Spudich et al., 2007). PIP2 localization at the active sites of endocytosis recruits myosin VI during clathrin-coated structures assembly (Cremona & De Camilli, 2001; Di Paolo & De Camilli, 2006).

D. melanogaster myosin VI, Jaguar, is broadly expressed during development and in the adult fly and is required for oogenesis, cell motility, asymmetric cell division, spermatogenesis (Kellerman & Miller, 1992; Mermall & Miller, 1995; Hicks et al., 1999; Petritsch et al., 2003). In the syncytial blastoderm of *D. melanogaster* embryos, myosin VI is involved in the formation of pseudo-cleavage furrows, and its inhibition leads to actin cortical network disorganization, and abnormal mitotic spindles leading to chromosome missegregation (Mermall et al., 1994; Mermall & Miller, 1995). In addition, Jaguar is essential during asymmetric cell division in neuroblasts since it transports the cell fate determinant Miranda, required for the correct orientation of the mitotic spindle along the apical-basolateral axis (Petritsch et al., 2003). During spermatid individualization, Jaguar accumulates at the individualization complex, a group of cytoskeletal proteins assembled around the spermatid nuclei. This is required for spermatid enclosure by the plasma membrane during spermatid individualization. Reduction of Jaguar levels in testis leads to male sterility due to defects in membrane remodelling during spermatid individualization (Hicks et al., 1999). In the individualization complex, myosin VI is important for actin assembly at sites of membrane remodelling (Rogat & Miller, 2002). Jaguar was suggested to stabilize the branched actin network at the individualization complex as it remains bound to F-actin with a slow turnover, suggesting that Jaguar acts as a crosslinker or an actin anchor (Noguchi et al., 2006).

Mammalian cells express myosin VI at membrane protrusions of the cell, Golgi complex and in endocytic and exocytic vesicles (Buss et al., 1998; Aschenbrenner et al., 2003; Warner et al., 2003). In polarised human cells, myosin VI can be expressed as four alternative splicing isoforms which have different tail sizes: with a large insert, with a small insert, with or without

both inserts in the tail region (Buss et al., 2001). No known motifs are described in these inserts. The myosin VI isoform with the large insert is involved in clathrin-mediated endocytosis. The myosin VI isoforms with no inserts are targeted to the Golgi and endosomes where they sort and deliver specific cargo to the basolateral surface of Madin-Darby Canine Kidney (MDCK) cells (Au et al., 2007). In HeLa cells, myosin VI has a role during cytokinesis (Arden et al., 2007). Myosin VI localizes in the contractile ring and then it accumulates at higher levels in the contractile ring during abscission, the midbody ring. Myosin VI also localizes in trafficking-vesicles that go in and out of the midbody region. In these cells, perturbation of myosin VI leads to cytokinesis failure and multinucleation due to defects during abscission. Myosin VI is thought to be implicated in transcription by RNA polymerase II. Transcription is inhibited by antibodies against myosin VI (Vreugde et al., 2006). Myosin VI binds to RNA polymerase II via its cargo binding domain on the tail and to DNA through the motor domain. Myosin VI binding to RNA polymerase II and DNA is essential for transcription (Fili et al., 2017, Fili & Toseland, 2020). In response to transcription stimuli, myosin VI actively moves into the nucleus (Grosse-Berkenbusch et al., 2020). During transcription, RNA polymerase II is clustered within the nucleus in transcription active zones. Myosin VI knockdown disrupts RNA Polymerase II localization, changes chromatin organization and decreases gene expression. Altogether these results suggest that myosin VI could act as an anchor for RNA polymerase II to maintain it at the transcription sites (Zorca et al., 2015)

In *C. elegans,* the myosin VI homologue, defective spermatogenesis 15 (SPE-15), is responsible for sorting cellular components during spermatocyte formation. *Spe-15* mutants fail to segregate mitochondria, endoplasmic reticulum and Golgi to the newly formed spermatocytes (Kelleher et al., 2000). SPE-15 drives the cytokinesis that leads to spermatid separation. In addition, it acts together with NMII, NMY-2, to perform correct spermatogenesis. Simultaneous perturbation of NMY-2 and SPE-15 blocks residual body formation, a structure responsible for the storage of undesired cellular contents from the spermatids (Hu et al., 2019). Depletion of HUM-8, another myosin VI, leads to embryonic lethality and low progeny brood size (Skop et al., 2004), but its function remains unknown.

Myosin VI expression is upregulated in prostate and breast cancer, as well as in gastroesophageal and lung carcinomas (Dunn et al., 2006). Also, there is a correlation between the aggressiveness of ovarian cancers and the levels of myosin VI expression (Yoshida et al., 2004). In In human cultured ovarian cells, similar to what happens in *D. melanogaster* ovarian border cells, myosin VI binds to adhesion proteins pushing on newly

polymerized F-actin resulting in forward movement of the cell (Geisbrecht & Montell, 2002). The cell movement contributes to cell migration, which is usually increased during tumour invasion.

1.6.4 Class VII

Class VII myosins were first discovered in *D. melanogaster* (Cheney et al., 1993). These class of myosin are mainly involved in moving cargos along F-actin, and maintain the correct function of the inner ear, intestine microvilli and eye retina.

Myosins VII have a typical head domain, a neck region with four or five IQ motifs, and a long tail (Kiehart et al., 2004; Richards & Smith, 2005; Foth et al., 2006, Figure 1.15). The tail has a predicted coiled-coil domain (not present in vertebrate myosin VIIb and *C. elegans* myosin VII), followed by a myosin Tail Homology 4 domain (MyTH4), a FERM domain, and an SH3 domain. The functional relevance of MyTH4 domain is not known but this domain has been implicated in myosin X binding to microtubules (Weber et al., 2004). The FERM domain is mostly described to interact with membrane receptors (Chishti et al., 1998) but in myosin VII it can also bind directly to F-actin (Lee & Liu, 2004; Yang et al., 2009). Additionally, these domains have been shown to work together to mediate myosin binding to other proteins such as harmonin (Boëda et al., 2002), usherin (Michalski et al., 2007) and shroom2 (Etournay et al., 2007). The SH3 domain is also responsible for binding myosin VII to other proteins involved in adhesion such as protocadherin 15 (PCDH15) and kelch-like ECH-associated protein (KEAP1) (Velichkova et al., 2002; Senften et al., 2006).

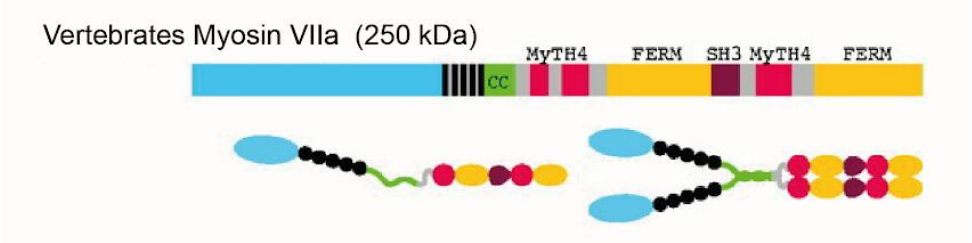

Figure 1.15 Schematic showing myosin VII structure as a monomer or a dimer. The motor domains are in blue, IQ domains are in black. Colored boxes in the tail represent different regions: a single SH3 domain in dark red; one coiled-coil (CC) domain in green; three MyTH4 domains in red, and two FERM domains in yellow (Figure adapted from (Krendel & Mooseker, 2005); used under permission).

Myosin VII has a slow ATPase cycle and high duty ratio when compared with other myosins (Udovichenko et al., 2002; Inoue & Ikebe, 2003; Yang et al., 2005; Yang et al., 2006; Watanabe, 2007). Myosins with these properties are prone to exert tension and therefore myosin VII may act as a tensor. *In vitro*, myosin VIIa moves towards the barbed end of F-actin (Inoue & Ikebe, 2003) with velocities similar to those of other myosins (Udovichenko et al., 2002; Inoue & Ikebe, 2003; Yang et al., 2006). An artificial myosin VII dimer moves processively on F-actin in a hand-over-hand mechanism, which together with its high duty ratio suggests that myosin VII is a processive motor with a step-size of 35 nm (Sato et al., 2017). However, myosin VII dimerization *in vivo* remains to be demonstrated. Most of myosins VII have a coiled-coil domain but due to its small size it is not sufficient for myosin VII dimerization (Inoue & Ikebe, 2003; Watanabe, 2007; Yang et al., 2006). Nonetheless, *in vitro* studies based on gel filtration analysis and the mobility in native gel show that myosin VII can form dimers through other domains in the tail (Inoue & Ikebe, 2003).

Myosin VII is found in vertebrates, *D. melanogaster* and *C. elegans* and mostly binds to CAM, but at least in humans myosins VII can function when bound to LCs (Table 1.4).

Organism	myosin VII proteins (number of IQ domains)	LCs/proteins binding to IQ domains	References
Caenorhabditis elegans	HUM-6 (4)	N/I	(Baker & Titus, 1997)
Drosophila melanogaster	myosinVIIa or crinkled (5), myosinVIIb (5)	CAM	(Yamashita et al., 2000; Umeki et al., 2009)
Homo Sapiens	MYO7A (5), MYO7B (5)	CAM Light Chain	(Sellers, 2000; Coluccio et al., 2008; Heissler & Manstein, 2012; Sakai et al., 2015)

Table 1.4 Myosins VII expressed in several organisms. Table indicates the organisms in which myosin VII is found (first column), the protein names and the number of IQ domains in each myosin (second column), the type of protein that binds to the IQ domains (third column), and the references in which the information was obtained (fourth column). N/I: non-identified.

Myosin VII regulation can be achieved in different manners. First, the binding to other proteins can be regulated by MYTH-4, FERM and SH3 domains (Li & Yang, 2016). Second, the tail domain is also capable of activating myosin VII. Myosin VII adopts a back-folded auto-inhibited conformation in which the tail is bound to the head domain leading to reduction of ATP consumption (Umeki et al., 2009; Sakai et al., 2015). Third, increased Mg^{2+} leads to reduced myosin VII ATPase activity *in vitro*, likely due to increased myosin affinity for ADP (Heissler & Manstein, 2011). Ca^{2+} also regulates myosin VII. Higher levels of Ca^{2+} induce a conformational change of the CAM that is bound to the distal IQ domain of myosin VII. This abolishes the interaction between the tail and the head domain leading to the open, active conformation (Umeki et al., 2009).

In mammalian, myosin VIIa is expressed in testis, kidney, lung, inner ear, retina, and the ciliated epithelium of the nasal mucosa (Hasson & Lakatos, 1998; Wolfrum et al., 1998). In MDCK cells, myosin VIIa co-localizes and binds to vezatin, a transmembrane protein of adherens junctions that associates with the cadherin-catenin complex (Kussel-Andermann, 2000). In HeLa cells it co-localizes and binds to Shroom Family Member 2 (SHROOM2), a sub-membranous protein of the cell junction (Etournay et al., 2007). It also binds to KEAP1, a sub-membranar protein present in an adhesion structure between Sertoli cells in the testis (Velichkova et al., 2002). Myosin VIIa binds to MAP2B, a microtubule-associated protein (Todorov et al., 2001). In addition, myosin VIIa binds to six proteins involved in Usher syndrome two PDZ domain-containing proteins, harmonin (USH1C) and whirlin (USH2D); a cadherin-like protein, protocadherin 15 (PCDH15/USH1F); a cytoskeleton-associated protein, sans (USH1G); and two transmembrane proteins, usherin (USH2A) and Vlgr1 (USH2C) to ensure cohesion of the stereocilia (Boëda et al., 2002; Delprat et al., 2005; Reiners et al., 2005).

Myosin VIIa is localized in the connecting cilium retinal pigment epithelium (RPE) (Hasson et al., 1995). Myosin VIIA (MYO7A) is associated with the connecting cilium membrane and the periciliary membrane (Liu et al., 1997). MYO7A mutant mice display melanosome mislocalization (Gibbs et al., 2004) and melanosomes move freely and faster (Wu et al., 1998) indicating that myosin VIIa is required for correct melanosome transport. The same mutants display mild electrophysiological defects (Libby & Steel, 2001), and a higher resistance to acute light damage (Williams & Lopes, 2011) likely due to defects in Retinoid Isomerohydrolase (RPE65) transport by MYO7A (Williams & Lopes, 2011). RPE65 is an enzyme responsible for the regeneration of the visual pigment (Jin et al., 2005). In contrast to humans, myosin VIIa-deficient mice or zebrafish do not show retinal degeneration.

Antibodies against myosin VIIb strongly label the microvilli of the intestine and kidney (Chen et al., 2001). During intestinal epithelial differentiation, adhesion complexes are responsible for organizing the microvilli. These adhesion complexes are enriched at the microvilli distal tips where they mediate the adhesion of neighbouring protrusions. Myosin VIIB (MYO7B) is also enriched at the tips of microvilli where it transports the proteins of the intermicrovillar adhesion complex and its loss results in intermicrovillar adhesion disruption (Weck et al., 2016). Myosin VII can also bind to microtubules *in vitro* (Weber et al., 2004), but whether this occurs *in vivo* remains unknown.

In *Drosophila*, myosin VIIa is expressed in embryos and throughout development in the head, thorax, and male and female abdomens (Kiehart et al., 2004). Perturbation of myosin VIIa (*crinkled* mutants) is lethal. Few mutant flies develop until adulthood (due to maternal load of myosin VIIa) but they are infertile and have reduced lifespan. Hair and bristle shape are defective, and they have impaired hearing since the auditory organ is incorrectly organized (Todi et al., 2005).

In *C. elegans,* no function for heavy chain unconventional myosin 6 (HUM-6), the myosin VII homologue, is described. Animals depleted of HUM-6 are not sterile, the embryos develop until adulthood without major defects (Kamath, 2003; Sönnichsen et al., 2005).

Loss-of-function mutations in human MYO7A cause Usher syndrome type I, which leads to deafness and blindness (Weil et al., 1996; Weil et al., 1997; El-Amraoui & Petit, 2005). Myosin VII is essential for proper vision and hearing in humans. However, it localizes in other human epithelial cells where its function is unknown.

1.6.5 Class IX

Class IX myosins were first found in mammals (Bement et al., 1994; Reinhard et al., 1995), and have only been described in animals so far. They are involved in many processes such as vesicular membrane trafficking, cell shape, cell adhesion and migration.

They have a typical myosin structure with two distinctive features: a N-terminal extension and an insert within the head domain that is thought to be involved in the actin interaction (Schröder et al., 1993). Depending on the organism, myosin IX can have from four to six IQ domains. The long-tail region does not have coiled-coil propensity, suggesting this is a single-headed myosin (Reinhard et al., 1995; Inoue et al., 2002; Post et al., 2002). The tail regions include two domains that are not usually found in the myosin family, a C1 domain

(Zn^{2+} binding motif) and a RHOA GAP domain (Figure 1.16). The C1 domains of other proteins, like the Rac-specific GAP, interact with lipids (Canagarajah et al., 2004), however its function in myosin IX molecule remains unclear. The RHOA GAP domain in the tail interacts with RHOA GTPase both *in vitro* and *in vivo* and leads to RHOA inactivation (Reinhard et al., 1995; Muller et al., 1997).

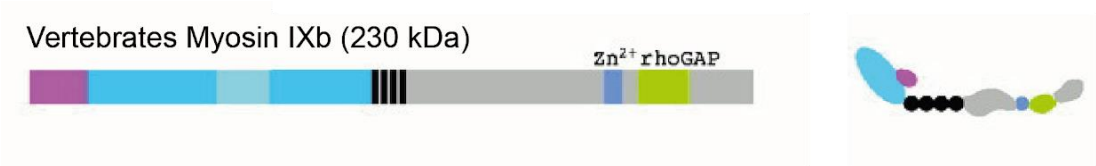

Figure 1.16 Schematic showing myosin IX structure. The motor domain is blue with an insert in light blue. The IQ domains are in black; the extension in the head is pink. Colored boxes in the tail domains represent different regions: a Zn^{2+}binding domain in blue on the tail and a RHOA GAP domain in green (Figure adapted from (Krendel & Mooseker, 2005); used under permission)

Myosin IX is a slow motor myosin with a step-size of 16 nm (Post et al., 1998, Post et al., 2002; Inoue et al., 2002; O'Connell & Mooseker, 2003; Nalavadi et al., 2005; Xie, 2010). Myosin IXB (MYO9B) is the only myosin in which ATP-hydrolysis is the rate-limiting step of the ATPase cycle (Nalavadi et al., 2005; Kambara & Ikebe, 2006). MYO9B spends a long time bound to ATP, which generally would lead to weak affinity for actin. However, MYO9B has higher affinity for actin in the ATP-bound state. An *in vitro* study suggests that two ATP-bound MYO9B populations may exist. One population has high-affinity, and it is bound to actin, and the other is free. These populations can interconvert, but the mechanism is unknown (Nalavadi et al., 2005). Truncated recombinant MYO9B without the C1 and GAP domains moves towards the minus end of F-actin (Inoue et al., 2002), suggesting that these domains are essential for determining movement directionality.

Myosin IX is found in vertebrates and in *C. elegans* (Table 1.5). Interestingly, myosin IX is not found in *D. melanogaster* (Odronitz & Kollmar, 2007).

Organism	myosin Ix proteins (number of IQ domains)	LCs/proteins binding to IQ domains	References

Caenorhabditis elegans	HUM-7	N/I	(Wallace et al., 2018)
Homo Sapiens	MYO9A or MYR7 and MYO9B or MYR5	CAM	(Post et al., 1998; Liao et al., 2010)

Table 1.5 Myosins IX expressed in several organisms. Table indicates the organism in which myosin IX is found (first column), the protein names and the number of IQ domains in each myosin (second column), the type of protein that binds to IQ domains (third column) and the references in which this information was obtained (fourth column). N/I: non-identified.

Myosin IX is regulated by CAM (Reinhard et al., 1995; Post et al., 1998). In addition, it has been suggested that an intramolecular interaction between the head and the tail can also regulate MYO9B (Nalavadi et al., 2005; Kambara & Ikebe, 2006; Van den Boom et al., 2007). Kinases regulate myosin IX. MYO9B phosphorylation by protein C kinase occurs *in vitro*, and a phosphoproteome analysis of HeLa cells revealed that MYO9A and MYO9B are phosphorylated on the tail domain (Reinhard et al., 1995; Chieregatti & Bahler, 1996; Olsen et al., 2006).

Vertebrate myosin IX is expressed in multiple tissues (Reinhard et al., 1995; Wirth et al., 1996; Omelchenko & Hall, 2012; Gorman et al., 1999). MYO9B modulates the activity of RHOA, RHOB, and RHOC *in vitro* (Graf et al., 2000). Myosin IXA (MYO9A) is expressed in maturing ependymal epithelial cells in the brain, and Myo9A knock-out mice display irregular epithelial cell morphology and disrupted organization of intercellular junctions in the brain. In the same study, Caco-2 cells depleted of MYO9A show increased RHOA-signalling and have defects in differentiation, cell morphology and cell junction assembly (Abouhamed et al., 2009). MYO9A depletion also leads to actin cytoskeleton disorganization and adhesion disruption of bronchial epithelial cells which culminates in cell scattering (Omelchenko & Alan, 2012). In these cells, MYO9A regulates the formation of cell junction-associated actin bundles during the initial cell-cell contact. The expression of the RHOA GAP domain partially rescued the cell scattering phenotype indicating that in cell junctions, RHOA must be inactive.

In melanoma cells, MYO9B accumulates in regions with high F-actin turnover such as lamellipodia, membrane ruffles, and filopodia and this localization depends on the motor

domain of MYO9B (Van den Boom et al., 2007). In mouse macrophages, myosin IX has a role in cell shape and motility. Macrophages lacking MYO9B have a contracted shape and do not spread or polarize. This occurs due to an increase of active RHOA and RLC phosphorylation. The defects in the shape can be rescued with the addition of Rho inhibitors. Macrophages lacking MYO9B move slowly, and the addition of a RHO inhibitor restores motility. These cells do not present the large sheet-like membrane protrusions characteristic of lamellipodia. In addition, actin levels are lower when MYO9B is perturbed (Van den Boom et al., 2007).

In *C. elegans*, like in other systems, heavy chain unconventional myosin 7 (HUM-7) was shown to act as a RHOA GAP (Wallace et al., 2018) and it localizes in the muscles and in the adjacent cells of nerve axons, possibly glia. HUM-7 is required for normal neuronal migration. A null *hum-7* mutant produces a small percentage of dead embryos that have problems during morphogenesis. Some embryos display a 'gut on the exterior' (Gex) phenotype, which is usually associated with epidermal ventral migration failure, and some embryos are arrested during development, indicating problems during elongation. The use of ectopic HUM-7 expression in embryonic epithelial cells allowed to show that HUM-7 can regulate actin dynamics. In these embryos, depletion of HUM-7 increases actin levels and the cells exhibit more protrusions than controls. Additionally, NMY-2 levels in embryonic epidermal cells are increased after HUM-7 depletion, which suggests that HUM-7 can also regulate NMII via RHOA inactivation (Wallace et al., 2018).

Myosin IX perturbation is associated with disease. Knockout of MYO9A leads to severe hydrocephalus in mice (Abouhamed et al., 2009). A mutated MYO9B increases the risk of coeliac disease (Monsuur et al., 2005) and MYO9B overexpression is observed in type I diabetes patients that also present increased intestinal permeability (Sapone et al., 2006).

1.6.6 Class XII

Class XII myosins have so far only been described in *nematodes* (Baker & Titus, 1997; Figure 1.17). Hum-4 is the only *C. elegans* gene encoding eight isoforms of this myosin XII (Sellers, 2000). Heavy chain unconventional myosin 4 (HUM-4) contains regions for binding ATP and actin, but they are more divergent from those in other classes, suggesting different biochemical properties. The N-terminus has a large extension (~150 amino acid) due to two insertions in the head domain (248 to 259 and 301 to 332 amino-acids positions, respectively) that are not found in other myosins. The second insert might change the activity

of this motor due to its proximity to the P-loop. The neck contains two IQ motifs. The tail has two MyTH4 domains, with unknown function. There are no mutants or relevant studies concerning HUM-4 function, kinetics, or localization. However, large RNAi screens revealed that its depletion does not cause embryonic lethality, worm sterility nor visible defects in animal morphology (Maeda et al., 2001; Kamath, 2003; Sönnichsen et al., 2005).

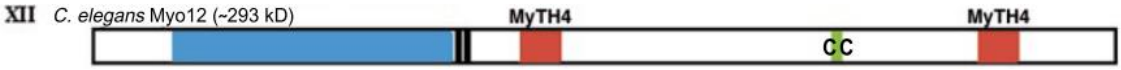

Figure 1.17 Schematic shows myosin XII structure. The motor domain is blue, IQ domains are in black. Colored boxes in the tail domains represent different regions: a single coiled-coil domain in green (CC) and two MyTH4 domains in red (Figure adapted from (Mermall et al., 1998); used under permission).

1.7 Caenorhabditis elegans

1.7.1 Model of study

C. elegans became a model organism in the 1960s, in the hands of Sydney Brenner and colleagues. Since then, this model organism has been used in several areas of research, such as genomics, cell biology, neuroscience, and aging. It was the first multicellular organism to have its whole genome sequenced, and the many similarities between the cellular and molecular processes in *C. elegans* and other animals make it a major model organism in biology. *C. elegans* is a small and transparent nematode that lives in temperate soil environments and subsists by feeding on bacteria. In the laboratory setting it can be easily grown using inexpensive agar plates and *E. coli* as food source. Other advantages that justify its use are its short life cycle (Figure 1.18), compact genome and an eutelic animal. *C. elegans* genome is completely sequenced and most of its genes have human homologues, thus, gene mutations associated with disease can be easily studied in *C. elegans* (*C. elegans* Sequencing Consortium, 1998; Kaletta & Hengartner, 2006). *C. elegans* mostly exists as hermaphrodites but can also exist as males. Males arise rarely in the natural population (0.1%) by spontaneous nondisjunction of chromosome X during meiosis of the hermaphrodite germline. However, through mating of males and hermaphrodites, a higher frequency of male progeny can be achieved (up to 50%). Genetic crosses using *C. elegans* are straightforward. Mating between hermaphrodites and males with different genetic backgrounds can be used to generate new strains. Strains can be kept

as frozen stocks at -80 ªC for long periods of time. In the absence of food *C. elegans* can switch to a dauer larval stage that can survive for months (Cassada & Russell, 1975). Despite its simple anatomy, the animal displays many complex behaviors such as locomotion and egg-laying (Rankin, 2002; De Bono, 2003).

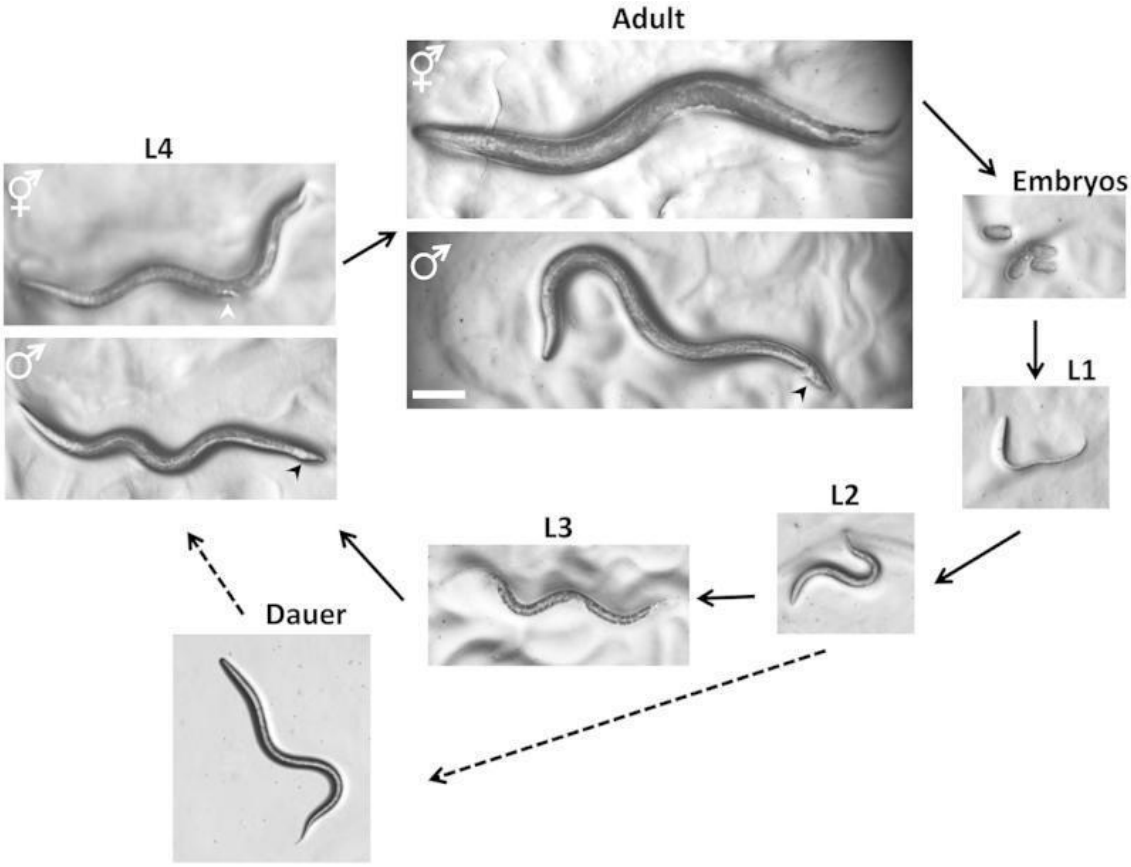

Figure 1.18 *C. elegans* Life Cycle. Animal development occurs throughout the four larval stages, but sex can only be distinguished at the L4 stage. At the L4 stage, hermaphrodites have an elongated tail and a developing vulva (white arrowhead). In adults, hermaphrodites have embryos and an elongated tail. The males have a slimmer girth than hermaphrodites and a fan-shaped tail (black arrowhead). Embryos can develop by the fertilization of oocytes by the hermaphrodite sperm or by the male sperm through mating. The dauer larvae are thinner than all the other larval stages. Bar 0.1 mm. (Figure reprinted from (Corsi et al., 2015); used under permission)

A comprehensive database, the Wormbase, includes genes, phenotypes, mutants, and strains available in *C. elegans* (*C. elegans* Sequencing Consortium, 1998; Stein et al., 2001). The RNA interference (RNAi) pathway, first discovered and characterized in *C. elegans* (Fire et al., 1998), constitutes an easy and quick way to study genes by reverse

genetics. RNAi is particularly useful in *C. elegans* embryos because of the architecture of the oocyte-producing gonad. Double-stranded RNAs (dsRNA) can be conveniently administered by injection, feeding, or soaking of animals. The introduction of dsRNA triggers the degradation of the corresponding mRNA in all tissues and the target protein already existing in the gonad is continually packed into newly formed oocytes (Figure 1.19). As a result, protein levels in fertilized embryos gradually decrease after RNA treatment. Importantly, the rate of protein depletion is mostly independent of the protein's intrinsic turnover properties, because even proteins with long half-lives are gradually diluted out from the gonad by being packaged into oocytes. Therefore, embryos with different degrees of a depleted protein can be assessed, and gradually more severe phenotypes can be characterized.

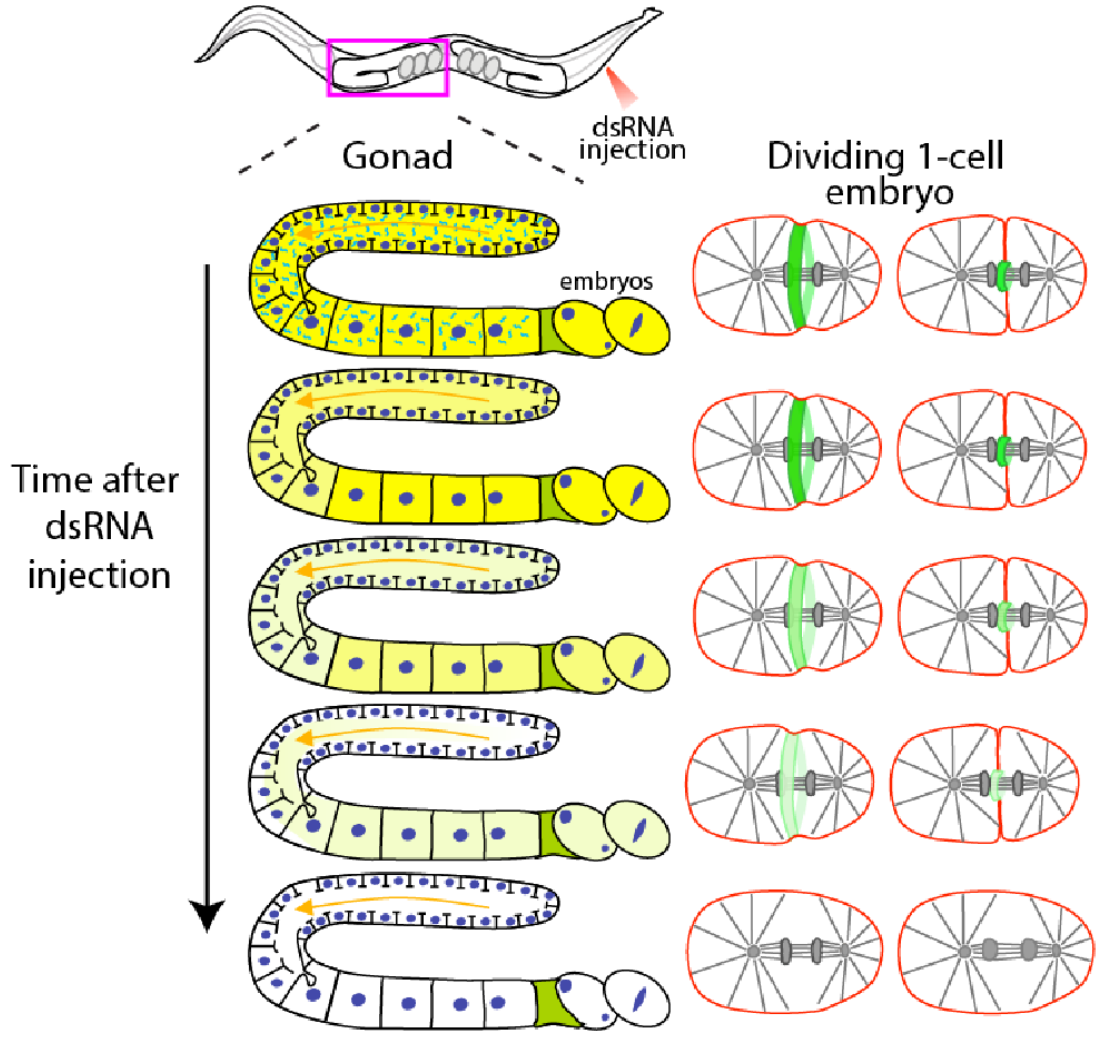

Figure 1.19 RNA interference (RNAi) in *C. elegans*. Injection of dsRNA against the gene of interest triggers the degradation of the corresponding mRNA in the gonad. Protein levels in newly fertilized embryos gradually

decrease after dsRNA injection. The decreased levels of proteins on the gonads are reflected on the embryos (Reprinted from WormBook under a Creative Commons Attribution License (CC BY 2.5.)

The use of CRISPR-CAS9 (clustered regularly interspaced short palindromic repeats-CRISPR-associated protein 9) is straightforward in *C. elegans*. This constitutes a powerful tool to directly modify the *C. elegans* genome (Hsu et al., 2014). CRISPR-Cas9 is a natural bacterial defence system against viral DNA that was adapted to genome editing in different organisms. Bacteria use DNA from invading viruses to create DNA segments known as clustered regularly interspaced short palindromic repeats (CRISPR) arrays. If infected again by the virus, the bacteria produce RNA segments from the CRISPR arrays to target the virus's DNA. Then, bacteria use CRISPR-associated protein 9 (Cas9) to cleave the viral DNA, stopping the replication of the virus. This system can be applied in model organisms to insert specific mutations, delete a domain or an entire gene, or insert fluorescent/biochemical tags. The modified genes are expressed in the natural context, resulting in more reliable results. In *C. elegans*, CRISPR-CAS9 is an alternative or complementary technique to transgenesis methods such as microparticle gene bombardment (Praitis et al., 2001) or Mos1 single-copy insertion of transgenes (Frøkjær-jensen et al., 2009).

1.7.2 Advantages of studying early embryonic cytokinesis in C. elegans

The *C. elegans* early embryo is a compelling biological system to conduct quantitative live imaging assays due to the stereotypical embryonic cell divisions, which is of great importance for the study of cell division and, more specifically, cytokinesis. A single animal lays 300 embryos, each of them having relatively large dimensions (around 50-µm length and 30 µm wide), which facilitates its observation under the microscope. Mutant or fluorescently tagged versions of a protein of interest are easily expressed in the embryo for live fluorescence imaging. Cytokinesis is stereotypical and slight defects can be easily detected. It is completed within 4-5 minutes which facilitates image acquisition with high temporal resolution. Different degrees of protein depletion can be achieved by changing the total time of RNAi treatment and at least two proteins can be depleted simultaneously. The existence of temperature sensitive mutants provides a simple manner to inactivate a protein in the desired stage of cytokinesis (Davies et al., 2014). Embryos can also be permeabilized and treated with drugs of interest at the desired moment (Carvalho et al., 2011). Moreover, in contrast to cell cultures, cellular divisions occur within a physiological context. Cultured

cells divide while adhered to a substrate, which may impose artificial constraints on cytokinesis and does not reflect the situation encountered in the context of tissue.

CHAPTER 2

AIMS

2. AIMS

Myosins are a superfamily of proteins, composed of many classes that exist within the same organism, potentially having diverse functions, cooperating or working redundantly. This thesis focuses on the study of the role of myosins during cytokinesis in the *C. elegans* one-cell embryo. Cytokinesis essentially depends on NMII, but similar to what happens in fission yeast other myosins can be involved. Moreover, recent evidence from human cells show that myosins can cooperate or compensate for one another (Beach & Hammer, 2015; Billington et al., 2015). NMY-2 is one of the three NMII in *C. elegans*, and it is known to form a complex with the RLC myosin light chain 4 (MLC-4) and ELC myosin light chain 5 (MLC-5). NMY-2, MLC-4 and MLC-5 are essential for cytokinesis to happen. However, if other myosins cooperate with or compensate for NMY-2 function during cytokinesis remains unclear.

The first aim of the thesis consisted in further exploring the importance of NMY-2 during cytokinesis and to examine whether other myosins can cooperate with NMY-2. NMY-2 roles during cytokinesis were characterized by taking advantage of a temperature-sensitive mutant and progressive depletion by RNAi. Several other myosins were individually depleted, and their importance for embryo viability and animal brood size was assessed. To explore if other myosins can cooperate with NMY-2, individual myosins were depleted in an NMY-2 sensitized background. The second aim of this thesis was to investigate the importance of NMY-2 motor activity during cytokinesis. It is widely considered that contractile ring contraction depends on the motor ability of NMII to translocate F-actin. However, alternative views exist, where NMII acts as a passive crosslinker, and actin filament depolymerization leads to network contraction. It has also been described that COS-7 cells and mouse cardiomyocytes null for NMIIB fail cytokinesis and this phenotype can be rescued by the expression of a motor-dead NMIIB mutant (Ma et al., 2012). As *in vivo* studies of myosin motor activity are limited, mutant animals with compromised motor activity were generated and mutant embryos were examined while undergoing the first embryonic division.

The third aim was to investigate the existence of plasma membrane-bound NMY-2 during cytokinesis. *In vitro* assays were used to check whether NMY-2 could directly bind to the plasma membrane. *In vivo* assays to test the association of NMY-2 with the plasma membrane during cytokinesis included assessing NMY-2 behaviour in the presence of gradually less F-actin in the contractile ring or in the absence of F-actin.

CHAPTER 3

MATERIAL AND METHODS

3. MATERIAL AND METHODS

3.1 *C. elegans* strains maintenance

C. elegans strains were grown in standard nematode growth medium (NGM) plates using *E. coli* OP50 strain as a food source (Stiernagle, 2006). An initial culture of *E. coli* OP50 was obtained by streaking out some bacteria from a glycerol stock onto a LB agar plate [10 g/L Bacto-tryptone, 5 g/L Bacto-yeast, 5 g/L NaCl and 15 g/L agar, pH 7.5]. Bacteria colonies were left to grow overnight at 37 (Byerly et al., 1976). A single colony of OP50 was inoculated on LB liquid medium and grown overnight at 37 ºC. The bacterial suspension was used for seeding NGM plates. Medium size plates (60 mm diameter) were used for general strain maintenance, and large plates (100 mm diameter) were used for growing larger quantities of worms for freezing. NGM [3 g/L NaCl, 17 g/L agar, and 2.5 g/L peptone] was sterilized by autoclaving at 110 ºC for 30 minutes. After cooling, 1 M $CaCl_2$, 5 mg/mL cholesterol in ethanol, 100 mM $MgSO_4$ and 100 mM KH_2PO_4 were added. Using sterile procedures, NGM solution was dispensed into plates using a peristaltic pump (Wheaton Science Products). This pump was adjusted in order to dispense a constant amount of NGM agar into each plate. Plates were left to dry at room temperature for 2-3 days, seeded with 250 µL of *E. coli* OP50 liquid culture in the case of medium NGM plates or 750 µL in the case of large NGM plates, and left at room temperature for one day before storage. *C. elegans* stocks were maintained at 20 °C. When *C. elegans* stocks became contaminated a standard alkaline bleach protocol was used to clean up the animals (Stiernagle, 2006). The bleach kills the contaminants and hermaphrodites but soaks onto the plate before the embryos hatch. The next day the larvae crawl onto the *E. coli* OP50 lawn and are transferred to a clean seeded NGM plate.

3.2 Generation of transgenic and CRISPR/CAS9 gene edited strains

In chapter 5: Re-encoded nmy-2 transgene fused to mCherry in strain GCP22 was generated by Mos1 mediated single copy transgene insertion (MosSCI) onto chromosome II, tTi5605 VV (Frøkjær-jensen et al., 2009; Frøkjær-Jensen et al., 2012). The nmy-2 promoter region (5.2 kb), ORF and 3'UTR (1.3 kb) were cloned as overlapping fragments from genomic DNA. A region of ~400 bp in exon 12 was re-encoded so that transgenic nmy-2, and not endogenous nmy-2, could be specifically depleted by RNAi. mCherry was cloned

from pDC122 and all fragments were assembled with pCFJ151 backbone through Gibson assembly (Gibson et al., 2009). Single copy transgene insertions were generated by injecting a mixture of target plasmid pAC71, plasmid with transposase pCFJ601, and plasmids carrying selection markers, pCFJ90, pCFJ104 and pGH8, into the strain EG6429 as described previously (Frøkjær-Jensen et al., 2008; Frøkjær-Jensen et al., 2012). Transgene integrations were confirmed by PCR of regions spanning each side of the insertion, sequencing of the entire genomic DNA locus and by fluorescence microscopy.

To generate point mutants in *nmy-2* and *unc-54*, the endogenous loci of *nmy-2* and *unc-54* were modified using the CRISPR/Cas9 technique. Two or three single guide RNAs (sgRNAs) were cloned into the pDD162 vector (Dickinson et al., 2013) and injected together with a single stranded repair template carrying the modified sequence of interest flanked by 35-50 bp homology regions (IDT ultramer) in the gonads of young adult N2 hermaphrodites. All sgRNAs and repair templates used are listed in Table 3.2. To this end, we describe a co-conversion strategy, using CRISPR/Cas9 in which screening for a dominant phenotypic oligonucleotide-templated conversion event at one locus can be used to enrich for custom modifications at another unlinked locus. Injection mixes contained a sgRNA and a repair template to insert the R92C mutation in the *dpy-10* gene, which causes a dominant roller phenotype in modified animals (Levy et al., 1993; Arribere et al., 2014). All point mutations were verified by genomic DNA sequencing. To remove possible unknown mutations, all mutants were subjected to six rounds of outcrossing with N2 animals. *Nmy-2(S251A)* and *nmy-2(R252A)* homozygous animals were sterile and could not be propagated. To maintain and propagate these animals, two approaches were taken. In the first approach *nmy-2(S251A)* and *nmy-2(R252A)* animals were balanced with hT2, by crossing *nmy-2(S251A)*/+ or *nmy-2(R252A)*/+ animals with the balancer strain JK2739 to generate the strains GCP629 and GCP513, respectively. Heterozygous mutant animals were fertile and easily identifiable, and homozygous animals were sterile and their gonads were analysed in Figure 2A. In the second approach, we were able to keep the *nmy-2(S251A)* and *nmy-2(R252A)* animals in homozygosity after crossing the strains GCP629 and GCP513 with GCP22 to generate the strains GCP618 and GCP592, respectively, which contained the point mutations in the endogenous nmy-2 gene in chromosome I and a wild-type copy of mCherry-labelled and re-encoded nmy-2 in chromosome II. The presence of the wild-type version of nmy-2 kept the animals fertile and embryos viable. The strains used in this thesis are listed in Table 3.1.

Table 3.1 *C. elegans* strains used in the thesis

EG6429	oxSi36[unc-47::GFP unc-119(+)]IV; unc-41(e268)V
GCP21	ltIs157 [pAC16;pie-1::Life-Act::GFP; unc-119 (+)]; ltIs37 [pAA64; Ppie-1::mCherry::his-58; unc-119 (+)] IV
GCP113	unc-119(ed3) III; nmy-2(cp13[nmy-2::gfp + LoxP]) I; ltIs37 [pAA64; Ppie-1::mCherry::his-58; unc-119 (+)] IV
GCP159	unc-119(ed3)III; prtSi8[pAC95;Pnmy-2:nmy-2reencoded::GFP::StrepTagII::3'UTRnmy-2; cb-unc-119(+)]II;weIs21 [pJA138; Ppie-1::mCherry::β-tubulin::pie-1 3'UTR)] IV
GCP179	nmy-2(cp13[nmy-2::gfp + LoxP]) I; ltIs44 [pAA173; Ppie-1::mCherry::PH(PLC1delta1); unc-119 (+)]
GCP179	nmy-2(cp13[nmy-2::gfp + LoxP]) I; ltIs44 [pAA173; Ppie-1::mCherry::PH(PLC1delta1); unc-119 (+)]
GCP21	ltIs157 [pAC16; Ppie-1::Life-Act::GFP; unc-119 (+)]; ltIs37 [pAA64; Ppie-1::mCherry::his-58; unc-119 (+)] IV
GCP22	ltIs157 [pAC16;Ppie-1::Life-Act::GFP; unc-119 (+)]; unc-119(ed3)III; prtSi2[pAC71; Pnmy-2:: re-encoded nmy-2::mCherry::StrepTagII::3'UTRnmy-2; cb-unc-119(+)]II

GCP227	unc-119(ed3)III; prtSi182[pAC238; Pmlc-5:mlc-5 reencoded::mKate2::StrepTagII::3'UTRmlc-5; cb-unc-119(+)]II
GCP239	unc-119(ed3)III; nmy-2(ne3409) I; prtSi4[pAC72; Pmlc-4:mlc-4reencoded::GFP::StrepTagII::3'UTRmlc-4; cb-unc-119(+)]II; ltIs37 [pAA64; Ppie-1::mCherry::his-58; unc-119 (+)] IV
GCP400	unc-119(ed3)III; ltIs37 [pAA64; Ppie-1::mCherry::his-58; unc-119 (+)]; [Pani-1::GFP::ANI-1; cb-unc-119(+)]IV
GCP401	nmy-2[prt38(S250A)]I; ltIs157 [pAC16; Ppie-1::Life-Act::GFP; unc-119 (+)]; ltIs37 [pAA64; Ppie-1::mCherry::his-58; unc-119 (+)] IV
GCP420	nmy-2 [prt37(R718C)]I; ltIs157 [pAC16;Ppie-1::Life-Act::GFP; unc-119 (+)]; ltIs37 [pAA64; Ppie-1::mCherry::his-58; unc-119 (+)] IV
GCP50	unc-119(ed3)III; prtSi4[pAC72; Pmlc-4:mlc-4reencoded::GFP::StrepTagII::3'UTRmlc-4; cb-unc-119(+)]II; ltIs37 [pAA64; Ppie-1::mCherry::his-58; unc-119 (+)] IV
GCP513	nmy-2 [prt100(R252A)]I/hT2 [bli-4(e937) let-?(q782) qIs48] (I;III).
GCP523	unc-54[prt98(S239A)]I
GCP524	unc-54[prt97(R710C)]I
GCP565	unc-54[prt99(R241A)]I
GCP592	nmy-2 [prt100(R252A)]I; ltIs157 [pAC16;Ppie-1::Life-Act::GFP; unc-119 (+)]; unc-119(ed3)III; prtSi2[pAC71; Pnmy-2:: re-encoded nmy-2::mCherry::StrepTagII::3'UTRnmy-2; cb-unc-119(+)]II

GCP618	nmy-2 [prt113(S251A)]I; ltIs157 [pAC16;Ppie-1::Life-Act::GFP; unc-119 (+)]; unc-119(ed3)III; prtSi2[pAC71; Pnmy-2::re-encoded nmy-2::mCherry::StrepTagII::3'UTRnmy-2; cb-unc-119(+)]II
GCP619	unc-54[prt112(S240A)]I
GCP629	nmy-2 [prt113(S251A)]I/hT2 [bli-4(e937) let-?(q782) qIs48] (I;III
GCP752	unc-119 (ed3) III;nmy-2 (cp52[nmy-2::mkate2]) I; ltIs157 [pAC16;Ppie-1::Life-Act::GFP; unc-119 (+)]; ltIs37 [pAA64; Ppie-1::mCherry::his-58; unc-119 (+)] IV
JK2739	mcm-4(e1466) dpy-5(e61) I/hT2 [bli-4(e937) let-?(q782) qIs48] (I;III)
N2	*C. elegans wild-type* strain
RZB213	[plst-1(msn190[plst-1::GFP])] IV
RZB250	[cyk-1 (knu83 C-terminal GFP, unc-119 (+)); unc-119(ed3)] III; zuIs15 nmy-2::mCherry); ltIs37 [Ppie-1::mCherry::his-58;unc-119(+)] IV

Table 3.2 List of CRISPR/Cas9 single guide RNAs (sgRNAs) and repair templates used in this study

Gene/Mutation	**Repair template***	**Diagnosis PCR and restriction enzyme**	**sgRNA sequence**

nmy-2(S250A)	aaccggatcatgggccagcttgaggaacagcttttgcaagcaaatcccatTctTgaAgcAttTggaaacagtaagacagtgaagaacgataatGcTagCagatttgtgagtgatcataacttttaaatgcacgcatcgttaaattttt	Forward primer: ACTCTGGCTTGTTCTGCGTT Reverse primer: GCACGCGAGATTTCTCCAG Restriction enzyme: NheI	sgRNA#1 CAAGCAAATCCCATACTCG sgRNA#2 ATCCCATACTCGAGGCTTT sgRNA#3 TGATCACTCACAAATCTAC
nmy-2(S251A)	aaccggatcatgggccagcttgaggaacagcttttgcaagcaaatcccatTctTgaAgcAttTggaaacagtaagacagtgaagaacgataatAGCGCTagatttgtgagtgatcataacttttaaatgcacgcatcgttaaattttt	Forward primer: ACTCTGGCTTGTTCTGCGTT Reverse primer: GCACGCGAGATTTCTCCAG	

		Restriction enzyme: Eco47III	
nmy-2(R252A)	aaccggatcatgggccagcttgaggaacagcttttgcaagcaaatcccatTctTgaAgcAttTggaaacagtaagacagtgaagaacgataattcTagCGCTtttgtgagtgatcataacttttaaatgc	Forward primer: ACTCTGGCTTGTTCTGCGTT Reverse primer: GCACGCGAGATTTCTCCAG Restriction enzyme: Eco47III	

nmy-2(R718C)	cacgaaaagaaacatggagttctcaacgctcatcttgttcttgatcaattGagatgcaacggagtgttAgaaggaattTGCatatgTcgtcaaggattccctacgcggctcccgttccaagaattccgtcaacgcta	Forward primer: TCATTTGTTCAACGCCTCAA Reverse primer: cacgacattgagcttggaaagattcaat Restriction enzyme: NdeI	sgRNA#1 CCGCGTAGGGAATCCTTGA sgRNA#2 GAATTCGTATATGCCGTCA sgRNA#3 TTAAGATGCAACGGAGTGT
unc-54(S239A)	ccttcggtaacgccaagactgtccgtaacaacaacGcGtcAcgCttTggaaagttcatccgtatccacttcaacaagcacgg	Forward primer: AAGACCACGAGAACCAGTCT Reverse primer: CGTACATGTTGGATGCCTTC	sgRNA#1 ACAACAACTCTTCCCGTTT sgRNA#2 CGGATGAACTTTCCGAAAC

		Restriction enzyme: MluI	sgRNA#3 ACGGATG AACTTTCC GAAA
unc-54(S240A)	ccttcggtaacgccaagactgtccgtaacaacaacAGCGcTcgtttcggaaagttca tccgtatccacttcaacaa	Forward primer: AAGACCAC GAGAACCA GTCT Reverse primer: CGTACATG TTGGATGC CTTC Restriction enzyme: Eco47III	

unc-54(R241A)	tcggtaacgccaagactgtccgtaacaacaactcaAGcGCtttTggaaagttcatccgtatccacttcaacaagcacgg	Forward primer: AAGACCACGAGAACCAGTCT Reverse primer: CGTACATGTTGGATGCCTTC Restriction enzyme: Eco47III	
unc-54(R710C)	ctttggttctcaaccagcttacctgcaacggagtCCtCgaGggCatATgTatttgcCgTaaAggattccccaacagaacccttcatccagacttcgt	Forward primer: CGAGAAGAACAAGGACCCCC Reverse primer: TGCGAAGCTTCTCCTCCTTG	sgRNA#1 GAATCAGAATTTGCAGAAA sgRNA#2 GGAATCAGAATTTGCAGAA

		Restriction enzyme: NdeI	sgRNA#3 CCTGCAA CGGAGTG TTGGA

*Bases in uppercase indicate silent mutations introduced to avoid repair template recognition by Cas9 and/or to introduce a restriction site (underlined bases) for diagnostic PCR of genomic edits.

3.3 Generation of list of myosin heavy chains in *C. elegans*

In chapter 4: Myosins listed in a previous work (Odronitz & Kollmar, 2007) were aligned and analysed.

In figure 7, the myosin protein sequences for NMY-2 and MYH1 alignment were obtained from the WormBase and UNIPROT databases, respectively, with the following accession numbers: F20G4.3|NMY-2 and P13538|MYH1_CHICKEN.

Myosin protein sequences for alignments in figure 8 were obtained from the WormBase database with the following accession numbers: F52B10.1|NMY-1; F20G4.3|NMY-2; Y11D7A.14|NMY-3; R06C7.10|MYO-1; T18D3.4|MYO-2; K12F2.1|MYO-3; F58G4.1|MYO-5; F45G2.2|MYO-6; F11C3.3|UNC-54; F29D10.4|HUM-1; F36D4.3|HUM-2; F47G6.4|SPE-15; F46C3.3|HUM-4; T02C12.1|HUM-5; T10H10.1|HUM-6; F56A6.2|HUM-7; Y66H1A.6|HUM-8; F43C9.3|HUM-10; R102.5|ALLO-1; F28D1.2|ATZ-1; C18C4.7| C18C4.7 and; F59A2.6|GOLG-4.

All the sequences were aligned using Jalview software (Waterhouse et al., 2009) and the MUSCLE method with default settings was applied (Edgar, 2004). From 22 putative

myosins, 17 are likely to act as myosin. The information of these myosins listed on Table 3.3 was taken from the WormBase database (http://www.wormbase.org).

Table 3.3 Myosins that are found in WormBase. The first column corresponds to the accession number, the second to gene name, the third to the myosin class and the last to the phenotypes described in WormBase and references where those phenotypes were described.

Accession number	Gene	Class	Phenotypes on WormBase (References)
F52B10.1	nmy-1	II	L1 larvae are dumpy and lumpy (Piekny, 2003; Kamath, 2003); range of embryonic lethal (Kamath, 2003);; locomotion defects (Kamath, 2003); roller phenotype (Sönnichsen et al., 2005; Piekny, 2003); Spermatheca defects (Kovacevic et al., 2013); Sterile (Kamath, 2003);
F20G4.3	nmy-2	II	P granule localization is defective (Cheeks et al., 2004); Maintains UNC-45 correct localization (Kachur et al., 2008); reduced apoptosis in the germline (Green et al., 2011); asymmetric cell division defects in early embryos (Sönnichsen et al., 2005); defects in axon fasciculation (Schmitz et al., 2007); defects in body wall muscle myosin organization (Meissner et al., 2009); PI(4,5)P2 accumulation in cytoplasm or nucleus of germ cells (Green et al., 2011); defects in cleavage furrow initiation (Skop et al., 2004); defects in early embryo cytokinesis (Poteryaev et al., 2005); defects in cytoplasmic streaming (Niwayama et al., 2011); embryonic lethal (Piano et al., 2002; Piekny, 2003; Kamath, 2003; Simmer et al., 2003; Skop et al., 2004; Sönnichsen et al., 2005); defects in endoplasmic reticulum symmetry (Poteryaev et al., 2005)
Y11D7A.14	nmy-3	II (previously annotated as Myosin XVII)	no phenotypes (sterility, embryonic viability, animal morphology) described in large RNAi screens (Kamath, 2003; Sönnichsen et al., 2005)
R06C7.10	myo-1	II	resistance to paralysis on aldicarb (Sieburth et al., 2005); embryonic lethal (Sönnichsen et al., 2005; Simmer et al., 2003); larval arrest (Simmer et al., 2003); larval lethal (Sieburth et al., 2005); reduced brood size (Gottschalk et al., 2005)

T18D3.4	myo-2	II	no phenotypes (sterility, embryonic viability, animal morphology) described in large RNAi screenings (Maeda et al., 2001; Sönnichsen et al., 2005)
K12F2.1	myo-3	II	Displaced body muscle (Waterston, 1989; Williams & Waterston, 1994); hypersensitivity to the drug methylmethanesulfonate (MMS) (van Haaften et al., 2006); embryonic lethal (Martin et al., 2002); larval arrest (Simmer et al., 2003); locomotion defects (Martin et al., 2002; Simmer et al., 2003); moderately sensitive to ionizing radiation (van Haaften et al., 2006); embryos are paralyzed at the 1.5- fold stage (Williams & Waterston, 1994); strong suppression of yolk uptake by oocytes (Balklava et al., 2007); sluggish phenotype (Kamath, 2003); Sterile (Kamath, 2003);
F58G4.1	myo-5	II	no phenotypes (sterility, embryonic viability, animal morphology) described in large RNAi screens (Maeda et al., 2001; Kamath, 2003; Sönnichsen et al., 2005)
F45G2.2	myo-6	II	resistance to paralysis on aldicarb (Sieburth et al., 2005)
F11C3.3	unc-54	II	defects in axon fasciculation (Dixon & Roy, 2005); bag phenotype (Trent et al., 1983); defect in body muscle cells (Brenner, 1974); defects in egg laying (Park & Horvitz, 1986; Fire et al., 1991; Timmons et al., 2001; Arribere et al., 2014); resistance to lay eggs in imipramine, levamisole, phentolamine and serotonin (Trent et al., 1983); embryonic arrest (Fire et al., 1998); paralyzed (Fire et al., 1991); larval arrest (Fire et al., 1998); defects in locomotion (Timmons et al., 2001; Arribere et al., 2014; Feldman et al., 2014; Dostal et al., 2010; Timmons et al., 2001; Fire et al., 1998); defects in muscle arm development (Dixon & Roy, 2005; Alexander et al., 2009); reduced sperm pseudopods (Nelson et al., 1982); thin (Park & Horvitz, 1986)
F47G6.4	spe-15	VI	embryonic lethal (Ceron et al., 2007); hermaphrodites with defects in self-fertilize (L'Hernault et al., 1988); defects in oocyte morphology (Ceron et al., 2007); reduced brood size (Ceron et al., 2007); lay of unfertilized oocytes (L'Hernault et al., 1988)

F29D10.4	hum-1	I	resistance to paralysis on aldicarb (Sieburth et al., 2005)
F36D4.3	hum-2	V	no phenotypes (sterility, embryonic viability, animal morphology) described in large RNAi screens (Maeda et al., 2001; Kamath, 2003; Sönnichsen et al., 2005)
F46C3.3	hum-4	XII	no phenotypes (sterility, embryonic viability, animal morphology) described in large RNAi screens (Maeda et al., 2001; Kamath, 2003; Sönnichsen et al., 2005)
T02C12.1	hum-5	I	more than two motoneuron commissures not reaching the dorsal cord (Schmitz et al., 2007)
T10H10.1	hum-6	VII	no phenotypes (sterility, embryonic viability, animal morphology) described in large RNAi screens (Kamath, 2003; Sönnichsen et al., 2005)
F56A6.2	hum-7	IX	defects on axon guidance and branching (Chen et al., 2014; Wallace et al., 2018); embryonic elongation defects (Wallace et al., 2018); embryonic lethal (Wallace et al., 2018); gut on the exterior of the embryos (Wallace et al., 2018)
Y66H1A.6	hum-8	VI	embryonic lethal, reduced brood size and germline morphology defects (Skop et al., 2004)

3.3 Synchronization of animals in L1 stage

L1 worms were synchronized by bleaching for the embryonic viability tests. To do so, a plate full of adult worms was rinsed with M9 medium (86 mM NaCl, 42 mM Na_2HPO_4, 22 mM KH_2PO_4, and 1 mM $MgSO_4$). The suspension was centrifuged at 1300 xg during 2 min and the supernatant removed. The worm pellet was washed with M9 medium and centrifuged in the same conditions. The supernatant was removed and to each pellet the following solution was added: 70 mM NaCl, 0.5 N NaOH, 0.89% bleach (4% sodium hypochlorite). Then the mixture was vortexed for 5 minutes until worms disintegrated completely releasing the eggs. M9 was added to dilute bleach and the mixture was centrifuged at 1300 xg for 2 min to

recover the egg pellet. The recovered eggs were washed twice with M9 like in previous steps. Finally, eggs were left to hatch overnight in M9 with shaking at 20 ºC. The next day the suspension was plated on unseeded plates and briefly air-dried.

3.4 RNA interference by animal injection

To produce dsRNA, primers with tails containing T3 and T7 promoters were used to amplify regions from genomic N2 DNA (gDNA) or cDNA (Table 3.4). PCR products were separated on agarose 1 % gels containing 2 µL of Midori Green (DNA staining solution) per 100 mL of 1x TAE buffer (40 mM Tris, 20 mM Glacial acetic acid, 1mM EDTA, pH 8). The gel was then visualized on a Gel doc system (Biorad). The bands of interest were excised with a scalpel under UV light, and the DNA was purified with the NucleoSpin Gel and PCR Clean-up Kit (Macherey-Nagel). Manufacturer's instructions were followed. Purified PCR products were used as templates for independent T3 and T7 *in vitro* transcription reactions (MEGAscript, Invitrogen). The transcription reaction was left incubating for 5 hours at 37 ºC and the resulting single-stranded (ssRNA) was then purified using the NucleoSpin RNA Clean-up (Macherey-Nagel) according to manufacturer's instructions. Purified ssRNA products were annealed in soaking buffer (3× soaking buffer: 10.9 mM Na_2HPO_4, 5.5 mM KH_2PO_4, 2.1 mM NaCl, 4.7 mM NH_4Cl) by incubating at 68 °C for 10 minutes and then at 37 °C for 30 minutes. Double-stranded RNA (dsRNA) was aliquoted in working volumes and kept at - 80 ºC until used.

In chapter 4: RNAi-mediated depletion of NMY-1, MYO-1 and MYO-3 was performed by injecting the dsRNA of interest in the gonad of L4 stage *C. elegans* (Table 3.4). The time of *nmy-1(RNAi)* and *myo-1(RNAi)* treatment was 48 hours. In the case of MYO-3 depletion, where penetrant depletion caused worm sterility, a shorter RNAi treatment of 40 hours was performed.

In chapter 6: RNAi-mediated depletion of CYK-1, ECT-2, RHO-A, MLC-4, CYK-4, ANI-1, HMR-1, SAX-7 and NMY-2 was performed by injecting the dsRNA of interest in the gonad of L4 stage *C. elegans* (Table 3.4).

Table 3.4 List of primers used for producing dsRNAs for injection.

Name	Oligo 1 (5´-3´)	Oligo 2 (5´-3´)	RNAi timing (h)
cyk-1	TAATACGACTCACTATAGGG GGCATTCTTCAAGGATCAA	AATTAACCCTCACTAAAGGTG GTGAGATTTGCGATGTTC	21-45
ect-2	TAATACGACTCACTATAGGT GGATCCGATTCTCGAACTT	AATTAACCCTCACTAAAGGAC ATTTGGCTTTGTGCTTCC	21
rho-a	TAATACGACTCACTATAGGT GGCTGCGATTAGAAAGAAG	AATTAACCCTCACTAAAGGCC TCACGAATTCCGTCCTTA	21
mlc-4	TAATACGACTCACTATAGGC TTAATCGGAGCATCTCTAAA G ; TAATACGACTCACTATAGGG CTCCCGCAAAACCGTAAAC	AATTAACCCTCACTAAAGGCT CCCGCAAAACCGTAAAC; CTTAATCGGAGCATCTCTAAA G	27
cyk-4	TAATACGACTCACTATAGGC GCAAGCTGTGGAAAGATTC	AATTAACCCTCACTAAAGGTT GCGATGTCACGAGTTGTT	23
ani-1	AATTAACCCTCACTAAAGGC CCAGTTTTTCCCCTCAGAT	TAATACGACTCACTATAGGAA ATTCCCGGTTTTGTCTCC	48
hmr-1	AATTAACCCTCACTAAAGGG AGTTCTAAGAGGCTCTGGGT G	TAATACGACTCACTATAGGTT CCGACCTGAACGGAGAAC	48
sax-7	AATTAACCCTCACTAAAGGT GGTCCAAGTGCAACTCAAG	TAATACGACTCACTATAGGCG GTTCTCTTCCTTGCTCAC	48
nmy-2	CCCAAGATATCAATTGAATCT CGGTTGAAGGAA	CCCCCGATATCGACTGCATTT CACGCATCTTATG	32

nmy-1	ATTAACCCTCACTAAAGGGG CAACATCAACTGACGAG	TAATACGACTCACTATAGGGA GCATCGAGAAGATCGTC	48
myo-1	AATTAACCCTCACTAAAGGA ATTGACCGACGAGGCCTTT	TAATACGACTCACTATAGGCG ACCACCTCCGGCCTTA	48
myo-3	AATTAACCCTCACTAAAGGC ATTGCTCAATTGGAAGCCAG A	TAATACGACTCACTATAGGCA GGAAATGTAAGCGGGTCAA	40

3.5 RNAi by animal feeding

RNAi was performed by feeding worms with bacteria that expressed the dsRNA of interest. DNA fragments of interest were amplified using the primers in Table 3.5 from N2 cDNA or gDNA. L4440 plasmid and amplified DNA fragments were digested with EcoRV (Fermentas Fast Digest®) for one hour at 37 °C, and the digestion products were separated in agarose gels and purified as described in section 3.4. Digested L4440 was incubated with calf intestinal phosphatase (Roche®) for 30 minutes at 37 °C. The purified PCR fragment was incubated with T4 Polynucleotide Kinase (Thermo Scientific) for 20 minutes at 37 °C and for 10 minutes at 75 °C. Ligation reactions were carried out with T4 DNA ligase (New England Biolabs) with the supplied buffer, using a 7:1 insert to plasmid ratio and overnight incubation at 16 °C (total volume 10 µL). For transformations, 100 µL aliquots of TOP10 *E. coli* competent cells were thawed on ice and mixed with 5 µL of the ligation reactions. The mixture was incubated for 20 minutes on ice, heat-shocked at 42 °C for 1 minute and cooled-down on ice for 2 minutes. Then, 500 µL of Super Optimal broth with Catabolite repression (SOC) was added, and the cells were incubated on a shaking incubator at 37 °C for 45 minutes. After incubation, the suspension was spread on agar plates containing 100 mg/mL ampicillin and 5 mg/mL tetracycline. The plates were incubated overnight at 37 °C. Then, single colonies were tested for correct insertion and final plasmids were transformed into HT115 *E. coli*, which were used to feed worms after IPTG induction.

In chapter 4: Besides MYO-3, NMY-1, and NMY-2, all other myosins HCs were depleted by using the vectors from the Ahringer library (Kamath, 2003); RNAi feeding library distributed by Source BioScience, United Kingdom). Bacteria expressing the dsRNA of interest were

grown overnight at 37 °C in LB with 100 µg/mL ampicillin, 5 mg/mL tetracycline and 1 mM Isopropyl β-d-1-thiogalactopyranoside (IPTG). The overnight culture was grown until an OD600 of 1.6. The bacterial culture (100 µL/plate) was spread onto 6 cm NGM agar plates. Plates were dried at room temperature for three days to induce RNA expression. After IPTG induction, animals were transferred to these plates: For penetrant depletions, synchronized L1-stage animals were incubated for 72 hours at 20 °C, in cases where depletion caused worm sterility, like NMY-2 and MYO-3, a shorter RNAi treatment was performed.

For the *nmy-2(RNAi)* time-course, different levels of NMY-2 depletion were achieved by varying the time of RNAi or age of animals at the beginning of the RNAi treatment: L4-stage animals were fed for 20 to 40 hours at 20 °C, or adult animals were fed for 9 to 14 hours.

In chapter 5: As protein levels in newly fertilized embryos gradually decrease with increasing duration of RNAi treatment (Kirkham et al., 2003; Velarde et al., 2007), different RNAi conditions were used to deplete NMY-2 depending on the desired level of depletion. RNAi treatment conditions were different depending on the use of nmy-2_RNA#1, nmy-2_RNA#2 or nmy-2_RNA#3:

In experiments where specific depletion of transgenic NMY-2::mCherry^{sen} was desired (labelled as nmy-2::mCherry^{sen}(*RNAi*) in the figures), nmy-2_RNA#2 was used in GCP22, GCP618 or GCP592 L4 hermaphrodites at 20 °C. Mild depletions (22-26 hours of RNAi treatment) were used in Figures 4A, 4B, 4D, 4E, 6A, and 7A-D; in these conditions most embryos were able to complete cytokinesis. Penetrant depletions (36-38 hours of RNAi treatment) were used in Figure 4B, 4C and 7E; in these conditions all 1-cell embryos failed cytokinesis. More penetrant depletions (38-48 hours of RNAi treatment) were used in Figure 3D; in these conditions hermaphrodites presented non-compartmentalized gonads and stopped producing embryos and embryos laid at earlier time points were not viable.

In *nmy-2*(*RNAi*) experiments where the purpose was to deplete endogenous NMY-2 to an extent that did not preclude cytokinesis (labelled as nmy-2(*RNAi*)), nmy-2_RNA#1 was used in L4 hermaphrodites at 20 °C (Figure 6, S3). Mild depletions (26-28 hours of RNAi treatment) were used in GCP21, GCP401 and GCP420 strains in Figures 5F, 5H and S5H; in these conditions most *nmy-2(S250A)* and all *nmy-2(R718C)* embryos were able to complete cytokinesis albeit slower than controls. Partial depletions (30-32 hours of RNAi treatment) were used in GCP21 strain (Figure 6B), GCP179 strain (Figure S3A-C) and in GCP22 strain (Figure S3D-G); in these conditions most embryos were able to complete

cytokinesis albeit slower than controls. In Figure S3D-G both endogenous and transgenic NMY-2::mCherry were simultaneously depleted using nmy-2_RNA#3.

Depletion of MYO-3 was accomplished by incubating L1 hermaphrodites of strains GCP565 and GCP619 (Figure 1D), GCP523 (Figure S4A) and GCP524 (Figure S5B) for 72 hours at 20°C. Depletion of MYO-3, UNC-54 or simultaneous depletion of MYO-3 and UNC-54 in Figures 1D, 1F, 1G, S4A and S5B were performed by feeding L1 hermaphrodites of N2 strain for 72 hours at 20 °C. For double RNAi of *myo-3* and *unc-54*, bacteria expressing each of the constructs were mixed 1:1 before seeding the RNAi plates (Figure 1F).

In chapter 6: For Latrunculin A treatments in experiments in figures 5-12, embryos were permeabilized by partial depletion of PERM-1. Bacteria expressing the dsRNA targeting perm-1 (Ahringer library; Source Bioscience) were grown overnight at 37°C in LB with 100 µg/ml ampicillin. The overnight culture was diluted 1 50 in LB with 100 µg/ml ampicillin and grown at 37°C until an OD600 of 0.4. The bacterial culture (100 µl/plate) was spread onto 6 cm NGM agar plates containing 0.001 mM IPTG. Plates were dried at room temperature for 2 hours to induce dsRNA expression. After IPTG induction, animals were fed with these bacteria for 21 hours at 20°C.

Table 3.5 Primers used for producing dsRNAs expression vectors.

Name	Gene target	Forward primer	Reverse primer
nmy-2_RNA#1	nmy-2 (does not target re-encoded nmy-2:mCherry^{sen})	GGCCCGATATCATGAACAACGAGCTTGAAAG	GGCACGATATCAGCCTCCTGGATAGCC

nmy-2_RNA#2	re-encoded nmy-2:mCherry^{sen} (does not target endogenous nmy-2)	GGCCCGATATCATGAATAATGAACTCGAGTCAATC	GGCCCGATATCACGTTCTTGAATGGCC
nmy-2_RNA#3	nmy-2 and re-encoded nmy-2:mCherry^{sen}	CCCAAGATATCAATTGAATCTCGGTTGAAGGAA	CCCCCGATATCGACTGCATTTCACGCATCTTATG

3.6 Embryonic Viability

All embryonic viability tests were performed by injection or feeding RNAi at 20 °C.

In chapter 4: In most cases, L1-stage animals were grown in feeding RNAi plates for 64 hours. After this period, 9 worms were singled out onto fresh plates with bacteria expressing the corresponding dsRNA. Eight hours later, the adult worm was removed, and the embryos laid were left to hatch at 20°C. In the case of NMY-1 and MYO-1 depletions, L4-stage animals were injected with dsRNA and grown for 44 hours in OP50 *E. coli* plates. Adult animals were singled out and left to lay eggs for 8 hours before the animal was removed. In all cases, 24 hours later, unhatched and hatched progeny on each plate were counted. Percent embryonic viability was calculated by dividing the number of hatched embryos by the total number of progeny.

In chapter 5: In Figures S4E and S5F, L4 hermaphrodites of strains GCP21, GCP401 or GCP420 were placed on NGM plates and singled out onto fresh plates after 40 hours at 20 °C. Adult gravid hermaphrodites were let to lay eggs for eight hours. In Figure 3D, GCP22, GCP618 or GCP592 L4 hermaphrodites were placed on plates with bacteria expressing nmy-2_RNA#2 for 40 hours at 20 °C. Adult hermaphrodites were then singled out onto fresh RNAi plates and let to lay eggs for 8 hours. In all cases animals were removed after the egg laying interval and embryos were left to hatch at 20 °C for 24 hours before counting. The

number of hatched and unhatched (dead) embryos was counted and the percent embryonic viability was calculated by dividing the number of hatched embryos by the total number of progeny. To measure egg laying rates in Figures 1E, S4B and S5C, L4 hermaphrodites of strains N2, GCP523, GCP524, GCP565 or GCP619 were placed on NGM plates and singled out onto fresh plates after 40 hours at 20 °C. Adult hermaphrodites were let to lay eggs for eight hours. The rate was calculated by dividing the total number of eggs by the number of laying hours.

3.7 Imaging

Gravid hermaphrodites were dissected, and one-cell embryos mounted on 2% agarose pads in a drop of M9 were imaged at 20 °C. Images were acquired on a spinning disk confocal system (Andor Revolution XD Confocal System; Andor Technology) with a confocal scanner unit (CSU-22; Yokogawa) mounted on an inverted microscope (Ti-E, Nikon) equipped with a 60× 1.42 oil-immersion Plan-Apochromat objective, solid-state Laser 488 nm (250 mW) and Laser 561 nm (250 mW). For image acquisition, an electron multiplication back-thinned charge-coupled device camera (iXon; Andor Technology) with 1x1 binning was used. Acquisition parameters, shutters, and focus were controlled by Andor iQ3 software. For central plane imaging in one-cell embryos, 6 × 1–μm z stacks were collected in the 488-nm and 561-nm channels every 10 seconds through the center of the embryo. For cortical imaging in one-cell embryos, 7 × 0.5–μm z stacks were collected in the 488-nm and 561-nm channel every 5 seconds. Exposure time was 100 milliseconds for the 488-nm and 561-nm channels. All imaging was performed in temperature-controlled rooms kept at 20 ºC.

In chapter 4: Rapid temperature shifts were performed using a CherryTemp fast heater-cooler system (Cherry Biotech). In this case, live imaging of one-cell *nmy-2(ne3409)* embryos was performed under no compression in the CherryTemp device at different temperatures: permissive temperature 16°C, semi-restrictive temperatures 24°C and restrictive temperature 26°C. Temperature upshift was performed during live imaging at the desired time points during cytokinesis.

3.8 Image analysis, quantifications, and statistics

All microscopy image processing and measurements were done using Fiji (ImageJ; National Institutes of Health (Schindelin et al., 2012) and Matlab (MathWorks). Z-stacks taken on the

cell cortex were projected using the maximum intensity projection tool. Images within each panel were scaled equally. The equatorial region of the central plane was selected to create the kymograph, using the Make Montage tool.

In chapter 5: Selected regions of 4-second time lapse movies (presented in movie 1 for wild-type, S251A and R252A NMY-2_{HMM} complexes) were used to create 300 seconds time projections presented in Figures 2I and 5D by using the Temporal Color Code tool with the fire color scale.

Coomassie stained SDS-PAGE gels were digitized in a GS-800 Calibrated Imaging Densitometer (Bio-Rad) and relative band intensity quantified in Image-Lab 5.2.1 (Bio-Rad). For each myosin mutant, the ability of NMY-2 to co-sediment with F-actin was quantified by dividing the intensity of the band corresponding to NMY-2 S1 fragment in the pellet by the sum of intensities of the NMY-2 S1 fragment bands in the supernatant and pellet. Graph plotting, linear regressions and statistical analyses were performed with Prism 7 or 8 (GraphPad Prism Software). Dissociation constant (Kd) estimations in Figures 2E and 5C were performed by fitting a 'one-site specific binding' model using a least squares nonlinear regression (GraphPad Prism Software). Error bars represent the 95 % CI of the mean except in Figure 2E and 5C where they represent the standard deviation (SD). Statistical significance tests were performed using a student t-test or one-way ANOVA with Bonferroni correction for multiple comparisons as indicated in figure legends.

3.9 Measurement of cytokinesis, ring assembly and furrow initiation time intervals, and ring constriction rate

Measurement of cytokinesis, ring assembly and furrow initiation time intervals, as well as overall ring constriction rate were performed during cytokinesis in one-cell embryos. This analysis only included embryos that completed ring constriction. Cytokinesis time was the interval between anaphase onset and the time when the contractile ring reached a diameter of ~ 5 µm. Ring assembly time was the time interval between anaphase onset and the establishment of a shallow deformation in the equatorial region (time point when the equator shows first sign of deformation). Furrow initiation time corresponded to the time interval between the establishment of the shallow deformation and the time when the plasma membranes of the nascent daughter cells became juxtaposed to one another (back-to-back membrane configuration). During ring constriction, the distance between the two sides of

the ring was measured on the z-plane where this was the widest at each time point and plotted against time. Ring constriction rate was the slope of the linear region between ~70 % and 30 % ingression. All these intervals were determined based on imaging of the embryo central plane.

3.10 Fluorescence intensity measurements

In chapter 4: To quantify the levels of NMY-2::GFP at the tip of the cytokinetic furrow in one-cell embryos, the mean fluorescence intensity in a 10-pixel wide, 30-pixel long (1.8x5.3 µm) box drawn over the tip of the furrow at 50% ingression was determined, and the mean camera background was subtracted.

In chapter 5: To quantify the levels of Lifeact::GFP at the tip of the cytokinetic furrow in one-cell embryos, the mean fluorescence intensity in a 10-pixel wide, 30-pixel long (1.8x5.3 µm) box drawn over the tip of the furrow at 50 % ingression was determined and the mean camera background was subtracted (Figure 6A). The average intensity at the furrow tip is presented as a percentage of the corresponding controls. In Figure 6B, quantification of actin levels in the contractile ring of ABa cells was done in GCP22 4-cell embryos by measuring the mean LifeAct::GFP fluorescence intensity in a manually traced 0.7-µm line over the circumference of the ring. The mean fluorescence intensity in a circle drawn over the cytoplasm at each time point was subtracted. Before quantification, each time lapse movie was corrected for fluorescence intensity decay using the ImageJ bleach correction tool and the simple ratio method. Data from multiple rings were pooled and plotted against ring perimeter. The mean of data points that fell in overlapping 5-µm intervals was calculated and plotted against the perimeter at the center of each interval.

In Figure S3C, NMY2::mCherry^{sen} intensity was calculated by measuring the average fluorescence intensity of a 130x35 pixel box placed over the cortical equatorial band and the camera mean fluorescence background was subtracted (a 40x40 pixel box placed outside of the embryos).

3.11 Analysis of band width and bundle alignment at the equatorial cortex

In chapter 5: Equatorial actin band width in Figure 7C was the length of a line traced across the band, perpendicularly to the division plane in cortical projections at shallow deformation. Values were normalized to embryo length along the anterior-posterior axis measured in the central plane and averaged for each condition. In Figure S3C, NMY2::mCherry^{sen} intensity was calculated by measuring the average fluorescence intensity of a 130x35 pixel box placed over the cortical equatorial band. The camera mean fluorescence background was subtracted (a 40x40 pixel box placed outside of the embryos). Deviation from vertical alignment (º) over time in Figure 7D was measured using the Directionality plugin for ImageJ. A region of interest of 30 x 70 pixel corresponding to the furrow region was selected for each movie. The average directionality (angle , in degrees), was then calculated for every frame of each movie using the local gradient orientation method. Deviation from vertical alignment (in degrees) was calculated for each angle , by subtracting the value of this angle to 90º. Absolute numbers were plotted.

3.12 Preparation of worm protein extracts and immunoblotting

In chapter 5: For protein sample preparation in Figures 3C and S4D, sixty L4 hermaphrodites of each of the strains: N2, GCP22, GCP592 GCP618, or GCP401 were grown on NGM plates for 46 hours at 20 ºC and pelleted at 750 xg. Animals were washed three times in M9 medium with 0.1 % Triton X-100. Lysis was performed by resuspending the pellet in 1x Laemmli buffer with ⅓ volume of quartz sand (Sigma). Tubes were subject to three 5-minute cycles of alternating boiling at 95 ºC and vortexing after which the quartz sand was pelleted, and the supernatant recovered. Protein samples were resolved by SDS-PAGE in a 7.5 % acrylamide gel and transferred to 0.2-µm nitrocellulose membranes (GE Healthcare). Membranes were blocked with 5 % nonfat dry milk in TBST (20 mM Tris, 140 mM NaCl, and 0.1 % Tween, pH 7.6) and probed at 4 °C overnight with the following primary antibodies: anti-NMY-2 antibody, 1:10000 (rabbit polyclonal against residues 945-1368); anti-α-tubulin, 1:5000 (mouse monoclonal DM1-α, catalogue #T6199 Sigma). Membranes were washed three times with TBS-T, incubated with HRP-conjugated secondary antibodies goat anti-rabbit 1:5000 (catalogue #111-035-144, Jackson ImmunoResearch) or goat anti-mouse 1:5000 (catalogue #115-035-003, Jackson ImmunoResearch) for 1 hour at room temperature, and washed three times with TBST. Blots were visualized by

chemiluminescence using Pierce ECL Western Blotting Substrate (Thermo Fisher Scientific) and imaged in a ChemiDoc™ XRS+ System with Image Lab™ Software (Bio-Rad).

3.13 Protein alignments

In chapter 5: Myosin protein sequences for alignments shown in Figures 1B, 1C, S1 and S5A were obtained from the Uniprot database with the following accession numbers: P08799|MYS2_DICDI; G5EBY3|G5EBY3_CAEEL; Q20641|Q20641_CAEELQ99323|MYSN_DROME; F1QC64|F1QC64_DANRE; F8W3L6|F8W3L6_DANRE; F1R3G4|F1R3G4_DANRE; 93522|O93522_XENLA; Q04834|Q04834_XENLA; Q8VDD5|MYH9_MOUSE ;Q61879|MYH10_MOUSE; Q6URW6|MYH14_MOUSE; P35579|MYH9_HUMAN; P35580|MYH10_HUMAN; Q7Z406|MYH14_HUMAN; P02566|MYO4_CAEEL and aligned using the Jalview software (Waterhouse et al., 2009) and the muscle algorithm with default parameters (Edgar, 2004).

3.14 Protein expression and purification

In chapter 5: Sequences of wild-type nmy-2 S1 fragments (corresponding to amino acids 1-874) or nmy-2 HMM fragments (corresponding to amino acids 1-1364), full length mlc-4 and mlc-5 and let-502 were amplified from *C. elegans* cDNA and cloned into pACEbac1 expression vector using a Gibson assembly approach (Gibson et al., 2009). Nmy-2 constructs were tagged N-terminally with 6×His followed by a linker (coding for GlySerGlySerGly). Let-502 (1-469) and myosin light chains mlc-4 and mlc-5 were tagged N-terminally with a Strep-tag II followed by a linker (coding for GlySerGlySerGly) using the primers indicated in Table 3.6. For establishment of point mutations NMY-2 S250A, S251A, R252A, the wild-type vectors were used for site directed mutagenesis using the primers indicated in Table 3.6. To obtain the let-502(1-469) pACEbac1 vector, the pACEbac1 containing full length let-502 was amplified using back-to-back primers indicated in Table S4 in order to delete the coding sequence downstream of amino acid 469. The resulting vector was re-ligated in a single reaction combining PNK kinase for PCR product phosphorylation (NEB), DpnI for template removal by digestion (Thermo-Fisher Scientific) and DNA T4 ligase (NEB). All plasmids were transformed in DH5-alpha or TOP10 competent bacteria and

sequences confirmed by Sanger DNA sequencing. Plasmid information is summarized on Table 3.7.

Table 3.6 Primers used in this study

Sequence	**Target (gene/plasmid)**	**Purpose**
Forward: GAGCTCACCTAGCTAGAAGTCTTT **Reverse**: CGAGATGATGTCATTATTACCGCTGG	nmy-2 (gDNA)	pCFJ151-Pnmy2 5.2kb:: re-encoded nmy2::mCherryStreptagII::3'nmy2 1.2kb (pAC71) nmy-2 promoter fragment
Forward: CCAGCGGTAATAATGACATCATCTCG **Reverse**: CCCTTTGAGACCATCTGCAGGTTGC	nmy-2 (pAC65)	pCFJ151-Pnmy2 5.2kb::re-encoded nmy2::mCherryStreptagII::3'nmy2 1.2kb (pAC71) nmy-2 open reading frame fragment
Forward: CCCTTTGAGACCATCTGCAGGTTGCG **Reverse**: CCGTACGTCTCGAGTCTAGAGGAATATC	nmy-2 (pAC65)	pCFJ151-Pnmy2 5.2kb::re-encoded nmy2::mCherryStreptagII::3'nmy2 1.2kb (pAC71) nmy-2 3'UTR fragment
Forward: CGCAACCTGCAGATGGTCTCAAAGGG	mCherry (pDC122)	pCFJ151-Pnmy2 5.2kb:: re-encoded nmy2::mCherryStreptagII::3'nmy2 1.2kb (pAC71)

Reverse: CCCTTTGAGACCATCTGCAGGTTGCG		mCherry fragment
Forward: AAGCTTGTCGAGAAGTACTAGAGGATCATAATC **Reverse:** GCCGCTACCAGAGCCATGG	pACEbac1	pACEbac1-6xHis::nmy2 (1-854) (pAC429) backbone+6xHis tag fragment
Forward: ACCATGGCTCTGGTAGCGGCACATCATCTCGACAAAAAGATGATGAG **Reverse:** TAGTACTTCTCGACAAGCTTTTAGTTGCGAACTGAGTCGCGGTCT	nmy-2 (cDNA)	pACEbac1-6xHis::nmy2 (1-854) (pAC429) nmy-2 ORF fragment
Forward: ACCATGGCTCTGGTAGCGGCACATCATCTCGACAAAAAGATGATGAG **Reverse:** TTAATCTTCTTCGAGCTGACGAATTT	nmy-2 (cDNA)	pACEbac1-6xHis::nmy2 (1-1354) (pAC514) nmy-2 1-1354 ORF fragment
Forward: AAGCTTGTCGAGAAGTACTAGAGGATCATAATC **Reverse:** GCCGCTACCAGAGCCTTTTTC	pACEbac1	pACEbac1-StreptagII::mlc-4 (pAC437) pACEbac1-StreptagII::mlc-5 (pAC438) backbone+StrepTagII fragment

Forward: AAAAAGGCTCTGGTAGCGGCGCCTCCCGCAAAACCGTAAAC **Reverse:** TAGTACTTCTCGACAAGCTTTTAAGCCTCATCCTTGTCCTTGG	mlc-4 (cDNA)	pACEbac1-StreptagII::mlc-4 (pAC437) mlc-4 ORF fragment
Forward: AAAAAGGCTCTGGTAGCGGCGACGATTTGGCTGATTGTCGTG **Reverse:** AGTACTTCTCGACAAGCTTTTAGGAGTTCATGACAGCGCG	mlc-5 (cDNA)	pACEbac1-StreptagII::mlc-5 (pAC438) mlc-5 ORF fragment
Forward: AAAAAGGCTCTGGTAGCGGCGAGCAGGATGAGCTGCGTG **Reverse:** TAGTACTTCTCGACAAGCTTACTATTGATAGATTGTGGAAGAG	let-502 (cDNA)	pACEbac1-StreptagII::let-502 (pAC522) let-502 full length ORF fragment
Forward: TAGTAAGCTTGTCGAGAAGTAC **Reverse:** TTCGAATTCTCGGTTTTTC	pACEbac1-streptagII::LET-502 (pAC522)	pACEbac1-StreptagII::let-502 (1-469)(pAC527)
Forward: GACAGTGAAGAACGATAATGCCA	pACEbac1-6xhis::NMY-2 (1-854) (pAC429)	pACEbac1-6xHis::nmy-2 (S250A) (1-854) (pAC451)

GTAGATTTGGAAAGTTC **Reverse:** GAACTTTCCAAATCTACTGGCATTATCGTTCTTCACTGTC	pACEbac1-6xHis::NMY-2 (1-1354) (pAC514)	pACEbac1-6xHis::nmy2 (S250A)(1-1354) (pAC515)
Forward: CAGTGAAGAACGATAATTCCGCTAGATTTGGAAAGTTCATTC **Reverse:** GAATGAACTTTCCAAATCTAGCGGAATTATCGTTCTTCACTG	pACEbac1-6xHis::NMY-2 (1-854) (pAC429) pACEbac1-6xHis::NMY-2 (1-1354) (pAC514)	pACEbac1-6xHis::nmy2 (S251A)(1-854) (pAC453) pACEbac1-6xHis::nmy2 (S251A)(1-1354) (pAC516)
Forward: GTGAAGAACGATAATTCCAGTGCATTTGGAAAGTTCATTCGCG **Reverse:** CGCGAATGAACTTTCCAAATGCACTGGAATTATCGTTCTTCAC	pACEbac1-6xHis::NMY-2 (1-854) (pAC429) pACEbac1-6xHis::NMY-2 (1-1354) (pAC514)	pACEbac1-6xHis::nmy2 (R252A)(1-854) (pAC452) pACEbac1-6xHis::nmy2 (R252A)(1-1354) (pAC517)
Forward: CGGAGTGTTGGAAGGAATTTGTATATGCCGTCAAGGATTC **Reverse:** GAATCCTTGACGGCATATACAAATTCCTTCCAACACTCCG	pACEbac1-6xHis::NMY-2 (1-854) (pAC429)	pACEbac1-6xHis::nmy2 (R781C)(1-854) (pAC476)

Table 3.7 Plasmids used in this study

Plasmid	Source	Reference	Use
Peft-3::Cas9 + Empty sgRNA	Addgene	RRID:Addgene_47549	Expression of CAS-9 and guide RNAs
pCFJ151	Addgene	RRID:Addgene_19330	Generation of MosSCI strains
pCFJ601	Addgene	RRID:Addgene_34874	MosSCI strains co-injection markers
pCFJ90	Addgene	RRID:Addgene_19327	MosSCI strains co-injection markers
pCFJ104	Addgene	RRID:Addgene_19328	MosSCI strains co-injection markers
pGH8	Addgene	RRID:Addgene_19359	MosSCI strains co-injection markers
L4440	Addgene	RRID:Addgene_1654	Plasmid for RNAi by feeding
pCFJ151-Pnmy2 5.2kb::nmy2 reenc::mCherryStreptag::3'nmy2 1.2kb	This study	pAC71	Plasmid for generation of NMY-2::mCherry^{sen} (GCP22)
pACEBac1-6xHis::nmy-2(1-874)_WT	This study	pAC429	Plasmid for Baculovirus expression 6xHis NMY-2 S1
pACEBac1-6xHis::nmy-2(1-874)_S250A	This study	pAC451	Plasmid for Baculovirus

			expression 6xHis NMY-2(S250A) S1
pACEBac1-6xHis::nmy-2(1-874)_S251A	This study	pAC453	Plasmid for Baculovirus expression 6xHis NMY-2(S251A) S1
pACEBac1-6xHis::nmy-2(1-874)_R252A	This study	pAC452	Plasmid for Baculovirus expression 6xHis NMY-2(R252A) S1
pACEBac1-6xHis::nmy-2(1-1354)_WT	This study	pAC514	Plasmid for Baculovirus expression 6xHis NMY-2 HMM
pACEBac1-6xHis::nmy-2(1-1354)_S250A	This study	pAC515	Plasmid for Baculovirus expression 6xHis NMY-2 (S250A) HMM
pACEBac1-6xHis::nmy-2(1-1354)_S251A	This study	pAC516	Plasmid for Baculovirus expression 6xHis NMY-2(S251A) HMM
pACEBac1-6xHis::nmy-2(1-1354)_R252A	This study	pAC517	Plasmid for Baculovirus expression 6xHis NMY-2(R252A) HMM
pACEBac1-StreptagII::mlc-4	This study	pAC437	Plasmid for Baculovirus expression StreptagII

			MLC-4
pACEBac1-StreptagII::mlc-5	This study	pAC438	Plasmid for Baculovirus expression StreptagII MLC-5
pACEBac1-StreptagII::Let-502(1-469)	This study	pAC527	Plasmid for Baculovirus expression StreptagII LET-502(1-469)

Bacmid recombination was performed in DH10EMBacY bacteria (Geneva Biotech) and Sf21 cells were transfected with each of the bacmids using X-tremeGene HP DNA Transfection Reagent (Roche). Virus production was performed as previously described (Bieniossek et al., 2008). For large-scale expression of NMY-2_{S1} or NMY-2_{HMM} complexes, NMY-2_{S1} or NMY-$2_{HMM,}$ MLC-4 and MLC-5 baculoviruses were used to co-infect 500-mL cultures of Sf21 cells (0.8×10^6 cells/ml, SFM4 medium; Hyclone). Cells were harvested by centrifugation at 3000 xg for 5 minutes. Pellets were resuspended in lysis buffer (15 mM MOPS, 300 mM NaCl, 15 mM $MgCl_2$, 0.1 % Tween 20, 1 mM EDTA, 3 mM NaN_3, 1 mM DTT, pH 7.3) supplemented with EDTA-free Complete Protease Inhibitor Cocktail (Roche), sonicated, and incubated for 20 minutes with 1 mM ATP to detach myosin from actin. Lysates were then cleared by centrifugation at 34000 xg for 40 minutes. NMY-2 S1 complexes were purified by batch affinity chromatography using Strep-Tactin Sepharose (IBA). Beads were washed with wash buffer (10 mM MOPS, 500 mM NaCl, 5 mM $MgCl_2$, 0.1 % Tween 20, 1 mM EDTA, 3 mM NaN_3, 1 mM DTT pH 7.3) supplemented with 1 mM ATP in the first wash and eluted on a gravity column with elution buffer (10 mM MOPS, 500 mM NaCl, 2.5 mM Desthiobiotin, 3 mM NaN_3, 1 mM DTT, pH 7.3). S1 complexes were further purified by size-exclusion chromatography using a Superose 6 increase 10/300 column (GE HealthCare) pre-equilibrated with 10 mM MOPS, 500 mM NaCl, 1 mM EDTA, pH 7.3. Fractions containing the NMY-2 S1 complex were pooled and concentrated in 50 MWCO Amicon Ultra-15 Centrifugal Filter Units (Merck-Millipore). NMY-2 HMM complexes were purified by a tandem Strep-Tactin-His tag affinity chromatography approach. The purification in Strep-Tactin Sepharose was similar to that used for NMY-2 S1 complex purification, except that Tween-20 was excluded from the lysis and wash buffers and 10 mM imidazole was added to the

lysis buffer. Eluates from Strep-Tactin affinity chromatography were then incubated with Ni-NTA beads (Thermo Fisher Scientific), washed with wash buffer 2 (10 mM MOPS, 500 mM NaCl, 25 mM imidazole, 3 mM NaN_3, 1 mM DTT) and eluted in elution buffer 2 (10 mM MOPS, 500 mM NaCl, 250 mM imidazole, 3 mM NaN_3, 1 mM DTT, pH 7.3). The eluate was concentrated using 50 MWCO Amicon Ultra-15 Centrifugal Filter Units (Merck-Millipore) and dialysed overnight in low salt buffer (10 mM MOPS, 25 mM KCl, 2 mM $MgCl_2$ 1 mM EDTA, pH 7.3). After dialysis the samples were centrifuged at 2000 xg for 5 minutes and supernatants stored. For both NMY-2 S1 and HMM complexes, glycerol and DTT were added to a final concentration of 10 % (vol/vol) and 1 mM, respectively. Aliquots were flash-frozen in liquid nitrogen and stored at −80 °C.

LET-502(1-469) baculoviruses were used to infect large scale Sf21 cultures and extracted from lysed cells, following similar procedures as described above but using lysis/ wash buffer (50 mM Tris, 150 mM NaCl, 3 mM NaN_3 10 % glycerol, 1 mM DTT) supplemented with EDTA-free Complete Protease Inhibitor Cocktail (Roche). Protein was then purified by batch affinity chromatography using Strep-Tactin Sepharose (IBA). Beads were washed with lysis/wash buffers and eluted on a gravity column with elution buffer 3 (50 mM Tris, 150 mM NaCl, 3 mM NaN_3 10 % glycerol, 2.5 mM Desthiobiotin). Eluates were concentrated in a 10 MWCO Amicon Ultra-15 Centrifugal Filter Units (Merck-Millipore) and dialysed overnight in dialysis buffer 2 (50 mM Tris, 150 mM NaCl, 3 mM NaN_3, 10 % glycerol). Samples were flash frozen and stored at -80 ºC.

3.15 F-actin co-sedimentation assays

In chapter 5: *Wild-type* or mutant NMY-2 S1 complexes were dialysed overnight in actin buffer (5 mM Tris, 0.2 mM $CaCl_2$, 50 mM KCl, 2 mM $MgCl_2$, 1 mM DTT, pH 8). All proteins were pre-cleared by centrifugation at 150000 xg for 1 hour in an Optima XP centrifuge with a TLA-100 rotor (Beckman-Coulter) prior to assay. F-actin was prepared from lyophilized human platelets (Cat. # APHL99 Cytoskeleton Inc.) or rabbit muscle G-actin. Rabbit muscle G-actin was extracted from muscle acetone powder (Sigma M6890) as described in (Sellers, 1998) and lyophilized by freeze-drying after adding 2 mg of sucrose per milligram of G-actin. Lyophilized G-actin was resuspended in water and polymerization was induced by addition of 10x actin polymerization buffer (final concentration: 5 mM Tris, 0.2 mM $CaCl_2$, 50 mM KCl, 2 mM $MgCl_2$, 1 mM ATP) to obtain a 21 µM F-actin stock. F-actin used in each round of co-sedimentation assays was from the same batch and source. For the co-sedimentation

assays in the presence of 1 mM ATP, an equal amount (approximately 2µM) of each variant of NMY-2 S1 complex was incubated with 14.7 µM F-actin (final concentration) or a similar volume of F-actin buffer (negative control), for 30 minutes at room temperature. A similar approach was used for the estimation of the dissociation constant (Kd) by incubating 0.5 µM of each NMY-2 S1 complex with different amounts of actin as indicated in the plots of Figures 2E and 5C. Samples were then centrifuged at 150000 xg for 1.5 hours at room temperature. Supernatants (SI) were carefully removed and Laemmli sample buffer was added to 1x final concentration. Pellets (PI) were resuspended in 30 µL of water and mixed by pipetting every 2 minutes over a period of 10 minutes on ice. Laemmli sample buffer was added to obtain 1x final concentration. To determine the ability of different versions of NMY-2 to detach from F-actin, pellets prepared as above were resuspended in actin polymerization buffer containing 50 mM ATP (without F-actin) over a period of 10 minutes on ice. After 30 minutes of incubation at room temperature, samples were centrifuged at 150000 xg for 1.5 hours at room temperature. Supernatant and pellet fractions (SII, PII) were collected and prepared for loading in gels as described above. After addition of Laemmli sample buffer, all samples were incubated for 4 minutes at 95 ºC to denature proteins and run on 20-4 % TGX gradient precast gels (Bio-Rad) using Tris-Glycine-SDS running buffer. Gels were stained with Blue Safe Coomassie stain (NZYtech) according to manufacturer's instructions (Figure 2C, 2F, 2H, 5A, S2 and S5D). To verify the bands corresponding to NMY-2 S1 fragments, immunoblotting with the mouse His-H8 antibody against the 6xHis tag (1:2500, catalogue #05-949 Merck Millipore) and a goat anti-mouse HRP-conjugated secondary antibody (1:5000, Jackson ImmunoResearch) was performed as described in the immunoblotting section.

3.16 *In vitro* phosphorylation assay

In chapter 5: *In vitro* phosphorylation of MLC-4 was performed according to (Haldeman et al., 2014). Twenty µg of NMY-2 HMM complexes were mixed with 0.5 µM of LET-502(1-469) in phosphorylation buffer (20 mM MOPS, 0.1 mM EGTA, 5 mM $MgCl_2$, 50 mM NaCl and 1 mM $CaCl_2$). The phosphorylation reaction was initiated by adding 2 mM ATP to the mix. The mix was then incubated for 1 hour at 24 ºC. The samples were then precipitated with 3 volumes of acetone at -20 ºC and centrifuged at 15000 xg for 5 minutes. Acetone was removed and protein pellets were resuspended in urea sample buffer (8 M urea, 33 mM Tris-glycine, pH 8.6, 0.17 mM EDTA, 10 mM DTT added immediately before use), to a final

concentration of ~3.3 µg/µL. The whole volume was loaded without prior heating in 4-20 % TGX gradient 10-well precast gels (Bio-Rad) using Tris-Glycine running buffer. Gels were stained with Blue Safe Coomassie stain (NZYtech) according to manufacturer's instructions (Figure 2H).

3.17 *In vitro* motility assay

In chapter 5: *In vitro* motility assays were performed according to (Sellers, 1998). Actin was polymerized from lyophilized G-actin as described for co-sedimentation assays and a 2 µM stock was labelled by incubating F-actin overnight with Rhodamine-phalloidin (1 unit of phalloidin for 100 µL of F-actin; Molecular Probes, Thermo Fisher Scientific) in labelling buffer (10 mM MOPS, 0.1 mM EGTA, 3 mM NaN_3). Motility chambers consisted of a microscopy slide taped to a 18x18 cm No. 1.5H coverslip (Marienfeld, Germany) previously coated with 1 % nitrocellulose (2 % Collodion solution for microscopy, diluted to 1 % with amyl acetate; Sigma-Aldrich). Two pieces of double-sided tape (Tesa) were used to form a ~7 mm-wide channel inside the chamber. NMY-2 HMM complexes at 1 µg/µL in a high salt solution (20 mM MOPS, 0.1 mM EGTA, 5 mM $MgCl_2$, 500 mM NaCl) were flowed into the chamber. BSA solution (20 mM MOPS, 0.1 mM EGTA, 5 mM $MgCl_2$, 500 mM NaCl 1 % BSA) was then flowed to block the sites of the coverslip that did not bind NMY-2. Low salt buffer (20 mM MOPS, 0.1 mM EGTA, 5 mM $MgCl_2$, 50 mM NaCl) was used to remove any excess of unbound BSA. To block myosin dead heads and induce phosphorylation of MLC-4, the chamber was incubated with a solution containing unlabeled actin, LET-502 (1-469) and ATP (20 mM MOPS, 0.1 mM EGTA, 5 mM $MgCl_2$, 50 mM NaCl, 1 mM $CaCl_2$, 0.5 µM LET-502 (1-469), 5 µM unlabelled actin, 1 mM ATP) for four minutes. After washing, labelled F-actin solution (20 nM Rhodamine-phalloidin F-actin, 1 mM DTT, 20 mM MOPS, 0.1 mM EGTA, 5 mM $MgCl_2$, 50 mM NaCl) was flowed into the chamber. Unbound labelled F-actin was removed with low salt buffer and assay buffer added (20 mM MOPS, 0.1 mM EGTA, 5 mM $MgCl_2$, 25 mM KCl, 50 mM DTT, 1 mM ATP and 0.7 % methylcellulose solution). Chambers were imaged at 21 ºC every 2 seconds for 300 seconds total, using the same microscope setup described above and the perfect focus system (Nikon) to maintain focus overtime.

3.18 F-Actin and DNA labelling of body wall muscles and gonads

In chapter 5: Phalloidin labelling of muscle actin shown in Figures 1G and S4C was done in N2 adult animals depleted of UNC-54 or GCP523, GCP565 and GCP619 adult hermaphrodites. Animals were collected and washed twice in M9 buffer, fixed with 4 % paraformaldehyde (20 % aqueous solution, Electron Microscopy Sciences) diluted in 1x cytoskeleton buffer (10 mM MES-KOH, pH 6.1, 138 mM KCl, 3 mM $MgCl_2$, 2 mM EGTA) containing 0.32 M sucrose (Cramer and Mitchison, 1993) for 15 minutes, permeabilized with acetone at -20 ºC for 5 minutes, washed with PBS containing 0.5 % Triton X-100 and 30 mM glycine (PBS-TG) for 10 minutes, and stained with 1:40 Oregon Green-phalloidin (Molecular Probes, Thermo Fisher Scientific) in PBS-TG for 30 minutes. After three 10-minute washes with PBS-TG, animals were mounted with ProLong Antifade containing DAPI (Molecular Probes, Thermo Fisher Scientific). Labelling of gonads shown in Figure 3A was done as described above in N2, GCP513 and GCP623 animals, but only the DAPI-staining of the gonads is shown.

In Figure 4A, DNA labelling of gonads was done in living GCP22, GCP592 and GCP618 adult hermaphrodites depleted of NMY-2::mCherry^{sen}. Animals were transferred to a drop of water containing OP50 bacteria (1:10 dilution of a saturated culture) and 2 mg/mL Hoechst 33342 (Thermo Fisher Scientific) to label DNA and incubated for 1.5 hours. After a recovery period of 30-60 minutes in NGM plates seeded with OP50, animals were anesthetized with levamisole (1 mg/mL, Sigma) and mounted on 2 % agarose pads for imaging.

3.19 Liquid thrashing assays

In chapter 5: For liquid thrashing assays, N2, GCP523, GCP524, GCP565 or GCP619 hermaphrodites were synchronized at the L1 stage by performing alkaline bleach treatment of adult gravid hermaphrodites (0.8% bleach, 250 mM NaOH; Stiernagle, 2006) to extract embryos, which were left to hatch overnight in M9 medium. L1 hermaphrodites were then plated and grown at 20 ºC. Young adult hermaphrodites were transferred to an M9 droplet and left to acclimatize for 2 minutes after which images were acquired at ~40 fps average. Body bends swimming frequencies in Figures 1D, 1F, 5A, S4B were automatically quantified using the wrMTrck plugin with standard parameters (Nussbaum-Krammer et al., 2015) in

ImageJ. Image background was removed by subtracting the average intensity projection of the stack and animals were segmented using Otsu intensity thresholding.

3.20 PIP binding assay

In chapter 6: For the experiments in figure 2, 6xHIS::NMY-2/StreptagII::MLC-4/StreptagII::MLC-5, 6xHIS::NMY-2/StreptagII::MLC-5 and StreptagII::MLC-4 were expressed in Sf21 cells and purified. The purification was done by batch affinity chromatography using streptactin beads (as described in chapter 5 for the purification of HMM or S1 NMY-2 fragments, followed by size exclusion chromatography purification (as described for NMY-2 S1 fragments in chapter 5). Protein sizes were confirmed by SDS-PAGE coomassie staining and immunoblot with specific antibodies. For detection of 6xHIS::NMY-2/StreptagII::MLC-4/StreptagII::MLC-5, a mouse anti-6x Histidine tag antibody (clone HIS.H8 Millipore) was used at 1:2,500 as primary antibody and an HRP-conjugated anti-mouse antibody was used at 1:5,000 as secondary antibody. For detection of MLC-4, Strep-Tactin®-HRP conjugate was used at 1:100,000.PIP membranes were blocked with 10 mL of blocking buffer (PBS-T: PBS, 0.1% v/v Tween-20, supplemented with 3 % BSA) for one hour at room temperature (RT). Then, the protein(s) of interest was/were added to the PIP strip membranes: 0.5 µg/mL PI(4,5)P2 Grip™ (catalog G-4501) protein, 1 µg/mL of NMY-2/MLC-4/MLC-5, or 1 µg/mL of NMY-2/MLC-5 or 1 µg/mL of MLC-4, in 5 mL PBS-T 3% BSA. The membrane was incubated for one hour at room temperature with gentle agitation. Next, the protein solution was discarded, and the PIP strips were washed three times, with gentle agitation, in 5 mL PBS-T for 5 minutes. The following primary antibodies were diluted in PBS-T+3% BSA blocking solution: for the detection of GST-tagged PI(4,5)P2 Grip™, a rabbit anti-GST antibody was used at 1:5,000; for the detection of 6xHIS::NMY-2/StreptagII::MLC-4/StreptagII::MLC-5, a mouse anti-6x Histidine tag antibody (clone HIS.H8 Millipore) was used at 1:2,500. For MLC-4, Strep-Tactin®-HRP conjugate was used at 1:100,000. The membranes were incubated with the primary antibodies for one hour at room temperature with gentle agitation, washed, and then incubated with the following secondary antibody diluted in PBS-T + 3% BSA : for PI(4,5)P2 Grip™ an HRP-conjugated anti-rabbit-antibody was used at 1:5,000 for 6xHIS::NMY-2/StreptagII::MLC-4/StreptagII::MLC-5 and 6xHIS::NMY-2/StreptagII::MLC-5 an HRP-conjugated anti-mouse antibody was used at 1:5,000. The membranes were incubated for one hour at RT with gentle agitation. Finally, after washing, the bound protein was detected by

chemiluminescence using Pierce ECL Western Blotting Substrate (Thermo Fisher Scientific) and imaged in a ChemiDoc™ XRS+ System with Image Lab™ Software (Bio-Rad).

3.21 Statistical Analysis

Graph plotting, linear regressions, and statistical analyses were performed with Prism 6 or 7 (GraphPad Software). All error bars represent the 95% CI of the mean and statistical significance tests were performed using a student t-test or one-way ANOVA with Bonferroni correction, as indicated in figure legends.

CHAPTER 4

EXPLORING THE CONTRIBUTION OF SEVERAL MYOSINS TO EMBRYONIC CYTOKINESIS

4. EXPLORING THE CONTRIBUTION OF SEVERAL MYOSINS TO EMBRYONIC CYTOKINESIS

4.1 Introduction

Actomyosin networks comprising F-actin, class II myosin motors and their regulators mediate essential cellular mechanical processes like cell division, cell migration, cell adhesion, tissue morphogenesis, and muscle contraction (Munjal & Lecuit, 2014; Taylor & Weeds, 1976; Marston & Taylor, 1980; Smith & White, 1985; Chen, 2007; Even-Ram et al., 2007). In most non-muscle cells, contractility-dependent events require NMII motors that assemble into bipolar filaments capable of producing tension and generating force for actin filament sliding (Vicente-Manzanares et al., 2009). In human cells, NMII-mediated contractility requires the formation of bipolar myosin filaments that assemble after phosphorylation of the RLC threonine 18 and serine 19, which promotes NMII HC tail-to-tail interactions (Suzuki et al., 1978; Ikebe & Hartshorne, 1985; Trybus, 1989). These regulatory sites of phosphorylation are well conserved in different species (Dean & Spudich, 2006; Uehara et al., 2008; Hosoba et al., 2015). However, this paradigm is evolving, as isolated NMII hexamers (HC dimer bound to a pair of RLCs and a pair of ELCs with phosphorylated RLC) were recently isolated from cultured cells (Shutova et al., 2014). Moreover, NMIIA, NMIIB, and NMIIC are able to form heterotypic filaments through the tail *in vitro*, and these heterotypic filaments of NMIIA and NMIIB were observed in mammalian cells (Shutova et al., 2014; Beach et al., 2014; Beach & Hammer, 2015). In addition, NMIIA can form filaments with a myosin from class XVIII, both *in vitro* and in human cells (Billington et al., 2015). Myosin XVIII is a class of unconventional myosins that has not been described in *C. elegans*. Mammalian Myosin XVIIIA (MYO18A) is expressed in hematopoietic cells, in the vicinity of the Golgi, and mature macrophages (Furusawa et al., 2000; Mori et al., 2003; Mori et al., 2005; Cross et al., 2004), and is required for zebrafish embryonic muscle integrity (Cao et al., 2004). Myosin XVIIIB (MYO18B) is important for sarcomere assembly in the human striated muscle (Salamon et al., 2003). In osteosarcoma cells, it localizes in stress fibers where it is responsible for assembling NMII stacks (Jiu et al., 2019). NMII stacking occurs in human cells and is required for contractility to occur during cytokinesis (Fenix et al., 2016).

One of the fascinating cellular processes that depend on actomyosin contractility is cytokinesis. Constriction of the contractile ring during cytokinesis was previously thought to be solely dependent on NMII but it has recently been shown to depend also on other types

of myosins in fission yeast (Zambon et al., 2017; Laplante & Pollard, 2017; Laplante et al., 2015; Palani et al., 2017).

The contribution of mixed populations of myosin molecules likely contributes to the functional plasticity of non-muscle myosin motors and their involvement in disease. In this chapter, I analysed the consequences of depleting the different myosin HCs in embryonic viability and cytokinesis in the one-cell embryo.

In *C. elegans* depletion of NMY-2, one of the NMII HCs, leads to defects in cellularization in the oocyte-producing gonad, cytokinesis failure, and elongation defects during embryogenesis (Piekny, 2003; Liu et al., 2010; Green et al., 2011; Cuenca et al., 2003; Davies et al., 2014; Guo & Kemphues, 1996). During embryonic cytokinesis and in the gonads, NMY-2 is in a complex with the RLC MLC-4, and the ELC MLC-5 (Shelton et al., 1999; Gally et al., 2009; Ono & Ono, 2016). The second *C. elegans* NMII heavy chain, NMY-1, is thought to act together with MLC-4 to maintain the spermatheca structure and function (Kovacevic et al., 2013). These results suggest that MLC-4 might not be a specific binding partner of NMY-2 (Wirshing & Cram, 2017). The third NMII heavy chain in *C. elegans* is NMY-3, whose depletion does not affect embryo production, animal survival or animal morphology (Kamath, 2003; Sönnichsen et al., 2005).

Seventeen myosin HCs exist in *C. elegans*, but besides NMY-2, there is no information about their function during cytokinesis. Previous studies suggest that Myosin heavy chain 1 (MYO-1), Myosin heavy chain 2 (MYO-2), MYO-3, and Uncoordinated 54 (UNC-54) are conventional muscle myosins (Ardizzi & Epstein, 1987; Walker et al., 2002). MYO-1 and MYO-2 are expressed in the animal's pharynx indicating a role during food pumping (Ardizzi & Epstein, 1987; Walker et al., 2002). Genome-wide screens show that MYO-1 is required for embryo production and viability (Simmer et al., 2003; Sönnichsen et al., 2005). No functions are described for MYO-2, but its depletion does not interfere with embryo production, embryonic viability or lead to detectable morphological problems (Maeda et al., 2001; Sönnichsen et al., 2005). MYO-3 and UNC-54 localize at the gonadal contractile sheath cells, body wall, anal-intestine, and sex muscle cells (Ono & Ono, 2016; Ardizzi & Epstein, 1987). MYO-3 mutants show some embryonic lethality, larval arrest, body muscle displacement and body wall muscle disorganization (Waterston, 1989; Williams & Waterston, 1994; Martin et al., 2002; Kamath, 2003). MYO-3 depletion also leads to sterility (Kamath, 2003). UNC-54 perturbation leads to body wall muscle disorganization, highly impaired movement, and embryo accumulation inside the animal's body (Trent et al., 1983; Brenner, 1974; Park & Horvitz, 1986; Timmons et al., 2001; Fire et al., 1991; Arribere et al.,

2014; Dixon & Roy, 2005). Myosin heavy chain 5 (MYO-5) and Myosin heavy chain 6 (MYO-6) functions are not described yet but large RNAi screens show no defects as sterility, lethality or morphology (Kamath, 2003; Sönnichsen et al., 2005). Class I myosins include heavy chain unconventional myosin 1 (HUM-1) and HUM-5, and the only member of class V is HUM- 2. The localization or function of these three myosins remains unknown but their depletion does not generate sterile worms, the embryos are fully viable, and the animals are apparently normal (Maeda et al., 2001; Kamath, 2003; Sönnichsen et al., 2005). Heavy chain unconventional myosin 8 (HUM-8) and SPE-15 form the class VI in *C. elegans*. HUM-8 depletion leads to embryonic lethality, defects in germline morphology and reduced brood size (Skop et al., 2004). *Spe-15* mutants or SPE-15 depleted animals display several phenotypes such as sterility, abnormal spermatogenesis, reduced brood size, and embryonic lethality (L'Hernault et al., 1988; Ceron et al., 2007; Hu et al., 2019). There are no studies concerning HUM-6 function, the single myosin of Class VII. However large RNAi screens show that HUM-6 is not essential for embryo production, animal survival or normal morphology (Kamath, 2003; Sönnichsen et al., 2005). The single member of class IX, HUM-7, localizes in body wall muscle cells and pharynx (Wallace et al., 2018). *Hum-7* mutants or animals depleted of HUM-7 present abnormal neuronal migration, arrest during embryonic development, reduced F-actin levels in epidermal cell migration during embryonic morphogenesis, and embryonic lethality (Wallace et al., 2018). In epidermal cells, together with the axonal guidance receptor Sensory axon guidance 3 (SAX-3) and RHO-A, HUM-7 regulates NMY-2 levels and localization patterns (Wallace et al., 2018). HUM-4 is the only myosin belonging to the class XII of the myosin superfamily but no data on its function are available.

In this chapter I further explored the NMY-2 roles during cytokinesis by taking advantage of a temperature-sensitive mutant and RNAi depletions. I then assessed whether other myosin HCs cooperate with NMY-2 in this process.

4.2 Results

4.2.1 NMY 2/MLC-4/MLC-5 depletion by RNAi leads to cytokinesis failure

To understand the role of NMY-2 in the embryos, I filmed the first embryonic cytokinesis of control and NMY-2 depleted embryos expressing NMY-2::GFP, mCherry::PH (PH is a domain from mammalian phospholipase C, PLC1δ1, which binds to plasma membrane PIP2

(Audhya et al., 2005), and mCherry::HIS-58, a fluorescently-tagged histone 2B to label the chromatin (Figure 4.1). As NMY-2 is important for gonad function, I depleted NMY-2 after the gonad had been fully formed (Late L4 stage) and looked at embryos while the gonad was still capable of producing oocytes that could be fertilized in the spermatheca. In control embryos that were not subject to RNAi treatment, NMY-2 localized in the cytoplasm, spindle, cell cortex, and was enriched in the contractile ring (Figure 4.1 top panel). I measured the time between anaphase onset (when chromatids segregate to opposing sides of the cell) to the end of cytokinesis when two daughter cells can be observed. Control embryos took on average 237±18 seconds to complete cytokinesis. When NMY-2 was depleted, the contractile ring was not able to form, and consequently, cytokinesis failed. Significantly reduced signal of NMY-2::GFP was detected indicating that the RNAi depletion was effective (Figure 4.1 bottom panel).

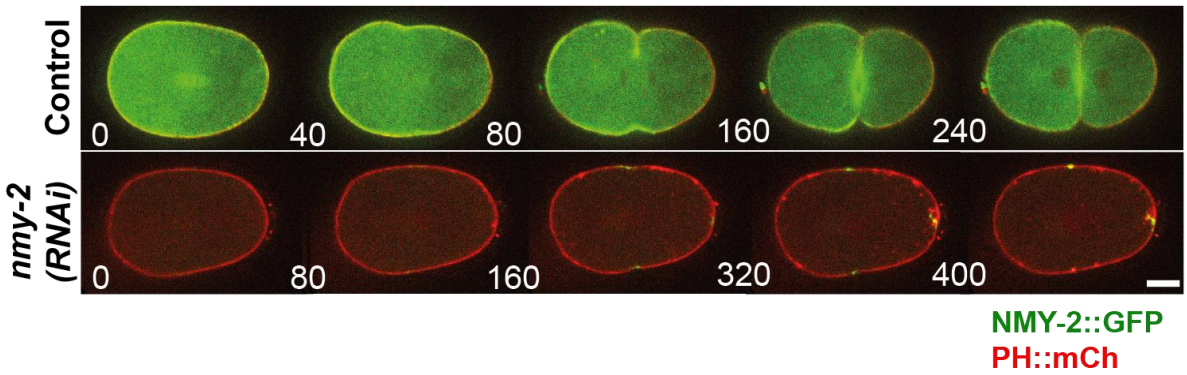

Figure 4.1 Embryos depleted of NMY-2 do not undergo cytokinesis. Central plane of *C. elegans* one-cell embryos expressing NMY-2::GFP (green) and PH::mCherry (red) undergoing cytokinesis. On the top row a control embryo undergoes cytokinesis successfully. On the bottom row, an NMY-2 depleted embryo did not form a contractile ring and failed cytokinesis. Times in the stills correspond to time after anaphase onset in seconds. Scale bar: 10µm.

Then, I assessed the effects of depleting the LCs MLC-4 and MLC-5 during cytokinesis. In Control embryos expressing NMY-2::GFP not treated with RNAi the contractile ring formed at the cell equator and cytokinesis successfully completed (Figure 4.2 top panel). Similar to NMY-2 depleted embryos, MLC-4 and MLC-5 depleted embryos did not form a contractile ring and failed cytokinesis. Interestingly, both depletions led to the appearance of NMY-2::GFP puncta, especially in the cytoplasm (Figure 4.2 middle and bottom panels). These results show that both MLC-4 and MLC-5 are essential for cytokinesis and required to properly localize NMY-2 during cytokinesis.

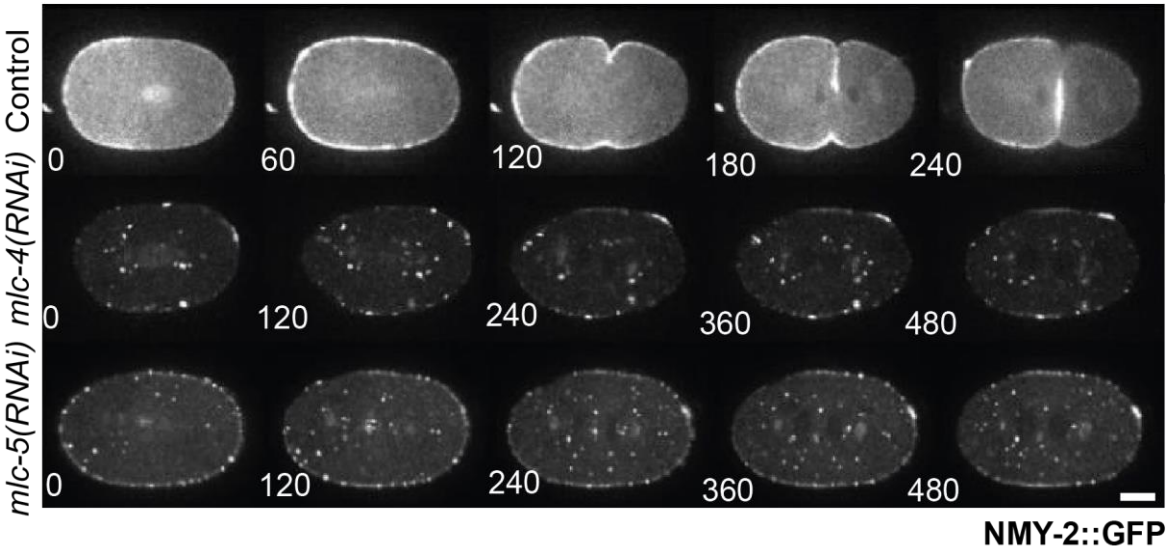

Figure 4.2 Embryos depleted of MLC-4 or MLC-5 do not undergo cytokinesis. Central plane of one-cell embryos is shown. The top row shows a control embryo in which a contractile ring forms at the cell equator, then it constricts and completes cytokinesis successfully. In MLC-4 and MLC-5 depleted embryos NMY-2 localizes in puncta, the contractile ring does not form, and cytokinesis does not occur. Numbers on stills correspond to time from anaphase onset in seconds. Scale bar: 10 µm.

4.2.2 NMY 2 inactivation at different stages of cytokinesis reveals that NMY 2 is essential during all stages of cytokinesis.

NMY-2 is required for processes such as polarity establishment that precede cytokinesis (Ou et al., 2010; Munro et al., 2004; Marston & Goldstein, 2006; Cuenca et al., 2003; Guo & Kemphues, 1996; Liu et al., 2010). Therefore, it is possible that the severe phenotype I described above may be the result of affecting other processes besides cytokinesis. In addition, furrow ingression does not occur and therefore it does not allow us to understand whether NMY-2 is necessary during ring constriction. In order to test the implications of perturbing NMY-2 specifically during cytokinesis, I used an NMY-2 temperature-sensitive (ts) mutant (*nmy-2(ne3409)*), in which the leucine 981 was mutated to a proline (Liu et al., 2010).

To quantitatively analyze the consequences of inactivating myosin at defined stages of cytokinesis, *nmy-2(ne3409)* embryos were submitted to a rapid temperature upshift from the permissive temperature (16 ºC) to the restrictive temperature (26 ºC) during different cytokinesis stages: i) between anaphase onset and the formation of a shallow equatorial deformation, the first indication of assembly of a competent ring (hereafter this time interval is referred to as ring assembly), ii) between shallow deformation and the folding of the plasma membrane in a back-to-back configuration (hereafter this time interval is designated

as furrow initiation), and iii) between back-to-back membrane configuration and 50% of furrow ingression. In all three stages, I observed that NMY-2 inactivation caused cytokinesis to practically stall (Figure 4.3A). When a rapid transition to the restrictive temperature was performed at stage i), the embryos did not initiate furrowing. When done at stages ii) or iii) in which cases furrow ingression had already initiated, the rate of ring constriction decreased to a negligible value (0.024±0.005 µm/s *versus* 0.20±0.01 µm/s in controls) (Figure 4.3A, B) and was always followed by regression.

Together, these results indicate that rapid inactivation of NMY-2 stalls cytokinesis progression even when the contractile ring has already formed and is undergoing constriction suggesting that NMY-2 is required for the normal pace of cytokinesis and that it is absolutely required throughout cytokinesis.

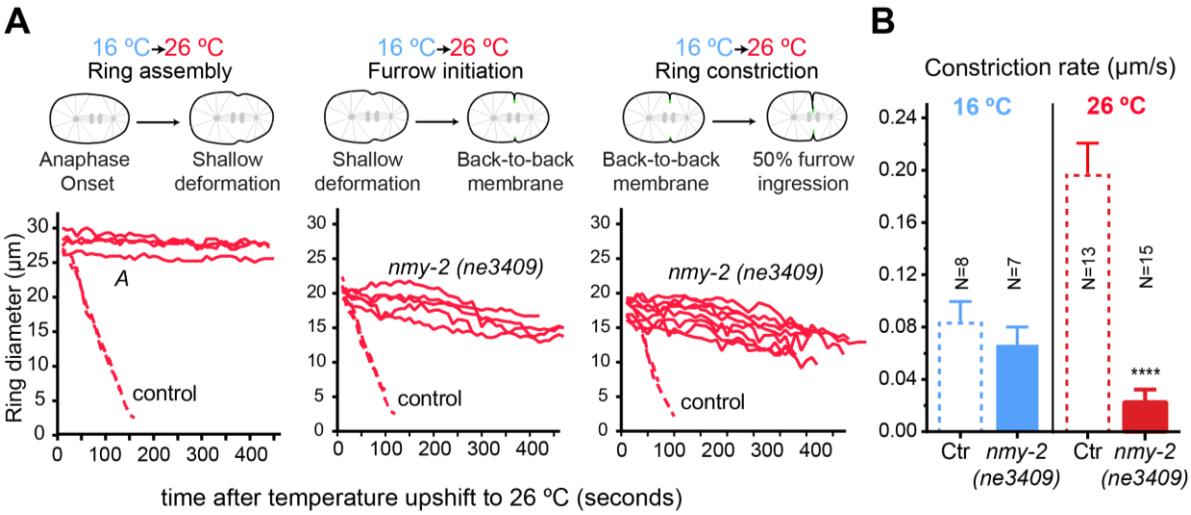

C

	control	*nmy-2(ne3409)*
16 ºC	NMII functional	NMII functional
26 ºC	NMII functional	NMII NOT functional

Figure 4.3 NMY-2 inactivation stalls cytokinesis progression (A) Contractile ring diameter over time in dividing control and *nmy-2(ne3409)* one-cell embryos. Temperature is upshifted from 16 ºC (permissive temperature) to 26 ºC (restrictive temperature) during ring assembly (left), furrow initiation (center), or ring constriction (right). (B) Ring constriction rate of control and *nmy-2(ne3409)* embryos when maintained at 16 ºC or upshifted to 26 ºC during furrow initiation or constriction. (C) Summary of the temperatures used and how NMY-2 functionality is affected. N corresponds to the number of one-cell embryos analysed. Error bars CI 95%;

Statistical significance was determined using t-test. p values **** p<0.00001.

4.2.3 Progressive depletion of NMY 2 by RNAi reveals that only a substantial decrease in its levels in the contractile ring affect cytokinesis kinetics

In order to understand the progression of the NMY-2 phenotype and how it affects cytokinesis, I conducted a time-course RNAi experiment to achieve a range of NMY-2 depletion levels. This was done in a strain expressing NMY-2::GFP from the endogenous locus, at physiological levels (Dickinson et al., 2013) to allow for the accurate assessment of NMY-2 levels in the contractile ring. Only one-cell embryos that completed cytokinesis were analyzed.

In control embryos, cortical NMY-2 is present throughout cytokinesis. When imaging the cortical layer of the embryo, NMY-2 is seen in patches that appear in the entire cortex after anaphase onset. NMY-2 then accumulates at the equatorial region before furrow ingression. When looking at the central plane of the embryo, NMY-2 is enriched at the tip of the furrow during furrow ingression.

To assess the degree of NMY-2 depletion in the RNAi time-course experiment, NMY-2::GFP levels were measured at the furrow tip at 50% constriction (Figure 4.4A'). The levels of NMY-2:GFP in control contractile rings varied between 60 to 150% when normalized to the average of all controls, which suggested that embryos can generally present a range of myosin levels (Figure 4.4B). The progressive reduction of NMY-2 levels was clearly observed both at the cell cortex and at the tip of the ingressing furrow (Figure 4.4B-D). Interestingly, as overall levels of NMY-2::GFP decreased, all the remaining NMY-2::GFP localized at the cell equator at the time of furrow initiation. Surprisingly, substantial impairment in both ring assembly and constriction only occurred when NMY-2::GFP levels were reduced below 20% of the average control myosin levels (Figure 4.4D-F). In the 0-20% NMY-2::GFP intensity interval, the average assembly time was 201±43 s (~2.7-fold increase when compared to controls), the furrow initiation time was 118±18 s (~2-fold increase when compared to controls), and the constriction rate was 0.13±0.01 μm/s (~25% reduction relative to controls) (Figure 4.4E).

In sum, the results suggest that although NMY-2 is essential for cytokinesis, the contractile ring is quite robust to reductions in NMY-2 levels, as embryos with a ~10-fold reduction in NMY-2 levels in the ring still manage to complete cytokinesis. Below a 20% threshold of NMY-2 in the ring, all stages of cytokinesis are substantially prolonged, showing again that

myosin is required for both ring assembly and constriction. The fact that only embryos with very low levels of NMY-2 left present cytokinesis delays may suggest that other myosins besides NMY-2 also contribute to cytokinesis allowing embryos to divide.

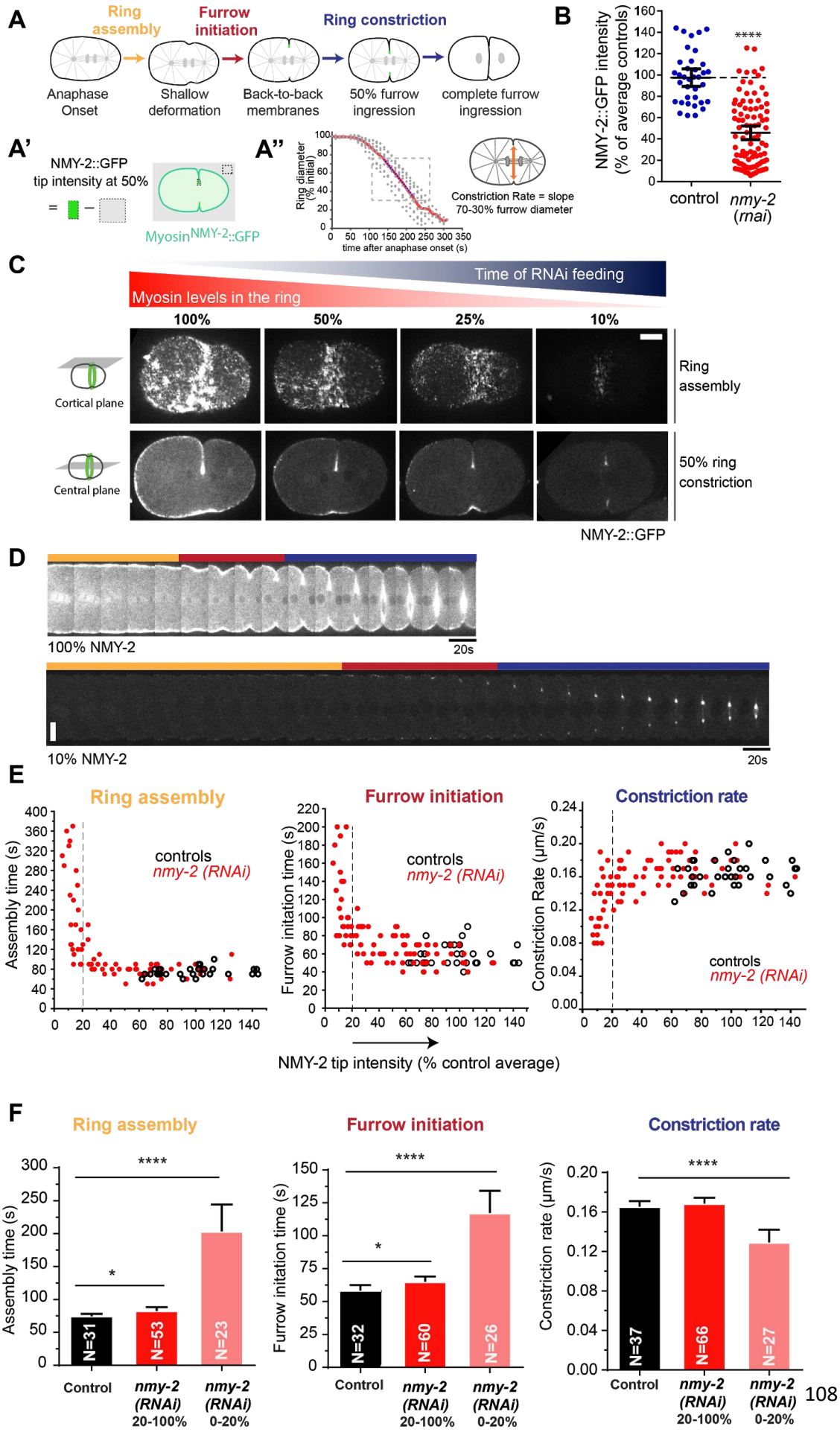
A
Ring assembly
Furrow initiation
Ring constriction
Anaphase Onset
Shallow deformation
Back-to-back membranes
50% furrow ingression
complete furrow ingression
A'
NMY-2::GFP tip intensity at 50%
MyosinNMY-2::GFP
A''
Ring diameter (% initial)
time after anaphase onset (s)
Constriction Rate = slope 70-30% furrow diameter
B
NMY-2::GFP intensity (% of average controls)
****
control
nmy-2 (rnai)
C
Time of RNAi feeding
Myosin levels in the ring
100%
50%
25%
10%
Cortical plane
Central plane
Ring assembly
50% ring constriction
NMY-2::GFP
D
100% NMY-2
20s
10% NMY-2
20s
E
Ring assembly
Furrow initiation
Constriction rate
Assembly time (s)
Furrow initation time (s)
Constriction Rate (µm/s)
controls
nmy-2 (RNAi)
NMY-2 tip intensity (% control average)
F
Ring assembly
Furrow initiation
Constriction rate
Assembly time (s)
Furrow initation time (s)
Constriction rate (µm/s)
****
*
N=31
N=53
N=23
N=32
N=60
N=26
N=37
N=66
N=27
Control
nmy-2 (RNAi) 20-100%
nmy-2 (RNAi) 0-20%

Figure 4.4 Embryos substantially depleted of NMY-2 complete cytokinesis. A) Cytokinesis can be divided into three stages. A´) Mean fluorescence intensity of NMY-2::GFP levels were measured at the furrow tip at 50% constriction like indicated. The camera background was subtracted. A´´) Constriction Rate was measured in the linear phase of constriction, by linear regression within 70 to 30 % of furrow ingression. B) NMY-2::GFP levels were normalized to control average. Control levels had a variation between 60 and 150% of NMY-2::GFP, while NMY-2 depleted embryos varied between 10% and 120%. C) Cortical and central views of embryos expressing different NMY-2::GFP levels at the furrow tip. D) Kymograph of the cleavage furrow region in embryos expressing 100% and 10% of NMY-2. In both cases, cytokinesis completes. E) Dot plots of ring assembly, furrow initiation, and constriction rate against the NMY-2::GFP levels in the tip of the contractile ring. Prolonged intervals were observed for NMY-2::GFP levels below 20%. F) Quantitative measurements of ring assembly, furrow initiation, and constriction rate show that all stages are affected in embryos that have less than 20% of NMY-2::GFP in the contractile ring. N corresponds to the analysed number of one-cell embryos undergoing cytokinesis. Error bars: CI 95%; Statistical significance was determined using t-test and by one-way ANOVA followed by Bonferroni's multiple comparison test. p values * p<0.01, **** p<0.00001.

4.2.4 NMY-1 does not worsen the cytokinesis phenotype of NMY 2 semi-inactivation

Given the results above, I investigated whether NMY-1, the other major NMII in *C. elegans,* could cooperate with NMY-2 during cytokinesis. To do that, I performed penetrant RNAi depletion of NMY-1 and observed what happens during cytokinesis. At this degree of depletion some worms were already sterile suggesting that the RNAi was efficient. The levels and pattern of localization of NMY-2::GFP were normal in NMY-1 depleted embryos and these completed cytokinesis similar to controls (Figure 4.5).

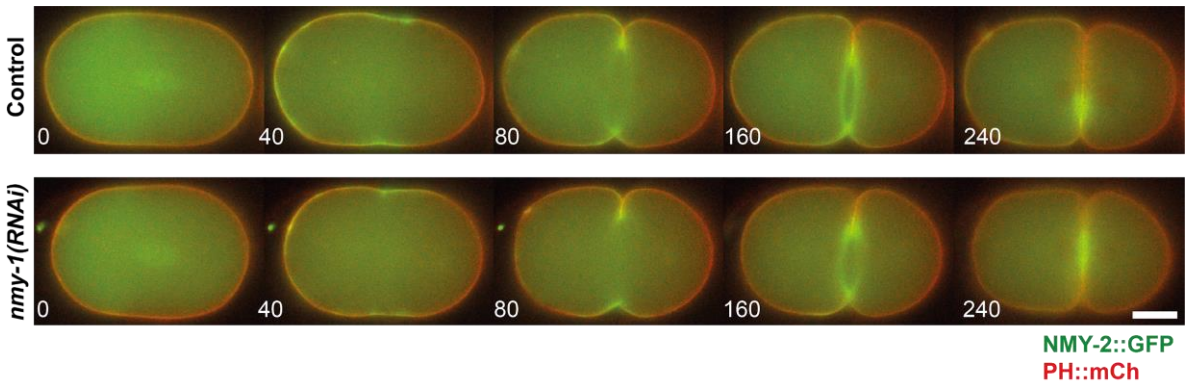

Figure 4.5 NMY-1 is not essential for cytokinesis. Control embryos expressing NMY-2::GFP and PH::mCherry form the contractile ring at the cell equator and complete cytokinesis 240 seconds after anaphase onset. Embryos depleted of NMY-1 display a similar behaviour. Numbers on stills correspond to time from anaphase onset in seconds. Scale bar:10 µm.

This result shows that in contrast to NMY-2, NMY-1 is not essential for successful cytokinesis. However, this does not exclude the possibility that NMY-1 may contribute to cytokinesis, since in NMY-1 depleted embryos, NMY-2 remains functional and might compensate for NMY-1. For this reason, I further investigated the role of NMY-1 during cytokinesis in the *nmy-2* temperature-sensitive mutant *nmy-2(ne3409)*. In this experiment, the temperature was up-shifted to a semi-restrictive temperature (24 ºC) that corresponds to a situation of NMY-2 partial inactivation, in which one-cell embryos slow down but do not fail cytokinesis (Figure 4.6A). *nmy-2(ne3409)* animals were depleted of NMY-1 while kept at the permissive temperature. NMY-2 was then partially inactivated at anaphase onset (Figure 4.6). I observed that in these conditions cytokinesis did not fail, and the time intervals were similar to those in embryos with NMY-2 partially inactivated that had not been depleted of NMY-1 (Figure 4.6A and 4.6B).

These results suggest that NMY-1 does not have a role during early embryonic cytokinesis, and it does not cooperate with NMY-2 in this cellular context.

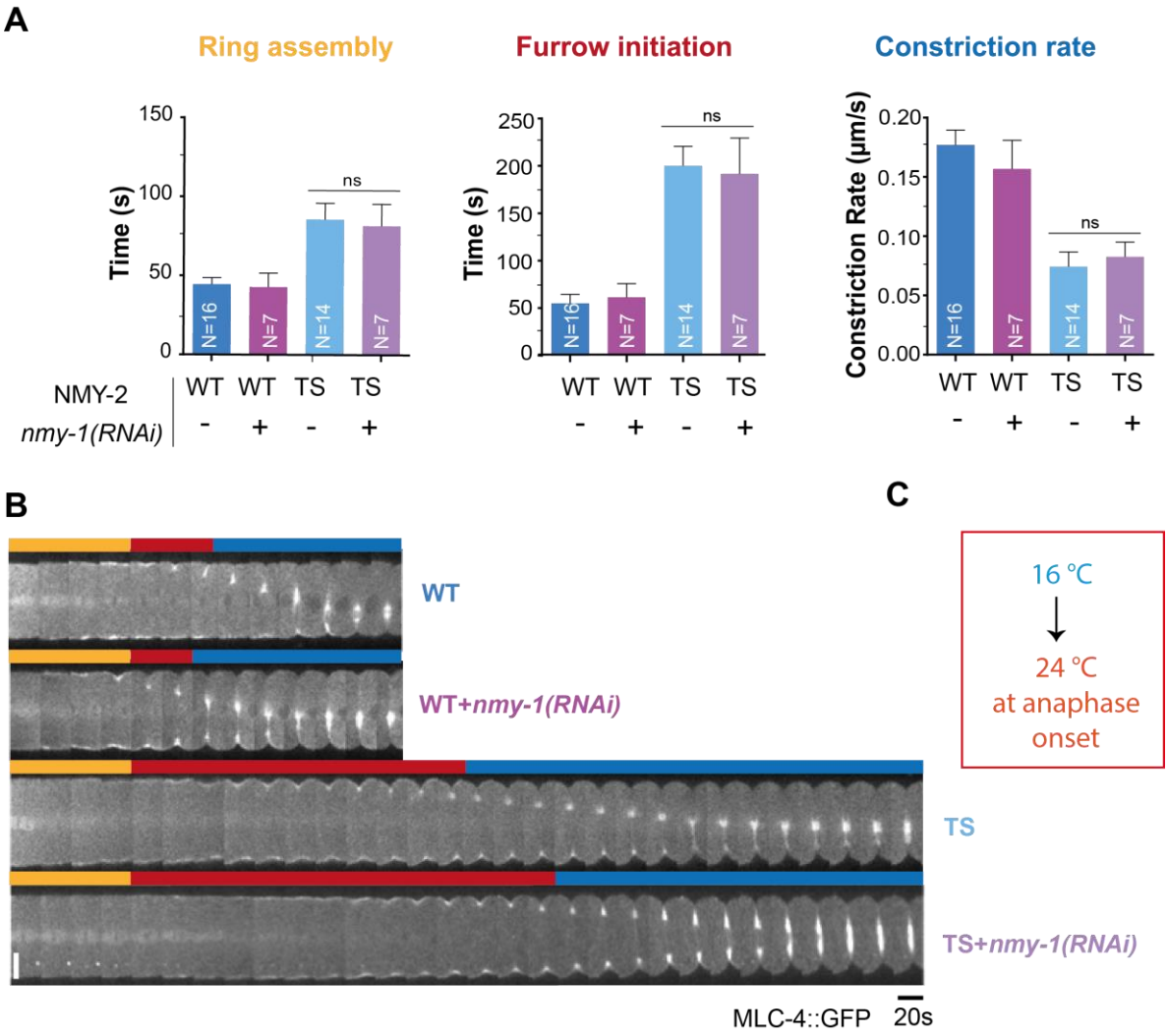

Figure 4.6 NMY-1 depletion does not enhance the NMY-2 depletion phenotype. A) Quantitative analysis shows that cytokinesis kinetics are similar when NMY-1 is depleted in both *wild-type* (WT) and *nmy2(ne3409)* (TS) backgrounds. B) Kymographs of the cleavage furrow region of representative examples of *wild-type* embryos (WT), *wild-type* embryos depleted of NMY-1 (WT+*nmy-1(RNAi)*), *nmy-2(ne3409)* embryos (TS), and *nmy-2(ne3409)* embryos depleted of NMYT-1 /TS+*nmy-1(RNAi)*), showing that cytokinesis takes the same time to complete with or without NMY-1. C) Embryos expressing MLC-4::GFP in *wild-type* and *nmy2(ne3409)*backgrounds were imaged at 16ºC until anaphase onset, time at which the temperature was changed to 24ºC to partially inactivate NMY-2. The color bars correspond to the contractile ring assembly (yellow); the furrow initiation (red) and constriction (blue) stages. N corresponds to the analysed number of one-cell embryos undergoing cytokinesis. Error bars: CI 95%; Statistical significance was determined using one-way ANOVA followed by Bonferroni's multiple comparison test. ns means no-significance. Scale bar: 10 µm.

4.2.5 Exploring the possibility that other myosins assist NMY 2 during embryogenesis and cytokinesis

4.2.5.1 There are 17 myosin heavy chains annotated in the C. elegans genome

In order to examine the involvement of other myosins in *C. elegans* cytokinesis I first did an *in silico* analysis of the *C. elegans* myosin genes. I based my analysis on proteins annotated as myosin in the WormBase (https://wormbase.org//) and on a previous report from Odronitz & Kollmar, 2007, in which the authors manually annotated the myosins of several species to elaborate an eukaryotic tree of life (Odronitz & Kollmar, 2007). I established a list of 22 putative myosins listed in Table 4.1. Note that since the beginning of this study several details have been updated: 1) HUM-3 is now SPE-15; 2) HUM-9 is now NMY-3; 3) R102.5 is now ALLO-1(Allophagy-defective 1), and is not annotated as myosin anymore; 4) F28D1.2 is now ATZ-1 (Abnormal transition zone 1); 5) C18C4.5 is now merged with C18C4.7 and 6) F59A2.2 is now merged with F59A2.6 that is annotated as GOLG-4 (Golgi associated coiled-coil protein homolog 4).

Accession Number	Protein Name	Myosin class
F52B10.1	NMY-1	II
F20G4.3	NMY-2	II
Y11D7A.14	NMY-3/HUM-9	II/ XVIIIA
R06C7.10	MYO-1	II
T18D3.4	MYO-2	II
K12F2.1	MYO-3	II
F58G4.1	MYO-5	II
F45G2.2	MYO-6	II
F11C3.3	UNC-54	II
F29D10.4	HUM-1	I

F36D4.3	HUM-2	V
F47G6.4	SPE-15/HUM-3	VI
F46C3.3	HUM-4	XII
T02C12.1	HUM-5	I
T10H10.1	HUM-6	VII
F56A6.2	HUM-7	IX
Y66H1A.6	HUM-8	VI
F43C9.3	HUM-10	-
R102.5	ALLO-1	-
F28D1.2	ATZ-1	-
C18C4.5 (now merged with C18C4.7)	--	II
F59A2.2 (now merged with F59A2.6)	GOLG-4	-

Table 4.1 Data from WormBase on predicted myosins in *C. elegans.* The first row indicates the accession number for each protein, the second row corresponds to the sequence name and the third indicates the myosin class described in the Wormbase.

To validate this list of candidate myosins I performed multiple sequence analysis to look for the conservation of key elements of the myosin HC head domain. These are essential for the actin-binding, ATPase function and are generally conserved: A-loop, P-loop, Switch I, Switch II, Relay helix, SH1 helix and Converter domain (Chinthalapudi et al., 2017); see section 1.5.1 in the introduction and Figure 4.7). In order to identify these elements, I started by aligning the NMY-2 sequence with that of chicken muscle myosin, whose three-dimensional structure has been determined by crystallography (Rayment et al., 1993), Figure 4.7).

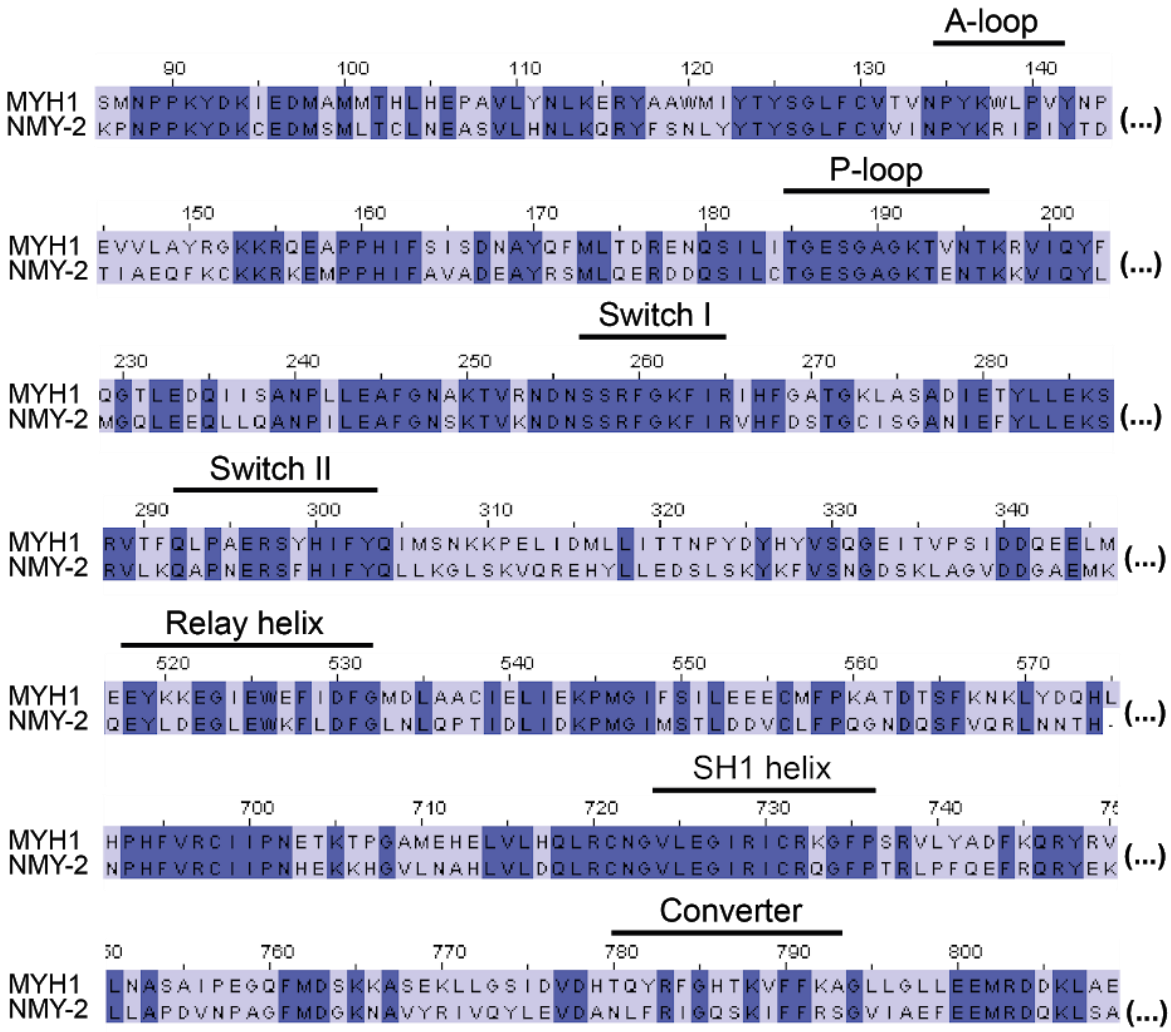

Figure 4.7 Motor domain alignment of *G. gallus* MYH1 (MYSS) and *C. elegans* NMY-2 shows high similarity. A-loop, P-loop, Switch I, Switch II, Relay helix, SH1 helix and Converter are indicated. Alignment in Jalview software using the MUSCLE multiple alignment method with default settings. Dark blue and light blue represent amino acids with higher or lower % of identity, respectively.

Then, I aligned the sequences of all the *C. elegans* myosins with that of NMY-2 and looked for the aforementioned sequence elements. Most putative myosins displayed a high degree of sequence conservation in these regions (Figure 4.8). However, this was not the case for heavy chain unconventional myosin 10 (HUM-10), ALLO-1, ATZ-1, C18C4.7 and GOLG-4 indicating these are probably not myosins. The overall amino acid identity is low, and the key motifs seem to be absent. The remainder myosins presented a high similarity between

the A-loop, P-loop, Switch I, Switch II, Relay helix, SH1 helix and Converter domain, strongly suggesting that these proteins are likely able to bind and translocate F-actin.

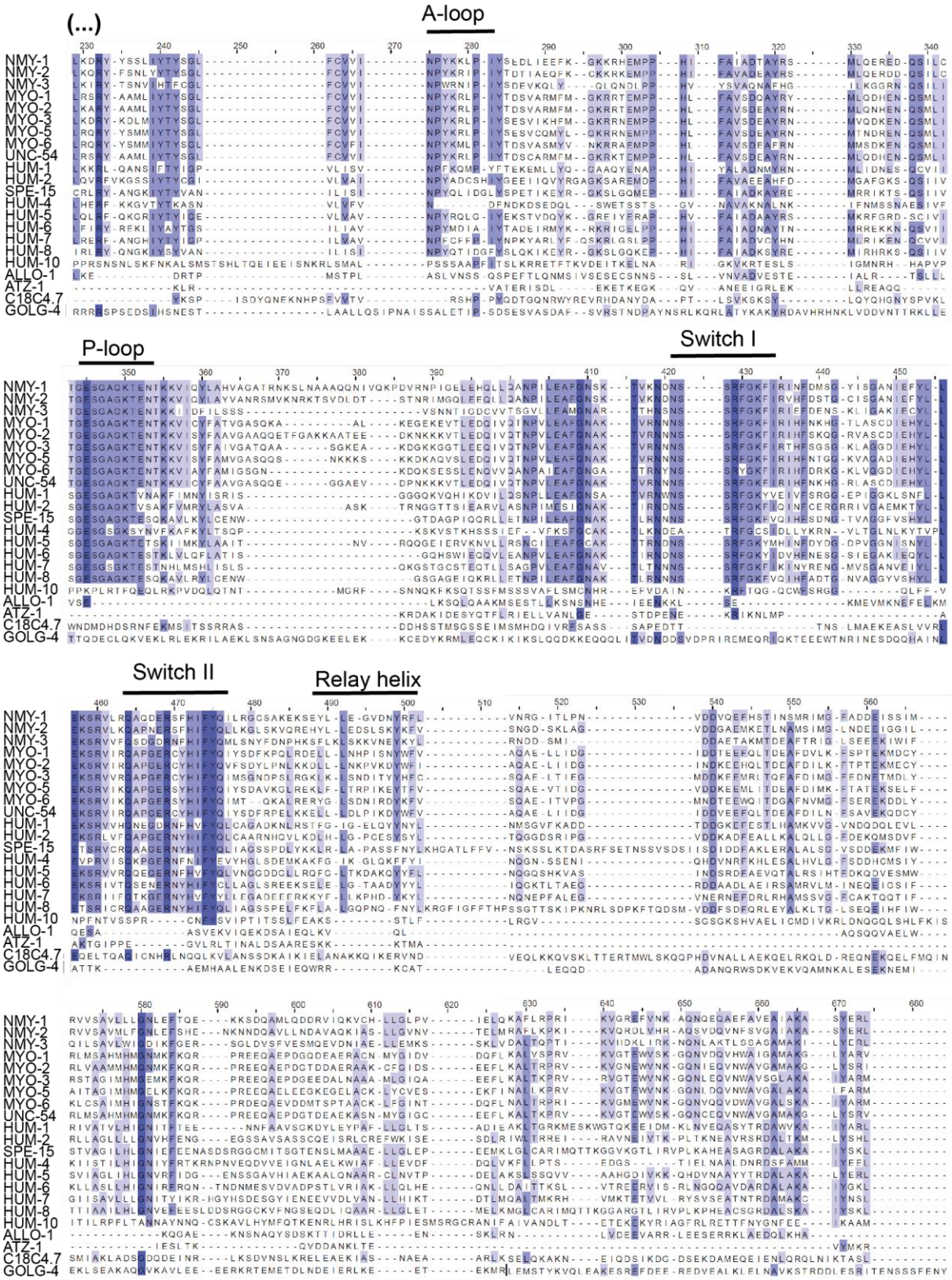
(...)
A-loop
P-loop
Switch I
Switch II
Relay helix
NMY-1
NMY-2
NMY-3
MYO-1
MYO-2
MYO-3
MYO-5
MYO-6
UNC-54
HUM-1
HUM-2
SPE-15
HUM-4
HUM-5
HUM-6
HUM-7
HUM-8
HUM-10
ALLO-1
ATZ-1
C18C4.7
GOLG-4

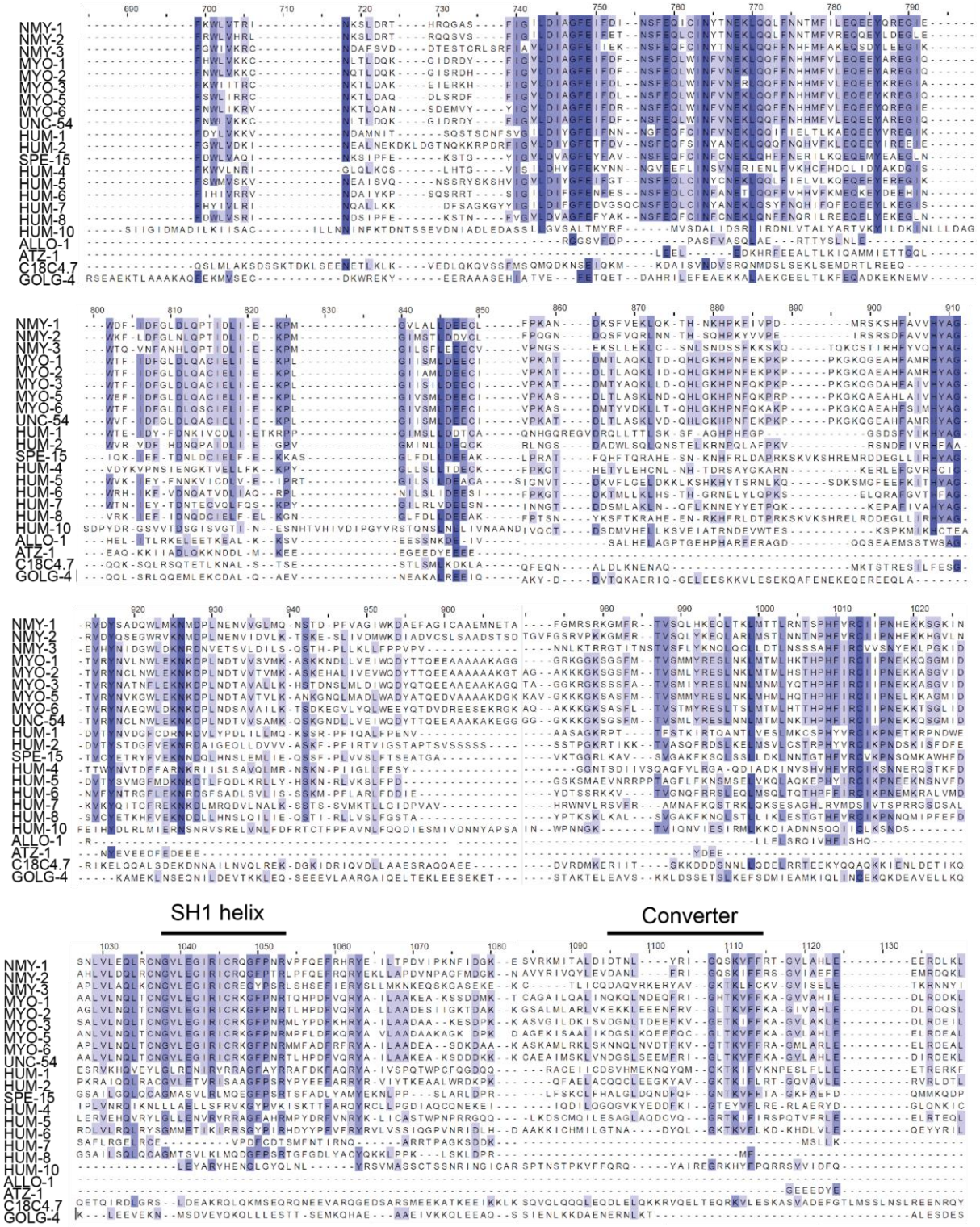

Figure 4.8 Putative myosins head domain alignment. Besides HUM-10, ALLO-1, ATZ-1, C18C4.7 and GOLG-4, all the other proteins are similar at sequence level. HUM-10, ALLO-1, ATZ-1, C18C4.7 and GOLG-4 do not seem to have the A-loop, the P-loop, Switch I, Switch II, Relay helix, and SH1 helix, or converter domain, which are essential for myosin function. Alignment in Jalview software using the MUSCLE multiple alignment method with default settings. Dark blue and light blue represent amino acids with higher or lower % identity, respectively.

The initial list of putative myosins had 22 candidates, but after this sequence analysis I concluded that only 17 have the amino-acid motifs required to be considered myosins and therefore excluded HUM-10, ALLO-1, ATZ-1, C18C4.7 and GOLG-4 from further analysis.

4.2.5.2 NMY 2 and MYO-1 depletion lead to decreased embryonic viability

In order to explore whether any of these myosins contributed to embryogenesis, I started by taking a general standard approach to determine embryonic viability after depleting each of them by RNAi. If any of them played an essential role in the embryo, embryos should arrest during development and not hatch. To determine embryonic viability, I depleted each of the genes by RNAi and counted the percentage of embryos that hatched relatively to the total number of laid embryos in comparison to controls. For RNAi depletions, animals in the L1 stage were fed with dsRNA targeting each of the myosins. In the case of NMY-1 and MYO-1, the dsRNA was injected because RNAi by feeding revealed not to be effective. The results obtained are displayed in Figure 4.9.

Animals depleted of NMY-2 or MYO-3 were sterile, suggesting that these myosins are crucial for gonad formation or maintenance, which is in agreement with previous reports (Kamath, 2003; Simmer et al., 2003; Green et al., 2011). NMY-2 depleted embryos were not viable in agreement with a role during embryonic development, whereas all embryos depleted of MYO-3 were viable. NMY-1 and MYO-1 depletion led to 33% and 38% of worm sterility, respectively, indicating a role in the gonads. UNC-54 depletion led to egg laying defects, and consequently, there were fewer embryos on the plate to count. However, they did form and hatched inside the parent (matricidal hatching). Depletion of the other myosins did not affect embryonic viability, which suggests that they are not essential during embryo development, or they act redundantly.

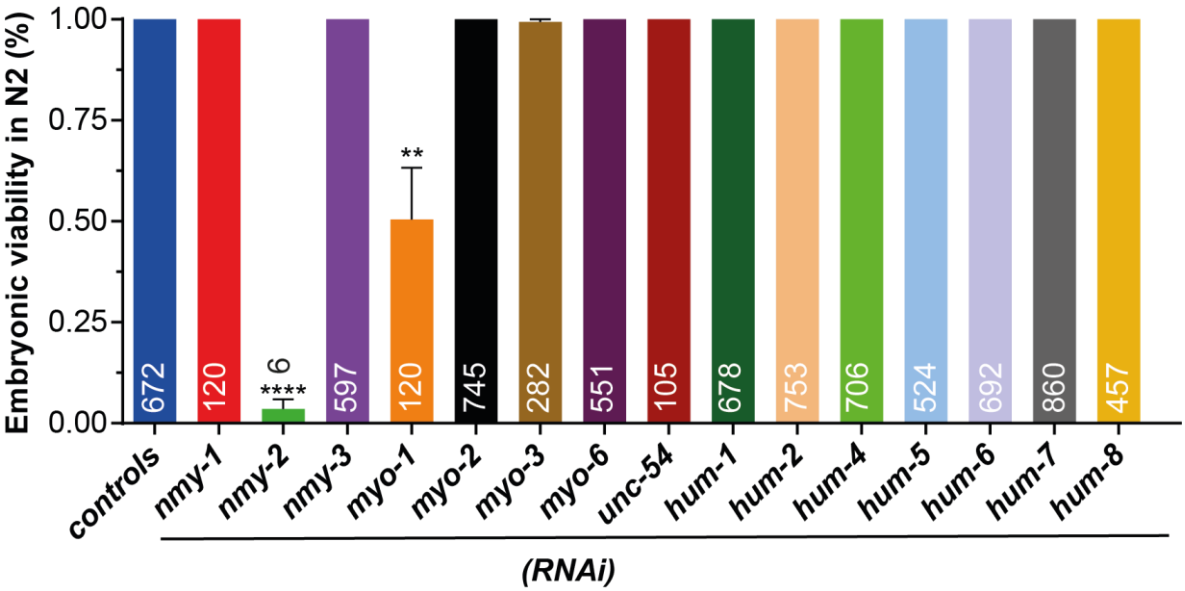

Figure 4.9 NMY-2 and MYO-1 depletion reduce embryo viability in the *wild-type* background. Data is from three independent experiments. Numbers in the bars correspond to the total number of embryos laid. Error bars: CI 95%. Statistical significance was determined using one-way ANOVA followed by Bonferroni's multiple comparison test. p values ** p<0.001, **** p<0.00001

Next, in order to test if the other myosins can cooperate with NMY-2, the embryonic viability assay was done in a *nmy-2* sensitized background, where NMY-2 function is partially compromised (Figure 4.10). For this effect I used a strain in which the sole source of NMY-2 is NMY-2(S250A), which has partially impaired motor activity (more details in Chapter 5). In the *nmy-2(S250A)* background, the embryonic viability is similar to the one observed in the *wild-type* background. In the *nmy-2(S250A)* background, animals depleted of NMY-2 and MYO-3 were sterile. Therefore, embryonic viability was again measured in embryos laid just before the animals became sterile. NMY-2 depleted embryos were not viable while embryos depleted of MYO-3 were fully viable. NMY-1 and MYO-1 depletions led to 33% of sterility. Only NMY-2 and MYO-1 were required for embryonic viability.

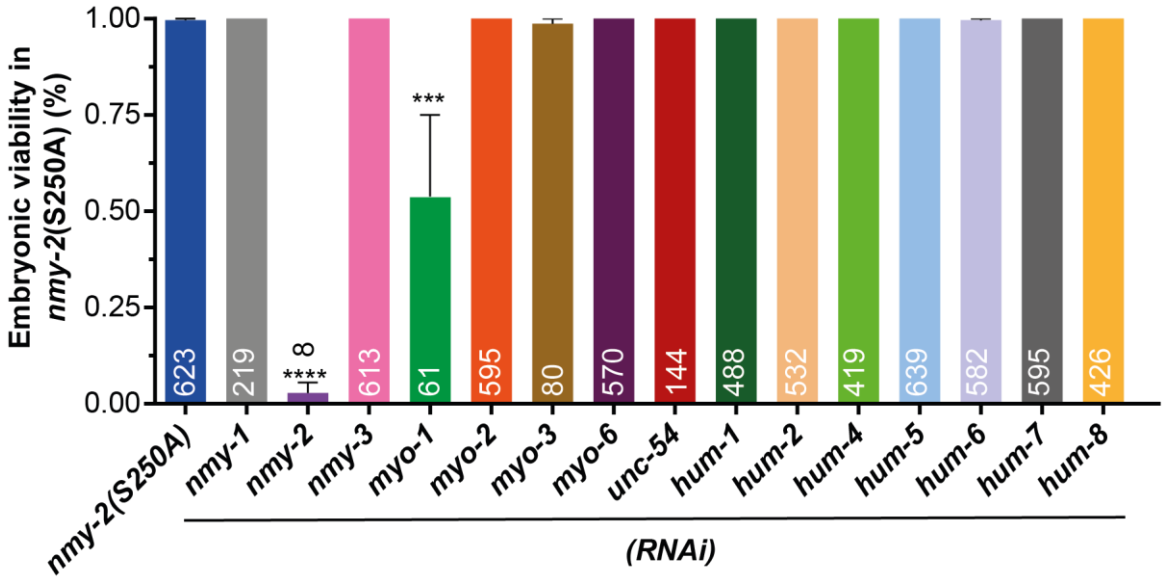

Figure 4.10 NMY-2 and MYO-1 depletion reduce embryonic viability in *nmy-2(S250A)* animals. Data is from three independent experiments. Numbers in the bars correspond to the total number of embryos laid. Error bars: CI 95%. Statistical significance was determined using one-way ANOVA followed by Bonferroni's multiple comparison test p values ***p<0.0001, **** p<0.00001.

4.2.5.3 MYO-1 contributes to embryonic cytokinesis

In order to understand if the defects in embryonic viability observed after MYO-1 depletion were caused by problems during cytokinesis, I depleted MYO-1 in *wild-type* and *nmy-2(S250A)* embryos. Cytokinesis timing from anaphase onset until the end of constriction was measured (Figure 4.11A). In the *wild-type* background (Figure 4.11B), MYO-1 depleted embryos presented delayed cytokinesis (266.7±18.4 s versus 207.5±5.9 s in *wild-type* animals). The *nmy-2(S250A)* embryos depleted of MYO-1 also displayed prolonged cytokinesis (314.3±22.9 s versus 268.3±17.1 s in *nmy-2(S250A)* animals, respectively). Analysis of ring constriction rate (Figure 4.12) revealed that in *wild-type* embryos rings constricted at 0.17±0.02 µm/s, but upon MYO-1 depletion, rings constricted at 0.14±0.02 µm/s. In *nmy-2(S250A)* embryos, the contractile rings constricted at 0.15±0.01 µm/s, and upon MYO-1 depletion constricted at 0.12±0.01 µm/s.

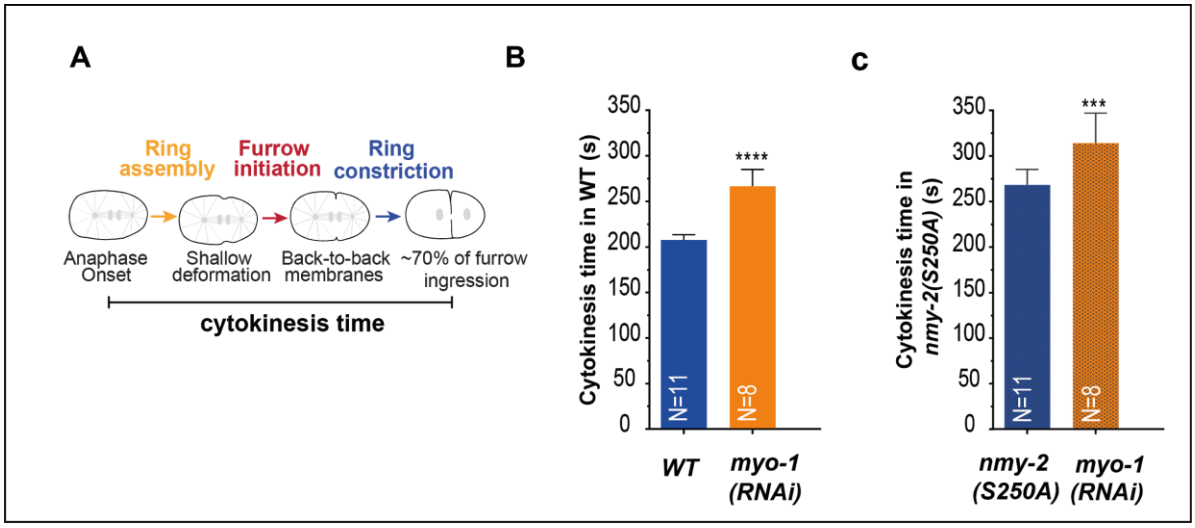

Figure 4.11 MYO-1 depletion leads to prolonged cytokinesis. A) Cytokinesis time was measured from anaphase onset until ~70% of furrow ingression (contractile ring with 10 µm of diameter). B) Cytokinesis timing of *wild-type* embryos (WT) depleted or not of MYO-1. C) Cytokinesis timing of *nmy-2(S250A)* embryos depleted or not of MYO-1. Error bars: CI 95%. N corresponds to the number of one-cell embryos analysed. Statistical significance was determined using one-way ANOVA followed by Bonferroni's multiple comparison test. p values ***p<0.0001, **** p<0.00001

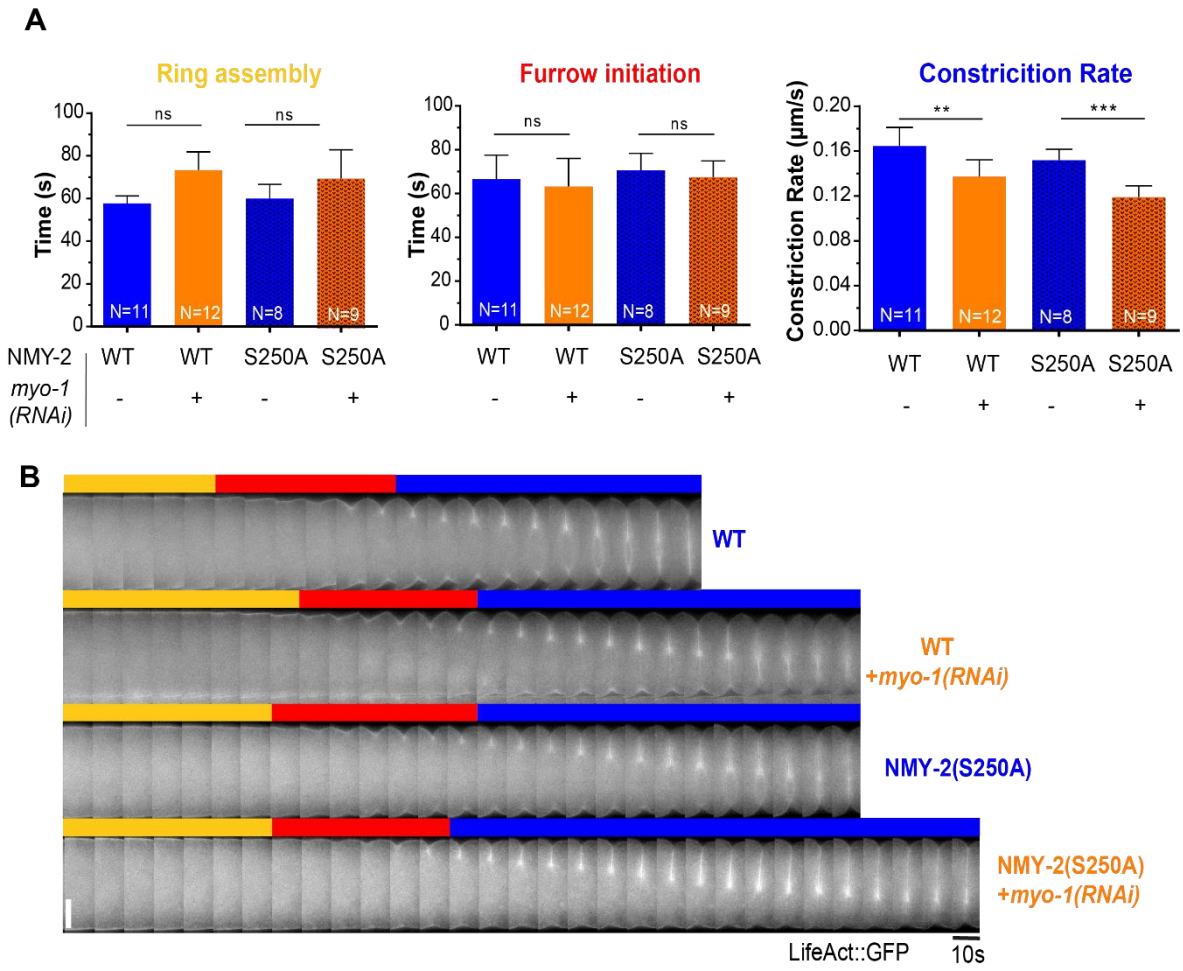

Figure 4.12 MYO-1 depleted embryos present ring constriction slowdown. A) Quantitative analysis shows that cytokinesis kinetics are slower when MYO-1 is depleted in both *wild-type* (WT) and *nmy-2(S250A)* (NMY-2(S250A)) backgrounds. B) Kymographs of the cleavage furrow region of representative examples of *wild-type* embryos (WT), *wild-type* embryos depleted of MYO-1 (WT+*myo-1(RNAi)*), *nmy-2(S250A)* (NMY-2(S250A)) embryos , and *nmy-2(S250A*) embryos depleted of MYO-1 (NMY-2(S250A)) +*myo-1(RNAi*), showing that cytokinesis takes longer to complete in the absence of MYO-1. The color bars correspond to contractile ring assembly (yellow); furrow initiation (red) and constriction (blue). N corresponds to the number of one-cell embryos analysed. Error bars: CI 95%; Statistical significance was determined using one-way ANOVA followed by Bonferroni's multiple comparison test. p values ** p<0.001, ***p<0.0001 ns means no-significance. Scale bar: 10 µm.

Together these results indicate that MYO-1 is important during ring constriction in both *wild-type* and *nmy-2(S250A)* backgrounds. I conclude that MYO-1 is necessary to set the normal pace of cytokinesis. In addition, MYO-1 may cooperate with NMY-2 since the ring constriction rate is further affected when MYO-1 is depleted in the *nmy-2(S250A)* background.

4.3 Discussion

Within a single organism, several types of myosins are expressed, which implies tissue, cell or process specificity. However, myosins can act redundantly or compensate for one another. In addition, recent studies suggest that myosins can cooperate by forming heterotypical filaments (Beach et al., 2014; Beach & Hammer, 2015; Billington et al., 2015). In this chapter, I investigated if other myosins can cooperate with NMY-2 in embryonic cytokinesis of *C. elegans.*

I show that NMY-2 plays essential roles in embryonic cytokinesis. NMY-2 severe depletion leads to cytokinesis failure. NMII is essential for cytokinesis in many different organisms (Lozanne & Spudich, 1987; Mabuchi & Okuno, 1977; Straight et al., 2003), but whether this absolute requirement is due to NMII motor or F-actin crosslinking functions will be discussed in Chapter 5.

To understand how the phenotype of depleting NMY-2 progresses with the progressive reduction of protein levels, I performed an NMY-2 RNAi time-course. Substantial impairment in both ring assembly and constriction only occurs when myosin levels were reduced below 20% of the average control, and cytokinesis only starts to fail in embryos that had less than 10% of the average control myosin levels. These results suggest that although NMY-2 is essential for cytokinesis, the contractile ring is quite robust to reductions in myosin levels, which can be due to an excess of myosin at the contractile ring. NMY-2 depletion reduces cortical tension (Silva et al., 2016; Tinevez et al., 2009). Tension in the surrounding cortex is expected to counteract contractile ring constriction, and it is possible that NMY-2 depleted embryos with low levels of myosin in the ring can constrict because of lower cortical resistance. It is also possible that, similar to what happens in human cells (Beach et al., 2014; Beach & Hammer, 2015; Billington et al., 2015; Jiu et al., 2019), other myosins may cooperate with NMY-2 during cytokinesis, allowing embryos to divide when NMY-2 is partially compromised.

NMY-2 depletion interferes with other embryonic processes, such as polarity establishment that occur before cytokinesis (Ou et al., 2010; Munro et al., 2004; Marston & Goldstein, 2006; Cuenca et al., 2003; Guo & Kemphues, 1996; Liu et al., 2010). These defects might exacerbate the NMY-2 depletion phenotype observed during cytokinesis. Additionally, it is possible that the lower constriction rate is due to a prolonged assembly of the contractile ring. In order to test the implications of perturbing NMY-2 solely during cytokinesis, I inactivated NMY-2 during ring assembly, shallow deformation, or ring constriction.

Independently of the stage, NMY-2 inactivation led to stalling of the furrow, and subsequently cytokinesis failure, indicating that NMII is required even when the contractile ring has already formed and is undergoing constriction.

NMY-1 is one of the three NMIIs expressed in *C. elegans*. NMY-1 depletion leads to some sterility and reduced production of embryos, suggesting a role in the gonads. Indeed, NMY-1 has been described to drive spermatheca contraction and its depletion results in embryos trapped inside this organ (Kovacevic et al., 2013; Wirshing & Cram, 2017). NMY-1 has also been described to antagonize NMY-2 function in the gonad ring canals in order to maintain their correct size (see section 1.5.3 in the introduction; Coffman et al., 2017). However, contradictory results show that NMY-1 does not localize in the gonad germ cells and NMY-1 depletion does not affect ring canal size (Priti et al., 2018). In addition, NMY-1 together with NMY-2 are required for proper *C. elegans* elongation (Piekny, 2003). I find that NMY-1 is not essential for embryonic viability, which indicates that embryonic cytokinesis does not fail. However, it is possible that embryos depleted of NMY-1 do not fail cytokinesis because NMY-2 compensates for NMY-1 function. I show that NMY-1 depletion per se does not cause any perturbation in the kinetics of cytokinesis in the one-cell embryo. If NMY-1 and NMY-2 cooperate, the cytokinesis phenotype of perturbing both should be more severe than perturbing NMY-2 alone. My results show that embryos with partially inactivated NMY-2 and depleted of NMY-1 had similar cytokinesis kinetics when compared to those embryos that solely had NMY-2 partially inactivated. This strongly indicates that NMY-1 does not contribute to the cytokinesis process, at least in the one-cell embryo, and the reduction of broodsize is likely due to problems during elongation.

NMY-3 head and neck domains are very similar to the amino acid sequence to those of NMY-1 and NMY-2. However, when the tail domain is compared, NMY-1 and NMY-2 are closer together than NMY-3. Therefore, NMY-3 is the most divergent NMII between all NMIIs in *C. elegans*. NMY-3 depletion did not affect embryonic viability or ability to produce embryos in the context of two large RNAi screens, suggesting that NMY-3 might not have essential role in gonads or during cytokinesis (Kamath, 2003; Sönnichsen et al., 2005)

My results suggest that the *C. elegans* NMY-1, NMY-2 and NMY-3 do not cooperate or have specific functions during cytokinesis (Taneja et al.,2020). This contrasts with human NMIIs, where NMII-A is important for contractile ring ingression and NMII-B is essential during abscission.

To test if other myosin HCs can cooperate with NMY-2, I performed an RNAi screen that included several *C. elegans* myosins in both *wild-type* and *nmy-2(S250A)* backgrounds. The latter carries a mutation in the ATPase site of NMY-2, which partially compromises its motor-activity. Expression of NMY-2(S250A) does not prevent embryonic cytokinesis from happening but reduces the robustness of the contractile ring, making it more sensitive to other perturbations (Chapter 5). In addition, *nmy-2(S250A)* mutants produce and lay embryos normally, which makes them a suitable tool to deplete other myosin HCs and assess phenotypes in a nmy-2 sensitized background.

Interestingly, I find that MYO-1 depletion led to some degree of sterility. MYO-1 depletion is associated with defects in embryos entering in the spermatheca (Wirshing & Cram, 2017), which may explain the lower number of embryos produced. Immunostaining with a specific antibody against MYO-1 or the expression transgenic LacZ under the myo-1 promoted (Pmyo-1::LacZ) followed by β-galactosidase staining suggested that MYO-1 is expressed in the pharynx muscle, along with MYO-2, where they likely have redundant functions in pumping food (Fire & Waterston, 1989; Ardizzi & Epstein, 1987). Reduced ability in pumping food is leads to a reduced feeding rate which can lead to slow growth, short lifespan, reduced brood size but not to embryonic lethality (Pazdernik & Schedl, 2013; Rodríguez-Palero et al., 2018). Therefore, the reduced embryonic viability observed in MYO-1 depleted animals might be associated with other functions, such as cytokinesis. Indeed, MYO-1 depleted embryos show slow cleavage furrow ingression, suggesting that MYO-1 plays a role during contractile ring constriction. Depletion of MYO-1 in *nmy-2(S250A)* background led to an aggravation of the cytokinesis phenotype, which indicates that MYO-1 and NMY-2 might cooperate during constriction. MYO-1 might form filaments and translocate linear F-actin in the contractile ring, or it could form heterotypic filaments with NMY-2 as described for human NMIIs (Beach et al., 2014; Beach & Hammer, 2015). However, we never observed cytokinesis failure, which suggests that embryonic lethality could be related to failure of cytokinesis in later divisions or other actomyosin-dependent processes during embryogenesis, like gastrulation and elongation.

It will be important to assess MYO-1 localization by generating a fluorescently tagged MYO-1 by directly editing the genomic locus of myo-1 by CRISPR-Cas9. One-cell embryos expressing this fluorescent MYO-1 could be imaged while undergoing cytokinesis. Since MYO-1 depletion reduced ring constriction rate, it is likely that it localizes at the ingressing furrow. Colocalization studies could then be performed to explore whether NMY-2 and MYO-1 have a similar localization during cytokinesis.

In order to further study myo-1 function, and due to the high sequence similarity, it may be possible to generate a temperature-sensitive mutant of myo-1 by changing the leucine 972 with a proline, homologous to the leucine 981 proline mutation present *nmy-2(ne3409*) ts mutant. This would allow for the temperature-dependent inactivation of MYO-1 during cytokinesis to assess its function at precise timings during cytokinesis. The assessment of the potential formation of heterotypic filaments between NMY-2 and MYO-1 could be done by applying similar protocols as described for human NMII (Beach & Hammer, 2015). To do so, one myosin would be fluorescently tagged at the head domain and the other at the tail. Embryos co-expressing both fluorescently tagged myosins would be imaged undergoing cytokinesis using super-resolution microscopy. Super-resolution studies in *C. elegans* embryos co-expressing different markers were already performed (Lardennois et al., 2019). The localization pattern and the distances between NMY-2 and MYO-1 signals can confirm if these can form heterotypic bipolar filaments. Biochemical approaches like co-immunoprecipitation or *in vitro* interactions would also confirm possible interactions between NMY-2 and MYO-1. Considering that MYO-1 is described as a muscle myosin (Ardizzi & Epstein, 1987), its muscle localization and function could also be further investigated using the novel tools described above.

Altogether, my results show that NMY-2 is the only myosin absolutely required for cytokinesis and is essential for all stages of cytokinesis. Interestingly, MYO-1 also contributes to cytokinesis, which brings novel information into the study of cell division – to my knowledge a conventional myosin with muscle-specific function has never been described as being involved in cytokinesis. MYO-1 localization and whether MYO-1 and NMY-2 cooperate or compensate for one another remains to be studied. As MYO-1 depletion leads to embryonic lethality and we observe no cytokinesis failure in the first embryonic division, it is possible that later embryonic cytokinesis events fail or that MYO-1 is essential for other functions during embryogenesis. In the future, it will be interesting to image embryonic development live to assess the stage when embryos arrest and further investigate MYO-1 function.

CHAPTER 5

CROSSLINKING ACTIVITY OF NON-MUSCLE MYOSIN II IS NOT SUFFICIENT FOR EMBRYONIC CYTOKINESIS IN *C. ELEGANS*

Contractile ring constriction during cytokinesis is thought to be mediated by actin filament translocation via myosin, nonetheless the importance of motor versus crosslinking activity of myosin and the role of actin depolymerization as driving forces for constriction have been a subject of discussion in model systems like yeast or human culture cells. Additionally, the studies on cytokinesis *in vivo* in animals are quite limited. In order to address how the contractile ring produces the force to form the cytokinetic furrow in in vivo, our team took advantage of CRISPR/Cas9 to directly edit the *C. elegans* genomic locus of *nmy-2* in order to generate NMY-2 point mutants with compromised motor activity. The impact of these mutants in embryonic cytokinesis was investigated. The work presented here was published in *Development* (2019 146: dev179150 doi: 10.1242/dev.179150). In this publication, I share first authorship with two other authors, and I contributed to methodology, formal analysis, investigation, data curation and writing - review & editing. Specifically, I contributed to the experimental data in figures 5.3, 5.4, 5.5 E-H, 5.6A, 5.7A-C, 5.E-F, S3A-F, and 5.S5H-G.

5. CROSSLINKING ACTIVITY OF NON-MUSCLE MYOSIN II IS NOT SUFFICIENT FOR EMBRYONIC CYTOKINESIS IN *C. ELEGANS*

5.1 Introduction

Cytokinesis is the final step of cell division that leads to the partitioning of the mother cell into two daughter cells, thereby ensuring that each daughter retains one copy of the replicated genome. Although cell-substrate adhesion may facilitate division in cultured cells (Dix et al., 2018; Kanada et al., 2005 Nagasaki et al., 2009; Neujahr et al., 1997), in fungi and animals cytokinesis primarily relies on the assembly and constriction of a distinct acto-myosin structure, the contractile ring, that forms at the cell equator. In animal cells, the contractile ring assembles beneath the plasma membrane after anaphase onset and subsequently constricts, folding the cell membrane inwards to achieve the physical separation between daughter cells (Green et al., 2012).

The major components of the contractile ring are filamentous actin (F-actin) and non-muscle myosin II (hereafter myosin). F-actin composes the scaffold of the contractile ring (Carvalho et al., 2009; Silva et al., 2016; Stachowiak et al., 2014; Wollrab et al., 2016) and F-actin dynamics in the ring are likely controlled by a variety of actin-binding proteins, including formins, profilin, cofilin, capping proteins and several crosslinkers such as α-actinin and fimbrin (Blanchoin et al., 2014).

Myosin is a motor protein that has traditionally been regarded as the engine that drives cytokinesis, but recent work has challenged this view (see below). Myosin is a hexameric complex composed of a dimer of heavy chains and two pairs of light chains. Each heavy chain has a N-terminal globular head that contains an ATP-binding pocket and an actin-binding site, a lever arm where the light chains bind, and a C-terminal coiled-coil domain involved in interactions that promote heavy chain dimerization and formation of multi-headed bipolar filaments (Niederman & Pollard, 1975; Vicente-Manzanares et al., 2009). ATP hydrolysis induces coupled conformational changes that are transmitted through the head subdomains to the lever arm. This generates a power stroke that causes myosin to move towards the actin filament barbed-end. In an interconnected F-actin network with antiparallel filament arrangement, this movement causes filaments to slide past one another and the network to contract. In addition, the ability to bind actin allows myosin filaments to exert tension and maintain the network connected. Ultrastructural studies show that the contractile ring consists primarily of unbranched filaments aligned parallel to the ring circumference and arranged in an antiparallel manner (Henson et al., 2017; Kamasaki et al., 2007; Maupin & Pollard, 1986; Sanger & Sanger, 1980; Schroeder, 1973). Additionally, myosin has been shown to form arrays of aligned filaments or stacks of filaments running parallel to actin filaments, an organization that is compatible with a purse-string mechanism where F-actin sliding by myosin motors would drive ring constriction (Beach et al., 2014; Fenix et al., 2016; Henson et al., 2017). However, although myosin is essential for cytokinesis in different model systems (Lozanne & Spudich, 1987; Mabuchi & Okuno, 1977; Straight et al., 2003), the specific requirement for myosin motor activity has been a subject of recent debate. Budding yeast is able to perform cytokinesis in the presence of a motor-less myosin (Lord et al., 2005; Mendes Pinto et al., 2012). In fission yeast, myosin motor activity appears to be required for ring constriction, but additional myosins also contribute (Laplante & Pollard, 2017; Laplante et al., 2015; Palani et al., 2017). In the amoeba *Dictyostelium discoideum*, specific mutations within the ATPase domain result in motor-dead myosins that, when expressed in suspension cells, cause growth phenotypes similar to or more severe than those of cells expressing no myosin, highlighting the importance of motor activity in this system (Sasaki et al., 1998; Shimada et al., 1997). Whether myosin motor activity is absolutely required in animal cells is less clear, as studies have relied on the use of the small molecule inhibitor blebbistatin, depletion/inactivation of myosin/myosin temperature-sensitive mutants or depletion or non-phosphorylatable mutants of the regulatory light chain that is required for myosin complex activation (Davies et al., 2014; Descovich et al., 2018; Jordan & Karess, 1997; Reymann et al., 2016; Straight et al., 2003). None of these

approaches can provide a definitive answer regarding the requirement for motor activity, as blebbistatin keeps myosin in a low actin affinity state (Allingham et al., 2005), depletion or inactivation of myosin does not differentiate between motor activity and F-actin crosslinking, and interfering with the regulatory light chain may affect other myosins or influence myosin localization and/or structure (Heissler & Sellers, 2015; Liu et al., 2016 Vasquez et al., 2014). The effect of specific motor-impairing mutations has been reported for the mammalian myosin IIB in COS-7 cells and mouse cardiomyocytes (Ma et al., 2012) and in this case the requirement for myosin motor activity was contested. Thus, how the contractile ring produces the force to form the cytokinetic furrow remains an important question.

The *C. elegans* embryo is particularly suited for the quantitative *in vivo* analysis of cytokinesis, as the embryo is large, and its divisions are stereotypical and temporally invariant. *C. elegans* possesses two non-muscle myosin II heavy chains: NMY-1 and NMY-2. NMY-2 has been shown to be essential for cytokinesis (Cuenca et al., 2003; Davies et al., 2014; Guo & Kemphues, 1996), whereas NMY-1 is required during late embryonic development (Piekny, 2003), in the adult somatic gonad and the spermatheca (Kovacevic et al., 2013; Priti et al., 2018; Wirshing & Cram, 2017). In this study, we assess the role of myosin motor activity during cytokinesis in the *C. elegans* early embryo by characterizing NMY-2 motor mutants generated by genome editing. Our results suggest that it is myosin motor activity, and not the ability of myosin to crosslink F-actin, that drives ring assembly by compacting and aligning F-actin bundles. Furthermore, we find that myosin motor activity determines the pace of constriction.

5.2 Results

5.2.1 Expression of motor-dead muscle myosins prevents C. elegans locomotion without substantially affecting actin organization in body wall muscles

To generate motor-dead myosin mutants in *C. elegans*, we took advantage of a previous alanine mutagenesis screen in the highly conserved switch I region of the ATPase domain of *D. discoideum* non-muscle myosin II, which yielded a series of mutants with compromised motor activity (Shimada et al., 1997). Based on the high sequence conservation among myosins, we chose two point mutations shown to yield motor-dead myosin in *D. discoideum*. These mutations correspond to S251A and R252A in NMY-2, and to S240A and R241A in

UNC-54, the main skeletal muscle myosin that is essential for animal movement and egg laying (Epstein & Thomson, 1974; Fire et al., 1991; Figure 5.1A-C, Figure 5.S1).

To assess the potential of these mutations to affect myosin motor activity in *C. elegans*, we first examined the consequences of introducing them into muscle myosin. Muscle fibers are composed of sarcomeres, which require myosin motor activity to contract. Although muscle and non-muscle myosin II present differences in ATP hydrolysis kinetics and motility rates, the principle underlying the change in molecular conformation that allows for the power stroke is identical in both motors and relies on extremely well-conserved regions, including the switch I loop of the ATP-binding site (Heissler & Sellers, 2016; Figure 5.1B,C, Figure 5.S1). Moreover, previous studies have established that the mechanistic effects of mutations in conserved myosin head residues are transposable between class II myosins and even between different myosin classes (Forgacs et al., 2009; Li et al., 1998; Onishi et al., 1998; Trivedi et al., 2012).

Using CRISPR/Cas9-based genome editing (Arribere et al., 2014), we introduced the two point mutations into UNC-54. We were able to generate homozygous animals expressing UNC-54(S240A) and UNC-54(R241A). To evaluate muscle function, we monitored animal locomotion and egg laying rates (Figure 5.1D,E). *unc-54(S240A)* and *unc-54(R241A)* adult animals displayed a drastic reduction in liquid locomotion [0.24±0.04 Hz in *unc-54(S240A)*, 0.23±0.13 Hz in *unc-54(S241A)* versus 1.6±0.1 Hz in wild-type animals] and were unable to lay eggs, as expected for strongly motor-impaired myosins. Residual movement observed in *unc-54(S240A)* and *unc-54(R241A)* animals was attributable to the secondary body wall muscle myosin MYO-3, as depletion of MYO-3 in either *unc-54* mutant led to paralysis on food plates and loss of motility in liquid (Figure 5.1D). Penetrant loss of movement was also observed when UNC-54 and MYO-3 were co-depleted by RNAi in wild-type animals (Figure 5.1F). As no neuronal roles have been described for UNC-54, it is reasonable to assume that decreased movement in *unc-54* animals is due to impairment of muscle contraction.

Interestingly, phalloidin staining of muscles in *unc-54(S240A)* and *unc-54(R241A)* adult animals revealed that actin organization was preserved (Figure 5.1G). This is in agreement with reports of nearly normal sarcomere organization and substantially decreased ability to move in *unc-54(s74)* animals, which express a point mutation in the myosin head domain (R270C) (Hwang et al., 2016; Moerman et al., 1982). In contrast, depletion of UNC-54 by RNAi resulted in wavy and irregular F-actin bundles (Figure 5.1G). This suggests that the motor activity of UNC-54 is not required for actin organization in adult muscles but is required for muscle contraction.

We conclude that mutating the highly conserved residues S240 and R241 results in inactive UNC-54 *in vivo*, in agreement with the effects of the mutations on non-muscle myosin II motor activity reported *in vitro* for *D. discoideum*. Of note, we also tested the mutation corresponding to R709C in mammalian non-muscle myosin IIB (Figure 5.S5A), a disease-related mutation in the SH1 helix (Ma et al., 2012). We found that muscle function was only partially impaired in *unc-54(R710C)* animals (Figure 5.S5B,C). UNC-54(R710C) is therefore unlikely to be motor-dead.

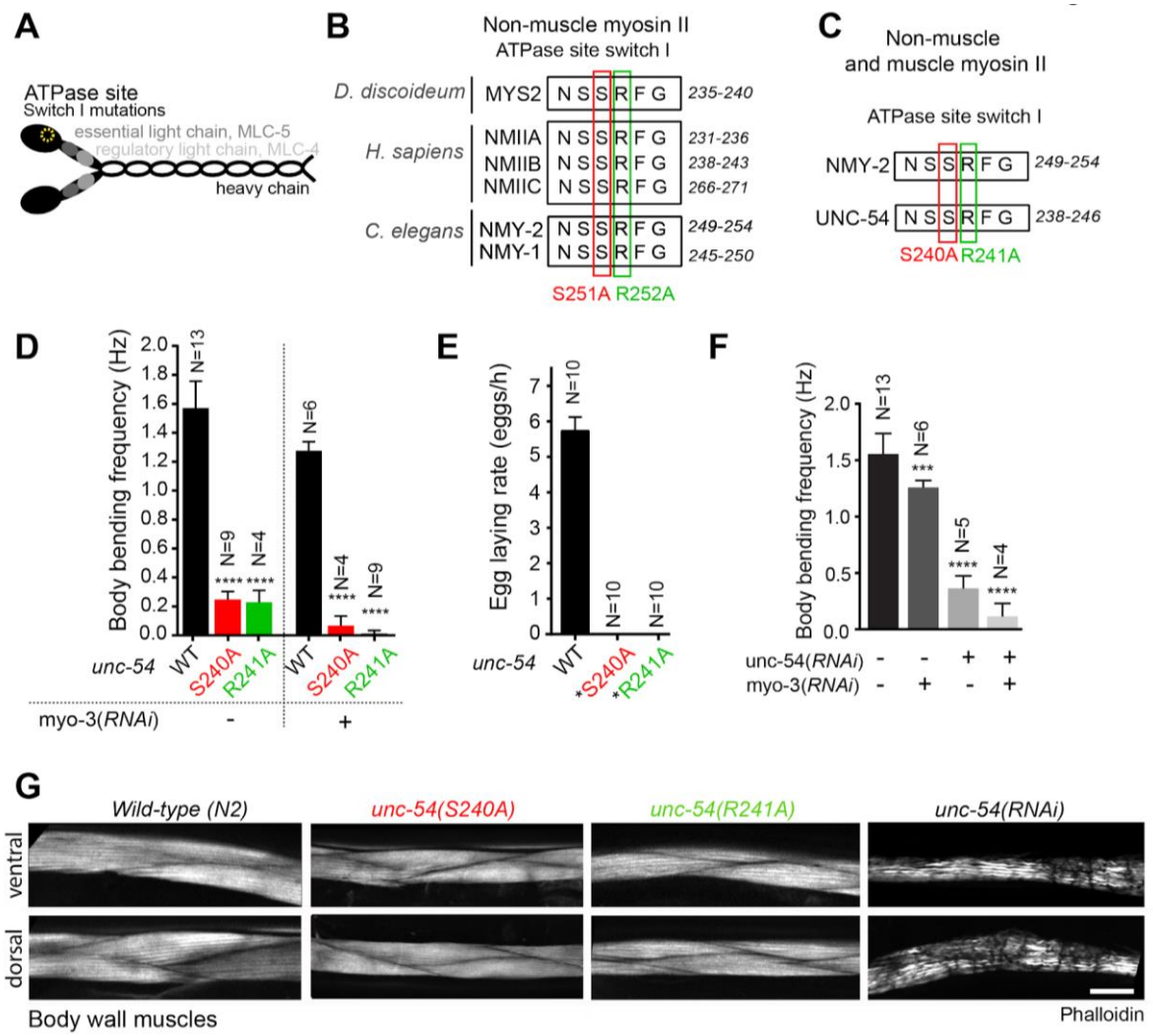

Figure 5.1 Muscle contraction as an *in vivo* readout of motor-impairment in myosin II mutants. (A) Schematic of the non-muscle myosin II hexamer. (B) Alignment of non-muscle myosin II sequences. The highly conserved residues S251 and R252A (numbered as in *C. elegans* NMY-2) mutated to alanine to obtain putative motor-dead myosins are marked by red and green boxes, respectively. (C) Residues S240 and R241 (numbered as in *C. elegans* UNC-54) mutated to alanine to obtain putative motor-dead muscle myosin are marked by red and green boxes, respectively. (D) Body bend frequency in liquid (mean±95% CI) in *wild-type* and *unc-54* motor mutant animals with and without depletion of the secondary muscle myosin MYO-3. (E) Egg-laying rate (mean±95% CI) in *wild-type* and *unc-54* mutant animals. Mutant animals do not lay eggs, but embryos are viable and develop normally inside the mother (asterisk). (F) Body bend frequency in liquid (mean±95% CI) in *wild-type* animals depleted of UNC-54 or MYO-3, or both. N is the number of analyzed animals in D, E and F. (G) Dorsal and ventral views of phalloidin-stained body wall muscles in animals with indicated genotypes and RNAi treatments. Statistical significance was determined using one-way ANOVA followed by Bonferroni's multiple comparison test; ****P≤0.0001, ***P≤0.001. Scale bar: 10 µm.

5.2.2 NMY-2(S251A) and NMY-2(R252A) bind but do not translocate F-actin in vitro

We next characterized the ability of corresponding NMY-2 mutants to bind and translocate F-actin *in vitro*. First, we assessed F-actin binding of NMY-2(S251A) and NMY-2(R252A) in high-speed co-sedimentation assays. His-tagged NMY-2 S1 fragments (residues 1-854; routinely used for actin binding and kinetic assays; (Manstein et al., 1989) carrying either mutation were purified along with the myosin regulatory (MLC-4) and essential (MLC-5) light chains from baculovirus-infected insect cells (hereafter NMY-2S1; Figure 5.2A). NMY-2S1 was incubated with or without F-actin in the presence of 0.7 mM ATP before ultracentrifugation (Figure 5.2B-D). In the absence of F-actin, all myosin was present in the supernatant (SI), indicating that wild-type and mutant NMY-2S1 are equally soluble. Conversely, in the presence of F-actin, all NMY-2S1 versions were found in the pellet (PI), showing that the mutants are capable of binding F-actin (Figure 5.2C,D). F-actin pelleted in the absence of myosin as expected, and no proteins corresponding to the size of the NMY-2 S1 fragment were present in the pelleted fraction (Figure 5.S2A). The identity of NMY-2S1 was confirmed by immunoblotting (Figure 5.2C). More of NMY-2(S251A)S1 and less of NMY-2(R252A)S1 pelleted with F-actin compared with wild-type NMY-2S1 (Figure 5.2C,D). Specifically, by performing the pelleting assay at different actin concentrations, we obtained a Kd of 0.062±0.016 µM, 2.46±0.69 µM and 0.66±0.13 µM for NMY-2(S251A)S1, NMY-2(R252A)S1 and wild-type NMY-2S1, respectively (Figure 5.2E). As a significant fraction of the ATP present in the buffer may be consumed during the course of the assay (thereby increasing the affinity of myosin for F-actin), the differences in Kd may in part reflect differences in the kinetics of ATP hydrolysis between wild-type and mutant myosins.

To determine whether the NMY-2 mutants were able to cycle between the F-actin bound and unbound states, we tested their ability to detach from F-actin pellets (PI) in the presence of high ATP concentrations. Myosin affinity for F-actin is determined by the status of the nucleotide bound to the ATPase pocket and is weak when bound to ATP (Spudich, 2001). PI pellets were resuspended in buffer containing 50 mM ATP in order to maintain myosin saturation (Figure 5.2B). After ultracentrifugation, the supernatant (SII) and pellet (PII) were analyzed (Figure 5.2F,G). Both wild type and NMY-2(R252A)S1 were almost completely displaced from PII, indicating that myosin detached from F-actin due to the high ATP concentration. NMY-2(S251A)S1 remained in PII, indicating that it either did not detach or was able to rebind F-actin even in the presence of high ATP.

To assess the ability of the NMY-2 mutants to translocate F-actin, we performed *in vitro* motility assays. Heavy meromyosin (HMM) fragments (residues 1-1354 based on (Hu et al., 2002; Figure 5.2A), which are better suited than S1 fragments for this type of assay, were purified together with MLC-4 and MLC-5 (hereafter NMY-2HMM; Figure 5.S2B). Activation of myosin contractility requires phosphorylation of its regulatory light chain and motility assays commonly use the calmodulin-dependent myosin light chain kinase (MLCK) for myosin activation (Sellers, 1998). However, this pathway does not seem to be required for embryonic cytokinesis in *C. elegans* (Batchelder et al., 2007), which is more dependent on the RhoA kinase LET-502 (Piekny & Mains, 2002). We produced a truncated version of this kinase, LET-502(1-469), which is homologous to the human ROCK1 minimal kinase domain (residues 3-415) previously shown to be active *in vitro* (Khandekar et al., 2006). Incubation of NMY-2HMM with LET-502(1-469) and ATP led to a shift of the MLC-4 band in a native gel (Figure 5.2H). Analysis of the shifted band by mass spectrometry confirmed that it corresponded to MLC-4 phosphorylated on residue S17 or T18 (not distinguishable). LET-502(1-469)-activated NMY-2HMM was attached to the bottom of a flow chamber and rhodamine-labelled F-actin was flowed into the chamber. Imaging of F-actin demonstrated that wild-type NMY-2HMM was able to translocate F-actin. In contrast, F-actin did not move in the presence of NMY-2(S251A)HMM or NMY-2(R252A)HMM. In the absence of kinase, all NMY-2HMM versions bound to F-actin but filaments remained mostly immobile (Figure 2I).

In summary, these results show that wild-type NMY-2HMM is capable of both binding and sliding F-actin *in vitro*, whereas NMY-2(S251A)HMM and NMY-2(R252A)HMM bind to but do not slide F-actin. While NMY-2(R252A)S1 appears to be able to cycle on and off F-actin similar to wild-type myosin, NMY-2(S251A)S1 is ATP insensitive and locked in a high actin-affinity conformation.

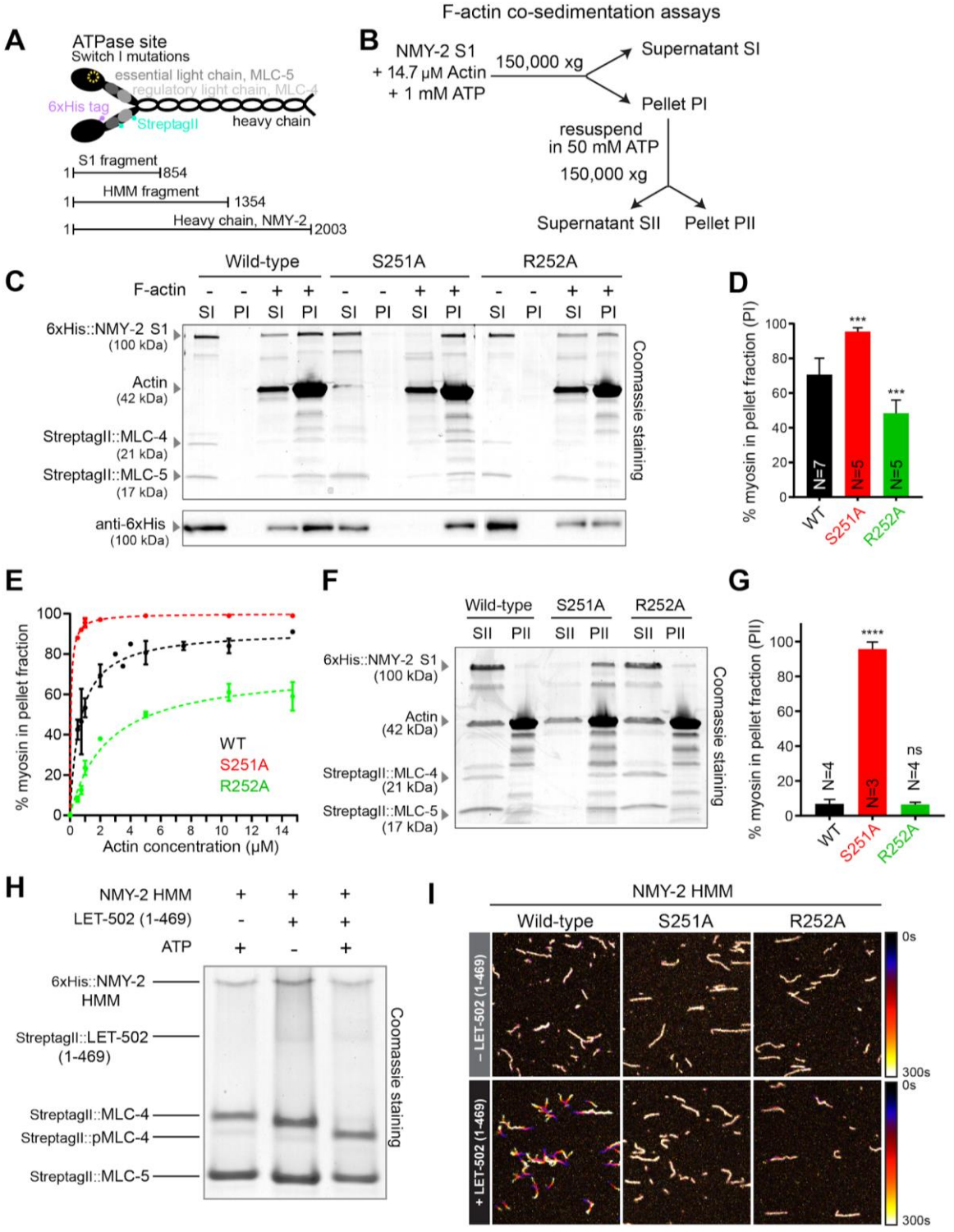

Figure 5.2 NMY-2(S251A) and NMY-2(R252A) bind but are unable to translocate actin filaments *in vitro*. (A) Schematic of the non-muscle myosin II depicting tags used for protein purification and S1 and HMM fragments. (B) Experimental procedure followed in C-G. (C) Coomassie-stained SDS-PAGE gel of SI and PI fractions from high-speed F-actin co-sedimentation assays (top). Immunoblot using an antibody against the 6xHistidine-tag (bottom). (D) Mean percentage ±95% CI of NMY-2 S1 present in PI, determined by measuring protein band intensities in Coomassie-stained SDS-PAGE gels as shown in C. (E) Mean percentage±s.d. of

NMY-2 S1 present in the pellet as a function of actin concentration. Dashed lines indicate the fitting of a one-site specific binding model using least-squares non-linear regression. (F) Coomassie-stained SDS-PAGE gel of SII and PII fractions from high-speed F-actin co-sedimentation assays. (G) Mean percentage±95% CI of NMY-2 S1 present in PII. (H) Coomassie-stained native gel of NMY-2HMM incubated with ATP, LET-502(1-469) or ATP and LET-502(1-469). (I) Time projections of selected regions showing F-actin sliding in the presence of wild-type or mutant NMY-2HMM in the absence or presence of LET-502(1-469). Color coding was used from black (0 s) to white (300 s). N is the number of independent experiments in D and G. Statistical significance was determined using one-way ANOVA followed by Bonferroni's multiple comparison test; ****P≤0.00001; ***P≤0.001; ns, not significant (P>0.05). Scale bar: 10 μm.

5.2.3 Myosin motor activity is essential for embryo production and development

Having established that NMY-2(S251A) and NMY-2(R252A) are motor-dead *in vitro*, we next used genome editing to introduce the mutations into NMY-2 *in vivo* (Arribere et al., 2014). Animals homozygous for either mutation exhibited severe gonad malformation and were consequently sterile (Figure 5.3A). To examine the impact of these mutants on embryogenesis, we introduced transgene-encoded wild-type NMY-2::mCherry into *nmy-2(S251A)* and *nmy-2(R252A)* animals. NMY-2::mCherry was expressed from the *nmy-2* promoter and 3′UTR and the transgene was partially re-encoded so it could be specifically depleted by RNAi (NMY-2::mCherrysen, sen indicating RNAi-sensitive; Figure 5.3B). The resulting strains were homozygous for both versions of NMY-2, which were expressed at similar levels (Figure 5.3C). The presence of NMY-2::mCherrysen allowed homozygous *nmy-2(S251A)* and *nmy-2(R252A)* mutants to develop normally into adulthood and lay viable eggs. When NMY-2::mCherrysen was penetrantly depleted using stringent RNAi conditions (see methods), *nmy-2(S251A)* and *nmy-2(R252A)* embryos were inviable (Figure 5.3D). These results demonstrate that NMY-2 motor activity is required for embryonic development.

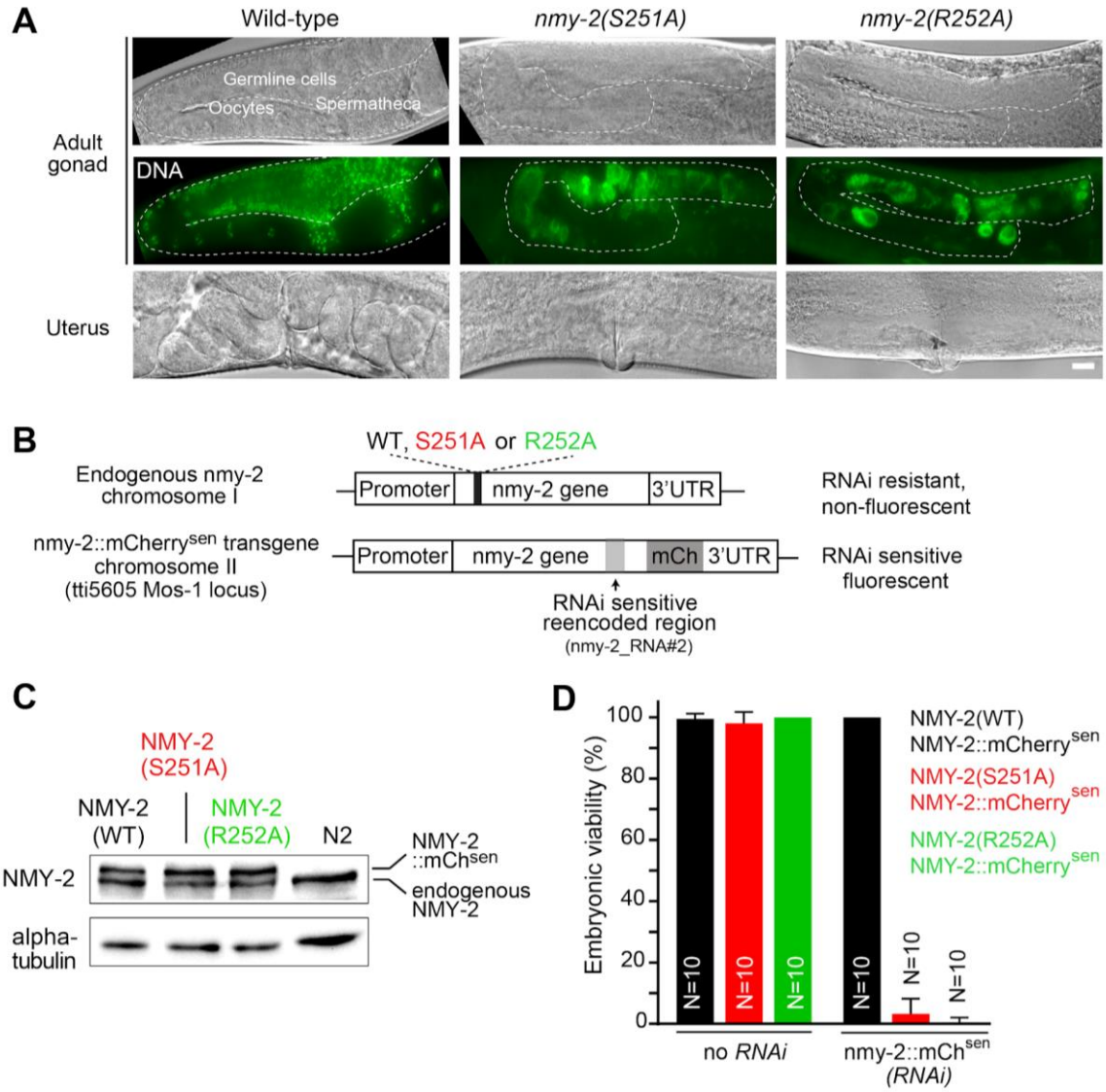

Figure 5.3 Motor-dead non-muscle myosin II does not support embryonic development. (A) Differential interference contrast images of the gonad (top) or uterus (bottom) in adult animals with indicated genotypes. Fluorescence images of DAPI-labelled DNA in the gonad region are shown in the central row. (B) Schematic of the endogenous and transgenic nmy-2 loci. Mutations were introduced in the endogenous nmy-2 gene on chromosome I by CRISPR/Cas9-mediated genome editing. A *wild-type* transgenic version of nmy-2 carrying a re-encoded region for RNAi sensitivity (sen) and fused to mCherry was introduced in single copy on chromosome II using MosSCI. (C) Immunoblot showing protein levels of endogenous NMY-2 and transgene-encoded NMY-2::mCherrysen in wild-type and mutant animals. α-Tubulin is used as loading control. (D) Embryonic viability (mean±95% CI) in the strains shown in B with or without penetrant depletion of NMY-2::mCherrysen. N denotes the number of animals whose embryonic progeny was examined. Statistical significance was determined using one-way ANOVA followed by Bonferroni's multiple comparison test; ****P≤0.0001. Scale bar: 10 μm

5.2.4 Motor-dead myosins do not support cytokinesis

Next, we asked whether NMY-2(S251A) and NMY-2(R252A) could support cytokinesis. Expression of the motor-dead myosins did not prevent wild-type NMY-2::mCherrysen from localizing in cortical patches during the first embryonic cytokinesis. However, myosin patches outside the cell equator were less abundant than in controls. The time of cytokinesis was not significantly affected (Figure 5.4E, -RNAi). When NMY-2::mCherrysen was penetrantly depleted by RNAi, *nmy-2(S251A)* and *nmy-2(R252A)* animals were sterile with non-compartmentalized gonads (data not shown). When we used less stringent RNAi conditions (mild NMY-2::mCherrysen depletion, see Materials and methods), the gonads of these animals presented multinucleated compartments, indicating problems with cytokinesis in this tissue (Figure 5.4A).

Although *nmy-2(S251A)* and *nmy-2(R252A)* animals became sterile after penetrant depletion of NMY-2::mCherrysen, we were able to examine the last fertilized one-cell embryos produced before onset of sterility. The majority of these embryos failed to initiate furrow ingression [69% in *nmy-2(S251A)*; 74% in *nmy-2(R252A)*; Figure 5.4B,C]. In the remaining embryos, the furrows ingressed partially, likely owing to the presence of residual wild-type NMY-2::mCherrysen (Figure 5.4B,C). We conclude that myosin motor activity is essential for cytokinesis.

To understand whether NMY-2(S251A) or NMY-2(R252A) affected a particular stage of cytokinesis, we performed mild depletions of NMY-2::mCherrysen. Under these conditions, the majority of mutant one-cell embryos completed cytokinesis but did so more slowly than wild-type embryos (490±45 s for S251A, 494±87 s for R252A, 219±14 s for controls; Figure 5.4D,E). We defined two intervals during early cytokinesis based on easily identifiable reference points: (1) the interval between anaphase onset and the formation of a shallow equatorial deformation, when contractile ring components are being recruited to the cell equator (‘ring assembly’); and (2) the interval between shallow deformation and the folding of the plasma membrane into a back-to-back configuration (‘furrow initiation’) (Figure 5.4D). To evaluate ring constriction, the rate of ring diameter decrease was calculated (Figure 5.4E). Abscission in *C. elegans* embryos only completes in the following round of cell divisions and was not analysed (Green et al., 2013). Mild depletion of NMY-2::mCherrysen in embryos expressing motor-dead myosins increased both intervals and slowed the ring constriction rate (0.11±0.01 µm/s for S251A, 0.12±0.01 µm/s for R252A, 0.18±0.01 µm/s for

controls; Figure 5.4D,E). The effects on cytokinesis were comparable with those obtained after partial depletion of NMY-2 in otherwise wild-type embryos (Figure 5.S3A-C). Interestingly, furrow initiation was already slightly delayed in *nmy-2(S251A)* and *nmy-2(R252A)* embryos without depleting NMY-2::mCherrysen, suggesting that the presence of motor-dead myosin interfered with the function of the wild-type version (-RNAi, Figure 5.4E).

Together, these data show that cytokinesis is progressively affected as the ratio of motor-dead to wild-type myosin increases. We conclude that myosin motor activity is required for ring assembly, furrow initiation and ring constriction, and that its ability to crosslink F-actin is therefore not sufficient for cytokinesis.

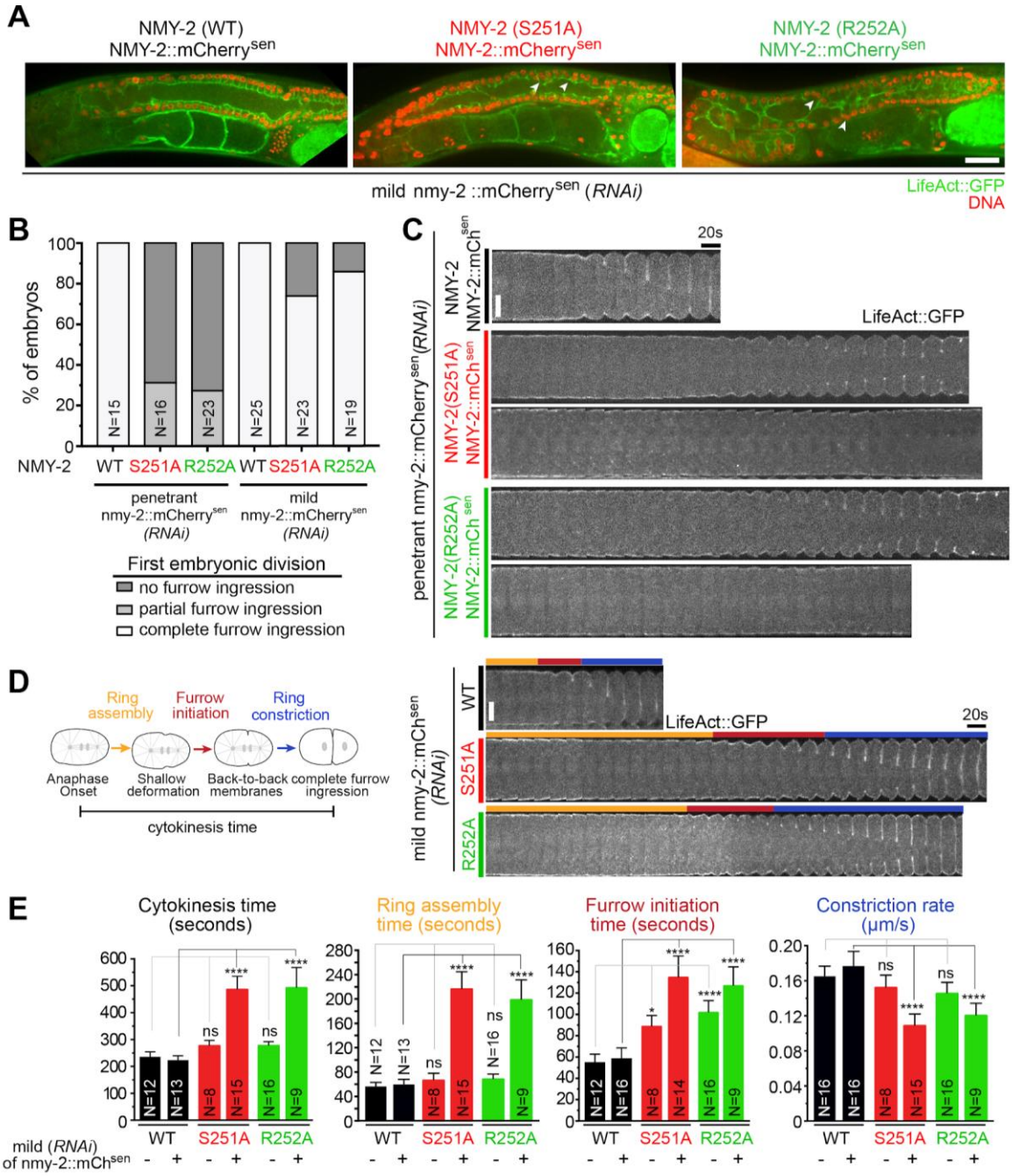

Figure 5.4 Motor activity of non-muscle myosin II is essential for cytokinesis. (A) Gonads of adult hermaphrodites with indicated genotypes. LifeAct::GFP labels gonad compartments and DNA is labelled with Hoechst 33342. Arrowheads indicate multinucleated compartments. (B) Percentage of embryos that complete (white), fail with partial ingression (light gray) or fail without ingression (dark gray) the first embryonic cytokinesis in animals with indicated genotypes after penetrant or mild depletion of NMY-2::mCherrysen. (C,D) Kymographs of the equatorial region of embryos with indicated genotypes after penetrant (C) or mild (D) depletion of NMY-2::mCherrysen. In C, two examples are shown for each mutant, one with partial furrow ingression and one with no furrow ingression. First frame corresponds to anaphase onset. Orange, red and blue bars indicate the intervals of ring assembly, furrow initiation and ring constriction, respectively, as depicted on the left in D. (E) Cytokinesis, ring assembly and furrow initiation time intervals and rate of ring constriction (mean±95% CI) in wild-type or mutant embryos subjected or not to mild depletion of NMY-2::mCherrysen. N is the number of

embryos analyzed. Statistical significance was determined using one-way ANOVA followed by Bonferroni's multiple comparison test; ****P≤0.0001; *P≤0.05; ns, not significant (P>0.05). Scale bars: 10 µm.

5.2.5 Partial impairment of myosin motor activity slows ring constriction and reduces the robustness of cytokinesis

We generated animals expressing NMY-2(S250A), which is predicted to result in a partially motor-impaired myosin (Shimada et al., 1997). Like S251 and R252, the S250 residue is located in the switch I region of the ATPase domain of myosin (Figure 5.1B, Figure 5.S1). We were able to generate homozygous animals expressing the equivalent mutation in muscle myosin: *unc-54(S239A)* (Figure 5.S4A-C). These animals displayed reduced locomotion in liquid (0.6±0.1 Hz versus 1.6±0.1 Hz in controls) and reduced egg-laying rate (3.7±0.5 eggs/h versus 5.8±0.3 eggs/h in controls), as expected for a myosin with partially-impaired motor activity (Figure 5.S4A,B). Body muscles in *unc-54(S239A)* animals presented a well-organized actin structure (Figure 5.S4C).

NMY-2(S250A)S1 co-sedimented with F-actin (Figure 5.5A,B), and its affinity for F-actin was similar to that of wild-type NMY-2S1 (0.66±0.13 µM for S250A and 0.66±0.21 µM for wild type). NMY-2(S250A)HMM was able to slide F-actin but movement was reduced compared with controls (Figure 5.5D, Figure 5.S4F).

Homozygous animals expressed NMY-2(S250A) at levels comparable with wild-type controls and were fully viable (Figure 5.S4D,E). Embryos expressing NMY-2(S250A) presented prolonged cytokinesis (263±7 s for S250A, 192±6 s for controls; Figure 5.5G). Ring assembly time was normal, but furrow initiation was delayed, and ring constriction rate was decreased (0.12±0.01 µm/s for S250A and 0.17±0.01 µm/s for controls; Figure 5.5G). We also generated NMY-2(R718C), which corresponds to R709C in mammalian myosin IIB (Figure 5.S5A). This mutant was able to bind F-actin similarly to wild type (Figure 5.S5D,E). Homozygous *nmy-2(R718C)* animals were fully viable and propagated normally (Figure S5F), and analysis of cytokinesis revealed delays similar to those observed in *nmy-2(S250A)* embryos (Figure 5.S5G). Together with the partial impairment of muscle function when the equivalent mutation was introduced into UNC-54 (Figure 5.S5B,C), these results are consistent with the idea that this mutation compromises, but does not abolish, myosin motor activity.

Next, we asked whether embryos expressing wild-type, NMY-2(S250A) or NMY-2(R718C) were sensitive to a decrease in overall myosin levels. After mild depletion of endogenous wild-type or mutant NMY-2, most embryos completed cytokinesis, albeit more slowly than non-depleted controls (441±26 s for S250A, 290±25 s for R718C, 271±9 s for wild type and 263±7 s for S250A no RNAi, 262±9 s for R718C no RNAi, 192±6 s for WT no RNAi; Figure 5.5F,H, Figure 5.S5G,H). Embryos with reduced levels of wild-type NMY-2 exhibited slight delays in ring assembly and furrow initiation, and a slight decrease in constriction rate (0.15±0.01 µm/s; Figure 5H). In contrast, embryos with reduced levels of NMY-2(S250A) exhibited substantial delays in ring assembly and furrow initiation and a substantial decrease in ring constriction rate (0.11±0.01 µm/s; Figure 5H). Additionally, four out of 22 *nmy-2(S250A)* embryos mildly depleted of NMY-2 failed cytokinesis, whereas all wild-type embryos completed cytokinesis successfully (18 out of 18). Mild depletion of NMY-2 in *nmy-2(R718C)* embryos decreased the ring constriction rate (0.13±0.01 µm/s; Figure 5.S5H) but did not affect the initial stages of cytokinesis nor lead to cytokinesis failure (Figure 5.S5H). We conclude that contractile rings with partially motor-impaired NMY-2 are less resilient to a decrease in myosin levels than rings with wild-type NMY-2.

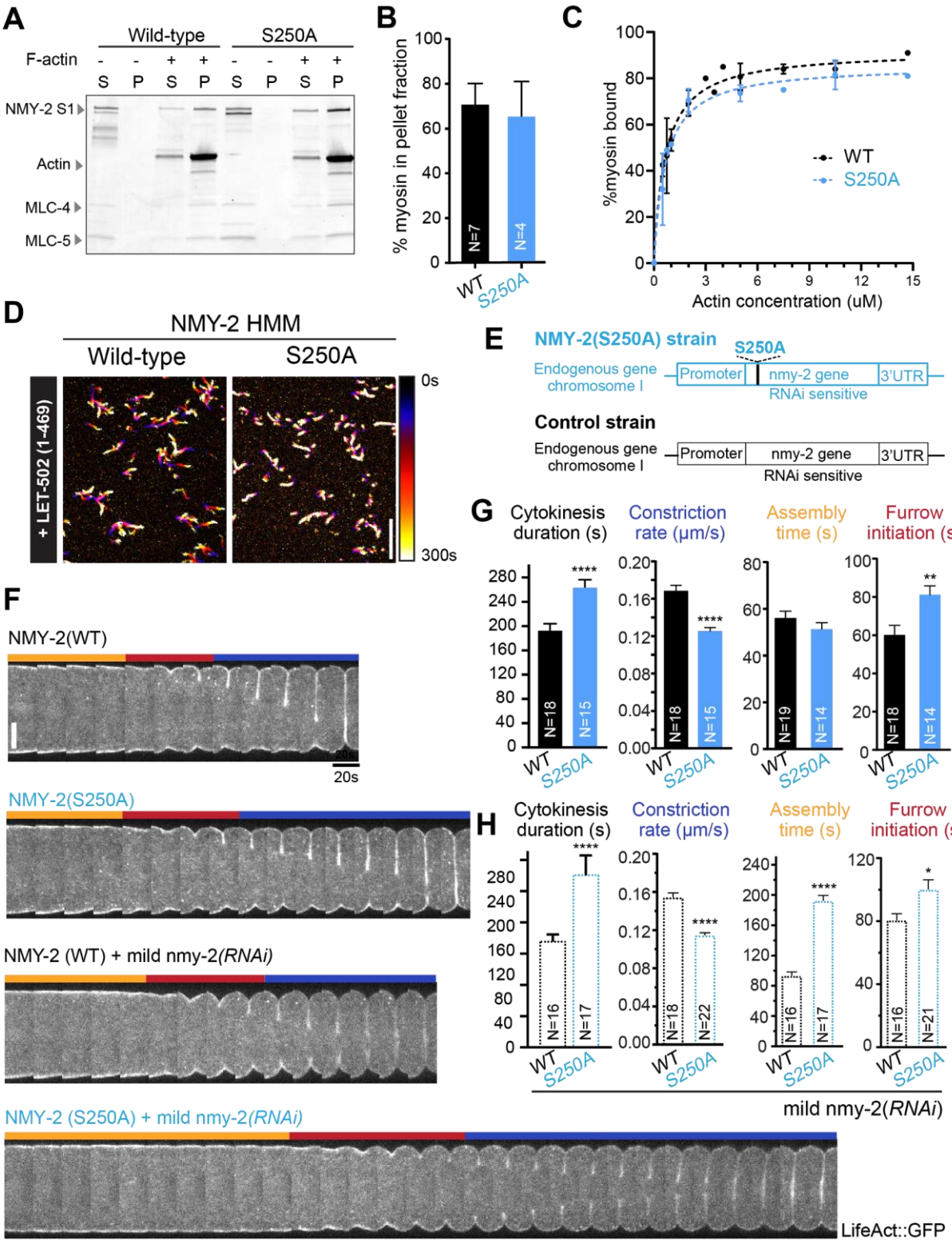

Figure 5.5 Partial impairment of non-muscle myosin II motor activity slows ring constriction and reduces cytokinesis robustness. (A) Coomassie-stained SDS-PAGE gel of supernatant (S) and pellet (P) fractions from high-speed F-actin co-sedimentation assays, where wild-type NMY-2S1 or NMY-2(S250A)S1 were incubated with 14.7 µM F-actin and 0.7 mM ATP before ultracentrifugation. (B) Mean percentage±95% CI of NMY-2 S1 present in the pellet, determined by measuring protein band intensities in Coomassie-stained SDS-PAGE gels as shown in A. (C) Mean percentage±s.d. of NMY-2 S1 present in the pellet as a function of actin concentration.

Dashed lines indicate the fitting of a one-site specific binding model using least-squares non-linear regression. (D) Time projections of movies of F-actin sliding in the presence of NMY-2HMM or NMY-2(S250A)HMM after phosphorylation by LET-502(1-469). Color coding was used from black (0s) to white (300s). (E) Schematic of the nmy-2 locus after introduction of the S250A mutation by CRISPR/Cas9-mediated genome editing. (F) Kymographs of the equatorial region of wild-type or S250A embryos with and without mild depletion of NMY-2. First frame corresponds to anaphase onset. Orange, red and blue bars indicate the intervals of ring assembly, furrow initiation and ring constriction, respectively, as depicted on the left in Figure 4D. (G,H) Cytokinesis, ring assembly and furrow initiation time intervals and rate of ring constriction (mean±95% CI) in wild-type or S250A embryos without (G) or with (H) mild NMY-2 depletion. N is the number of independent experiments in B, and the number of analyzed embryos in G,H. Statistical significance was determined using one-way ANOVA followed by Bonferroni's multiple comparison test; ****P≤0.0001; *P≤0.05; ns, not significant (P>0.05). Scale bars: 10 µm.

5.2.6 Perturbation of myosin levels or motor activity does not change actin levels during ring constriction

We also examined whether myosin modulated actin levels in the contractile ring. We found that the concentration of LifeAct::GFP in the constricting ring at 50% ingression was unaltered in all conditions tested: one-cell embryos expressing NMY-2(S250A), embryos expressing NMY-2(S251A) or NMY-2(R252A) in the presence of normal or decreased levels of NMY-2::mCherrysen, and wild-type NMY-2-expressing embryos partially depleted of NMY-2 (Figure 5.6A). In addition, as in control embryos, the concentration of LifeAct::GFP in the contractile ring remained constant throughout constriction after partial NMY-2 depletion (Figure 5.6B). We conclude that neither lowering myosin levels nor impairing myosin motor activity affects actin levels in the constricting ring.

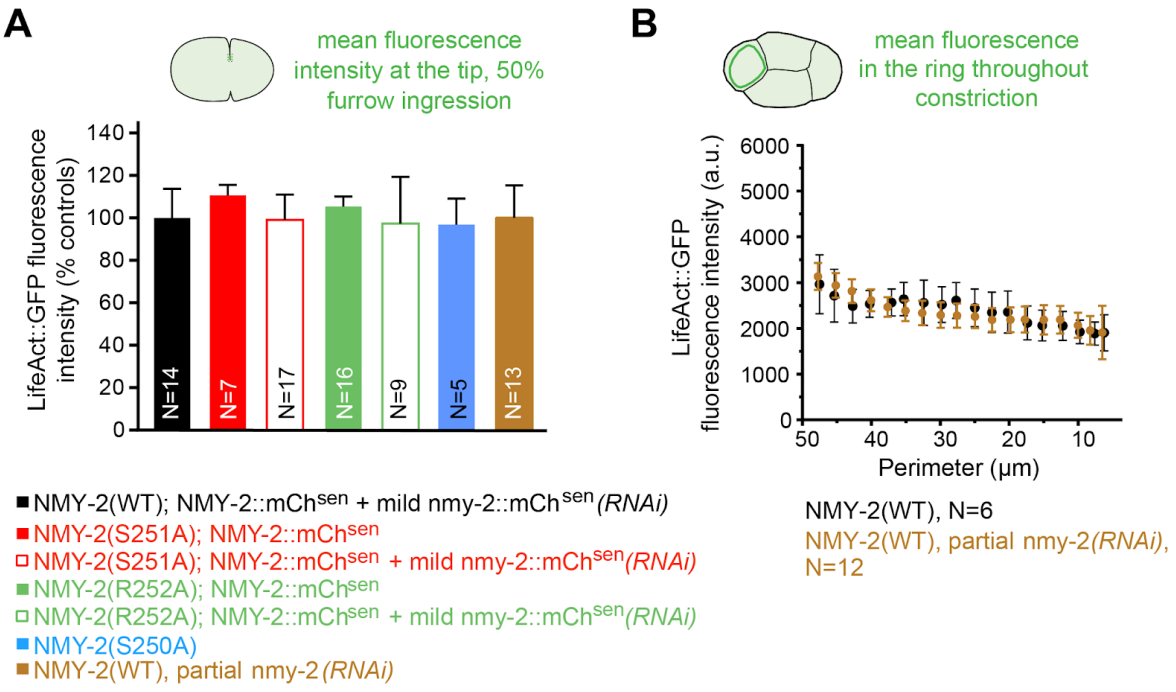

Figure 5.6 Impairment of non-muscle myosin II motor activity does not affect F-actin levels in the constricting contractile ring. (A) LifeAct::GFP levels (mean±95% CI) in the contractile ring at 50% furrow ingression in embryos with indicated genotypes and RNAi treatments (measured region is indicated in the schematic on top). Values were normalized to corresponding controls, which are NMY-2(WT);NMY-2::mChsen and NMY-2(WT). (B) Quantification of LifeAct::GFP levels (mean±95% CI) during ring constriction in the ABa cell of four-cell embryos, where the ring can be observed end-on. N is the number of embryos analyzed. Statistical significance was determined using one-way ANOVA followed by Bonferroni's multiple comparison test; ns, not significant (P>0.05).

5.2.7 Myosin motor activity is required for F-actin alignment at the division plane, compaction of the equatorial actin band and deformation of the equator

To better understand how decreasing NMY-2::mCherrysen levels in embryos expressing myosin motor-dead mutants impacts contractile ring formation and furrow initiation, we examined F-actin bundle behavior and actomyosin recruitment to the cell equator (Figure 5.7A,B). After mild depletion of NMY-2::mCherrysen in control embryos, formation of an equatorial band of actin (LifeAct::GFP) and myosin (NMY-2::mCherrysen) was promptly followed by equatorial deformation. Analysis of F-actin bundle orientation at the equator revealed fast bundle alignment perpendicular to the anterior-posterior embryo axis with maximum bundle alignment occurring shortly after shallow deformation (Figure 5.7D). In *nmy-2(S251A)* or *nmy-2(R252A)* embryos mildly depleted of NMY-2::mCherrysen, equatorial accumulation of actin occurred at a similar time to that in controls, but deformation of the cell equator was substantially delayed. Myosin recruitment to the cell equator was slower in myosin mutants than in controls, and myosin levels increased beyond control levels during furrow initiation (Figure 5.7A). Some F-actin bundles at the cell equator were slanted relative to the division plane (Figure 5.7A,B), and the width of the actin equatorial band was broader than in controls (Figure 5.7C). Analysis of F-actin bundle deviation from vertical alignment revealed that bundle alignment was slow and continued during furrow initiation (Figure 5.7D). In *nmy-2(S251A)* or *nmy-2(R252A)* embryos depleted of NMY-2::mCherrysen that failed to initiate furrowing, most F-actin bundles were slanted (Figure 5.7E). Partial depletion of NMY-2 in otherwise wild-type embryos led to the formation of a broad equatorial actin band with some slanted bundles, but enough myosin accumulated to allow for bundle alignment and furrowing (Figure 5.S3E-G). Once equatorial myosin reached a level that corresponded to 13.9±0.1% of that of controls (Figure 5.S3D), equatorial deformation ensued.

Together, these results indicate that motor-dead myosin does not support furrowing and that a threshold of motor-competent myosin needs to be reached for furrow initiation. We

conclude that myosin motor activity is required for equatorial band compaction, actin filament bundle orientation and equatorial deformation (Figure 5.7F).

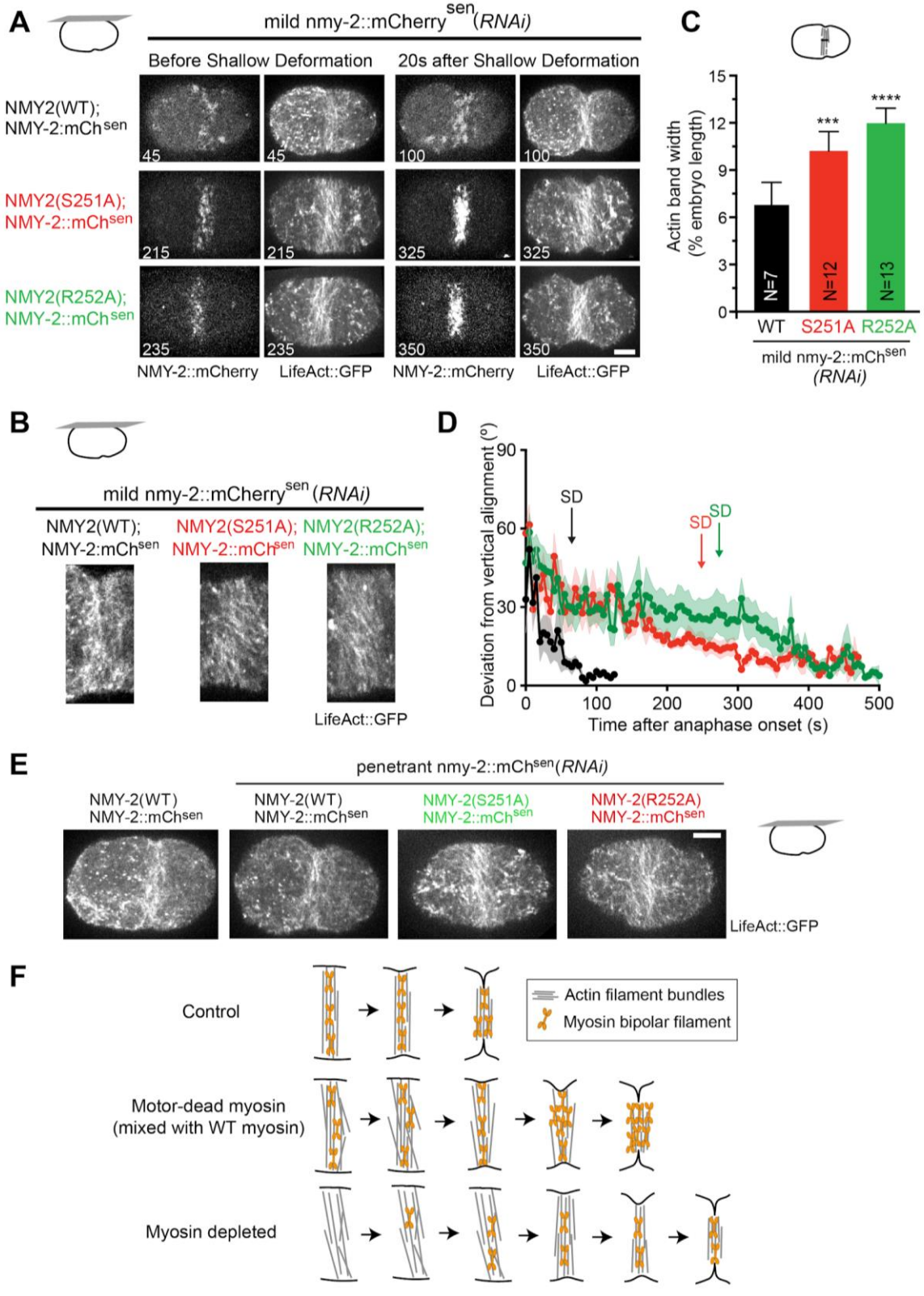

Figure 5.7 Equatorial accumulation of motor-competent myosin is rate limiting for furrow initiation. (A) Frames of time-lapse movies of one-cell embryos of the indicated genotypes co-expressing LifeAct::GFP and NMY-2::mCherrysen after mild depletion of NMY-2::mCherrysen. Numbers on frames indicate time after

anaphase onset. (B) Higher magnification of the cortical equatorial actin band in embryos of the indicated genotypes. (C) Width of equatorial actin band (mean±95% CI, normalized to embryo length) at shallow deformation for embryos of the indicated genotypes after mild depletion of NMY-2::mCherrysen. N is the number of analyzed embryos. (D) Deviation from vertical alignment of F-actin bundles (mean±s.e.m.) measured between anaphase onset and back-to-back membrane configuration in embryos of the indicated genotypes after mild depletion of NMY-2::mCherrysen. Average onset of equatorial shallow deformation (SD) is indicated. (E) Frames showing the equatorial actin band in embryos of the indicated genotypes after penetrant depletion of NMY-2::mCherrysen. (F) Summary of results. Statistical significance in C was determined using one-way ANOVA followed by Bonferroni's multiple comparison test; ****P≤0.0001; ***P≤0.001. Scale bars: 10 µm.

5.3 Discussion

5.3.1 Myosin motor activity is required for cytokinesis

We combined *in vivo* and *in vitro* characterization of two motor-dead and two partially motor-impaired myosins to show that myosin motor activity is essential for cytokinesis in *C. elegans* embryos. Our data reveal that motor-dead NMY-2(S251A) and NMY-2(R252A), which bind but do not translocate F-actin, fail to support cytokinesis in the early embryo. *nmy-2(S251A)* or *nmy-2(R252A)* embryos completed cytokinesis in the presence of transgene-encoded wild-type NMY-2 but did so with slightly slower kinetics than controls. This indicates that motor-dead NMY-2 hinders the activity of wild-type NMY-2, perhaps through the formation of heterotypic filaments, like those made up of different non-muscle myosin II isoforms or different myosin classes (Beach et al., 2014; Billington et al., 2015; Shutova et al., 2014). Indeed, co-polymerization of different non-muscle myosin II isoforms was shown to result in the formation of filaments with intermediate motile properties (Melli et al., 2018). The importance of myosin motor activity is reinforced by the observation that embryos whose only source of non-muscle myosin is partially motor-impaired NMY-2(S250A) or NMY-2(R718C) were delayed in cytokinesis. In addition, *nmy-2(S250A)* embryos were more sensitive to a reduction in overall myosin levels than wild-type embryos, indicating that in the presence of motor-impaired myosin more myosin molecules are needed to complete cytokinesis.

Our results imply that the ability of myosin to crosslink F-actin is not sufficient for cytokinesis and therefore contrast with results in COS-7 cells and mouse cardiomyocytes, where myosin was proposed to exert tension in a motor-independent manner during cytokinesis (Ma et al., 2012). We note that of the three myosin mutants presumed to be motor-dead in that report, NMIIA(N93K) was recently shown not to be motor-dead (Heissler et al., 2018) and our *in vivo* characterization of NMY-2(R718C) and UNC-54(R710C), which are equivalent to NMIIB(R709C), strongly argues that this myosin mutant is also not motor-dead. This is in

agreement with the characterization of the corresponding mutation in mammalian NMIIA, R702A, which was reported to translocate F-actin at half the velocity of wild-type NMIIA (Hu et al., 2002). The third myosin mutant analyzed by Ma et al. is NMIIB(R234A), which is equivalent to NMY-2(R252A). This mutant was recently proposed to be a bona fide motor-dead mutant in mammalian myosins (Heissler et al., 2018). NMIIB(R234A) was able to ameliorate cytokinesis defects in COS-7 cells depleted of NMIIB, while we show that NMY-2(R252A) does not support cytokinesis in the *C. elegans* embryo. The *Dictyostelium discoideum* mutant MYS2(R238A), which corresponds to NMY-2(R252A) and NMIIB(R234A), caused very slow cell growth when cultured in suspension, but supported apparently normal cytokinesis when cells grew adhered to a surface (Shimada et al., 1997). This indicates that cytokinesis operates differently when cells divide while adhering to a surface. Indeed, some adherent cultured cells can divide with a compromised contractile ring in an adhesion-dependent manner by migrating away in opposite directions during cell division (Dix et al., 2018; Kanada et al., 2005; Nagasaki et al., 2009; O'Connell et al., 1999).

5.3.2 Myosin motor activity is required during furrow ingression

We observed that in embryos co-expressing motor-dead NMY-2(S251A) or NMY-2(R252A) with low levels of transgene-encoded wild-type myosin (i.e. after mild RNAi of NMY-2::mCherrysen), the rate of contractile ring constriction slowed substantially. These embryos were also delayed in contractile ring assembly and furrow initiation presented reduced F-actin bundle alignment and increased actin band width at the cell equator before furrow ingression. Therefore, it is possible that defects in F-actin architecture contribute to the slowdown in ring constriction in these mutants. However, embryos solely expressing partially motor-impaired NMY-2(S250A) or NMY-2(R718C), which bind F-actin similarly to wild-type NMY-2, assembled contractile rings with normal timing and appearance, yet were still delayed in furrow initiation and had a slower rate of ring constriction. Thus, ring constriction slowdown in *nmy-2(S250A)* and *nmy-2(R718C)* embryos is unlikely to be a consequence of improperly assembled contractile rings. This indicates that myosin motor activity continues to be required after the contractile ring is formed and that motor activity sets the contraction speed of the F-actin network of the ring. Our results therefore argue against the hypothesis that contractile stress induced by passive F-actin crosslinking combined with F-actin treadmilling is sufficient to drive ring constriction independently of myosin motor activity (Mendes Pinto et al., 2012; Oelz et al., 2015). Our data are in agreement with that obtained for contractile rings isolated from fission yeast expressing a myo2 mutant (myo2-E1-Sup1,

carrying G345R, Q640H and F641I mutations) that binds tightly to actin but does not translocate F-actin *in vitro* (Palani et al., 2017). Contrary to controls, isolated mutant rings did not constrict in the presence of ATP. Interestingly, 65% of *S. pombe* cells expressing myo2-E1-Sup1 were able to complete cytokinesis because of the compensating activity of Myp2 (another myosin II isoform) and perhaps Myo51 (a myosin V), which are both normally dispensable (Palani et al., 2017).

It is possible that myosin motor activity contributes to contractile ring constriction by determining F-actin turnover, as proposed previously (Guha et al., 2005; Mendes Pinto et al., 2012; Murthy & Wadsworth, 2005; Wilson et al., 2010). The concentration of actin in the contractile ring remains constant throughout constriction, which indicates that there is net depolymerization of F-actin as the ring becomes smaller (Carvalho et al., 2009). We observe that the rate of contractile ring constriction slows in myosin motor mutants, yet the concentration of actin in the ring at 50% of ingression is the same as in controls. This indicates that rings that constrict more slowly due to impaired myosin motor activity experience proportionally slower net depolymerization of F-actin such that the actin concentration in the ring remains the same as in controls.

Myosin has been implicated in disassembling F-actin networks (Backouche et al., 2006; Haviv et al., 2008; Medeiros et al., 2006; Reymann et al., 2012; Wilson et al., 2010), likely through F-actin buckling. F-actin buckling has been proposed to be caused by myosin filaments with slightly different velocities (Lenz et al., 2012), and F-actin buckles have a higher curvature and should therefore be more prone to severing (Murrell & Gardel, 2012; Schramm et al., 2017; Vogel et al., 2013). Our analysis of actin levels in the constricting ring in myosin motor mutants is consistent with the idea that myosin motor activity disassembles F-actin. Net depolymerization of F,-actin could directly drive ring constriction or it could keep ring structure optimized for myosin-driven contractility.

5.3.3 Furrow initiation occurs once sufficient amounts of motor-competent myosin have accumulated at the equator

We show that cytokinesis is successful in embryos co-expressing equal amounts of wild-type and motor-dead myosin, and that similar amounts of NMY-2::mCherrysen are recruited to the equator in *nmy-2(WT)*, *nmy-2(S251A)* and *nmy-2(R252A)* embryos. By contrast, when motor-dead myosin is present in excess of wild-type myosin, i.e. after mild depletion of NMY-

2::mCherrysen in *nmy-2(S251A)* or *nmy-2(R252A)* embryos, we observe enhanced recruitment of NMY-2::mCherrysen to the cell equator (Figure 5.7A). We speculate that the excess of motor-dead myosin may favor the formation of homotypic motor-dead filaments that hinder contractility. In this scenario, more wild-type myosin would need to be recruited to the equator to achieve sufficient contractility for furrow initiation. Our results also reveal that when NMY-2 is substantially depleted by RNAi in wild-type animals, equatorial deformation occurs when myosin levels at the equator have reached 14% of control levels. This is consistent with the idea that when total myosin levels are low, less equatorial myosin is required for furrow initiation because there is also less cortical tension that resists furrowing (Silva et al., 2016). Overall, our results support the idea that a threshold level of myosin-based contractility is required to initiate furrowing. We propose that the accumulation of motor-competent myosin at the equatorial region is rate limiting for furrow initiation and that proper F-actin alignment at the division plane, compaction of the equatorial actin band and deformation of the equator are dependent on myosin motor activity.

How myosin is recruited to the cell equator is still debated and may involve a diffusion-retention mechanism dependent on local RhoA activation (Bement et al., 2005; Kimura et al., 1996; Uehara et al., 2010), myosin mechanosensitivity and catch-bonding behavior (Capitanio et al., 2012; Guo & Guilford, 2006; Vernerey & Akalp, 2016), and/or equator-directed cortical flows (Bray & White, 1988; Khaliullin et al., 2018; Reymann et al., 2016). If equator-directed flows contribute to the accumulation of excess NMY-2::mCherrysen in the ring when motor-dead myosin is present, then other cortical components, such as anillin and septins, may also accumulate in excess. It will also be interesting to address how myosin motor mutants affect cortical actin flows, which have been described to drive alignment and compaction of F-actin in the ring and to be myosin dependent (Reymann et al., 2016).

5.3.4 Motor activity of major muscle myosin is dispensable for F-actin organization in adult muscle

We used motility assays to show that our myosin motor mutants were defective in translocating F-actin *in vitro*. However, this does not necessarily reflect the situation *in vivo*, where a variety of actin regulators co-exist. We used muscle contraction as an *in vivo* readout of motor-impairment in myosin II mutants. Animals expressing UNC-54(S240A) or

UNC-54(R241A), which are equivalent to NMY-2(S251A) and NMY-2(R252A), respectively, displayed a dramatic reduction in movement (with residual movement depending on the other muscle myosin, MYO-3) and were unable to lay eggs. As both of these behaviors depend on the contraction of muscle sarcomeres, these results strongly suggest that the mutations result in motor-dead muscle myosin. Interestingly, and in contrast to UNC-54 depletions, F-actin organization in adult muscle was not overtly affected by motor-dead UNC-54. This is in agreement with results from flight muscles in *Drosophila melanogaster* that suggested that muscle myosin motor activity is largely dispensable for the high-order organization of F-actin during sarcomere maturation (Loison et al., 2018). The movement of animals expressing UNC-54(S239A), which is equivalent to NMY-2(S250A), was reduced but not abolished, in agreement with the prediction that this mutation produces partially motor-impaired myosin.

Overall, our data and previous studies of other myosin II proteins suggest that mutating specific highly conserved residues in the switch I loop of the ATP binding site consistently produces motor-dead and partially motor-impaired myosin in different myosin II families. Therefore, these mutations should be useful to study the role of myosin II motor activity in a variety of tissues.

5.4 Supplemental Data

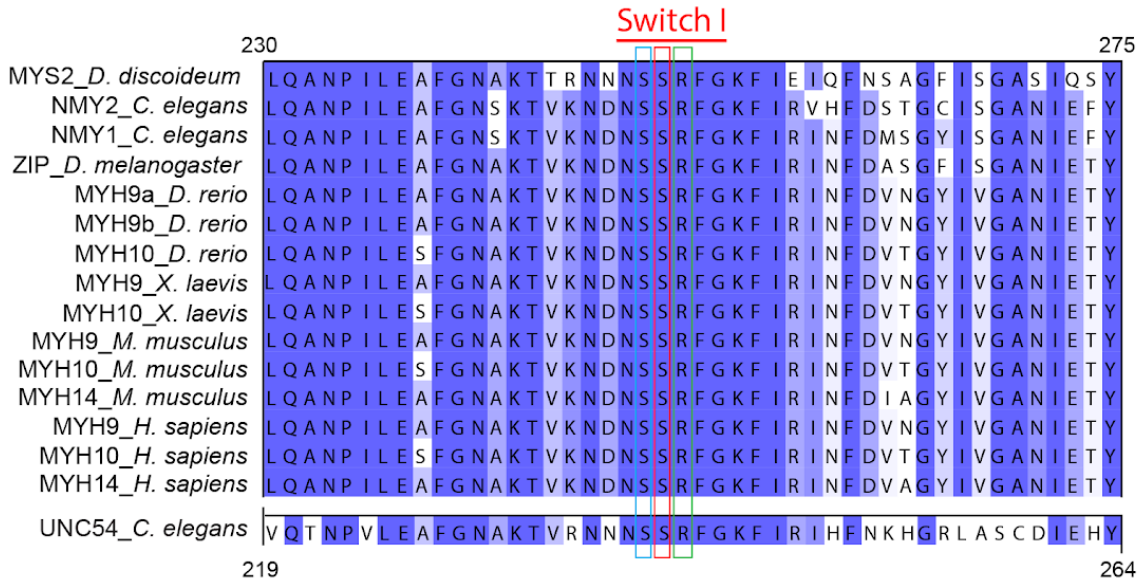

Figure 5.S1 Conservation between non-muscle myosin IIs from different species. Alignment of non-muscle

myosin IIs of several species along with *C. elegans* muscle myosin heavy chain B (UNC-54) showing conservation of the ATPase domain containing the switch I motif. Residues mutated in this study are boxed in cyan, red and green.

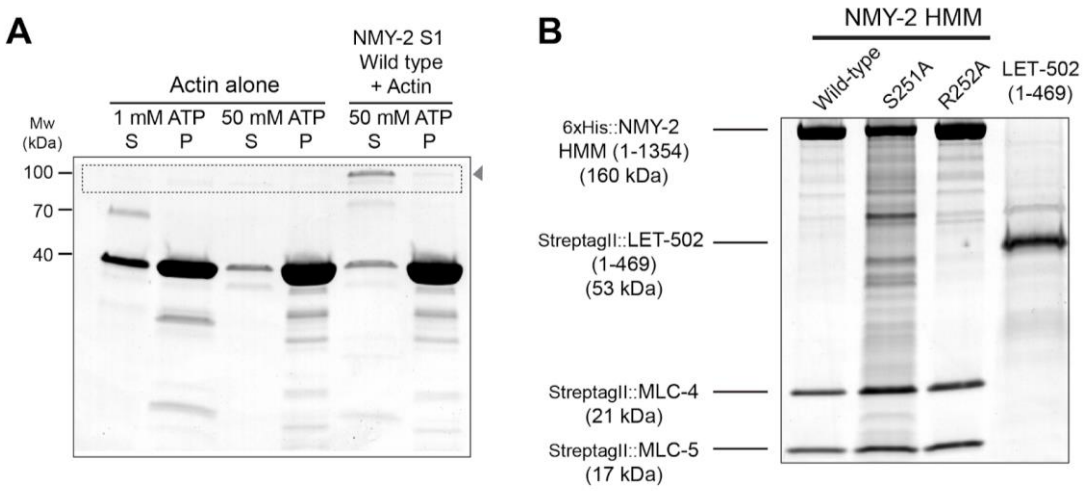

Figure 5.S2 F-actin samples used in high-speed co-sedimentation assays and NMY-2HMM and LET-502(1-469) used for motility assays. (A) Coomassie-stained SDS-PAGE gel of high-speed F-actin co-sedimentation in the absence of myosin showing supernatant and pellet fractions I in the presence of 0.7 mM ATP (lanes 1 and 2) and after resuspension with 50 mM ATP (lanes 3 and 4), or in the presence of wild-type NMY2 and resuspended in 50 mM ATP. (B) Coomassie-stained SDS-PAGE gel of purified NMY-2(1- 1354) HMM fragments in complex with MLC-4 and MLC-5 (lanes 1-3) and purified LET-502(1- 469).

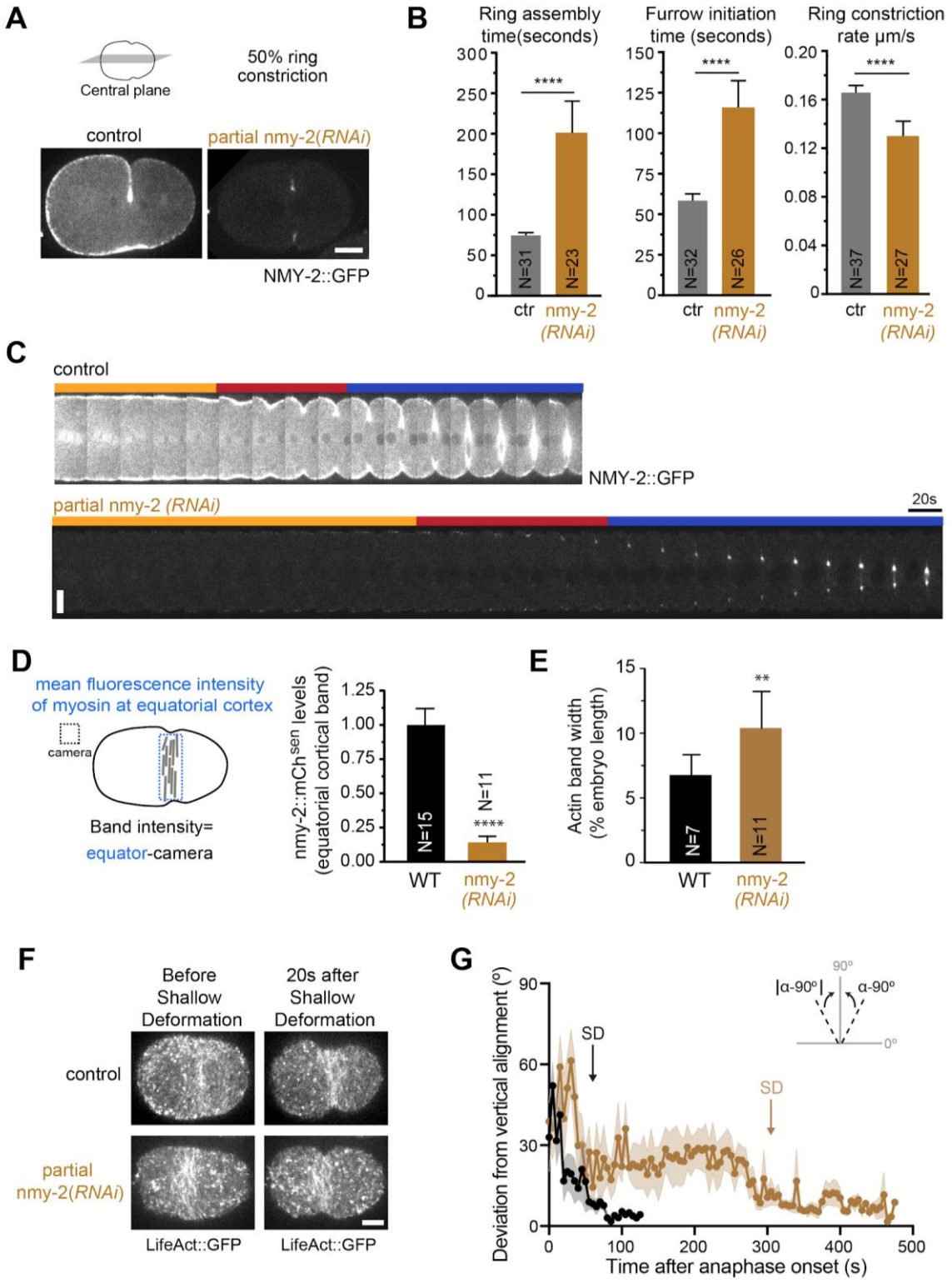
A
Central plane
50% ring constriction
control
partial nmy-2(RNAi)
NMY-2::GFP
B
Ring assembly time(seconds)
Furrow initiation time (seconds)
Ring constriction rate µm/s
****
N=31
N=23
N=32
N=26
N=37
N=27
ctr
nmy-2 (RNAi)
C
control
NMY-2::GFP
partial nmy-2 (RNAi)
20s
D
mean fluorescence intensity of myosin at equatorial cortex
camera
Band intensity=
equator-camera
nmy-2::mCh^sen levels (equatorial cortical band)
N=15
N=11
WT
nmy-2 (RNAi)
E
Actin band width (% embryo length)
**
N=7
N=11
F
Before Shallow Deformation
20s after Shallow Deformation
control
partial nmy-2(RNAi)
LifeAct::GFP
G
Deviation from vertical alignment (°)
SD
Time after anaphase onset (s)
|α-90°|
α-90°

Figure 5.S3 Partial depletion of NMY-2 in *wild-type* embryos allows cytokinesis to complete, albeit more slowly than in controls. (A) Central plane at 50 % furrow ingression of a control embryo and an embryo partially depleted of NMY-2 expressing NMY-2::GFP. (B) Ring assembly and furrow initiation time intervals and rate of ring constriction (mean±95% CI). (C) Kymographs of furrow region. Time zero corresponds to anaphase onset. Orange, red and blue bars indicate the intervals of ring assembly, furrow initiation and ring constriction, as depicted in Figure 4D. (D) Quantification of mean NMY2::mCherrysen levels at the equatorial cortex, measured as indicated on the left. Note that nmy2(RNAi) depletes both endogenous NMY-2 and transgene-encoded NMY-2::mCherrysen. N is the number of embryos analyzed. (E) Equatorial actin band width normalized to embryo length at shallow deformation. (F) Stills of one-cell embryos expressing LifeAct::GFP before and after equatorial shallow deformation. (G) Deviation from vertical alignment of F-actin bundles (mean±SEM), measured between anaphase onset and back-to-back membrane configuration. Average onset of equatorial shallow deformation (SD) is indicated. Statistical significance was determined using the t-test; **** P≤0.0001, ** P≤0.01. Scale bars, 10 µm.

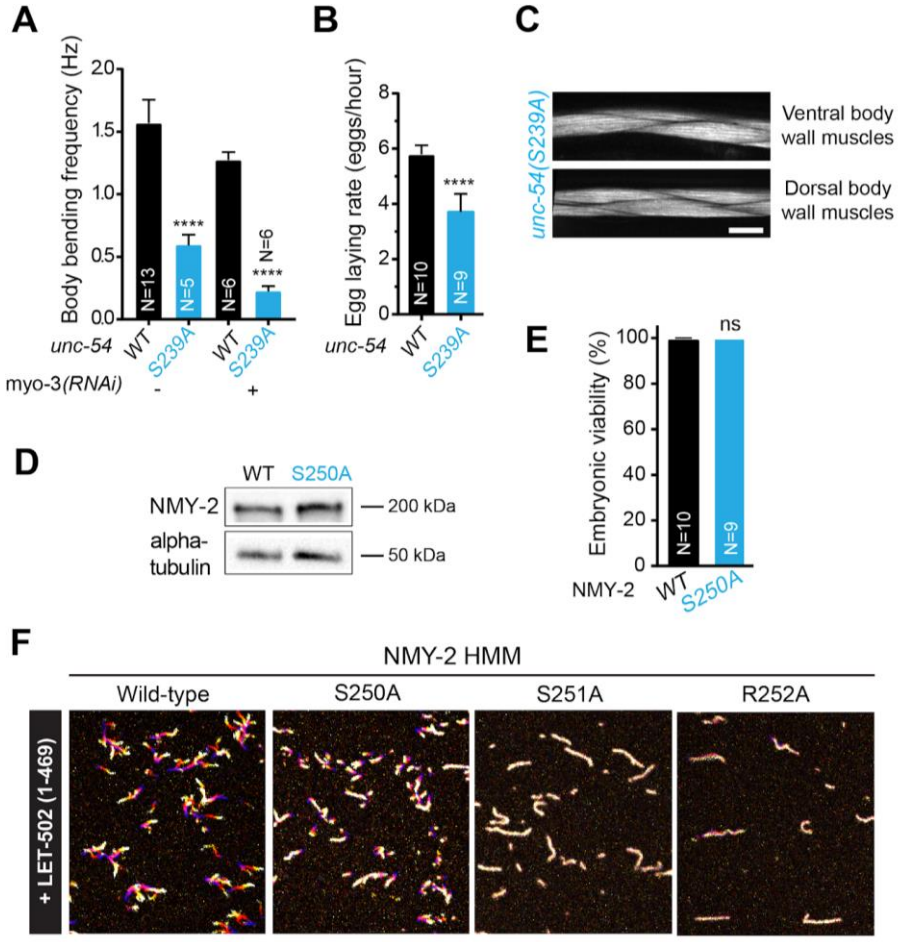

Figure 5.S4 Additional characterization of NMY-2(S250A) and UNC-54(S239A) mutants. (A) Body bend frequency in liquid (mean±95% CI) in wild-type and unc-54(S239A) animals with and without depletion of MYO-3. (B) Egg laying rate (mean±95% CI) in *wild-type* and *unc54(S239A)* animals. (C) Phalloidin staining of body wall muscles in *unc-54(S239A)* animals. (D) Immunoblot showing NMY-2 levels in *wild-type* and *nmy-2(S250A)* animals. α-tubulin is used as loading control. (E) Embryonic viability (mean±95% CI) in *wild-type* or *nmy-2(S250A)* animals. (F) Time projections of movies of F-actin sliding in the presence of wild-type, S250A, S251A or R252A NMY-2 HMMs after phosphorylation by LET-502(1-469). Color coding was used from black (0s) to white (300s). N is the number of animals analyzed in A and B and the number of animals whose progeny was analyzed in E. Statistical significance was determined using oneway ANOVA followed by Bonferroni's multiple comparison test; **** P≤0.0001, ns=not significant (P>0.05). Scale bars, 10 µm.

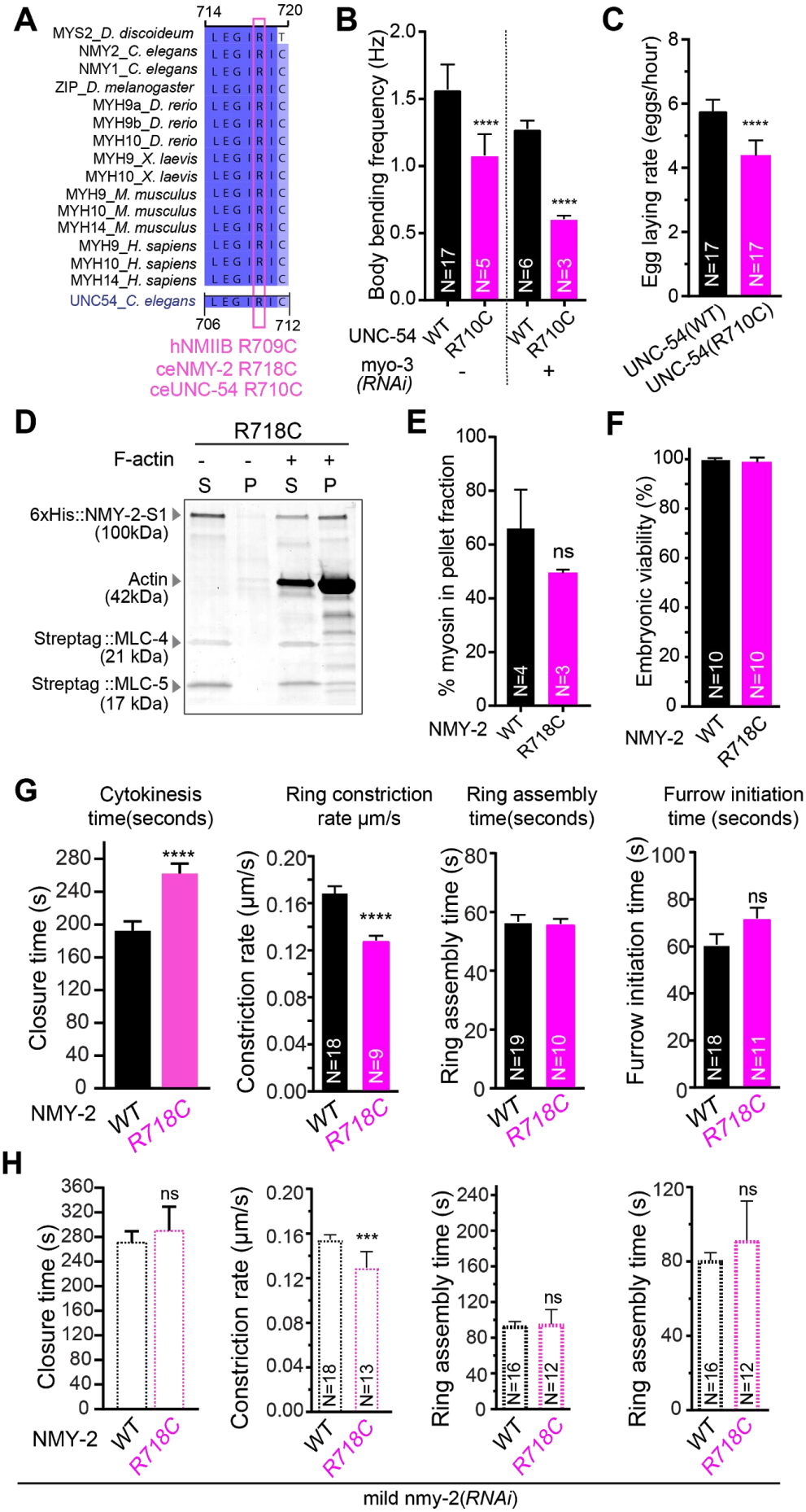
A
714
720
MYS2_D. discoideum
NMY2_C. elegans
NMY1_C. elegans
ZIP_D. melanogaster
MYH9a_D. rerio
MYH9b_D. rerio
MYH10_D. rerio
MYH9_X. laevis
MYH10_X. laevis
MYH9_M. musculus
MYH10_M. musculus
MYH14_M. musculus
MYH9_H. sapiens
MYH10_H. sapiens
MYH14_H. sapiens
UNC54_C. elegans
706
712
hNMIIB R709C
ceNMY-2 R718C
ceUNC-54 R710C
B
Body bending frequency (Hz)
UNC-54
myo-3 (RNAi)
WT
R710C
N=17
N=5
N=6
N=3
C
Egg laying rate (eggs/hour)
UNC-54(WT)
UNC-54(R710C)
N=17
N=17
D
R718C
F-actin
S
P
6xHis::NMY-2-S1 (100kDa)
Actin (42kDa)
Streptag ::MLC-4 (21 kDa)
Streptag ::MLC-5 (17 kDa)
E
% myosin in pellet fraction
NMY-2
WT
R718C
N=4
N=3
ns
F
Embryonic viability (%)
N=10
N=10
G
Cytokinesis time(seconds)
Closure time (s)
Ring constriction rate µm/s
Constriction rate (µm/s)
Ring assembly time(seconds)
Ring assembly time (s)
Furrow initiation time (seconds)
Furrow initiation time (s)
N=18
N=9
N=19
N=10
N=18
N=11
H
N=18
N=13
N=16
N=12
N=16
N=12
mild nmy-2(RNAi)

Figure 5.S5 NMY-2(R718C), which is equivalent to human NMIIB(R709C), is not motor-dead. (A) Alignment of non-muscle myosin IIs of several species along with C. elegans muscle myosin heavy chain UNC-54 showing conservation of the SH1 helix region. (B) Body bend frequency in liquid (mean±95% CI) in wild-type and unc-54(R710C) animals with and without depletion of MYO-3. (C) Egg laying rate (mean±95% CI) in wild-type and unc-54(R710C) animals. (D) Coomassie-stained SDS-PAGE gel of high-speed F-actin co-sedimentation assays in which the NMY-2(R718C)S1 was incubated with and without 14.7 μM of F-actin before ultracentrifugation. (S) indicates the supernatant and (P) the pellet fractions. (E) Percentage (mean±95% CI) of NMY2S1 present in the pellet, determined by measuring protein band intensities in Coomassie-stained SDS-PAGE gels as shown in (D). (F) Embryonic viability (mean±95% CI) in wild-type or nmy2(R718C) animals. (G, H) Cytokinesis, ring assembly and furrow initiation time intervals and rate of ring constriction (mean±95% CI) in *wild-type* and *nmy-2(R718C)* embryos with and without mild depletion of NMY-2. N is the number of analyzed animals in B and C, the number of animals whose progeny was analyzed in F, the number of independent experiments in E, and the number of analyzed embryos in G and H. Statistical significance was determined using one-way ANOVA followed by Bonferroni's multiple comparison test; **** P≤0.0001, ** P≤0.01, ns=not significant (P>0.05)

CHAPTER 6

INVESTIGATING THE EXISTENCE OF PLASMA MEMBRANE-BOUND NON-MUSCLE MYOSIN II DURING CYTOKINESIS

6. INVESTIGATING THE EXISTENCE OF PLASMA MEMBRANE-BOUND NON-MUSCLE MYOSIN II DURING CYTOKINESIS

6.1 Introduction

There is evidence that the binding of NMII to membranes is important for various of its cellular roles. NMII is involved in vesicle transport along F-actin in clam oocytes (DePina et al., 2007) and in the formation and transport of Golgi vesicles in mammalian cells (Ikonen et al., 1997; Durán et al., 2003). NMII was also shown to localize to the plasma membrane of HeLa cells in interphase when F-actin is depolymerized by Latrunculin A (Liu et al., 2016). *In vitro* experiments showed that recombinant mammalian NMII can directly bind to negatively charged liposomes and this binding substantially increases in the absence of the RLC (Liu et al., 2016). During cytokinesis the existence of a membrane bound myosin population has not been thoroughly explored.

In *D. melanogaster* neuroblasts, NMII RLC was shown to be anchored in the plasma membrane through the Phosphatidylinositol 4-phosphate (PI(4)P) transfer protein, Vibrator, and that Vibrator regulates cell division (Koe et al., 2018).

In *S. pombe*, the contractile ring forms from the coalescence of nodes of proteins, where all the contractile ring machinery is located (Wu et al., 2006; Vavylonis et al., 2008; Pollard & Wu, 2010). F-actin grows from the nodes, and NMII grabs and pulls on the F-actin from neighbouring nodes, leading to node coalescence. The use of advanced high-resolution microscopy allowed the determination of the node architecture at a nanometer resolution, and by using this technique, NMII was described to have its tail near the plasma membrane while its head domain points towards the cytoplasm (Laporte et al., 2011; Laplante et al., 2016). Anillin Mid1p, F-BAR Cdc15p, IQGAP Rng2p, and the formin Cdc12p were shown to form the base of the node that anchors the ends of NMII tails to the plasma membrane. This arrangement was proposed to be equivalent to the NMII bipolar filaments of animals and amoebas, but with radial geometry. A more recent coarse-grained computational model for cytokinesis suggested that contractile ring constriction in the presence of nodes, would result in membrane folds that have not been observed (Nguyen et al., 2018). In the model, which takes in account the existing data described above as well as recent electron cryotomography data (Swulius et al., 2018), and the participation of unipolar and bipolar myosin during cytokinesis, bipolar myosins bound to F-actin in the ring drive contraction, while membrane-bound, unipolar myosins, transmit force to the membrane. Given all these, it is possible that during cytokinesis two myosin pools co-exist, one that forms bipolar

filaments through the tail that interdigitates F-actin and another that binds to the plasma membrane in a direct or indirect manner through the tail and to F-actin via the head domain. In this chapter, I assessed if such a membrane-bound pool exists in *C. elegans* and if this pool plays a role during cytokinesis. My results suggest that NMII NMY-2 can directly bind phospholipids and that a pool of NMY-2 that binds the plasma membrane is likely to exist during cytokinesis in the early *C. elegans* embryo.

6.2 Results

6.2.1 NMY- 2 has putative membrane binding sites

Since NMY-2 has no described membrane-binding domains, I started by exploring whether NMY-2 could have unstructured domains that could mediate membrane binding. To do that, I used the BH-search software (Brzeska et al., 2010), which was developed to identify or predict unstructured membrane-binding domains comprising basic and hydrophobic amino-acids. The software is optimized for cytoskeletal proteins, kinases and GTP-binding proteins that bind lipids through less structured regions (Brzeska et al., 2010). Other predictive softwares exist but they are based in potential membrane-penetrating regions or lipid-binding sites with highly defined tertiary structures (Lemmon, 2008), which do not exist in myosins that are known to bind to the plasma membrane as those from class I (Doberstein et al., 1992; Brzeska et al., 2010). The score is an updated hydrophobicity scale that considers both the distribution of hydrophobic and basic amino acids which are the ones that usually bind to the plasma membrane. I found that NMY-2 has three potential binding sites (Figure 6.1), the first two being in the head domain, and the third in the neck domain. This prediction suggests that NMY-2 may be able to directly bind to the plasma membrane and may not require an adaptor.

Sequence 1 :EMBOSS_001

Peak 1: 835 - 847 (13 aa) : area 2.19
Peak 2: 450 - 454 (5 aa) : area 0.34
Peak 3: 446 - 448 (3 aa) : area 0.21

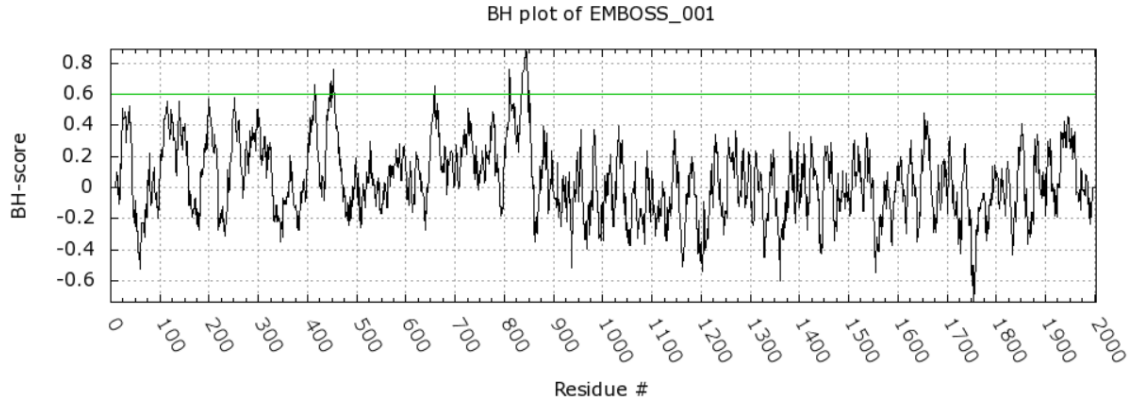

Figure 6.1 Potential membrane-binding sites in NMY-2 determined by BH-search software. Three NMY-2 regions are putative binding sites to the plasma membrane. The score of the amino acids on positions 446-448, 450-454 and 835-847 is above the 0.6 scale cut-off, which indicates that these residues have the hydrophobicity required for the attachment to the plasma membrane.

6.2.2 NMY-2-MLC-4-MLC-5 complex binds directly to phospholipids in vitro

To test whether NMY2 can directly bind phospholipids in vitro, we used PIP strips, which are hydrophobic membranes that have been spotted with eight phosphoinositides and seven other biologically important lipids. As it has been shown that mammalian NMII can bind to phospholipids via the RLC binding site and that *D. melanogaster* RLC directly binds to phospholipids (Liu et al., 2016 ; Koe et al., 2018), we tested the ability of MLC-4 alone, NMY-2 in a complex with both MLC-4 and MLC-5, and NMY-2 in a complex just with MLC-5 to bind the PIP strips. All these were purified by myself and my co-supervisor by affinity chromatography followed by size exclusion chromatography. As a positive control we used a commercial recombinant glutathione S-transferase (GST)-tagged PLC-δ1 PH domain protein that binds PIP2. The lipidic membranes were incubated with 6xHIS::NMY-2/StreptagII::MLC-4/StreptagII::MLC-5, 6xHIS::NMY-2/StreptagII::MLC-5 or StreptagII::MLC-4 and bound protein was then detected through an immunoassay with specific antibody against the anti-GST, anti-6xHIS, or anti-StreptagII purification tags.

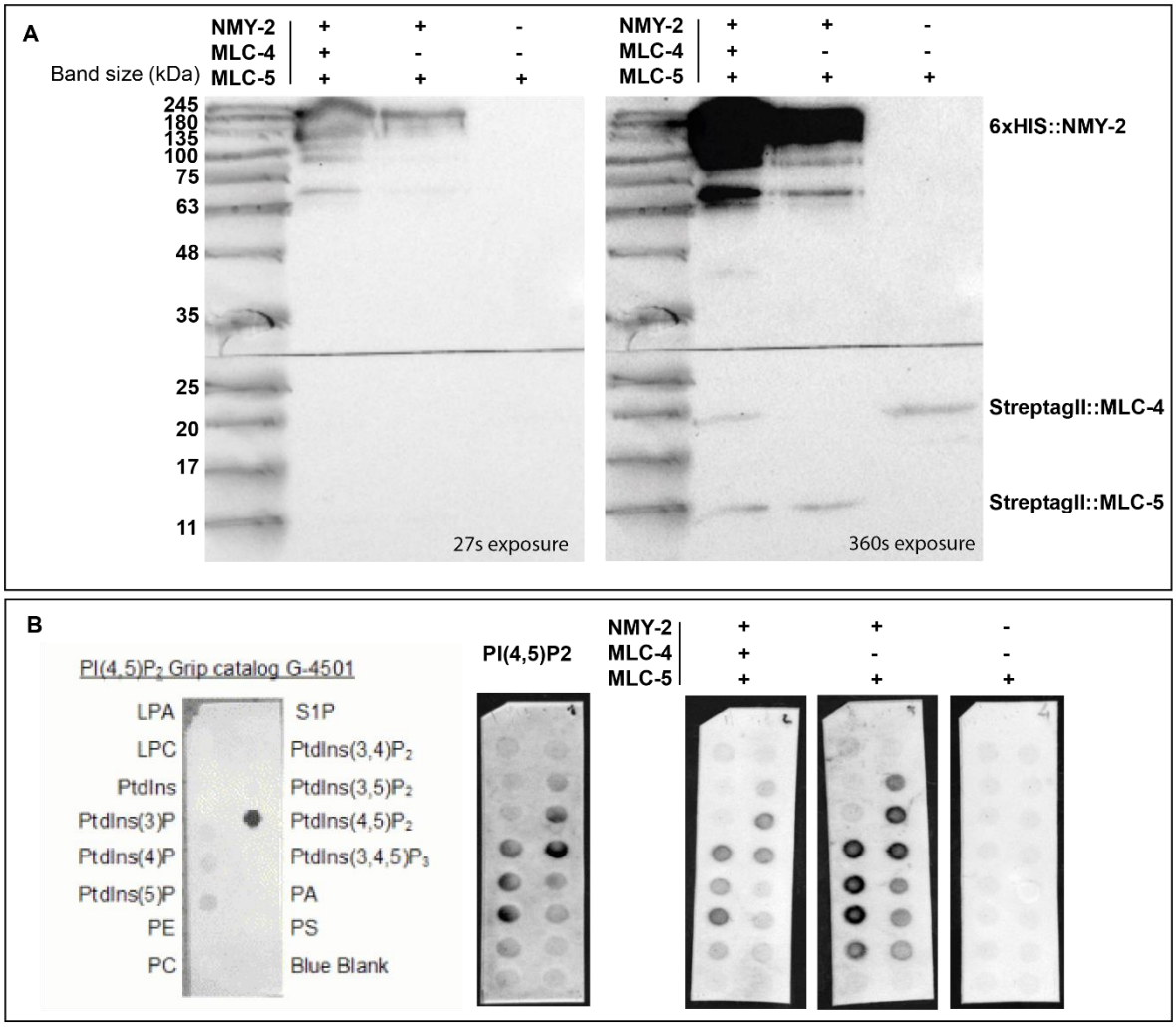

Figure 6.2 NMY-2 is capable of binding phospholipids *in vitro*. In the left, a positive control, a recombinant GST-tagged PLC-δ1 PH domain protein that specifically binds PIP2. In the right the PIPstrip assay with the several conditions tested. NMY-2-MLC-4-MLC-5 complex and NMY-2-MLC-5 bind to Phosphatidylinositol 3-phosphate (PtdIns(3)P), Phosphatidylinositol 4-phosphate (PtdIns(4)P), Phosphatidylinositol 5-phosphate (PtdIns(5)P), Phosphatidylethanolamine (PE), Phosphatidylinositol 3,4-bisphosphate (PtdIns(3,4)P2), Phosphatidylinositol 3,5-bisphosphate (PtdIns(3,5)P2), Phosphatidylinositol 4,5-bisphosphate (PtdIns(4,5)P2), Phosphatidylinositol 3,4,5-trisphosphate (PtdIns(3,4,5)P3), Phosphatidic acid (PA) and Phosphatidylserine (PS). MLC-4 alone does not bind to any phospholipid.

Our results suggest that NMY-2 can bind to several phospholipids when in a complex with both light chains or just the essential light chain and that MLC-4 alone is not able to bind to any phospholipid (Figure 6.2). NMY-2 was able to bind to different types of phosphatidylinositols (PtdIns), Phosphatidylethanolamine (PE), Phosphatidic acid (PA) and Phosphatidylserine (PS) phospholipids, which are the main components of the plasma membrane. This suggests that NMY-2 can bind directly to the plasma membrane *in vivo*.

6.2.3 A substantial decrease of F-actin in the contractile ring does not lead to a decrease in NMY-2 levels

Formins are large multidomain proteins that associate with actin barbed ends and are responsible for assembling the non-branched F-actin that forms the contractile ring during cytokinesis (Vavylonis & Horan, 2017; see section 1.1, chapter 1). In *C. elegans* CYK-1 is the only formin that is essential for cytokinesis (Swan, 1998; Severson et al., 2002; Davies et al., 2014). Depletion of CYK-1 prevents F-actin bundle formation in the contractile ring and leads to cytokinesis failure (Severson et al., 2002; Davies et al., 2014; Chan et al., 2019). If all the NMY-2 in the contractile ring is bound to CYK-1-nucleated F-actin, then the amount of NMY-2 present in the contractile ring should decrease as the amount of CYK-1 is progressively reduced.

In order to assess this, gradual depletion of CYK-1 was performed through a RNAi time-course experiment, in which dividing one-cell embryos with different degrees of CYK-1 depletion were analysed. L4 animals expressing NMY-2::GFP from the endogenous nmy-2 locus were injected with a dsRNA against cyk-1 and the cytokinesis phenotype was assessed between 21 hours and 45 hours after RNAi injection. Longer treatments of RNAi resulted in no furrow ingression and were not considered for this analysis. The amount of CYK-1 remaining was inferred from the time of RNAi treatment, as at the time I performed this experiment, a strain expressing a fluorescent version of endogenous CYK-1 was not available (Figure 6.3). Cytokinesis kinetics of CYK-1 depleted embryos were assessed as previously performed in chapter 4. by measuring the time interval between anaphase onset and equatorial shallow deformation (ring assembly), the time interval between shallow deformation and the early furrowing stage that consists of a folded back-to-back plasma membrane (furrow initiation), and the rate of ring constriction. To assess NMY-2::GFP levels in the contractile ring of each example, I measured the fluorescence intensity within a box placed over the tip of the furrow at 50% ingression and subtracted the camera background. Independently of the level of CYK-1 depletion, the ring assembly duration remained similar to controls (55±3.34 s in 37-45 hours interval vs 52±2.72 s in controls; Figure 6.3B). The furrow initiation time increased with decreasing CYK-1 levels (203±35 s in 37-45 hours interval vs 50±4.27 s in controls; Figure 6.3B). Contractile rings constricted progressively slower as the duration *cyk-1(RNAi)* increased, and the last window of RNAi treatment duration (0.10±0.04 µm in 37-45 hours interval vs 0.17±0.02 µm in controls; 37-45 hours) resulted in a reduction of constriction rate of 43% when compared to controls. Measurement

of NMY-2::GFP levels at the furrow tip revealed that these did not change when I compare embryos with the longest RNAi treatment and controls (1472±219 U.A. in 37-45 hours interval vs 1257±298 U.A. in controls; Figure 6.3C). I also assessed the correlation between the rate of constriction and myosin intensity in the contractile ring (Figure 6.3D). The distribution obtained showed that NMY-2::GFP levels in the contractile ring did not decrease with the ring constriction rate. As with progressively less CYK-1, progressively less F-actin is expected to exist in the contractile ring, these data indicate that in these conditions at least part of NMY-2 may not be bound to F-actin. Some of these results were integrated in a manuscript of which I am third author, showing that CYK-1 and the ARP2/3 complex are the principal F-actin nucleators during contractile ring constriction and both modulate cytokinesis kinetics. We found that CYK-1 levels at the contractile ring and the surrounding cortex were increased when ARP2/3 was depleted suggesting that ARP2/3 inhibits CYK-1 activity at the cell cortex (Chan et al., 2019).

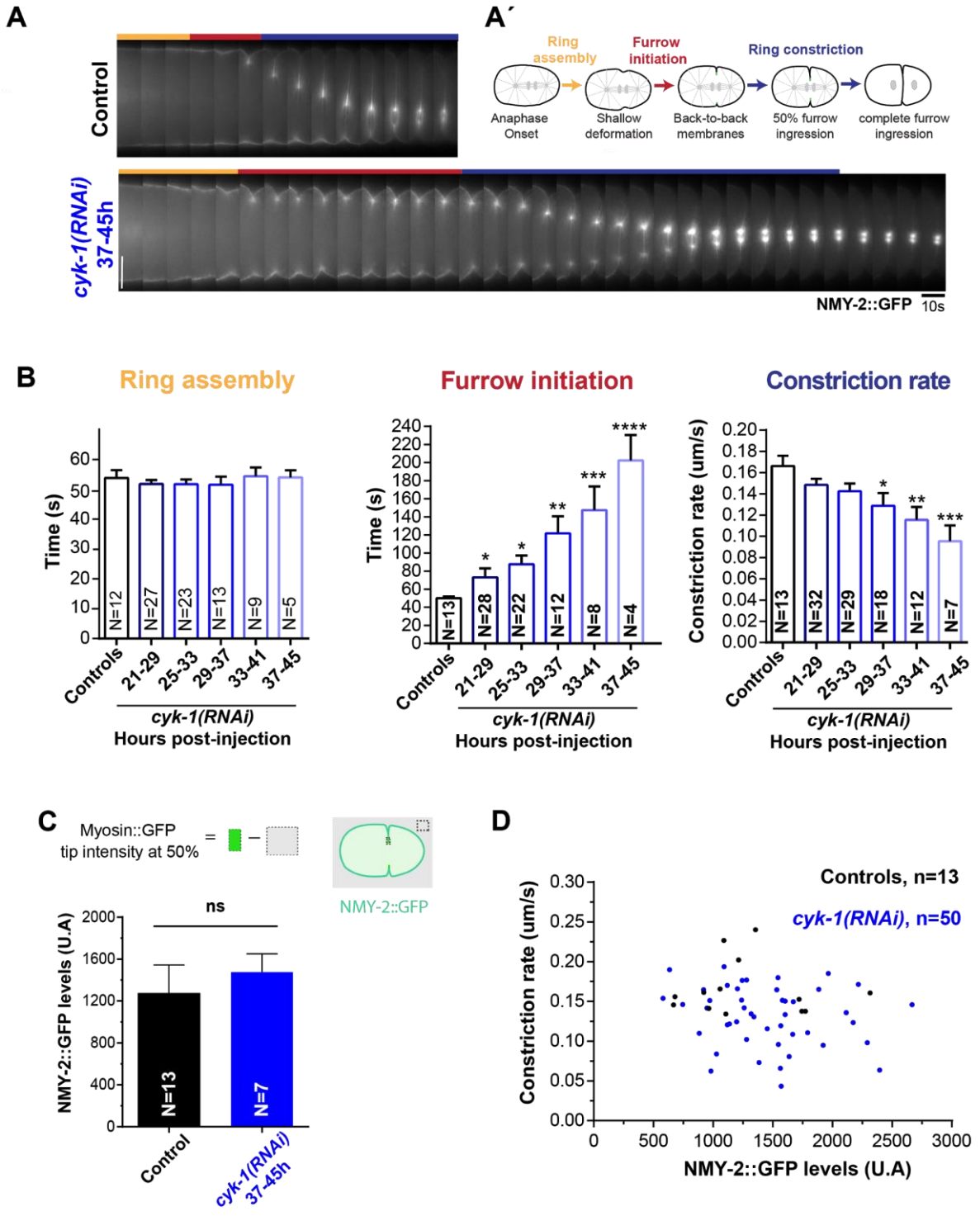

Figure 6.3 Partial depletion of CYK-1 impairs furrow initiation and slows down contractile ring constriction without affecting NMY-2 levels. A) Kymographs of the cleavage furrow region in control or CYK-1 partially depleted embryos expressing NMY-2::GFP. First frame corresponds to anaphase onset. Yellow, red, and blue bars indicate the intervals of ring assembly, furrow initiation and constriction rate, respectively. A´) Cytokinesis can be divided into three stages. B) Mean duration of the cytokinesis intervals described in (A) measured in control embryos and embryos increasingly depleted of CYK-1, using an RNAi time-course regime. Furrow initiation and constriction rate were delayed in embryos depleted of CYK-1. C) Mean fluorescence

intensity of NMY-2::GFP levels measured at the tip of the furrow at 50% ingression in both controls and embryos depleted of CYK-1 for 37-45h showing that NMY-2::GFP levels are similar in both conditions. D) Constriction rate as a function of NMY-2::GFP levels measured at the tip of the furrow at 50% ingression in both controls and CYK-1 depleted embryos. N corresponds to the analysed number of one-cell embryos undergoing cytokinesis. Error bars: CI 95%. Statistical significance was determined using one-way ANOVA followed by Bonferroni's multiple comparison test; p values * p<0.01, ** p<0.001, *** p<0.0001, **** p<0.00001. Scale bar: 10 µm.

6.2.4 In the presence of Latrunculin A, NMY-2 remains associated with the plasma membrane

In order to understand if NMY-2 is able to associate with the plasma membrane in the absence of F-actin during cytokinesis, I treated dividing one-cell embryos expressing NMY-2::mKate2 and LifeAct::GFP with Latrunculin A. Latrunculin A sequesters actin monomers thereby inhibiting F-actin polymerization and leading to overall F-actin network depolymerization (Figure 6.4; Spector et al., 1983). If NMY-2 localization to the plasma membrane or cell cortex fully depends on its binding to F-actin, then all NMY-2 should become cytoplasmic in the presence of Latrunculin A. If this does not happen, NMY-2 is likely able to associate with the plasma membrane.

In order to perform drug treatments, *C. elegans* embryos must be permeabilized, otherwise the embryo eggshell does not allow the entrance of drugs. To do so, I used a well-established permeabilization treatment for *C. elegans* embryos (Carvalho et al., 2011). In this treatment, animals are subjected to partial *perm-1(RNAi)* which permeabilizes the embryos eggshell without affecting early embryonic divisions (Carvalho et al., 2011). To assess the permeability status of the embryos I used a fluorescent dye that binds to membranes, FM4-64. In permeable embryos, the dye entered the eggshell and was able to label the plasma membrane, whereas no labelling was observed in non-permeable embryos

In controls, before anaphase onset, a time point that was identified by the visualization of the mCherry labelled Histone 2B (mCherry::HIS-58) in the center of the embryo, both NMY-2::mKate2 and Lifeact::GFP localized in small patches throughout the cortex with higher incidence on the anterior side of the embryo. After anaphase onset, NMY-2::mKate2 and Lifeact::GFP concentrated at the equator of the cell where the contractile ring started to form: LifeAct::GFP formed filamentous structures while NMY-2::mKate2 appeared in patches (Figure 6.4).

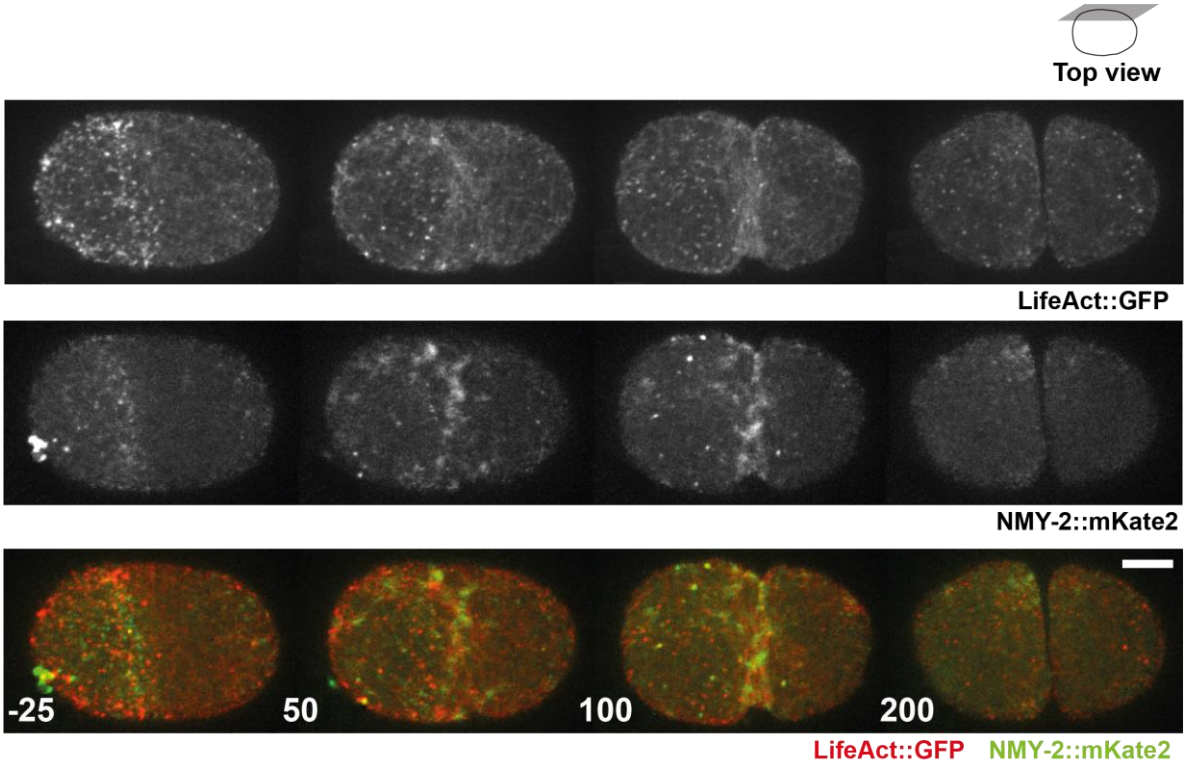

Figure 6.4 LifeAct::GFP and NMY-2::mKate2 partial co-localize at the embryo cortex and are enriched at the cell equator during cytokinesis. Top view of one-cell embryo co-expressing LifeAct::GFP, a fluorescent probe for actin, and NMY-2::mKate2. Before anaphase onset actin and NMY- 2 localize at the cortex and after anaphase start to enrich at the cell equator. Numbers on stills correspond to time from anaphase onset in seconds. Scale bar: 10 µm.

In *perm-1*(*RNAi*) embryos, both NMY-2::mKate2 and LifeAct::GFP localized into small patches at the embryo cortex before Latrunculin A addition (Figure 6.5). When 10 µM Latrunculin A was added at anaphase onset, cortical LifeAct::GFP signal started decreasing, and completely cleared from the cell surface 184±52 s after Latrunculin A addition. This indicates F-actin depolymerization in the embryo.

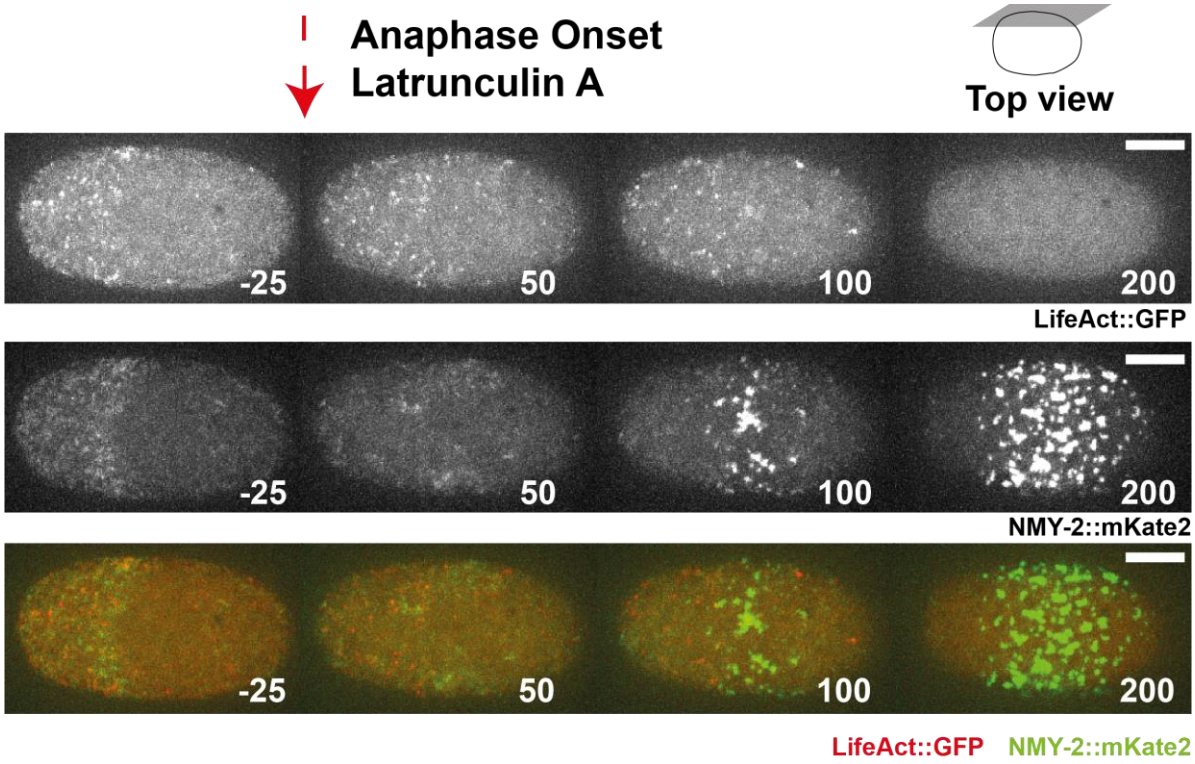

Figure 6.5 Latrunculin A addition at anaphase onset (time zero) leads to F-actin depolymerization and myosin accumulation at the plasma membrane. Top view of a one-cell embryo when treated with Latrunculin A. Numbers on stills correspond to time from anaphase onset in seconds. Scale bar: 10 µm.

The behavior of NMY-2::mKate2 was the following: First, NMY-2::mKate2 started to appear as puncta at the cell surface (60±8 s after Latrunculin A addition). Second, some NMY-2::mKate2 started to be pulled towards the centrosomes (80±11 s). This behaviour seemed to correspond to invaginations of the plasma membrane due to pulling by spindle microtubules, as previously described (Redemann et al., 2010; and section 6.2.5 below; Figure 6.6). Third, NMY-2::mKate2 signal was cleared from the cell poles (119±15 s). Fourth, NMY-2::mKate2 accumulated solely at the cell equator at a time similar to that when control embryos in the absence of Latrunculin A would start furrow ingression (126±18 s). Finally, the number of events of NMY-2::mKate2 being pulled from the surface to the centrosomes increased (200±24 s), starting soon after F-actin had depolymerized likely because of the even more weakened cell surface. This last event persisted at least until the point when I stopped imaging the embryos, about 300 s after anaphase onset (normal furrow closure takes on average 237±18 s from anaphase onset; Figure 6.6).

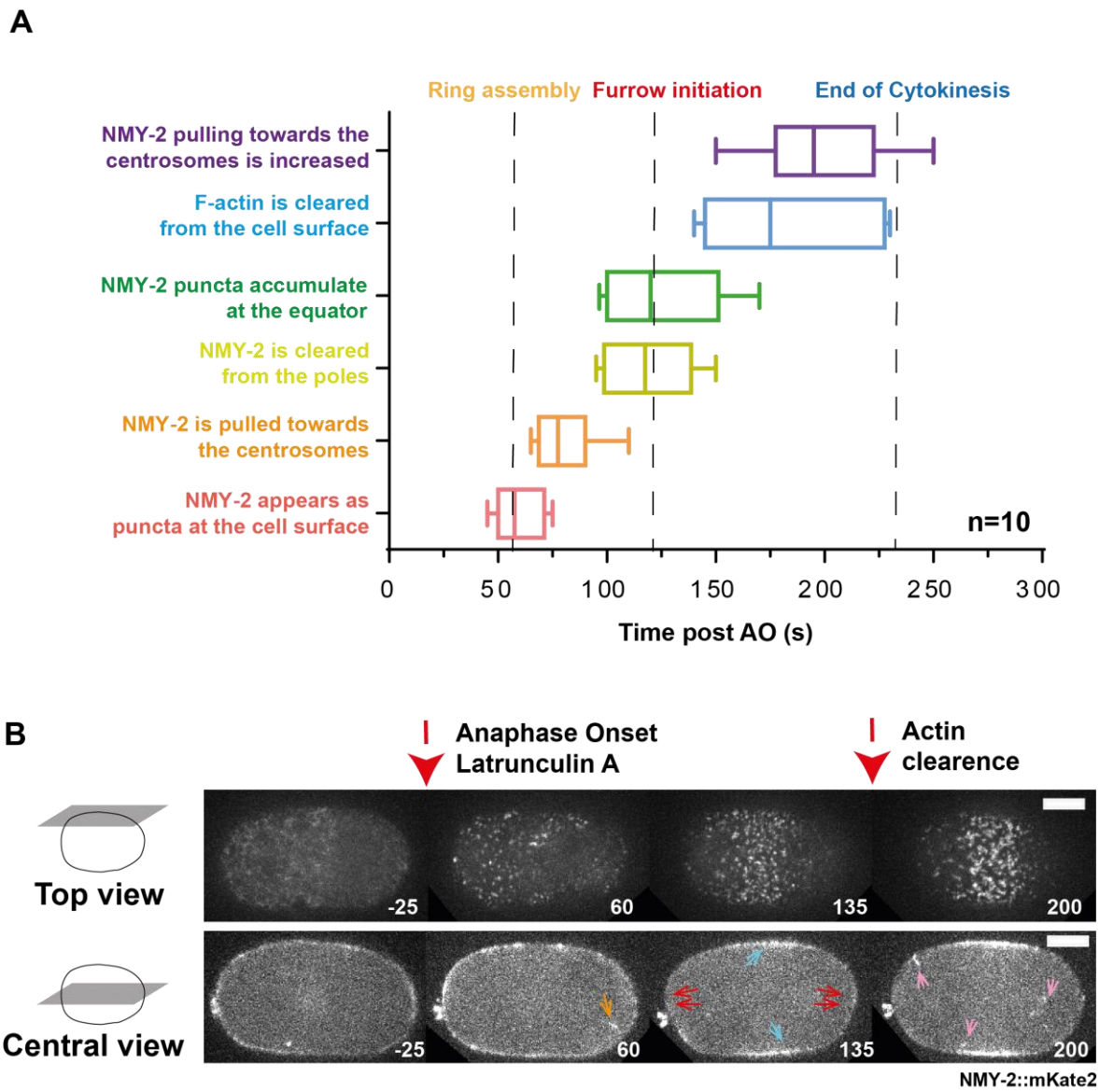

Figure 6.6 NMY-2::mKate2 remains associated with the plasma membrane and it is pulled towards the centrosomes after Latrunculin A addition. A) Localization of NMY-2::mKate2 and LifeAct::GFP was assessed after Latrunculin A addition. Each color represents an observed event as described on the y axis. Actin clearance was judged by LifeAct::GFP signal. Average timings of contractile ring assembly, furrow initiation and end of cytokinesis in normal conditions are marked with dashed lines. n=10 is the number of embryos analysed. AO corresponds to anaphase onset. In the box plot, the line within the box marks the mean; whiskers at the left and right of the box indicate the 10th and 90th percentiles, respectively. B) Top and central views of a one-cell embryo treated with Latrunculin A at anaphase onset. First column shows a time point prior to Latrunculin A addition (time=-25s). After Latrunculin A addition, NMY-2::mKate2 starts to form puncta at the cell surface and some is pulled towards the centrosomes (orange arrow). NMY-2::mKate2 is cleared from the cell poles (red arrows) and accumulates in puncta at the equator (blue arrows and top view). After F-actin is completely cleared from the cell surface, as judged by Lifeact::GFP signal (see figure 6.4), NMY-2::mKate2 starts to be increasingly pulled into the cytoplasm (pink arrows). Numbers on stills correspond to time from anaphase onset in seconds. Scale bar: 10 µm.

These results indicate that the F-actin network is successfully cleared from the cortical layer in Latrunculin A treated embryos, and that in its presence NMY-2 must associate with the plasma membrane as it still accumulates at the embryo equator similar to embryos that were not treated with Latrunculin A.

6.2.5 Astral microtubules remove NMY-2 from the cell surface in the absence of a cortical F-actin layer

The F-actin-based cell cortex is essential to dictate cell surface mechanical properties. When F-actin is decreased, the cell surface weakens (Gilden & Krummel, 2010; Chugh et al., 2017; Trichet et al., 2008), and microtubules pull on the plasma membrane more easily than in a normal condition (Redemann et al., 2010). To assess whether NMY-2 that seemed to fall from the cortex during Latrunculin A treatment was due to microtubule pulling on the cell surface Nocodazole, which inhibits microtubule polymerization, and Latrunculin A were simultaneously added at anaphase onset to one-cell embryos expressing NMY-2::GFP and mCherry::TBB-1, a β-tubulin probe that labels microtubules (Figure 6.7). In embryos treated with Latrunculin A only, the spindle appeared normal, and NMY-2::GFP at the plasma membrane/cortex seemed to be pulled towards the centrosomes (pink arrows). With time, NMY-2::GFP was cleared from the poles and accumulated at the cell equator. In embryos treated with Latrunculin A and Nocodazole, mCherry::TBB-1 signal decreased over time and the puncta of NMY-2::GFP stopped being pulled from the cell surface. In contrast to what happens in embryos treated with Latrunculin A only, NMY-2::GFP was dispersed through the cell surface, remaining at the cell poles and not preferentially accumulating at the equator (white arrows in Latrunculin A treated embryos and yellow arrows in Latrunculin A and Nocodazole treated embryos).

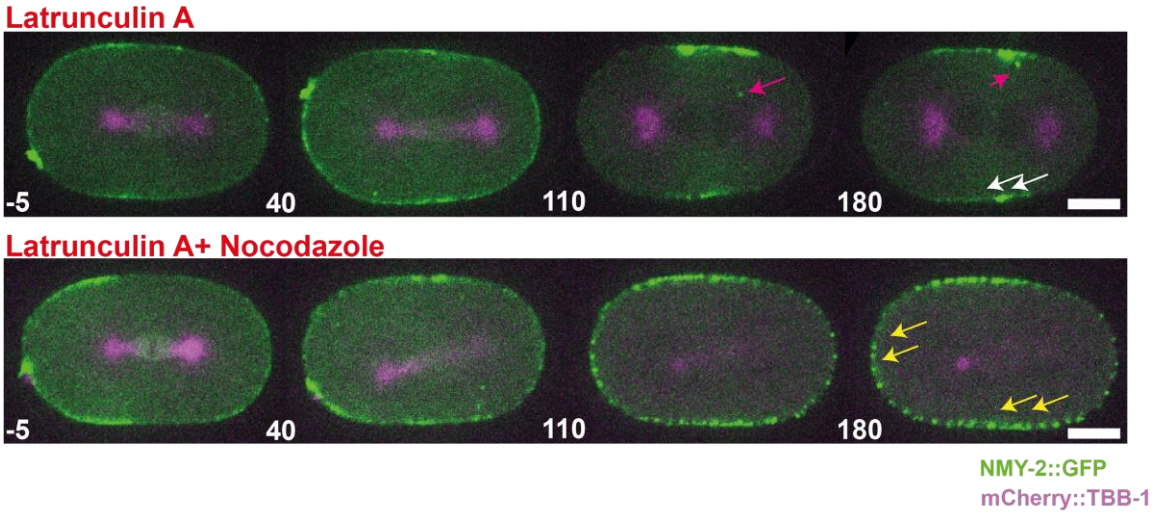

Figure 6.7 Microtubules pull and remove NMY-2 from the cell surface and inhibit NMY-2 accumulation at the cell poles. Central views of embryos treated with Latrunculin A (top row) or Latrunculin A and Nocodazole (bottom row) are shown. In the Latrunculin A-treated embryo, mCherry::TBB-1 signal on the mitotic spindle is maintained over time. NMY-2::GFP is pulled from the cell surface towards the centrosomes (pink arrows). Ultimately, NMY-2::GFP is cleared from the poles and accumulates at the cell equator (white arrows at the cell equator). In the embryo simultaneously treated with Latrunculin A and Nocodazole, mCherry::TBB-1 signal is reduced with time. Some NMY-2::GFP puncta start to be pulled by the microtubules, but as microtubules depolymerize no more NMY-2::GFP puncta are pulled. NMY-2::GFP is not cleared from the poles and does not preferentially accumulate at the cell equator (yellow arrows). Numbers on stills correspond to time from anaphase onset in seconds. Scale bar: 10 µm

I conclude that in the absence of the F-actin cortical layer, the cell surface is weakened, and the astral microtubules pull on the plasma membrane, contributing to the removal of material from the surface onto the cytoplasm. This action may be important for the event of polar clearance that normally happens during cytokinesis.

6.2.6 Different actomyosin cytoskeleton proteins remain associated with the plasma membrane after depolymerization of F-actin

To find out whether NMY-2's ability to bind to the plasma membrane in the absence of F-actin was direct or required other proteins I first imaged embryos expressing fluorescently tagged proteins that are known to be part of the actomyosin cytoskeleton during cytokinesis (Figure 6.8), in the presence of Latrunculin A. The localization pattern of the NMII RLC and ELC (MLC-4::GFP and MLC-5::mKate2, respectively), anillin (ANI-1::GFP), and CYK-1 (CYK-1::GFP) was examined. In control embryos, all these probes accumulate at the equatorial cortex and at the tip of the cleavage furrow (Mangal et al., 2018; Chan et al., 2019; Singh et al., 2019). Similar to what happened in embryos expressing NMY-2::GFP, all these

fluorescent proteins remained associated with the plasma membrane and were pulled by microtubules after Latrunculin A addition (time point 200 s in Figure 6.8).

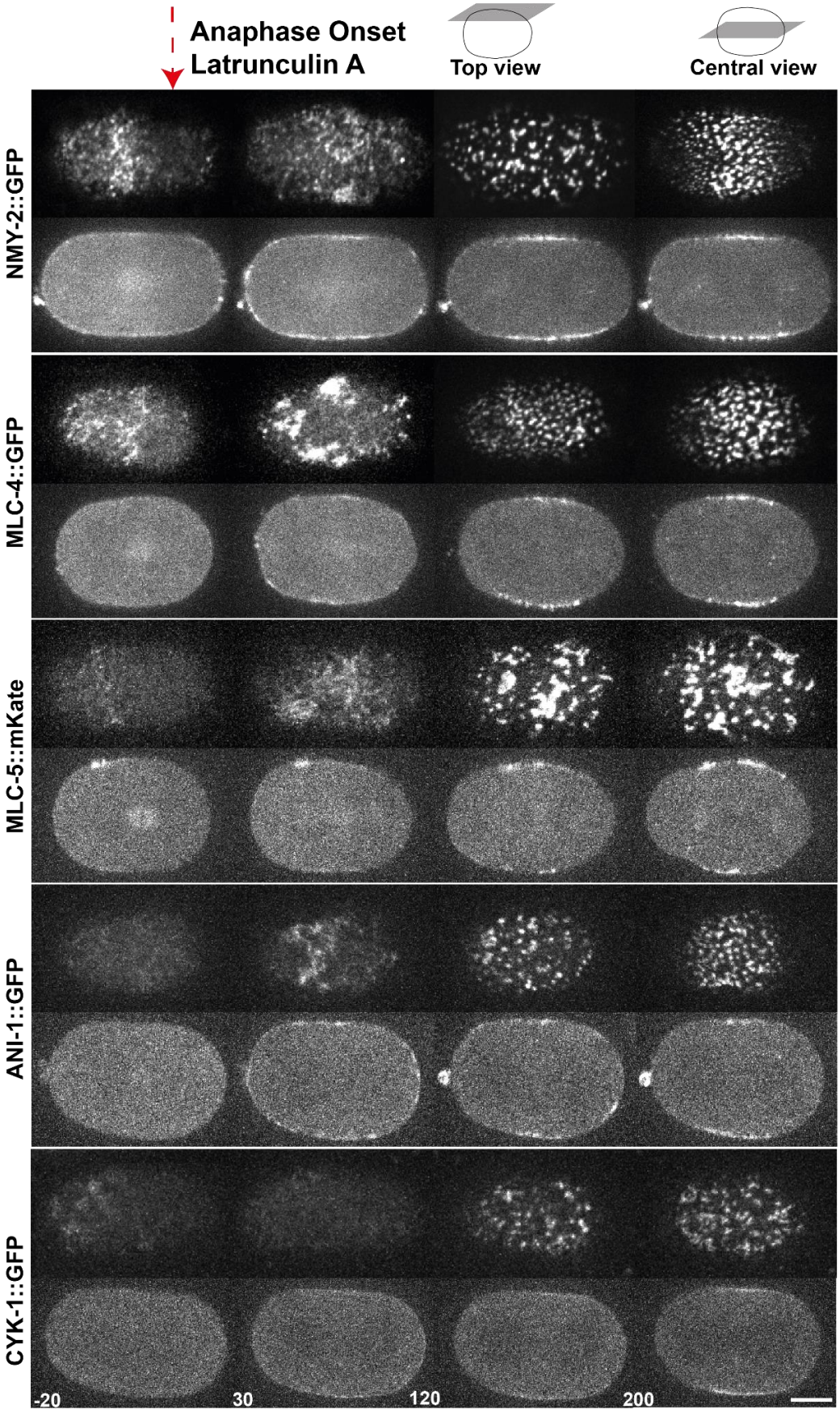
Anaphase Onset
Latrunculin A
Top view
Central view
NMY-2::GFP
MLC-4::GFP
MLC-5::mKate
ANI-1::GFP
CYK-1::GFP
-20
30
120
200

Figure 6.8 NMY-2 LCs, anillin ANI-1 and the formin CYK-1, like NMY-2, also remain associated with the plasma membrane in embryos treated with Latrunculin A. Top and central views of embryos expressing the indicated proteins and treated with Latrunculin A. Numbers on stills correspond to time from anaphase onset in seconds. Scale bar:10 µm

In contrast, a fluorescent probe of the F-actin crosslinker plastin (PLST-1), which only has actin binding domains in its structure (Ding et al., 2017) disappeared from the cell surface after Latrunculin A addition. This is the expected behavior for a protein that just binds to F-actin and these observations reinforce the idea that NMY-2 behaves differently (Figure 6.9).

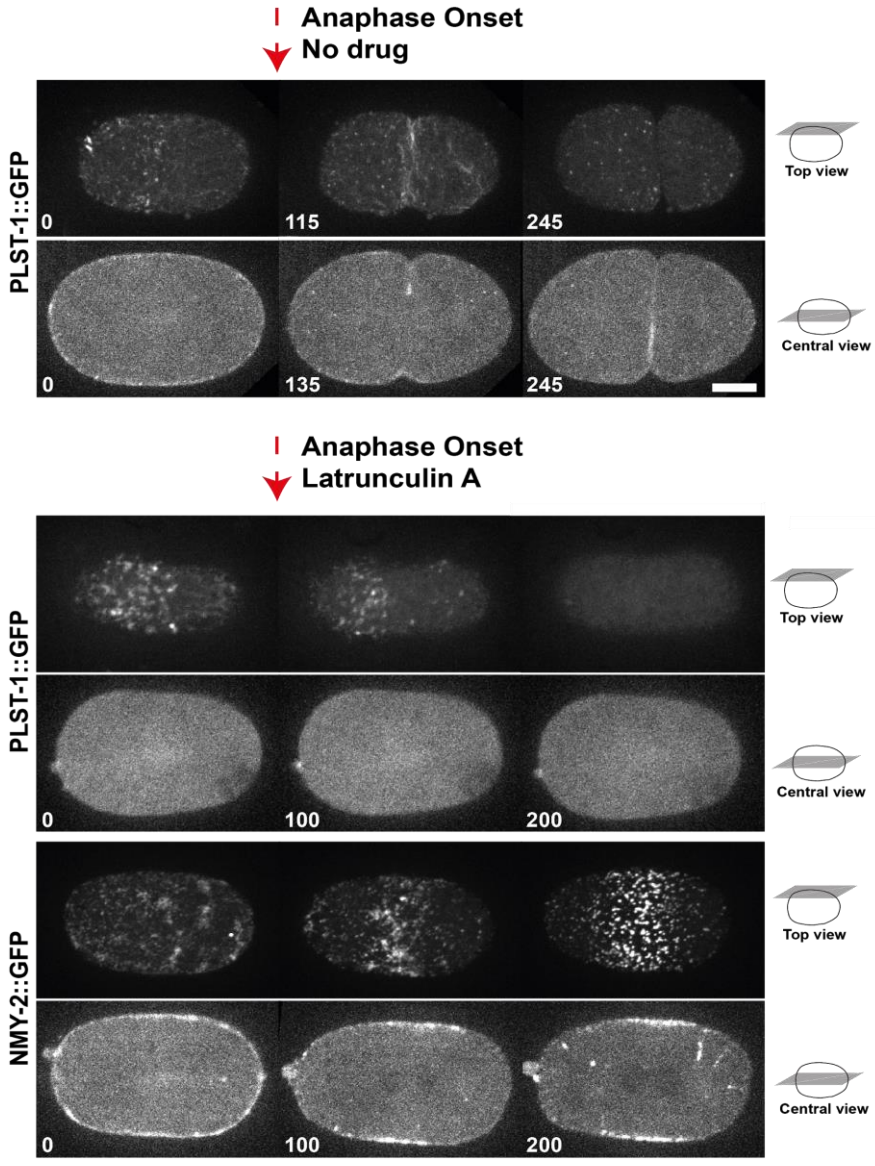

Figure 6.9 PLST-1::GFP is not observed at the cell surface after Latrunculin A treatment. Stills of one-cell embryos expressing PLST-1::GFP or NMY-2::GFP, drug treatment or no treatment, and top or central views of the embryo are indicated. In a control situation (no drug, top), PLST-1::GFP localizes at the cell cortex and

enriches in filamentous structures at the cell equator and at the tip of the ingressing furrow. In contrast to NMY-2::GFP, PLST-1::GFP does not stay associated with the plasma membrane when F-actin is depolymerized upon Latrunculin A treatment. Numbers on stills correspond to time from anaphase onset in seconds. Scale bar: 10 µm.

Altogether these results reveal that similar to NMY-2/MLC-4/MLC-5, other proteins from the actomyosin network are able to associate with the plasma membrane at least in the presence of Latrunculin A.

6.2.7 NMII activation status may influence binding to the plasma membrane

After I found that ANI-1, CYK-1, MLC-4 and MLC-5 were also able to remain bound to the plasma membrane upon Latrunculin A treatment, I checked whether any of them could be involved in anchoring NMY-2. MLC-4, RHO-A, CYK-4 and ECT-2 are required for NMII activation. Active RhoGTPase RHO-A, like in other systems, activates NMY-2 via phosphorylation of MLC-4 by ROCK, LET-502 (see chapter 1 section 1.4.1). Anillin localizes at the cell cortex and has myosin, actin and plasma membrane binding domains and therefore it may act as an actomyosin cytoskeleton scaffolder (Piekny & Maddox, 2010). It also limits NMY-2 localization on the cell cortex as its depletion leads to increased myosin levels at the cleavage furrow (Maddox et al., 2007). Cell adhesion proteins, like HMR-1 and SAX-7, localize at the plasma membrane and redundantly regulate NMY-2 localization in *C. elegans* (Grana et al., 2010; Padmanabhan et al., 2017). All these proteins are able to localize at the cell surface, which makes them suitable for possibly mediating the binding of NMY-2 to the plasma membrane. To do this, I combined depletion of ANI-1, MLC-4 and MLC-5 with Latrunculin A treatment in embryos expressing NMY-2::GFP (Figure 6.10). In addition, I also depleted RHO-A, CYK-4, ECT-2, Hammerhead embryonic lethal (HMR-1) and Sensory axon guidance 7 (SAX-7).

NMY-2::GFP levels seemed to be increased after double depletion of HMR-1 and SAX-7 or ANI-1, suggesting that they negatively regulate NMY-2 binding to the plasma membrane even in the absence of F-actin. In contrast, NMY-2::GFP levels were substantially decreased in RHO-A, ECT-2 or MLC-4 depleted embryos. As RHO-A, ECT-2 and MLC-4 are essential in the cascade that activates NMY-2, NMY-2 decreased levels after RHO-A, ECT-2 or MLC-4 depletion suggest that NMY-2 needs to be activated in order to associate with the plasma membrane. In addition, it seems that RHO-A and ECT-2 are essential to maintain NMY-2::GFP at the cell equator since in control embryos depleted of RHO-A or ECT-2, either

treated with Latrunculin A, NMY-2::GFP fails to accumulate at the equator and is dispersed throughout the embryo surface.

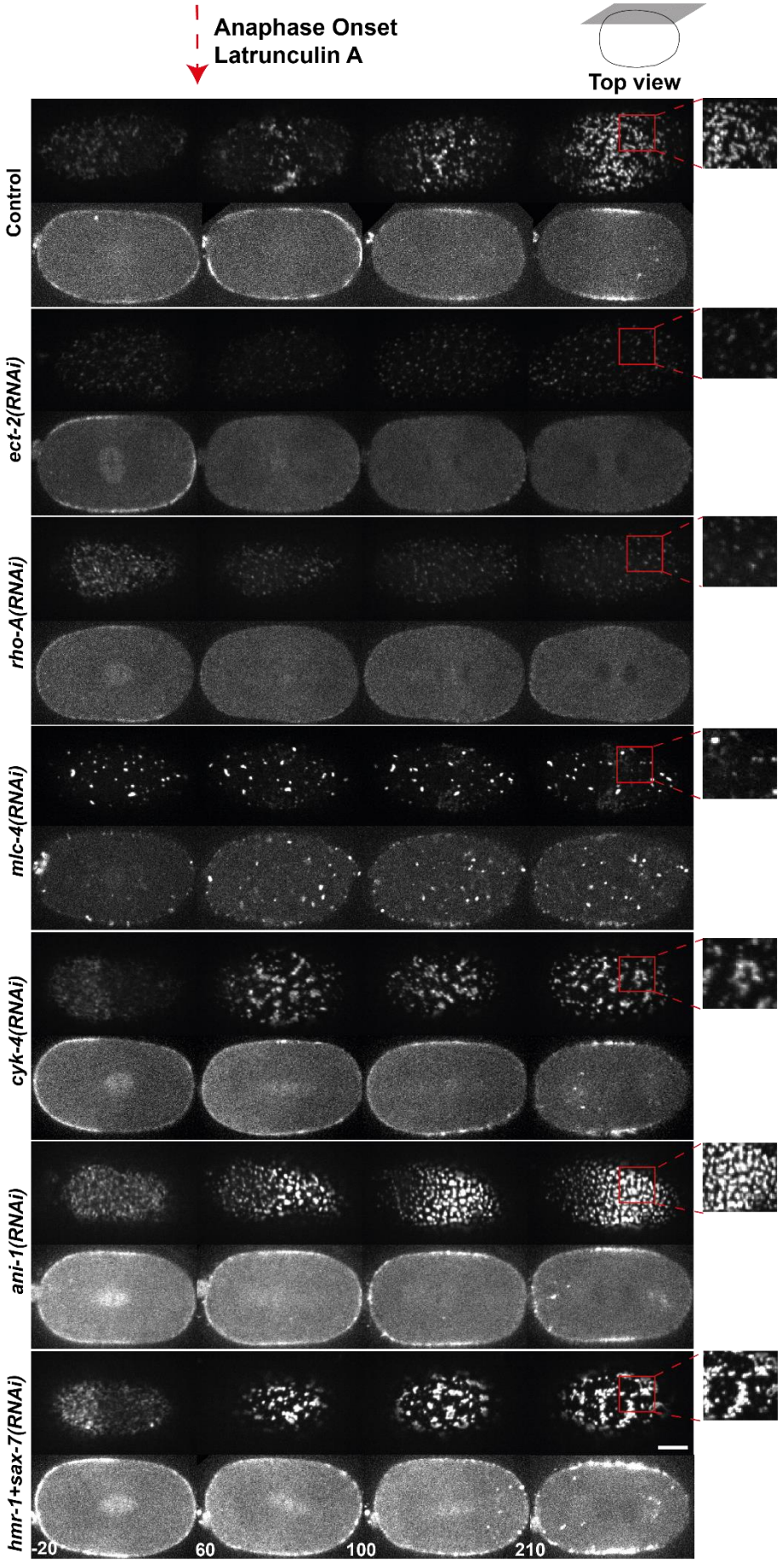
Anaphase Onset
Latrunculin A
Top view
Control
ect-2(RNAi)
rho-A(RNAi)
mlc-4(RNAi)
cyk-4(RNAi)
ani-1(RNAi)
hmr-1+sax-7(RNAi)
-20
60
100
210

Figure 6.10 Latrunculin A treatment in embryos depleted of MLC-4, RHO-A and ECT-2 lead to substantial decrease of NMY-2::GFP signal at the plasma membrane. NMY-2::GFP association with the plasma membrane is decreased in mlc-4(*RNAi*), rho-a(*RNAi*) and ect-2(*RNAi*) and looks increased in ani-1(*RNAi*) and hmr-1;sax-7(*RNAi*). Top views of the embryos are shown over time. Insets show a zoom of NMY-2::GFP signal associated with the plasma membrane in the different conditions. Time zero corresponds to anaphase onset when Latrunculin A was added. All the stills from the same column display the same timing in seconds after or before Latrunculin A addition (anaphase onset). Scale bar: 10 µm.

Qualitative analysis of NMY-2::GFP signal at the cell surface in a control situation and after ect-2*(RNAi)* revealed that: 1) NMY-2::GFP levels increased over time in control embryos treated with Latrunculin A at anaphase onset; 2) in embryos depleted of ECT-2, NMY-2::GFP levels were significantly lower when compared to those in controls and did not increase over time, and 3) embryos depleted of ECT-2 and treated with Latrunculin A showed reduced NMY-2::GFP signal similar to what was observed in the absence of Latrunculin A (Figure 6.11). NMY-2::GFP decreased levels in embryos depleted of ECT-2 that were not submitted to Latrunculin A treatment suggest that ECT-2, and therefore RHO-A activation, are required for maintaining NMY-2::GFP at the cell surface. In addition, the fact that NMY-2::GFP fails to localize at the equator in ECT-2 depleted embryos indicates that RHO-A activation is necessary for correct localization of NMY-2. Embryos depleted of ECT-2 that were treated with Latrunculin A also had a similar pattern of NMY-2::GFP localization when compared with those depleted of ECT-2 in the absence of Latrunculin A. This reveals that in the presence or absence of F-actin, active RHO-A is necessary for NMY-2 localization at the cell surface and to enrich NMY-2 at the equatorial cell surface. It is possible that ECT-2 and consequent RHO-A activation are necessary for NMY-2 cortical/membrane localization during cytokinesis, since the embryos I analysed still have residual ECT-2. This is because penetrant ECT-2 depletion results in sterile animals that do not produce embryos. This same reasoning is valid for RHO-A depletion.

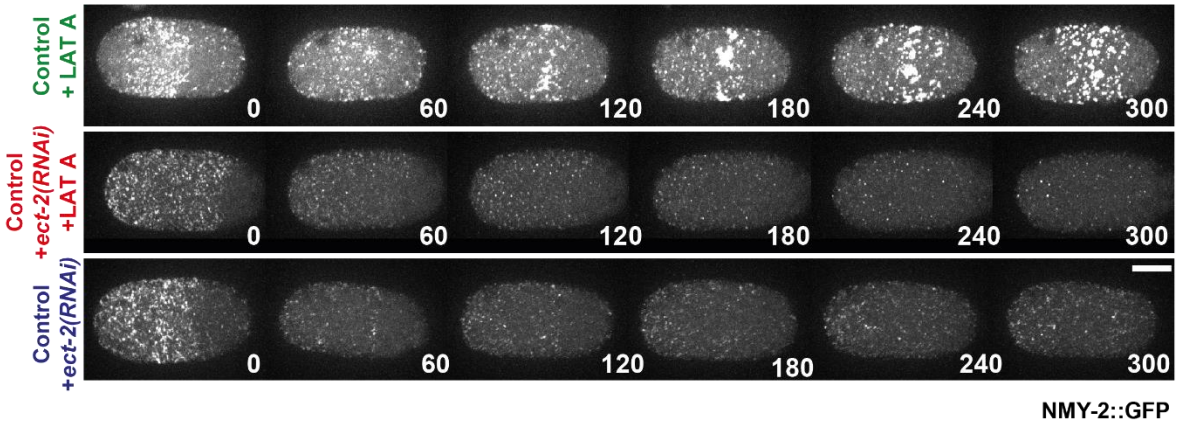

Figure 6.11 Latrunculin A treatment in ECT-2 depleted embryos leads to a substantial decrease of NMY-2::GFP signal at the plasma membrane. Top views a control embryo expressing NMY-2::GFP upon Latrunculin A addition (top row), and of ECT-2 depleted embryos in the presence (central row) or absence of Latrunculin A (bottom row). Time zero corresponds to anaphase onset. Numbers on stills correspond to time from anaphase onset in seconds. Scale bar: 10 µm

6.2.8 NMY-2 is unlikely to anchor ANI-1 in the plasma membrane

Anillin contains a PH domain located at the C-terminus that is responsible for plasma membrane-binding and is essential for normal cytokinesis in humans and *D. melanogaster* (Piekny & Glotzer, 2008; Liu et al., 2012; Oegema et al., 2000; Kim et al., 2017). Anillin is also able to bind to the plasma membrane via a C2 Domain (Sun et al., 2015). Additionally, anillin contains a myosin binding domain in its N-terminus (Straight et al., 2005; Kim et al., 2017). Together these domains enable simultaneous binding of Anillin to the plasma membrane and myosin. Having shown that both myosin and anillin remained associated with the plasma membrane upon Latrunculin A treatment, and that, in *S. pombe* contractile rings, the anillin-like protein Mid1p is at the base of the nodes where NMII is anchored, I hypothesised that anillin could be anchoring myosin to the plasma membrane. However, when I depleted ANI-1 in *C. elegans* one-cell embryos, the levels of NMY-2::GFP at the plasma membrane did not decrease upon Latrunculin A treatment (Figure 6.8). In fact, NMY-2::GFP levels increased in ANI-1 depleted embryos treated with Latrunculin A. This is reminiscent of what happens in constricting contractile rings depleted of ANI-1 in the absence of Latrunculin A (Maddox et al., 2007), which reveals that ANI-1 is able to regulate NMY-2 levels in the presence or absence of F-actin. These results indicate that it is unlikely that ANI-1 mediates NMY-2 association with the plasma membrane, during cytokinesis.

Conversely, to test if NMY-2 could be anchoring ANI-1 to the plasma membrane, I combined depletion of NMY-2 with Latrunculin A treatment in embryos expressing ANI-1::GFP (Figure

6.12). In embryos just treated with Latrunculin A, ANI-1::GFP started to accumulate as puncta at the equatorial plasma membrane (Figure 6.8). In NMY-2 depleted embryos treated with Latrunculin A, ANI-1::GFP was still able to accumulate at the plasma membrane in a seemingly similar amount but in more elongated structures that do not coalesce (Figure 6.12B).

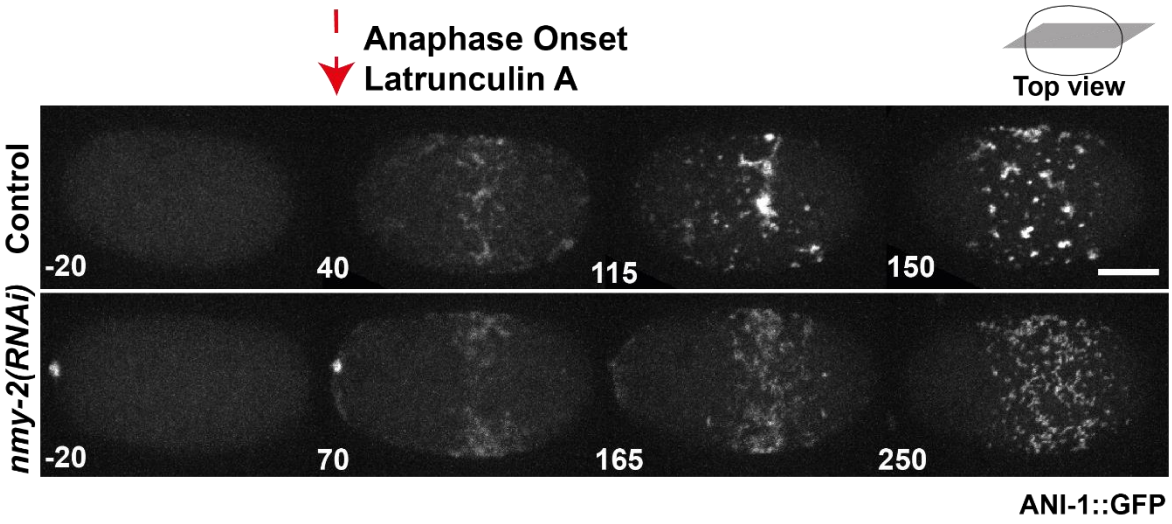

Figure 6.12 Latrunculin A treatment in embryos depleted of NMY-2 results in more elongated and dispersed structures of ANI-1::GFP at the plasma membrane. ANI-1::GFP localizes as patches in controls (top row), and it forms filamentous structures after nmy-2(*RNAi*) (bottom row). Stills of the top view of the embryos are shown. Time zero corresponds to anaphase onset when Latrunculin A was added. Scale bar: 10 µm.

Altogether these results suggest that NMY-2 do not regulate the ability of ANI-1 binding to the plasma membrane and therefore NMY-2 is anchoring ANI-1 to the plasma membrane during the cytokinesis of *C. elegans* one-cell embryo.

6.3 Discussion

In this chapter, I assessed the existence of a *C. elegans* NMII NMY-2 bound to the plasma membrane during cytokinesis. I found that NMY-2 has putative membrane-binding sites and that it can directly bind to phospholipids *in vitro*, suggesting a possible direct binding of NMY-2 to the plasma membrane *in vivo.* The use of Latrunculin A, during cytokinesis, allowed the observation that, indeed, NMY-2 remains associated with the plasma membrane when the F-actin network is depolymerized. Overall, my results suggest that a NMY-2 plasma membrane-bound pool is likely to exist during cytokinesis.

I showed that purified NMY-2 in a complex with MLC-4 and MLC-5 can bind to several phospholipids, PtdIns, PE, PA and PS, that are usual components of the plasma membrane. This result agrees with the finding that mammalian NMII binds to liposomes containing multiple PIPs (PtdIns, PS) (Liu et al., 2016). In contrast, our purified MLC-4 alone was not able to bind any of the phospholipids tested. This result contrasts with what was observed in a study using recombinant RLC from *D. melanogaster*, which revealed its ability to bind to several phosphatidylinositols (PtdIns), Phosphatidylethanolamine (PE) and Phosphatidic acid (PA) (Koe et al., 2018). In the future, the phospholipid binding assay should be performed in the presence of LET-502-phosphorylated MLC-4, to understand whether its phosphorylation status may influence its ability or the ability of NMY-2-MLC-4-MLC-5 to bind to phospholipids.

NMY-2 sequence analysis revealed that NMY-2 has three potential membrane-binding sites, two in the head domain and a 13 amino acid-long stretch in the IQ domain where the RLC binds. The latter would be in agreement with the idea that mammalian NMII binds to liposomes containing PIPs through its RLC-binding site. However, NMII binding to the plasma membrane via the head region or the IQ domains in the neck is unexpected since these sites are required for binding and translocation of F-actin and for NMII activation. Binding through the tail of the HC would be expected since 1) other myosins from different classes that bind to cellular membranes do it through their tail domain (see chapter 1, section 1.6), and 2) previous reports from *S. pombe* contractile rings indicate that the tail of the HC faces the plasma membrane and the head faces the cytoplasm (Laporte et al., 2011; Laplante et al., 2016). To test if these putative (and well conserved) sites can bind membranes, the affinity of the corresponding fluorescently labelled synthetic peptides to acidic phospholipid vesicles should be tested *in vitro* like previously described (Brzeska et al., 2010). To test their relevance in vivo, the nonpolar and basic amino acids of NMY-2 predicted to mediate this interaction could be mutated to polar or acidic amino acids since these are less prone to bind to phospholipids due to its hydrophilicity or negative charge. Mutated NMY-2 could be expressed in *C. elegans* and its localization and impact in cytokinesis assessed.

To start exploring the existence of a pool of NMY-2 that binds the plasma membrane during cytokinesis *in vivo*, I first performed a *cyk-1*(*RNAi*) time course experiment in embryos expressing NMY-2::GFP to understand how decreasing F-actin in the contractile ring would impact NMY-2 localization. The localization profile and signal intensity of NMY-2::GFP was not affected after CYK-1 depletion. This result could indicate that NMII is anchored in the

membrane and does not depend on the amount of F-actin in the ring. Alternatively, it is possible that all the NMY-2 is bound to the F-actin remaining in the ring. Given that the distance between the cortex and plasma membrane is 10 to 20 nm in Jurkat T cells (Clausen et al., 2017), and the diffraction-limited fluorescent imaging, distinguishing the localization of NMII bound to the plasma membrane or within the F-actin cortical layer is challenging. Nevertheless, if all the NMY-2 were bound to the F-actin remaining in the ring, this would likely lead to a higher tension within the contractile ring, which could be tested by performing laser microsurgery in the contractile ring (Silva et al., 2016). This technique allows the assessment of the biophysical properties of the contractile by simply cutting it.

Next, I looked at NMY-2 localization in the absence of the cortical F-actin layer, after adding Latrunculin A to permeabilized embryos expressing fluorescently tagged NMY-2. A significant portion of NMY-2 localized as puncta on the cell surface, namely at the cell equator, implying direct/indirect association with the plasma membrane. Whether or not these puncta correspond to the myosin clusters observed by Henson and colleagues (Henson et al., 2017) in fixed isolated cortices of dividing sea urchin eggs using structured illumination microscopy remains to be assessed. Their observations indicated that NMII structural organization at the equator evolves from separate clusters to linear aligned filaments, and that this reorganization seemed to be dependent on the presence of F-actin. An attractive possibility is that myosin initially binds to the plasma membrane and as F-actin are nucleated/elongated at the cell equator, NMII reorganizes into bipolar filaments that interdigitate the non-branched, circumferential F-actin. It would be interesting to perform live-imaging on how myosin reorganizes when Latrunculin A is washed out in *C. elegans* embryos.

The fact that MLC-4 and MLC-5 also remained associated with the plasma membrane with similar localization patterns as NMY-2 in controls and when the F-actin network is depolymerized by Latrunculin A during cytokinesis, indicates that NMY-2 associates with the plasma membrane in a complex with its LCs. This in turn indicates that the *in vivo* binding to the plasma membrane is unlikely to occur via NMY-2's neck domain. Interestingly, CYK-1 and ANI-1 also remained associated with the plasma membrane in the presence of Latrunculin A. This result raises the possibility that NMY-2 could be anchored in the plasma membrane through ANI-1 or CYK-1, or that, alternatively, NMY-2 could anchor ANI-1 and CYK-1 to the plasma membrane. Further examination in embryos co-expressing more than one fluorescent protein will be required to assess their co-localization.

To study whether NMY-2 could be anchored in the plasma membrane by anillin, I performed Latrunculin A treatment in embryos expressing NMY-2::GFP and depleted of ANI-1. In addition, I tested NMY-2 localization in embryos depleted of MLC-4, MLC-5, CYK-4, HMR-1+SAX-7 (that act redundantly in cell-adhesion in *C. elegans* (Grana et al., 2010), ECT-2 and RHO-A, all known to directly bind the plasma membrane and/or able to regulate NMII levels. I observed that NMY-2::GFP levels at the plasma membrane were increased when ANI-1 and HMR-1+SAX-7 were depleted, suggesting that these proteins do not anchor NMII to the plasma membrane *in vivo* but regulate the amount of NMY-2 that is able to associate with it. It is known that anillin depletion leads to increased NMY-2 levels at the cleavage furrow in the presence of F-actin (Maddox et al., 2007), and my results suggest that this regulation is independent of F-actin. It is also known that HMR-1 clusters negatively regulate RHO-A activity and NMY-2 levels at the cell cortex in untreated embryos (Padmanabhan et al., 2017), and my results indicate that HMR-1 depletion may facilitate NMY-2 association with the plasma membrane independently of F-actin.

Whether, conversely, NMII could mediate anillin recruitment to the plasma membrane was also assessed. Embryos expressing ANI-1::GFP depleted of NMY-2 and treated with Latrunculin A seemed to have similar levels of ANI-1::GFP at the cell surface, suggesting that NMY-2 does not mediate ANI-1 binding to the plasma membrane. Since NMY-2 full depletion leads to worm sterility it is not possible to have embryos completely devoid of NMY-2. It is therefore still possible that ANI-1's binding to the plasma membrane can be reduced when NMY-2 is totally absent. This hypothesis could possibly be test in the NMY-2 temperature-sensitive mutant embryos (*ne3409*) expressing ANI-1::GFP and treated with Latrunculin A. Acute inactivation of NMY-2 during cytokinesis by rapidly upshifting the temperature to 25 °C would allow for examining the localization of ANI-1::GFP when all myosin is inactivated. An alternative would be to use an anillin mutant that lacks the myosin binding domain, which has been mapped in other systems (Straight et al., 2005; Kim et al., 2017). If NMY-2 indeed regulates ANI-1 binding to the plasma membrane, such a mutated version of ANI-1 should not be able to localize at the plasma membrane upon Latrunculin A treatment. In *D. melanogaster* S2 cells, Anillin is also associated with the equatorial plasma membrane in the presence of Latrunculin A and depletion of NMII RLC does not affect its membrane association (Hickson & O'Farrell, 2008). MLC-4 depletion reduces NMY-2 levels at the cell cortex in *C. elegans* embryos (see chapter 4, Figure 4.2 or section 4.2.1) and one would expect that the phenotypes should be similar. However, the levels of NMY-2 at the contractile ring are higher in MLC-4 depleted embryos than those directly depleted of NMY-2 and using RLC as a reporter for NMII behavior is not so straightforward because the RLC

can localize independently of NMII HC or interact with different myosins (Heissler & Sellers, 2015). Therefore, it will be interesting to deplete MLC-4 (or MLC-5) and observe ANI-1::GFP localization at the plasma membrane in *C. elegans* embryos treated with Latrunculin A to compare the results with those obtained for NMY-2 depletion.

Depletion of ECT-2, RHO-A or MLC-4 revealed that NMY-2 association with the plasma membrane might depend on its activation. In embryos treated with Latrunculin A and depleted of MLC-4, RHO-A or ECT-2, the levels of membrane-bound NMY2 were substantially decreased. The reduction of NMY-2 levels at the plasma membrane reveals that MLC-4, RHO-A and ECT-2 target NMY-2 to the plasma membrane and that NMY-2 binding to the plasma membrane depends on NMY-2 activation: NMY-2 recruitment to the cell surface is mediated by RHO-A activation in *C. elegans* embryos (Nishikawa et al., 2017), and equatorial ECT-2 activates RHO-A, which leads to MLC-4 phosphorylation on residues threonine 17 and serine 18 by LET-502 during cytokinesis. RLC phosphorylation in these highly conserved residues allows for NMII conformational changes into a contractility-competent form (see section 1.5.2; Vicente-Manzanares et al., 2009). Interestingly, only in embryos depleted of RHO-A and ECT-2 depletions, and not of MLC-4, NMII was not able to accumulate at the equatorial region. It is possible that RHO-A and ECT-2 mediate NMY-2 localization at the cell equator, and MLC-4 is locally phosphorylated, and NMY-2 activated. Although NMY-2 is recruited to the cell equator in embryos depleted of MLC-4, its activation should not occur which leads to the loss or reduced ability of NMY-2 to bind to the plasma membrane. To further investigate this hypothesis, LET-502 depletion should be performed (in the presence or absence of Latrunculin A) to assess whether NMY-2::GFP localization at the plasma membrane is also substantially decreased, similar to that observed after RHO-A, ECT-2 or MLC-4 depletions. In the future, the ability of NMY-2 to bind to the plasma membrane should be tested in the presence of a MLC-4 mutant that cannot be phosphorylated on threonine 17 and serine 18 (MLC-4(TS17,18AA)), where threonine 17 and serine 18 are replaced with alanines). Mutant embryos expressing MLC-4(TS17,18AA) and NMY-2::mKate2 should be imaged in the presence and absence of Latrunculin A. Since NMY-2 bound to MLC-4(TS17,18AA) should be inactive, its use would allow us to understand if inactive myosin is able to bind the plasma membrane.

The crosslinked F-actin network beneath the plasma membrane is the most essential contributor to cellular tension (Gilden & Krummel, 2010; Chugh et al., 2017). Cytochalasin B, a drug that prevents actin polymerization by binding to the filaments barbed-end is known to reduce cortical tension (Charras et al., 2006). In *C. elegans* embryos, treatment with

Cytochalasin D results in membrane invaginations due to microtubule pulling on the weakened cell surface (Redemann et al., 2010). In my experiments with Latrunculin A, evidence for these invaginations was also observed, as all tested probes that remained at the plasma membrane after treatment, (NMY-2, MLC-4, MLC-5, ANI-1, and CYK-1), were pulled from the membrane toward the centrosomes. At least for NMY-2, this behavior was microtubule dependent as it did not occur in the presence of both Latrunculin A and Nocodazole. Interestingly, in these embryos NMY-2 remained spread throughout the whole cell surface and was not removed from the cell poles, suggesting that similar to what happens in untreated embryos, the astral microtubules regulate NMY-2 clearance from the embryo poles when the F-actin cortex is absent. In a normal control situation, there is equatorial enrichment of proteins required for contractile ring assembly, which is known to be regulated by two mechanisms: 1) cues from the central spindle that at anaphase onset lead to RHO-A activation and subsequent accumulation of the proteins required to form the contractile ring at the cell equator (see chapter 1 section 1.4.1; von Dassow et al., 2009; Green et al., 2012; D'Avino et al., 2015; Dechant & Glotzer, 2003) and 2) an inhibitory signal clears the proteins involved in contractile ring formation from the cell poles by the astral microtubules and protein phosphatase 1 at kinetochores, which leads to polar relaxation and local reduction of contractility (Dechant & Glotzer, 2003; Werner et al., 2007; Foe & von Dassow, 2008; Chen et al., 2008; Mangal et al., 2018). Our observations show that myosin clearance from the poles and its accumulation at the equator happen with the right timing in the presence of Latrunculin A. Thus, my data raise the possibility that the event of polar clearance may happen at the plasma membrane and not the cortical layer. Polar relaxation is thought to trigger cortical flows (Chen et al., 2008; Khaliullin et al., 2018; Werner et al., 2007), which are described to be required for contractile ring assembly (DeBiasio et al., 1996; Reymann et al., 2016; Salbreux et al., 2009). All these studies were done in the presence of an F-actin cortex and myosin was always considered to be cleared from the cortical layer. The idea of membrane flows is valid since membrane components have been shown to flow at the same velocity as cortical flows (Scholze et al., 2018).

In sum, my data suggest that NMY-2 can associate with the plasma membrane independently of F-actin during cytokinesis. The combination of our *in vitro* and *in vivo* data indicates that NMY-2 could be binding to the plasma membrane directly depending on its activation status. Understanding the contribution of membrane-bound myosin to cytokinesis in the presence of an F-actin cortex remains a challenge. The use of super resolution microscopy and the generation of myosin mutants that are motor-competent but unable to bind membranes will be key to advance.

CHAPTER 7

CONCLUSIONS AND PERSPECTIVES

7. CONCLUSIONS AND PERSPECTIVES

Myosins are a superfamily of motor proteins expressed among organisms. These are involved in many cell events such as muscle contraction, vesicle trafficking, and cytokinesis. Many myosin classes are expressed in a single organism, which supports the idea that each acts in a specific cell event, or that together they have complementary or redundant roles.

During cytokinesis, a contractile actomyosin ring must form in order to a single cell divide into two daughter cells. NMIIs from class II localize to the contractile ring and their function is essential for normal progression of this process. In yeast and human cells, different NMIIs can act during cytokinesis (Kitayama et al., 1997; Beach & Hammer, 2015; Taneja et al., 2020). Interestingly, myosins from other classes (myosin V and VI) were shown to also contribute to cytokinesis in *S. pombe* and to abscission in HeLa cells (Laplante et al., 2015; Zambon et al., 2017; Arden et al., 2007). More recently it was reported that the release of spermatids during spermatogenesis cytokinesis in *C. elegans* also requires a myosin VI (Kelleher et al., 2000; Hu et al., 2019).

In order to further explore which myosins can function during cytokinesis in animals, I used *C. elegans* one-cell embryos. Cell divisions in the early embryo are highly stereotypical and even subtle phenotypes associated with the depletion of each myosin are easy to detect by live imaging. I found that the only myosin essential for cytokinesis is NMY-2, one of the three NMIIs expressed in *C. elegans*. Contrary to what was observed in yeast and human cells, no phenotype was detected when the other NMIIs were depleted. Interestingly, I found that MYO-1, a conventional muscle myosin, is important for contractile ring constriction, which was unexpected because to my knowledge is the first time that, to my knowledge, a muscle myosin is described to function in a non-muscle context. I showed that both MYO-1 and NMY-2 function during contractile ring constriction, but if MYO-1 works independently of NMY-2 or if together they form heterotypic filaments remains to be studied. It will be important to investigate MYO-1 localization and possible co-localization with NMY-2 within the contractile ring.

I then explored a central question in the field that remains to be further addressed in animal cells. It is well accepted that NMII is essential for cytokinesis, but the relevance of its motor activity for the process remains controversial and poorly studied *in vivo* in animals. *C. elegans* has three NMIIs, but as I showed NMY-2 is the only NMII that is essential for cytokinesis in *C. elegans* embryos. To address if NMII motor activity is essential for cytokinesis, together with my colleagues, I used *C. elegans* one-cell embryos expressing

mutant NMY-2 with reduced (motor-impaired) or no (motor-dead) motor activity, that are able to bind to F-actin. The motor-impaired mutants complete cytokinesis albeit slower than controls and their contractile rings are more sensitive to a reduction in NMII levels. The motor-dead NMIIs do not support cytokinesis. We also show that NMII motor activity is important for contractile ring assembly, furrow initiation, and contractile ring constriction. In addition, embryos expressing the motor-dead mutants were not able to assemble and align a compact F-actin band at the cell equator where the contractile ring forms. Altogether our results show that NMII's crosslinking activity is not sufficient for cytokinesis to occur in the absence of motor-activity. In the future, it would be interesting to study how F-actin cortical flows are affected by the expression of NMII motor mutants because cortical flows were described to be dependent on NMII and required to generate a normal F-actin band at the cell equator (Reymann et al., 2016).

A second unexplored question about NMIIs is the existence and relevance of an NMII pool bound to the plasma membrane. During cytokinesis two NMII pools may exist, one consisting of NMII bipolar filaments that interdigitates F-actin and the other able to associate with the plasma membrane and F-actin (Laporte et al., 2011; Laplante et al., 2016). Some evidence exists that indeed NMII can associate with the plasma membrane (Liu et al., 2016) but the relevance of such a membrane-bound pool is not understood. I showed that NMII can bind to phospholipids *in vitro* indicating that NMII potentially binds to the plasma membrane *in vivo*. To test this, I used permeabilized *C. elegans* one-cell embryos and showed that when Latrunculin A, a drug that sequesters monomeric actin preventing new polymerization and triggering F-actin depolymerization, is added at anaphase onset NMY-2 remained associated with the plasma membrane. I found that NMY-2 at the plasma membrane was cleared from the poles due to signals from the microtubules and accumulated at the cell equator via ECT-2 and active RHO-A, suggesting that signals that normally regulate NMII at the cell cortex, regulate NMY-2 membrane-bound pool dynamics. NMY-2 binding to the plasma membrane seems to depend on its NMY-2 status since depletion of proteins that regulate its activation resulted in lower levels of NMY-2 at the plasma membrane. Accordingly, it will be important to observe if a constitutively inactive NMY-2 by expressing a MLC-4 that cannot be phosphorylated at the activation sites, can bind to the plasma membrane. In the future, it will be important to explore the consequences of expressing motor-competent NMII with a compromised plasma membrane-binding ability in the presence of an unperturbed F-actin network.

In sum, in my thesis work, I showed that *C. elegans* NMY-2 and NMY-2's motor activity are required throughout cytokinesis. Additionally, to NMY-2's important function in translocating F-actin, I found evidence that a NMY-2 membrane-bound pool may exist during cytokinesis, whose function may be relevant for this process. In addition, I obtained evidence for the involvement of a muscle class II myosin in embryonic cytokinesis, which to my knowledge has never been reported and therefore deserves in depth characterization in the future.

REFERENCES

Abouhamed, M., Grobe, K., Leefa Chong San, I. V., Thelen, S., Honnert, U., Balda, M. S., Matter, K., & Bähler, M. (2009). Myosin IXa regulates epithelial differentiation and its deficiency results in hydrocephalus. *Molecular Biology of the Cell*, *20*(24), 5074–5085.

Adam, J. C., Pringle, J. R., & Peifer, M. (2000). Evidence for Functional Differentiation among Drosophila Septins in Cytokinesis and Cellularization. *Molecular Biology of the Cell*, *11*(9), 3123–3135.

Adams, R. J., & Pollard, T. D. (1989). Binding of myosin I to membrane lipids. *Nature*, *340*(6234), 565–568.

Adelstein, R. S., & Anne Conti, M. (1975). Phosphorylation of platelet myosin increases actin-activated myosin ATPase activity. *Nature*, *256*(5518), 597–598.

Agarwal, P., & Zaidel-Bar, R. (2019). Principles of Actomyosin Regulation In Vivo. *Trends in Cell Biology*, *29*(2), 150–163.

Albanesi, J. P., Fujisaki, H., Hammer, J. A., Korn, E. D., Jones, R., & Sheetz, M. P. (1985). Monomeric Acanthamoeba myosins I support movement in vitro. *Journal of Biological Chemistry*, *260*(15), 8649–8652.

Albanesi, Joseph P., Hammer, Ja., & Korn, E. D. (1983). The interaction of F-actin with phosphorylated and unphosphorylated myosins IA and IB from Acanthamoeba castellanii. *Journal of Biological Chemistry*, *258*(16), 10176–10181.

Alexander, M., Chan, K. K. M., Byrne, A. B., Selman, G., Lee, T., Ono, J., Wong, E., Puckrin, R., Dixon, S. J., & Roy, P. J. (2009). An UNC-40 pathway directs postsynaptic membrane extension in Caenorhabditis elegans. *Development*, *136*(6), 911–922.

Allingham, J. S., Smith, R., & Rayment, I. (2005). The structural basis of blebbistatin inhibition and specificity for myosin II. *Nature Structural & Molecular Biology*, *12*(4), 378–379.

Almeida, C. G., Yamada, A., Tenza, D., Louvard, D., Raposo, G., & Coudrier, E. (2011). Myosin 1b promotes the formation of post-Golgi carriers by regulating actin assembly

and membrane remodelling at the trans-Golgi network. *Nature Cell Biology*, *13*(7), 779–789.

Altmann, K., Frank, M., Neumann, D., Jakobs, S., & Westermann, B. (2008). The class V myosin motor protein, Myo2, plays a major role in mitochondrial motility in Saccharomyces cerevisiae. *Journal of Cell Biology*, *181*(1), 119–130.

Amano, M., Ito, M., Kimura, K., Fukata, Y., Chihara, K., Nakano, T., Matsuura, Y., & Kaibuchi, K. (1996). Phosphorylation and activation of myosin by Rho-associated kinase (Rho-kinase). *The Journal of Biological Chemistry*, *271*(34), 20246–20249.

Anlaş, A. A., & Nelson, C. M. (2018). Tissue mechanics regulates form, function, and dysfunction. *Current Opinion in Cell Biology*, *54*, 98–105.

Arden, S. D., Puri, C., Au, J. S.-Y., Kendrick-Jones, J., & Buss, F. (2007). Myosin VI is required for targeted membrane transport during cytokinesis. *Molecular Biology of the Cell*, *18*(12), 4750–4761.

Ardizzi, J. P., & Epstein, H. F. (1987). Immunochemical localization of myosin heavy chain isoforms and paramyosin in developmentally and structurally diverse muscle cell types of the nematode Caenorhabditis elegans. *The Journal of Cell Biology*, *105*(6), 2763–2770.

Arif, E., Wagner, M. C., Johnstone, D. B., Wong, H. N., George, B., Pruthi, P. A., Lazzara, M. J., & Nihalani, D. (2011). Motor protein Myo1c is a podocyte protein that facilitates the transport of slit diaphragm protein Neph1 to the podocyte membrane. *Molecular and Cellular Biology*, *31*(10), 2134–2150.

Arribere, J. A., Bell, R. T., Fu, B. X., Artiles, K. L., Hartman, P. S., & Fire, A. Z. (2014). Efficient marker-free recovery of custom genetic modifications with CRISPR/Cas9 in Caenorhabditis elegans. *Genetics*, *198*(3), 837–846.

Aschenbrenner, L., Lee, T., & Hasson, T. (2003). Myo6 facilitates the translocation of endocytic vesicles from cell peripheries. *Molecular Biology of the Cell*, *14*(7), 2728–2743.

Attanapola, S. L., Alexander, C. J., & Mulvihill, D. P. (2009). Ste20-kinase-dependent TEDS-site phosphorylation modulates the dynamic localisation and endocytic function of the fission yeast class I myosin, Myo1. *Journal of Cell Science*, *122*(21), 3856–3861.

Au, J. S.-Y., Puri, C., Ihrke, G., Kendrick-Jones, J., & Buss, F. (2007). Myosin VI is required for sorting of AP-1B–dependent cargo to the basolateral domain in polarized MDCK cells. *The Journal of Cell Biology*, *177*(1), 103–114.

Audhya, A., Hyndman, F., McLeod, I. X., Maddox, A. S., Yates III, J. R., Desai, A., & Oegema, K. (2005). A complex containing the Sm protein CAR-1 and the RNA helicase CGH-1 is required for embryonic cytokinesis in Caenorhabditis elegans. *The Journal of Cell Biology*, *171*(2), 267–279.

Ayscough, K. R., Stryker, J., Pokala, N., Sanders, M., Crews, P., & Drubin, D. G. (1997). High rates of actin filament turnover in budding yeast and roles for actin in establishment and maintenance of cell polarity revealed using the actin inhibitor latrunculin-A. *The Journal of Cell Biology*, *137*(2), 399–416.

Backouche, F., Haviv, L., Groswasser, D., & Bernheim-Groswasser, A. (2006). Active gels: Dynamics of patterning and self-organization. *Physical Biology*, *3*(4), 264.

Bähler, M. (2000). Are class III and class IX myosins motorized signalling molecules? *Biochimica et Biophysica Acta (BBA) - Molecular Cell Research*, *1496*(1), 52–59.

Bahloul, A., Chevreux, G., Wells, A. L., Martin, D., Nolt, J., Yang, Z., Chen, L. Q., Potier, N., Van Dorsselaer, A., Rosenfeld, S., Houdusse, A., & Sweeney, H. L. (2004). The unique insert in myosin VI is a structural calcium-calmodulin binding site. *Proceedings of the National Academy of Sciences of the United States of America*, *101*(14), 4787–4792.

Baines, I. C., Brzeska, H., & Korn, E. D. (1992). Differential localization of Acanthamoeba myosin I isoforms. *The Journal of Cell Biology*, *119*(5), 1193–1203.

Baker, J. P., & Titus, M. a. (1997). A family of unconventional myosins from the nematode Caenorhabditis elegans. *Journal of Molecular Biology*, *272*(4), 523–535.

Balasubramanian, M. K., McCollum, D., Chang, L., Wong, K. C., Naqvi, N. I., He, X., Sazer, S., & Gould, K. L. (1998). Isolation and characterization of new fission yeast cytokinesis mutants. *Genetics*, *149*(3), 1265–1275.

Balklava, Z., Pant, S., Fares, H., & Grant, B. D. (2007). Genome-wide analysis identifies a general requirement for polarity proteins in endocytic traffic. *Nature Cell Biology*, *9*(9), 1066–1073.

Bassi, Z. I., Audusseau, M., Riparbelli, M. G., Callaini, G., & D'Avino, P. P. (2013). Citron kinase controls a molecular network required for midbody formation in cytokinesis. *Proceedings of the National Academy of Sciences*, *110*(24), 9782–9787.

Bassi, Z. I., Verbrugghe, K. J., Capalbo, L., Gregory, S., Montembault, E., Glover, D. M., & D'avino, P. P. (2011). Sticky/Citron kinase maintains proper RhoA localization at the cleavage site during cytokinesis. *Journal of Cell Biology*, *195*(4), 595–603.

Bastos, R. N., Penate, X., Bates, M., Hammond, D., & Barr, F. A. (2012). CYK4 inhibits Rac1-dependent PAK1 and ARHGEF7 effector pathways during cytokinesis. *The Journal of Cell Biology*, *198*(5), 865–880.

Batchelder, E. L., Thomas-Virnig, C. L., Hardin, J. D., & White, J. G. (2007). Cytokinesis is not controlled by calmodulin or myosin light chain kinase in the Caenorhabditis elegans early embryo. *FEBS Letters*, *581*(22), 4337–4341.

Batters, C., Arthur, C. P., Lin, A., Porter, J., Geeves, M. A., Milligan, R. A., Molloy, J. E., & Coluccio, L. M. (2004). Myo1c is designed for the adaptation response in the inner ear. *The EMBO Journal*, *23*(7), 1433–1440.

Beach, J. R., & Hammer, J. A. (2015). Myosin II isoform co-assembly and differential regulation in mammalian systems. *Experimental Cell Research*, *334*(1), 2–9.

Beach, J. R., Shao, L., Remmert, K., Li, D., Betzig, E., & Hammer, J. A. (2014). Nonmuscle Myosin II Isoforms Coassemble in Living Cells. *Current Biology*, *24*(10), 1160–1166.

Belyantseva, I. A., Boger, E. T., Naz, S., Frolenkov, G. I., Sellers, J. R., Ahmed, Z. M., Griffith, A. J., & Friedman, T. B. (2005). Myosin-XVa is required for tip localization of whirlin and differential elongation of hair-cell stereocilia. *Nature Cell Biology*, *7*(2), 148–156.

Bement, W. M., & Mooseker, M. S. (1995). TEDS rule: A molecular rationale for differential regulation of myosins by phosphorylation of the heavy chain head. *Cell Motility and the Cytoskeleton*, *31*(2), 87–92.

Bement, W. M., Benink, H. A., & von Dassow, G. (2005). A microtubule-dependent zone of active RhoA during cleavage plane specification. *Journal of Cell Biology*, *170*(1), 91–101.

Bement, W. M., Miller, A. L., & von Dassow, G. (2006). Rho GTPase Activity Zones and Transient Contractile Arrays. *BioEssays : News and Reviews in Molecular, Cellular and Developmental Biology*, *28*(10), 983–993.

Bement, W. M., Wirth, J. A., & Mooseker, M. S. (1994). Cloning and mRNA expression of human unconventional myosin-IC: a homologue of amoeboid myosins-I with a single IQ motif and an SH3 domain. *Journal of Molecular Biology*, *243*(2), 356–363.

Benesh, A. E., Nambiar, R., McConnell, R. E., Mao, S., Tabb, D. L., & Tyska, M. J. (2010). Differential localization and dynamics of class I myosins in the enterocyte microvillus. *Molecular Biology of the Cell*, *21*(6), 970–978.

Bezanilla, M., Forsburg, S. L., & Pollard, T. D. (1997). Identification of a second myosin-II in Schizosaccharomyces pombe: Myp2p is conditionally required for cytokinesis. *Molecular Biology of the Cell*, *8*(12), 2693–2705.

Bi, E., Maddox, P., Lew, D. J., Salmon, E. D., McMillan, J. N., Yeh, E., & Pringle, J. R. (1998). Involvement of an actomyosin contractile ring in Saccharomyces cerevisiae cytokinesis. *Journal of Cell Biology*, *142*(5), 1301–1312. https://doi.org/10.1083/jcb.142.5.1301

Bi, J., Chase, S. E., Pellenz, C. D., Kurihara, H., Fanning, A. S., & Krendel, M. (2013). Myosin 1e is a component of the glomerular slit diaphragm complex that regulates actin reorganization during cell-cell contact formation in podocytes. *American Journal of Physiology-Renal Physiology*, *305*(4), F532–F544.

Billington, N., Beach, J. R., Heissler, S. M., Remmert, K., Guzik-Lendrum, S., Nagy, A., Takagi, Y., Shao, L., Li, D., Yang, Y., Zhang, Y., Barzik, M., Betzig, E., Hammer, J. A., & Sellers, J. R. (2015). Myosin 18A coassembles with nonmuscle myosin 2 to form mixed bipolar filaments. *Current Biology*, *25*(7), 942–948.

Blanchoin, L., Boujemaa-Paterski, R., Sykes, C., & Plastino, J. (2014). Actin dynamics, architecture, and mechanics in cell motility. *Physiological Reviews*, *94*(1), 235–263.

Boëda, B., El Amraoui, A., Bahloul, A., Goodyear, R., Daviet, L., Blanchard, S., Perfettini, I., Fath, K. R., Shorte, S., & Reiners, J. (2002). Myosin VIIa, harmonin and cadherin 23, three Usher I gene products that cooperate to shape the sensory hair cell bundle. *The EMBO Journal*, *21*(24), 6689–6699.

Boguslavsky, S., Chiu, T., Foley, K. P., Osorio-Fuentealba, C., Antonescu, C. N., Bayer, K. U., Bilan, P. J., & Klip, A. (2012). Myo1c binding to submembrane actin mediates insulin-induced tethering of GLUT4 vesicles. *Molecular Biology of the Cell*, *23*(20), 4065–4078.

Bonafé, N., & Sellers, J. R. (1998). Molecular characterization of myosin {V} from {Drosophila} melanogaster. *Journal of Muscle Research and Cell Motility*, *19*(2), 129–141.

Bose, A., Guilherme, A., Robida, S. I., Nicoloro, S. M. C., Zhou, Q. L., Jiang, Z. Y., Pomerleau, D. P., & Czech, M. P. (2002). Glucose transporter recycling in response to insulin is facilitated by myosin Myo1c. *Nature*, *420*(6917), 821–824.

Brandstaetter, H., Kendrick-Jones, J., & Buss, F. (2012). Myo1c regulates lipid raft recycling to control cell spreading, migration and Salmonella invasion. *Journal of Cell Science*, *125*(Pt 8), 1991–2003.

Bray, D., & White, J. G. (1988). Cortical flow in animal cells. *Science*, *239*(4842), 883–888.

Brennan, I. M., Peters, U., Kapoor, T. M., & Straight, A. F. (2007). Polo-like kinase controls vertebrate spindle elongation and cytokinesis. *PloS One*, *2*(5).

Brenner, S. (1974). The Genetics Of Caenorhabditis Elegans. *Genetics*, *77*(1), 71–94.

Bringmann, H., & Hyman, A. A. (2005). A cytokinesis furrow is positioned by two consecutive signals. *Nature*, *436*(7051), 731–734.

Brockerhoff, S. E., Stevens, R. C., & Davis, T. N. (1994). The unconventional myosin, Myo2p, is a calmodulin target at sites of cell growth in Saccharomyces cerevisiae. *Journal of Cell Biology*, *124*(3), 315–323.

Brown, S. S. (1997). Myosins in yeast. *Current Opinion in Cell Biology*, *9*(1), 44–48.

Bryant, Z., Altman, D., & Spudich, J. A. (2007). The power stroke of myosin VI and the basis of reverse directionality. *Proceedings of the National Academy of Sciences*, *104*(3), 772–777.

Brzeska, H., Lynch, T. J., Martin, B., & Korn, E. D. (1989). The localization and sequence of the phosphorylation sites of Acanthamoeba myosins I. An improved method for

locating the phosphorylated amino acid. *Journal of Biological Chemistry*, *264*(32), 19340–19348.

Brzeska, H., Martin, B. M., & Korn, E. D. (1996). The catalytic domain of Acanthamoeba myosin I heavy chain kinase. I. Identification and characterization following tryptic cleavage of the native enzyme. *The Journal of Biological Chemistry*, *271*(43), 27049–27055.

Brzeska, Hanna, Guag, J., Remmert, K., Chacko, S., & Korn, E. D. (2010). An Experimentally Based Computer Search Identifies Unstructured Membrane-binding Sites in Proteins APPLICATION TO CLASS I MYOSINS, PAKS, AND CARMIL. *Journal of Biological Chemistry*, *285*(8), 5738–5747.

Brzeska, Hanna, Young, R., Knaus, U., & Korn, E. D. (1999). Myosin I heavy chain kinase: Cloning of the full-length gene and acidic lipid-dependent activation by Rac and Cdc42. *Proceedings of the National Academy of Sciences*, *96*(2), 394–399.

Brzeska, Hanna, Young, R., Tan, C., Szczepanowska, J., & Korn, E. D. (2001). Calmodulin-binding and Autoinhibitory Domains of *Acanthamoeba* Myosin I Heavy Chain Kinase, a p21-activated Kinase (PAK). *Journal of Biological Chemistry*, *276*(50), 47468–47473.

Burkard, M. E., Randall, C. L., Larochelle, S., Zhang, C., Shokat, K. M., Fisher, R. P., & Jallepalli, P. V. (2007). Chemical genetics reveals the requirement for Polo-like kinase 1 activity in positioning RhoA and triggering cytokinesis in human cells. *Proceedings of the National Academy of Sciences of the United States of America*, *104*(11), 4383–4388.

Buss, F., Arden, S. D., Lindsay, M., Luzio, J. P., & Kendrick Jones, J. (2001). Myosin VI isoform localized to clathrin coated vesicles with a role in clathrin mediated endocytosis. *The EMBO Journal*, *20*(14), 3676–3684.

Buss, F., Kendrick-Jones, J., Lionne, C., Knight, A. E., Côté, G. P., & Paul Luzio, J. (1998). The localization of myosin VI at the Golgi complex and leading edge of fibroblasts and its phosphorylation and recruitment into membrane ruffles of A431 cells after growth factor stimulation. *The Journal of Cell Biology*, *143*(6), 1535–1545.

Byerly, L., Cassada, R. C., & Russell, R. L. (1976). The life cycle of the nematode Caenorhabditis elegans: I. Wild-type growth and reproduction. *Developmental Biology*, *51*(1), 23–33.

C. elegans Sequencing Consortium. (1998). Genome sequence of the nematode {C}. elegans: A platform for investigating biology. *Science (New York, N.Y.)*, *282*(5396), 2012–2018.

Canagarajah, B., Leskow, F. C., Ho, J. Y. S., Mischak, H., Saidi, L. F., Kazanietz, M. G., & Hurley, J. H. (2004). Structural mechanism for lipid activation of the {Rac}-specific {GAP}, beta2-chimaerin. *Cell*, *119*(3), 407–418.

Canman, J. C., Lewellyn, L., Laband, K., Smerdon, S. J., Desai, A., Bowerman, B., & Oegema, K. (2008). Inhibition of Rac by the GAP activity of centralspindlin is essential for cytokinesis. *Science*, *322*(5907), 1543–1546.

Cao, L., Ding, X., Yu, W., Yang, X., Shen, S., & Yu, L. (2007). Phylogenetic and evolutionary analysis of the septin protein family in metazoan. *FEBS Letters*, *581*(28), 5526–5532.

Cao, T. T., Chang, W., Masters, S. E., & Mooseker, M. S. (2004). Myosin-Va binds to and mechanochemically couples microtubules to actin filaments. *Molecular Biology of the Cell*, *15*(1), 151–161.

Capitanio, M., Canepari, M., Maffei, M., Beneventi, D., Monico, C., Vanzi, F., Bottinelli, R., & Pavone, F. S. (2012). Ultrafast force-clamp spectroscopy of single molecules reveals load dependence of myosin working stroke. *Nature Methods*, *9*(10), 1013–1019.

Carlsson, L., Nyström, L.-E., Sundkvist, I., Markey, F., & Lindberg, U. (1977). Actin polymerizability is influenced by profilin, a low molecular weight protein in non-muscle cells. *Journal of Molecular Biology*, *115*(3), 465–483.

Carmena, M., Wheelock, M., Funabiki, H., & Earnshaw, W. C. (2012). The chromosomal passenger complex (CPC): From easy rider to the godfather of mitosis. *Nature Reviews Molecular Cell Biology*, *13*(12), 789–803.

Carter, S. B. (1967). Effects of Cytochalasins on Mammalian Cells. *Nature*, *213*(5073), 261–264.

Carvalho, A., Carmena, M., Sambade, C., Earnshaw, W. C., & Wheatley, S. P. (2003). Survivin is required for stable checkpoint activation in taxol-treated HeLa cells. *Journal of Cell Science*, *116*(14), 2987–2998.

Carvalho, A., Desai, A., & Oegema, K. (2009). Structural memory in the contractile ring makes the duration of cytokinesis independent of cell size. *Cell*, *137*(5), 926–937.

Carvalho, A., Olson, S. K., Gutierrez, E., Zhang, K., Noble, L. B., Zanin, E., Desai, A., Groisman, A., & Oegema, K. (2011). Acute drug treatment in the early C. elegans embryo. *PloS One*, *6*(9).

Cassada, R. C., & Russell, R. L. (1975). The dauerlarva, a post-embryonic developmental variant of the nematode Caenorhabditis elegans. *Developmental Biology*, *46*(2), 326–342.

Castrillon, D. H., & Wasserman, S. A. (1994). Diaphanous is required for cytokinesis in Drosophila and shares domains of similarity with the products of the limb deformity gene. *Development (Cambridge, England)*, *120*(12), 3367–3377.

Catlett, N. L., & Weisman, L. S. (1998). The terminal tail region of a yeast myosin-V mediates its attachment to vacuole membranes and sites of polarized growth. *Proceedings of the National Academy of Sciences*, *95*(25), 14799–14804.

Catlett, N. L., Duex, J. E., Tang, F., & Weisman, L. S. (2000). Two distinct regions in a yeast myosin-V tail domain are required for the movement of different cargoes. *The Journal of Cell Biology*, *150*(3), 513–526.

Caudron, F., & Barral, Y. (2009). Septins and the lateral compartmentalization of eukaryotic membranes. *Developmental Cell*, *16*(4), 493–506.

Ceron, J., Rual, J. F., Chandra, A., Dupuy, D., Vidal, M., & Van Den Heuvel, S. (2007). Large-scale {RNAi} screens identify novel genes that interact with the C. Elegans retinoblastoma pathway as well as splicing-related components with synMuv B activity. *BMC Developmental Biology*, *7*, 1–16.

Chan, F. Y., Silva, A. M., Saramago, J., Pereira-Sousa, J., Brighton, H. E., Pereira, M., Oegema, K., Gassmann, R., & Carvalho, A. X. (2019). The ARP2/3 complex prevents excessive formin activity during cytokinesis. *Molecular Biology of the Cell*, *30*(1), 96–107.

Chandrasekaran, R., Kenworthy, A. K., & Lacy, D. B. (2016). Clostridium difficile toxin A undergoes clathrin-independent, PACSIN2-dependent endocytosis. *PLoS Pathogens*, *12*(12).

Chang, D. C., & Meng, C. (1995). A localized elevation of cytosolic free calcium is associated with cytokinesis in the zebrafish embryo. *The Journal of Cell Biology*, *131*(6 Pt 1), 1539–1545.

Chang, F. (1999). Movement of a cytokinesis factor cdc12p to the site of cell division. *Current Biology*, *9*(15), 849-S2.

Charras, G. T., Coughlin, M., Mitchison, T. J., & Mahadevan, L. (2008). Life and times of a cellular bleb. *Biophysical Journal*, *94*(5), 1836–1853.

Charras, G. T., Hu, C.-K., Coughlin, M., & Mitchison, T. J. (2006). Reassembly of contractile actin cortex in cell blebs. *The Journal of Cell Biology*, *175*(3), 477–490.

Cheeks, R. J., Canman, J. C., Gabriel, W. N., Meyer, N., Strome, S., & Goldstein, B. (2004). C. elegans PAR proteins function by mobilizing and stabilizing asymmetrically localized protein complexes. *Current Biology*, *14*(10), 851–862.

Chen, C. S. (2007). Separate but not equal: Differential mechanical roles for myosin isoforms. *Biophysical Journal*, *92*(May), 2984–2985.

Chen, C.-H., Lee, A., Liao, C.-P., Liu, Y.-W., & Pan, C.-L. (2014). RHGF-1/PDZ-RhoGEF and retrograde DLK-1 signaling drive neuronal remodeling on microtubule disassembly. *Proceedings of the National Academy of Sciences*, *111*(46), 16568–16573.

Chen, W., Foss, M., Tseng, K.-F., & Zhang, D. (2008). Redundant Mechanisms Recruit Actin into the Contractile Ring in Silkworm Spermatocytes. *PLoS Biology*, *6*(9).

Chen, Z. Y., Hasson, T., Zhang, D. S., Schwender, B. J., Derfler, B. H., Mooseker, M. S., & Corey, D. P. (2001). Myosin-VIIb, a novel unconventional myosin, is a constituent of microvilli in transporting epithelia. *Genomics*, *72*(3), 285–296.

Cheney, R. E., & Mooseker, M. S. (1992). Unconventional myosins. *Current Opinion in Cell Biology*, *4*(1), 27–35.

Cheney, R. E., O'Shea, M. K., Heuser, J. E., Coelho, M. V., Wolenski, J. S., Espreafico, E. M., Forscher, P., Larson, R. E., & Mooseker, M. S. (1993). Brain myosin-V is a two-headed unconventional myosin with motor activity. *Cell*, *75*(1), 13–23.

Cheney, R. E., Riley, M. A., & Mooseker, M. S. (1993). Phylogenetic analysis of the myosin superfamily. *Cell Motility and the Cytoskeleton*, *24*(4), 215–223.

Cheng, J., Grassart, A., & Drubin, D. G. (2012). Myosin 1E coordinates actin assembly and cargo trafficking during clathrin-mediated endocytosis. *Molecular Biology of the Cell*, *23*(15), 2891–2904.

Chew, T.-L., Wolf, W. A., Gallagher, P. J., Matsumura, F., & Chisholm, R. L. (2002). A fluorescent resonant energy transfer–based biosensor reveals transient and regional myosin light chain kinase activation in lamella and cleavage furrows. *The Journal of Cell Biology*, *156*(3), 543–

Chieregatti, E., & Bahler, M. (1996). The myosin myr 5 is phosphorylated at multiple sites. *Molecular Biology Of The Cell*, *7*, 2167–2167.

Chinthalapudi, K., Heissler, S. M., Preller, M., Sellers, J. R., & Manstein, D. J. (2017). Mechanistic insights into the active site and allosteric communication pathways in human nonmuscle myosin-{2C}. *ELife*, *6*, 1–24.

Chishti, A. H., Kim, A. C., Marfatia, S. M., Lutchman, M., Hanspal, M., Jindal, H., Liu, S.-C., Low, P. S., Rouleau, G. A., & Mohandas, N. (1998). The FERM domain: A unique module involved in the linkage of cytoplasmic proteins to the membrane. *Trends in Biochemical Sciences*, *23*(8), 281.

Chuang, C.-H., Carpenter, A. E., Fuchsova, B., Johnson, T., de Lanerolle, P., & Belmont, A. S. (2006). Long-range directional movement of an interphase chromosome site. *Current Biology: CB*, *16*(8), 825–831.

Chugh, P., Clark, A. G., Smith, M. B., Cassani, D. A. D., Dierkes, K., Ragab, A., Roux, P. P., Charras, G., Salbreux, G., & Paluch, E. K. (2017). Actin cortex architecture regulates cell surface tension. *Nat Cell Biol*, *19*(6), 689–697.

Churchman, L. S., Ökten, Z., Rock, R. S., Dawson, J. F., & Spudich, J. A. (2005). Single molecule high-resolution colocalization of Cy3 and Cy5 attached to macromolecules

measures intramolecular distances through time. *Proceedings of the National Academy of Sciences*, *102*(5), 1419–1423.

Ciapa, B., Pesando, D., Wilding, M., & Whitaker, M. (1994). Cell-cycle calcium transients driven by cyclic changes in inositol trisphosphate levels. *Nature*, *368*(6474), 875–878.

Clark, K., Middelbeek, J., Dorovkov, M. V., Figdor, C. G., Ryazanov, A. G., Lasonder, E., & van Leeuwen, F. N. (2008). The α kinases TRPM6 and TRPM7, but not eEF-2 kinase, phosphorylate the assembly domain of myosin IIA, IIB and IIC. *FEBS Letters*, *582*(20), 2993–2997.

Clarke, M., & Spudich, J. A. (1977). Nonmuscle contractile proteins: The role of actin and myosin in cell motility and shape determination. *Annual Review of Biochemistry*, *46*(1), 797–822.

Clausen, M. P., Colin-York, H., Schneider, F., Eggeling, C., & Fritzsche, M. (2017). Dissecting the actin cortex density and membrane-cortex distance in living cells by super-resolution microscopy. *Journal of Physics D: Applied Physics*, *50*(6), 064002.

Coelho, M. V., & Larson, R. E. (1993). Ca (2+)-dependent phosphorylation of the tail domain of myosin-V, a calmodulin-binding myosin in vertebrate brain. *Brazilian Journal of Medical and Biological Research, 26*(5), 465–472.

Coffman, V. C., Kachur, T. M., Pilgrim, D. B., & Dawes, A. T. (2017). Antagonistic Behaviors of NMY-1 and NMY-2 Maintain Ring Channels in the C. elegans Gonad. *Biophysical Journal*, *111*(10), 2202–2213.

Coffman, V. C., Sees, J. A., Kovar, D. R., & Wu, J.-Q. (2013). The formins Cdc12 and For3 cooperate during contractile ring assembly in cytokinesis. *Journal of Cell Biology*, *203*(1), 101–114.

Coluccio, A. E., Rodriguez, R. K., Kernan, M. J., & Neiman, A. M. (2008). The yeast spore wall enables spores to survive passage through the digestive tract of Drosophila. *PLoS One*, *3*(8).

Coluccio, L. M., & Geeves, M. A. (1999). Transient Kinetic Analysis of the 130-kDa Myosin I (MYR-1 Gene Product) from Rat Liver A MYOSIN I DESIGNED FOR

MAINTENANCE OF TENSION? *Journal of Biological Chemistry*, *274*(31), 21575–21580.

Consortium*, T. C. elegans S. (1998). Genome Sequence of the Nematode C. elegans: A Platform for Investigating Biology. *Science*, *282*(5396), 2012–2018.

Cooper, J. A., & Sept, D. (2008). New insights into mechanism and regulation of actin capping protein. *International Review of Cell and Molecular Biology*, *267*, 183–206.

Corsi, A. K., Wightman, B., & Chalfie, M. (2015). A transparent window into biology: A primer on Caenorhabditis elegans. *Genetics*, *200*(2), 387–407.

Côté, G. P., Albanesi, J. P., Ueno, T., Hammer, J. A., & Korn, E. D. (1985). Purification from Dictyostelium discoideum of a low-molecular-weight myosin that resembles myosin I from Acanthamoeba castellanii. *The Journal of Biological Chemistry*, *260*(8), 4543–4546.

Cote, G. P., Albanesi, J. P., Ueno, T., Hammer, J. d, & Korn, E. D. (1985). Purification from Dictyostelium discoideum of a low-molecular-weight myosin that resembles myosin I from Acanthamoeba castellanii. *Journal of Biological Chemistry*, *260*(8), 4543–4546.

Coureux, P.-D., Sweeney, H. L., & Houdusse, A. (2004). Three myosin V structures delineate essential features of chemo ꟷmechanical transduction. *The EMBO Journal*, *23*(23), 4527–4537.

Coureux, P.-D., Wells, A. L., Ménétrey, J., Yengo, C. M., Morris, C. A., Sweeney, H. L., & Houdusse, A. (2003). A structural state of the myosin V motor without bound nucleotide. *Nature*, *425*(6956), 419–423.

Crawley, S. W., Roche, M. A. de la, Lee, S.-F., Li, Z., Chitayat, S., Smith, S. P., & Côté, G. P. (2006). Identification and Characterization of an 8-kDa Light Chain Associated with Dictyostelium discoideum MyoB, a Class I Myosin. *Journal of Biological Chemistry*, *281*(10), 6307–6315.

Cremona, O., & De Camilli, P. (2001). Phosphoinositides in membrane traffic at the synapse. *Journal of Cell Science*, *114*(6), 1041–1052.

Cross, J. A., & Dodding, M. P. (2019). Motor–cargo adaptors at the organelle–cytoskeleton interface. *Current Opinion in Cell Biology*, *59*, 16–23.

Cross, M., Csar, X. F., Wilson, N. J., Manes, G., Addona, T. A., Marks, D. C., Whitty, G. A., Ashman, K., & Hamilton, J. A. (2004). A novel 110 kDa form of myosin XVIIIA (MysPDZ) is tyrosine-phosphorylated after colony-stimulating factor-1 receptor signalling. *Biochemical Journal*, *380*(1), 243–253.

Cuenca, A. a, Schetter, A., Aceto, D., Kemphues, K., & Seydoux, G. (2003). Polarization of the C. elegans zygote proceeds via distinct establishment and maintenance phases. *Development (Cambridge, England)*, *130*(7), 1255–1265.

Cyr, J. L., Dumont, R. A., & Gillespie, P. G. (2002). Myosin-1c Interacts with Hair-Cell Receptors through Its Calmodulin-Binding IQ Domains. *Journal of Neuroscience*, *22*(7), 2487–2495.

D'Avino, P. P., & Capalbo, L. (2016). Regulation of midbody formation and function by mitotic kinases. *Seminars in Cell & Developmental Biology*, *53*, 57–63.

D'Avino, P. P., Giansanti, M. G., & Petronczki, M. (2015). Cytokinesis in animal cells. *Cold Spring Harbor Perspectives in Biology*, *7*(4), a015834.

D'Avino, P. P., Savoian, M. S., & Glover, D. M. (2004). Mutations in sticky lead to defective organization of the contractile ring during cytokinesis and are enhanced by Rho and suppressed by Rac. *Journal of Cell Biology*, *166*(1), 61–71.

D'Avino, P. P., Takeda, T., Capalbo, L., Zhang, W., Lilley, K. S., Laue, E. D., & Glover, D. M. (2008). Interaction between Anillin and RacGAP50C connects the actomyosin contractile ring with spindle microtubules at the cell division site. *Journal of Cell Science*, *121*(8), 1151–1158.

Dart, A. E., Tollis, S., Bright, M. D., Frankel, G., & Endres, R. G. (2012). The motor protein myosin 1G functions in FcγR-mediated phagocytosis. *Journal of Cell Science*, *125*(Pt 24), 6020–6029.

Davies, T., Jordan, S. N., Chand, V., Sees, J. A., Laband, K., Carvalho, A. X., Shirasu-Hiza, M., Kovar, D. R., Dumont, J., & Canman, J. C. (2014). High-Resolution Temporal Analysis Reveals a Functional Timeline for the Molecular Regulation of Cytokinesis. *Developmental Cell*, *30*(2), 209–223.

de Bono, M. (2003). Molecular approaches to aggregation behavior and social attachment. *Journal of Neurobiology*, *54*(1), 78–92.

De La Cruz, M. C., Ruiz-Torres, P., Alcamí, J., Díez-Marqués, L., Ortega-Velázquez, R., Chen, S., Rodríguez-Puyol, M., Ziyadeh, F. N., & Rodríguez-Puyol, D. (2001). Hydrogen peroxide increases extracellular matrix mRNA through TGF-β in human mesangial cells. *Kidney International*, *59*(1), 87–95.

De La Roche, M. A., Smith, J. L., Rico, M., Carrasco, S., Merida, I., Licate, L., Côté, G. P., & Egelhoff, T. T. (2002). Dictyostelium discoideum has a single diacylglycerol kinase gene with similarity to mammalian theta isoforms. *The Biochemical Journal*, *368*(Pt 3), 809–815.

Dean, S. O., & Spudich, J. a. (2006). Rho kinase's role in myosin recruitment to the equatorial cortex of mitotic Drosophila S2 cells is for myosin regulatory light chain phosphorylation. *PloS One*, *1*(1), e131–e131.

DeBiasio, R. L., LaRocca, G. M., Post, P. L., & Taylor, D. L. (1996). Myosin II transport, organization, and phosphorylation: Evidence for cortical flow/solation-contraction coupling during cytokinesis and cell locomotion. *Molecular Biology of the Cell*, *7*(8), 1259–1282.

Dechant, R., & Glotzer, M. (2003). Centrosome separation and central spindle assembly act in redundant pathways that regulate microtubule density and trigger cleavage furrow formation. *Developmental Cell*, *4*(3), 333–344.

Delprat, B., Michel, V., Goodyear, R., Yamasaki, Y., Michalski, N., El-Amraoui, A., Perfettini, I., Legrain, P., Richardson, G., & Hardelin, J.-P. (2005). Myosin XVa and whirlin, two deafness gene products required for hair bundle growth, are located at the stereocilia tips and interact directly. *Human Molecular Genetics*, *14*(3), 401–410.

DePina, A. S., Wöllert, T., & Langford, G. M. (2007). Membrane associated nonmuscle myosin II functions as a motor for actin based vesicle transport in clam oocyte extracts. *Cell Motility and the Cytoskeleton*, *64*(10), 739–755.

Descovich, C. P., Cortes, D. B., Ryan, S., Nash, J., Zhang, L., Maddox, P. S., Nedelec, F., & Maddox, A. S. (2018). Cross-linkers both drive and brake cytoskeletal remodeling and furrowing in cytokinesis. *Molecular Biology of the Cell*, *29*(5), 622–631.

Di Paolo, G., & De Camilli, P. (2006). Phosphoinositides in cell regulation and membrane dynamics. *Nature*, *443*(7112), 651–657.

Dickinson, D. J., Ward, J. D., Reiner, D. J., & Goldstein, B. (2013). Engineering the Caenorhabditis elegans genome using Cas9-triggered homologous recombination. *Nature Methods*, *10*(10), 1028.

Ding, S. S., & Woollard, A. (2017). Non-muscle myosin II is required for correct fate specification in the Caenorhabditis elegans seam cell divisions. *Scientific Reports*, *7*(1), 1–13.

Ding, W. Y., Ong, H. T., Hara, Y., Wongsantichon, J., Toyama, Y., Robinson, R. C., Nédélec, F., & Zaidel-Bar, R. (2017). Plastin increases cortical connectivity to facilitate robust polarization and timely cytokinesis. *Journal of Cell Biology*, *216*(5), 1371–1386.

Dix, C. L., Matthews, H. K., Uroz, M., McLaren, S., Wolf, L., Heatley, N., Win, Z., Almada, P., Henriques, R., & Boutros, M. (2018). The role of mitotic cell-substrate adhesion re-modeling in animal cell division. *Developmental Cell*, *45*(1), 132-145. e3.

Dixon, S. J., & Roy, P. J. (2005). Muscle arm development in Caenorhabditis elegans. *Development*, *132*(13), 3079–3092.

Doberstein, S. K., & Pollard, T. D. (1992). Localization and specificity of the phospholipid and actin binding sites on the tail of Acanthamoeba myosin IC. *Journal of Cell Biology*, *117*(6), 1241–1249.

Dominguez, R., Freyzon, Y., Trybus, K. M., & Cohen, C. (1998). Crystal structure of a vertebrate smooth muscle myosin motor domain and its complex with the essential light chain: Visualization of the pre–power stroke state. *Cell*, *94*(5), 559–571.

Donaudy, F., Ferrara, A., Esposito, L., Hertzano, R., Ben-David, O., Bell, R. F., Melchionda, S., Zelante, L., Avraham, K. B., & Gasparini, P. (2003). Multiple mutations of {MYO1A}, a cochlear-expressed gene, in sensorineural hearing loss. *American Journal of Human Genetics*, *72*(6),

Dorn, J. F., Zhang, L., Phi, T.-T., Lacroix, B., Maddox, P. S., Liu, J., & Maddox, A. S. (2016). A theoretical model of cytokinesis implicates feedback between membrane curvature and cytoskeletal organization in asymmetric cytokinetic furrowing. *Molecular Biology of the Cell*, *27*(8), 1286–1299.

Dostal, V., Roberts, C. M., & Link, C. D. (2010). Genetic mechanisms of coffee extract protection in a Caenorhabditis elegans model of β-amyloid peptide toxicity. *Genetics*, *186*(3), 857–866.

Douglas, M. E., Davies, T., Joseph, N., & Mishima, M. (2010). Aurora B and 14-3-3 coordinately regulate clustering of centralspindlin during cytokinesis. *Current Biology: CB*, *20*(10), 927–

Du, A., Sanger, J. M., Linask, K. K., & Sanger, J. W. (2003). Myofibrillogenesis in the first cardiomyocytes formed from isolated quail precardiac mesoderm. *Developmental Biology*, *257*(2), 382–394.

Dulyaninova, N. G., Malashkevich, V. N., Almo, S. C., & Bresnick, A. R. (2005). Regulation of Myosin-IIA Assembly and Mts1 Binding by Heavy Chain Phosphorylation. *Biochemistry*, *44*(18), 6867–6876.

Dunn, T. A., Chen, S., Faith, D. A., Hicks, J. L., Platz, E. A., Chen, Y., Ewing, C. M., Sauvageot, J., Isaacs, W. B., & De Marzo, A. M. (2006). A novel role of myosin VI in human prostate cancer. *The American Journal of Pathology*, *169*(5), 1843–1854.

Durán, J. M., Valderrama, F., Castel, S., Magdalena, J., Tomás, M., Hosoya, H., ... & Egea, G. (2003). Myosin motors and not actin comets are mediators of the actin-based Golgi-to-endoplasmic reticulum protein transport. *Molecular Biology of The Cell, 14*(2), 445-459.

Eda, M., Yonemura, S., Kato, T., Watanabe, N., Ishizaki, T., Madaule, P., & Narumiya, S. (2001). Rho-dependent transfer of Citron-kinase to the cleavage furrow of dividing cells. *Journal of Cell Science*, *114*(Pt 18), 3273–3284.

Edgar, R. C. (2004). MUSCLE: multiple sequence alignment with high accuracy and high throughput. *Nucleic Acids Research*, *32*(5), 1792–1797.

Edwards, K. A., & Kiehart, D. P. (1996). Drosophila nonmuscle myosin II has multiple essential roles in imaginal disc and egg chamber morphogenesis. *Development (Cambridge, England)*, *122*(5), 1499–1511.

El-Amraoui, A., & Petit, C. (2005). Usher I syndrome: Unravelling the mechanisms that underlie the cohesion of the growing hair bundle in inner ear sensory cells. *Journal of Cell Science*, *118*(20), 4593–4603.

Emoto, K., Inadome, H., Kanaho, Y., Narumiya, S., & Umeda, M. (2005). Local change in phospholipid composition at the cleavage furrow is essential for completion of cytokinesis. *Journal of Biological Chemistry*, *280*(45), 37901–37907.

Engelhardt, W. A., & Ljubimowa, M. N. (1939). Myosine and adenosinetriphosphatase. *Nature*, *144*(3650), 668–669.

Epstein, H. F., & Thomson, J. N. (1974). Temperature-sensitive mutation affecting myofilament assembly in Caenorhabditis elegans. *Nature*, *250*(5467), 579–580.

Espindola, F. S., Espreafico, E. M., Coelho, M. V., Martins, A. R., Costa, F. R., Mooseker, M. S., & Larson, R. E. (1992). Biochemical and immunological characterization of p190-calmodulin complex from vertebrate brain: A novel calmodulin-binding myosin. *The Journal of Cell Biology*, *118*(2), 359–368.

Espreafico, E. M., Cheney, R. E., Matteoli, M., Nascimento, A. A., De Camilli, P. V., Larson, R. E., & Mooseker, M. S. (1992). Primary structure and cellular localization of chicken brain myosin-V (p190), an unconventional myosin with calmodulin light chains. *The Journal of Cell Biology*, *119*(6), 1541–1557.

Espreafico, E. M., Coling, D. E., Tsakraklides, V., Krogh, K., Wolenski, J. S., Kalinec, G., & Kachar, B. (1998). Localization of myosin-V in the centrosome. *Proceedings of the National Academy of Sciences*, *95*(15), 8636–8641.

Estey, M. P., Di Ciano-Oliveira, C., Froese, C. D., Bejide, M. T., & Trimble, W. S. (2010). Distinct roles of septins in cytokinesis: SEPT9 mediates midbody abscission. *Journal of Cell Biology*, *191*(4), 741–749.

Etournay, R., Zwaenepoel, I., Perfettini, I., Legrain, P., Petit, C., & El-Amraoui, A. (2007). Shroom2, a myosin-VIIa- and actin-binding protein, directly interacts with ZO-1 at tight junctions. *Journal of Cell Science*, *120*(16), 2838–2850.

Even-Faitelson, L., & Ravid, S. (2006). PAK1 and aPKCζ regulate myosin II-B phosphorylation: A novel signaling pathway regulating filament assembly. *Molecular Biology of the Cell*, *17*(7), 2869–2881.

Even-Ram, S., Doyle, A. D., Conti, M. A., Matsumoto, K., Adelstein, R. S., & Yamada, K. M. (2007). Myosin IIA regulates cell motility and actomyosin-microtubule crosstalk. *Nat Cell Biol*, *9*(3), 299–309.

Fagarasanu, A., Fagarasanu, M., Eitzen, G. A., Aitchison, J. D., & Rachubinski, R. A. (2006). The peroxisomal membrane protein Inp2p is the peroxisome-specific receptor for the myosin V motor Myo2p of Saccharomyces cerevisiae. *Developmental Cell*, *10*(5), 587–600.

Fan, Y., Eswarappa, S. M., Hitomi, M., & Fox, P. L. (2012). Myo1c facilitates G-actin transport to the leading edge of migrating endothelial cells. *Journal of Cell Biology*, *198*(1), 47–55.

Fares, H., Peifer, M., & Pringle, J. R. (1995). Localization and possible functions of Drosophila septins. *Molecular Biology of the Cell*, *6*(12), 1843–1859.

Fath, K. R., Trimbur, G. M., & Burgess, D. R. (1994). Molecular motors are differentially distributed on Golgi membranes from polarized epithelial cells. *The Journal of Cell Biology*, *126*(3), 661–675.

Fededa, J. P., & Gerlich, D. W. (2012). Molecular control of animal cell cytokinesis. *Nature Cell Biology*, *14*(5), 440–447.

Feldman, N., Kosolapov, L., & Ben-Zvi, A. (2014). Fluorodeoxyuridine improves Caenorhabditis elegans proteostasis independent of reproduction onset. *PloS One*, *9*(1).

Fenix, A. M., Taneja, N., Buttler, C. A., Lewis, J., Van Engelenburg, S. B., Ohi, R., & Burnette, D. T. (2016). Expansion and concatenation of nonmuscle myosin IIA filaments drive cellular contractile system formation during interphase and mitosis. *Molecular Biology of the Cell*, *27*(9), 1465–1478.

Field, C. M., & Alberts, B. M. (1995). Anillin, a contractile ring protein that cycles from the nucleus to the cell cortex. *Journal of Cell Biology*, *131*(1), 165–178.

Field, C. M., Coughlin, M., Doberstein, S., Marty, T., & Sullivan, W. (2005). Characterization of anillin mutants reveals essential roles in septin localization and plasma membrane integrity. *Development*, *132*(12), 2849–2860.

Field, C., Li, R., & Oegema, K. (1999). Cytokinesis in eukaryotes: A mechanistic comparison. *Current Opinion in Cell Biology*, *11*(1), 68–80.

Field, S. J., Madson, N., Kerr, M. L., Galbraith, K. A., Kennedy, C. E., Tahiliani, M., Wilkins, A., & Cantley, L. C. (2005). PtdIns (4, 5) P2 functions at the cleavage furrow during cytokinesis. *Current Biology*, *15*(15), 1407–1412.

Fili, N., & Toseland, C. P. (2020). Unconventional myosins: How regulation meets function. *International Journal of Molecular Sciences*, *21*(1), 1–25.

Fili, N., Hari-Gupta, Y., Dos Santos, Á., Cook, A., Poland, S., Ameer-Beg, S. M., Parsons, M., & Toseland, C. P. (2017). NDP52 activates nuclear myosin VI to enhance RNA polymerase II transcription. *Nature Communications*, *8*(1).

Fire, A., Xu, S., Montgomery, M. K., Kostas, S. a, Driver, S. E., & Mello, C. C. (1998). Potent and specific genetic interference by double-stranded RNA in Caenorhabditis elegans. *Nature*, *391*(6669), 806–11.

Fire, A., Albertson, D., Harrison, S. W., & Moerman, D. G. (1991). Production of antisense RNA leads to effective and specific inhibition of gene expression in C. elegans muscle. *Development*, *113*(2), 503–514.

Flemming, W. (1882). *Zellsubstanz, kern und zelltheilung*. Vogel.

Foe, V. E., & von Dassow, G. (2008). Stable and dynamic microtubules coordinately shape the myosin activation zone during cytokinetic furrow formation. *The Journal of Cell Biology*, *183*(3), 457–470.

Forgacs, E., Sakamoto, T., Cartwright, S., Belknap, B., Kovács, M., Tóth, J., Webb, M. R., Sellers, J. R., & White, H. D. (2009). Switch 1 mutation S217A converts myosin V into a low duty ratio motor. *Journal of Biological Chemistry*, *284*(4), 2138–2149.

Foth, B. J., Goedecke, M. C., & Soldati, D. (2006). New insights into myosin evolution and classification. *Proceedings of the National Academy of Sciences*, *103*(10), 3681–3686.

Frank, D. J., Martin, S. R., Gruender, B. N. T., Lee, Y. S. R., Simonette, R. A., Bayley, P. M., Miller, K. G., & Beckingham, K. M. (2006). Androcam is a tissue-specific light chain for myosin VI in the Drosophila testis. *Journal of Biological Chemistry*, *281*(34), 24728–24736.

Friedman, A. L., Geeves, M. A., Manstein, D. J., & Spudich, J. A. (1998). Kinetic Characterization of Myosin Head Fragments with Long-Lived Myosin·ATP States. *Biochemistry*, *37*(27), 9679–9687.

Frøkjær-Jensen, C., Davis, M. W., Ailion, M., & Jorgensen, E. M. (2012). Improved Mos1-mediated transgenesis in C. elegans. *Nature Methods*, *9*(2), 117–118.

Frøkjær-Jensen, C., Davis, M. W., Hopkins, C. E., Newman, B. J., Thummel, J. M., Olesen, S.-P., Grunnet, M., & Jorgensen, E. M. (2008). Single-copy insertion of transgenes in {Caenorhabditis} elegans. *Nature Genetics*, *40*(11), 1375.

Frøkjær-jensen, C., Davis, M. W., Hopkins, C. E., Newman, B., Thummel, J. M., Olesen, S., Grunnet, M., & Jorgensen, E. M. (2009). Single copy insertion of transgenes in C. elegans. *Nature Genetics*, *40*(11), 1375–1383.

Fujii, T., Iwane, A. H., Yanagida, T., & Namba, K. (2010). Direct visualization of secondary structures of F-actin by electron cryomicroscopy. *Nature*, *467*(7316), 724–728.

Fujita-Becker, S., Dürrwang, U., Erent, M., Clark, R. J., Geeves, M. A., & Manstein, D. J. (2005). Changes in Mg2+ ion concentration and heavy chain phosphorylation regulate the motor activity of a class I myosin. *Journal of Biological Chemistry*, *280*(7), 6064–6071.

Fujiwara, K., Porter, M. E., & Pollard, T. D. (1978). Alpha-actinin localization in the cleavage furrow during cytokinesis. *Journal of Cell Biology*, *79*(1), 268–275.

Fujiwara, T., Bandi, M., Nitta, M., Ivanova, E. V., Bronson, R. T., & Pellman, D. (2005). Cytokinesis failure generating tetraploids promotes tumorigenesis in p53 -null cells. *Nature*, *437*(7061),

Fukui, Y., De Lozanne, A., & Spudich, J. A. (1990). Structure and function of the cytoskeleton of a Dictyostelium myosin-defective mutant. *Journal of Cell Biology*, *110*(2), 367–378.

Fukui, Y., Lynch, T. J., Brzeska, H., & Korn, E. D. (1989). Myosin I is located at the leading edges of locomoting Dictyostelium amoebae. *Nature*, *341*(6240), 328–331.

Furch, M., Fujita-Becker, S., Geeves, M. A., Holmes, K. C., & Manstein, D. J. (1999). Role of the salt-bridge between switch-1 and switch-2 of Dictyostelium myosin11Edited by A. R. Fersht. *Journal of Molecular Biology*, *290*(3), 797–809.

Furusawa, T., Ikawa, S., Yanai, N., & Obinata, M. (2000). Isolation of a novel {PDZ}-containing myosin from hematopoietic supportive bone marrow stromal cell lines. *Biochemical and Biophysical Research Communications*, *270*(1), 67–75.

Galganski, L., Urbanek, M. O., & Krzyzosiak, W. J. (2017). Nuclear speckles: Molecular organization, biological function and role in disease. *Nucleic Acids Research*, *45*(18), 10350–10368.

Gallagher, P. J., Garcia, J. G., & Herring, B. P. (1995). Expression of a novel myosin light chain kinase in embryonic tissues and cultured cells. *Journal of Biological Chemistry*, *270*(49), 29090–29095.

Gally, C., Wissler, F., Zahreddine, H., Quintin, S., Landmann, F., & Labouesse, M. (2009). Myosin II regulation during C. elegans embryonic elongation: LET-502/ROCK, MRCK-1 and PAK-1, three kinases with different roles. *Development (Cambridge, England)*, *136*(18), 3109–19.

Ganem, N. J., Storchova, Z., & Pellman, D. (2007). Tetraploidy, aneuploidy and cancer. *Current Opinion in Genetics & Development*, *17*(2), 157–162.

García, J. A., Yee, A. G., Gillespie, P. G., & Corey, D. P. (1998). Localization of myosin-Iβ near both ends of tip links in frog saccular hair cells. *Journal of Neuroscience, 18*(21), 8637-8647.

Gassmann, R., Carvalho, A., Henzing, A. J., Ruchaud, S., Hudson, D. F., Honda, R., Nigg, E. A., Gerloff, D. L., & Earnshaw, W. C. (2004). Borealin: A novel chromosomal passenger required for stability of the bipolar mitotic spindle. *Journal of Cell Biology*, *166*(2), 179–191.

Geisbrecht, E. R., & Montell, D. J. (2002). Myosin VI is required for E-cadherin-mediated border cell migration. *Nature Cell Biology*, *4*(8), 616–620.

Gérard, A., Patino-Lopez, G., Beemiller, P., Nambiar, R., Ben-Aissa, K., Liu, Y., Totah, F. J., Tyska, M. J., Shaw, S., & Krummel, M. F. (2014). Detection of rare antigen-

presenting cells through T cell-intrinsic meandering motility, mediated by Myo1g. *Cell*, *158*(3), 492–505.

Gibbs, D., Azarian, S. M., Lillo, C., Kitamoto, J., Klomp, A. E., Steel, K. P., Libby, R. T., & Williams, D. S. (2004). Role of myosin VIIa and Rab27a in the motility and localization of RPE melanosomes. *Journal of Cell Science*, *117*(26), 6473–6483.

Gibson, D. G., Young, L., Chuang, R., Venter, J. C., Iii, C. A. H., Smith, H. O., & America, N. (2009). Enzymatic assembly of DNA molecules up to several hundred kilobases. *Nature Methods*, *6*(5), 12–17.

Gilden, J., & Krummel, M. F. (2010). Control of cortical rigidity by the cytoskeleton: Emerging roles for septins. *Cytoskeleton*, *67*(8), 477–486.

Gillespie, P. G., Albanesi, J. P., Bähler, M., Bement, W. M., Berg, J. S., Burgess, D. R., Burnside, B., Cheney, R. E., Corey, D. P., & Coudrier, E. (2001). Myosin-I nomenclature. *The Journal of Cell Biology*, *155*(5), 703–704.

Gillespie, P. G., Wagner, M. C., & Hudspeth, A. J. (1993). Identification of a 120 kd hair-bundle myosin located near stereociliary tips. *Neuron*, *11*(4), 581–594.

Glotzer, M. (2001). Animal cell cytokinesis. *Annual Review of Cell and Developmental Biology*, *17*, 351–386.

Glotzer, Michael. (2005). The molecular requirements for cytokinesis. *Science (New York, N.Y.)*, *307*(5716), 1735–1739.

Glotzer, Michael. (2009). The 3Ms of central spindle assembly: Microtubules, motors and MAPs. *Nature Reviews Molecular Cell Biology*, *10*(1), 9–20.

Goldbach, P., Wong, R., Beise, N., Sarpal, R., Trimble, W. S., & Brill, J. A. (2010). Stabilization of the Actomyosin Ring Enables Spermatocyte Cytokinesis in Drosophila. *Molecular Biology of the Cell*, *21*(9), 1482–1493.

Golomb, E., Ma, X., Jana, S. S., Preston, Y. A., Kawamoto, S., Shoham, N. G., Goldin, E., Conti, M. A., Sellers, J. R., & Adelstein, R. S. (2004). Identification and Characterization of Nonmuscle Myosin II-C, a New Member of the Myosin II Family. *Journal of Biological Chemistry*, *279*(4), 2800–2808.

Goode, B. L., & Eck, M. J. (2007). Mechanism and function of formins in the control of actin assembly. *Annual Review of Biochemistry*, *76*, 593–627.

Goodson, H. V., & Spudich, J. A. (1995). Identification and molecular characterization of a yeast myosin I. *Cell Motility and the Cytoskeleton*, *30*(1), 73–84.

Goodson, Holly V, Andersen, B. L., Warrick, H. M., Pon, L. A., & Spudich, J. A. (1996). Synthetic lethality screen identifies a novel yeast myosin I gene MYO5: Myosin I proteins are required for polarization of the actin cytoskeleton. *Journal of Cell Biology*, *133*(6), 1277–1291.

Gorman, S. W., Haider, N. B., Grieshammer, U., Swiderski, R. E., Kim, E., Welch, J. W., Searby, C., Leng, S., Carmi, R., & Sheffield, V. C. (1999). The cloning and developmental expression of unconventional myosin IXA (MYO9A) a gene in the Bardet–Biedl syndrome (BBS4) region at chromosome 15q22–q23. *Genomics*, *59*(2), 150–160.

Gottschalk, A., Almedom, R. B., Schedletzky, T., Anderson, S. D., Yates, J. R., & Schafer, W. R. (2005). Identification and characterization of novel nicotinic receptor-associated proteins in Caenorhabditis elegans. *EMBO Journal*, *24*(14), 2566–2578.

Govindan, B., Bowser, R., & Novick, P. (1995). The role of Myo2, a yeast class V myosin, in vesicular transport. *The Journal of Cell Biology*, *128*(6), 1055–1068.

Graf, B., Bähler, M., Hilpelä, P., Böwe, C., & Adam, T. (2000). Functional role for the class IX myosin myr5 in epithelial cell infection by Shigella flexneri. *Cellular Microbiology*, *2*(6), 601–616.

Grana, T. M., Cox, E. A., Lynch, A. M., & Hardin, J. (2010). SAX-7/L1CAM and HMR-1/cadherin function redundantly in blastomere compaction and non-muscle myosin accumulation during Caenorhabditis elegans gastrulation. *Developmental Biology*, *344*(2), 731–744.

Green, R. A-, Paluch, E., & Oegema, K. (2012). Cytokinesis in animal cells. *Annual Review of Cell and Developmental Biology*, *28*, 29–58.

Green, R. A., Kao, H. L., Audhya, A., Arur, S., Mayers, J. R., Fridolfsson, H. N., Schulman, M., Schloissnig, S., Niessen, S., Laband, K., Wang, S., Starr, D. A., Hyman, A. A., Schedl, T., Desai, A., Piano, F., Gunsalus, K. C., & Oegema, K. (2011). A high-

resolution C. elegans essential gene network based on phenotypic profiling of a complex tissue. *Cell*, *145*(3), 470–482.

Green, R. A., Mayers, J. R., Wang, S., Lewellyn, L., Desai, A., Audhya, A., & Oegema, K. (2013). The midbody ring scaffolds the abscission machinery in the absence of midbody microtubules. *Journal of Cell Biology, 203*(3), 505-520.

Grosse-Berkenbusch, A., Hettich, J., Kuhn, T., Fili, N., Cook, A. W., Hari-Gupta, Y., Palmer, A., Streit, L., Ellis, P. J. I., & Toseland, C. (2020). Myosin VI moves on nuclear actin filaments and supports long-range chromatin rearrangements. *BioRxiv*.

Guertin, D. A., Trautmann, S., & McCollum, D. (2002). Cytokinesis in eukaryotes. *Microbiology and Molecular Biology Reviews, 66*(2), 155-178.

Guha, M., Zhou, M., & Wang, Y. (2005). Cortical Actin Turnover during Cytokinesis Requires Myosin II. *Current Biology*, *15*(8), 732–736. https://doi.org/10.1016/j.cub.2005.03.042

Guo, B., & Guilford, W. H. (2006). Mechanics of actomyosin bonds in different nucleotide states are tuned to muscle contraction. *Proceedings of the National Academy of Sciences*, *103*(26), 9844–9849.

Guo, S., & Kemphues, K. J. (1996). A non-muscle myosin required for embryonic polarity in Caenorhabditis elegans. *Nature*, *382*(6590), 455–458.

Gupta, P., Gauthier, N. C., Cheng-Han, Y., Zuanning, Y., Pontes, B., Ohmstede, M., Martin, R., Knölker, H.-J., Döbereiner, H.-G., & Krendel, M. (2013). Myosin 1E localizes to actin polymerization sites in lamellipodia, affecting actin dynamics and adhesion formation. *Biology Open*, *2*(12), 1288–1299.

Haldeman, B. D., Brizendine, R. K., Facemyer, K. C., Baker, J. E., & Cremo, C. R. (2014). The kinetics underlying the velocity of smooth muscle myosin filament sliding on actin filaments in vitro. *Journal of Biological Chemistry, 289*(30), 21055-21070.

Halsall, D. J., & Hammer, J. A. (1990). A second isoform of chicken brush border myosin I contains a 29-residue inserted sequence that binds calmodulin. *FEBS Letters*, *267*(1), 126–130.

Hammer, J. A., Jung, G., & Korn, E. D. (1986). Genetic evidence that Acanthamoeba myosin I is a true myosin. *Proceedings of the National Academy of Sciences of the United States of America*, *83*(13), 4655–4659.

Hammer, John A. (1991). Novel myosins. *Trends in Cell Biology*, *1*(2), 50–56.

Hanakam, F., Albrecht, R., Eckerskorn, C., Matzner, M., & Gerisch, G. (1996). Myristoylated and non ‐myristoylated forms of the {pH} sensor protein hisactophilin {II}: Intracellular shuttling to plasma membrane and nucleus monitored in real time by a fusion with green fluorescent protein. *The EMBO Journal*, *15*(12), 2935–2943.

Hasson, H. M., & Lakatos, N. (1998). *Sealing structure for medical instrument*. Google Patents.

Hasson, T., Gillespie, P. G., Garcia, J. A., MacDonald, R. B., Zhao, Y., Yee, A. G., Mooseker, M. S., & Corey, D. P. (1997). Unconventional myosins in inner-ear sensory epithelia. *The Journal of Cell Biology*, *137*(6), 1287–1307.

Hasson, Tama, & Mooseker, M. S. (1994). Porcine myosin-VI: characterization of a new mammalian unconventional myosin. *The Journal of Cell Biology*, *127*(2), 425–440.

Hasson, Tama, & Mooseker, M. S. (1996). Vertebrate unconventional myosins. *Journal of Biological Chemistry*, *271*(28), 16431–16434.

Hasson, Tama, Heintzelman, M. B., Santos-Sacchi, J., Corey, D. P., & Mooseker, M. S. (1995). Expression in cochlea and retina of myosin VIIa, the gene product defective in Usher syndrome type 1B. *Proceedings of the National Academy of Sciences*, *92*(21), 9815–9819.

Haviv, L., Gillo, D., Backouche, F., & Bernheim-Groswasser, A. (2008). A cytoskeletal demolition worker: Myosin II acts as an actin depolymerization agent. *Journal of Molecular Biology*, *375*(2), 325–330.

Heer, N. C., & Martin, A. C. (2017). Tension, contraction and tissue morphogenesis. *Development*, *144*(23), 4249–4260.

Hegan, P. S., Ostertag, E., Geurts, A. M., & Mooseker, M. S. (2015). Myosin Id is required for planar cell polarity in ciliated tracheal and ependymal epithelial cells. *Cytoskeleton*, *72*(10), 503–516.

Heissler, S. M., & Manstein, D. J. (2011). Comparative kinetic and functional characterization of the motor domains of human nonmuscle myosin-2C isoforms. *Journal of Biological Chemistry*, *286*(24), 21191–21202.

Heissler, S. M., & Manstein, D. J. (2012). Functional characterization of the human myosin-7a motor domain. *Cellular and Molecular Life Sciences*, *69*(2), 299–311.

Heissler, S. M., & Sellers, J. R. (2015). Four things to know about myosin light chains as reporters for non-muscle myosin-2 dynamics in live cells. *Cytoskeleton*, *72*(2), 65–70.

Heissler, S. M., & Sellers, J. R. (2016). Kinetic adaptations of myosins for their diverse cellular functions. *Traffic*, *17*(8), 839–859.

Heissler, S., Billington, N., Ma, X., Adelstein, R., & Sellers, J. (2018). Tools to study nonmuscle myosin-2 motor function revisited. *Biophysical Journal*, *114*(3), 318a.

Henson, J. H., Ditzler, C. E., Germain, A., Irwin, P. M., Vogt, E. T., Yang, S., Wu, X., & Shuster, C. B. (2017). The ultrastructural organization of actin and myosin II filaments in the contractile ring: New support for an old model of cytokinesis. *Molecular Biology of the Cell*, *28*(5), 613–623.

Hernandez, O. M., Jones, M., Guzman, G., & Szczesna-Cordary, D. (2007). Myosin essential light chain in health and disease. *American Journal of Physiology - Heart and Circulatory Physiology*, *292*(4).

Hicks, J. L., Deng, W. M., Rogat, A. D., Miller, K. G., & Bownes, M. (1999). Class VI unconventional myosin is required for spermatogenesis in Drosophila. *Molecular Biology of the Cell*, *10*(12), 4341–4353.

Hickson, G. R. X., & O'Farrell, P. H. (2008). Rho-dependent control of anillin behavior during cytokinesis. *Journal of Cell Biology*, *180*(2), 285–294.

Hodge, T., & Cope, M. J. T. V. (2000). A myosin family tree. *Journal of Cell Science*, *113*(19), 3353–3354.

Hokanson, D. E., & Ostap, E. M. (2006). Myo1c binds tightly and specifically to phosphatidylinositol 4,5-bisphosphate and inositol 1,4,5-trisphosphate. *Proceedings of the National Academy of Sciences*, *103*(9), 3118–3123.

Holmes, K. C., Popp, D., Gebhard, W., & Kabsch, W. (1990). Atomic model of the actin filament. *Nature*, *347*(6288), 44–49.

Honda, R., Körner, R., & Nigg, E. A. (2003). Exploring the functional interactions between Aurora B, INCENP, and survivin in mitosis. *Molecular Biology of the Cell*, *14*(8), 3325–3341.

Hosoba, K., Komatsu, S., Ikebe, M., Kotani, M., Wenqin, X., Tachibana, T., Hosoya, H., & Hamao, K. (2015). Phosphorylation of myosin II regulatory light chain by ZIP kinase is responsible for cleavage furrow ingression during cell division in mammalian cultured cells. *Biochemical and Biophysical Research Communications*, *459*(4), 686–691.

Houdusse, A., Kalabokis, V. N., Himmel, D., Szent-Györgyi, A. G., & Cohen, C. (1999). Atomic Structure of Scallop Myosin Subfragment S1 Complexed with MgADP: A Novel Conformation of the Myosin Head. *Cell*, *97*(4), 459–470.

Hsu, P. D., Lander, E. S., & Zhang, F. (2014). Development and applications of CRISPR-Cas9 for genome engineering. *Cell*, *157*(6), 1262–1278.

Hu, A., Wang, F., & Sellers, J. R. (2002). Mutations in human nonmuscle myosin IIA found in patients with May-Hegglin anomaly and Fechtner syndrome result in impaired enzymatic function. *Journal of Biological Chemistry*, *277*(48), 46512–46517.

Hu, J., Cheng, S., Wang, H., Li, X., Liu, S., Wu, M., Liu, Y., & Wang, X. (2019). Distinct roles of two myosins in C. Elegans spermatid differentiation. In *PLoS Biology* (Vol. 17).

Huxley, A. F., & Niedergerke, R. (1954). Structural changes in muscle during contraction: Interference microscopy of living muscle fibres. *Nature*, *173*(4412), 971–973.

Huxley, H. E. (1969). The mechanism of muscular contraction. *Science*, *164*(3886), 1356–1366.

Huxley, H., & Hanson, J. (1954). Changes in the cross-striations of muscle during contraction and stretch and their structural interpretation. *Nature*, *173*(4412), 973–976.

Hwang, H., Barnes, D. E., Matsunaga, Y., Benian, G. M., Ono, S., & Lu, H. (2016). Muscle contraction phenotypic analysis enabled by optogenetics reveals functional

relationships of sarcomere components in Caenorhabditis elegans. *Scientific Reports*, *6*, 19900.

Ikebe, M, & Hartshorne, D. J. (1985). Phosphorylation of smooth muscle myosin at two distinct sites by myosin light chain kinase. *Journal of Biological Chemistry*, *260*(18), 10027–10031.

Ikebe, Mitsuo. (1989). Phosphorylation of a second site for myosin light chain kinase on platelet myosin. *Biochemistry*, *28*(22), 8750–8755.

Ikonen, E., de Almeid, J. B., Fath, K. R., Burgess, D. R., Ashman, K., Simons, K., & Stow, J. L. (1997). Myosin II is associated with Golgi membranes: identification of p200 as nonmuscle myosin II on Golgi-derived vesicles. *Journal of cell science, 110*(18), 2155-2164.

Inoue, A., & Ikebe, M. (2003). Characterization of the motor activity of mammalian myosin VIIA. *Journal of Biological Chemistry*, *278*(7), 5478–5487.

Inoue, A., Saito, J., Ikebe, R., & Ikebe, M. (2002). Myosin IXb is a single-headed minus-end-directed processive motor. *Nature Cell Biology*, *4*(4), 302–306.

Itoh, S., Umemoto, S., Hiromoto, M., Toma, Y., Tomochika, Y., Aoyagi, S., Tanaka, M., Fujii, T., & Matsuzaki, M. (2002). Importance of NAD (P) H oxidase–mediated oxidative stress and contractile type smooth muscle myosin heavy chain SM2 at the early stage of atherosclerosis. *Circulation*, *105*(19), 2288–2295.

Ivarsson, R., Jing, X., Waselle, L., Regazzi, R., & Renström, E. (2005). Myosin 5a controls insulin granule recruitment during late phase secretion. *Traffic*, *6*(11), 1027–1035.

Iwaki, M., Tanaka, H., Iwane, A. H., Katayama, E., Ikebe, M., & Yanagida, T. (2006). Cargo-binding makes a wild-type single-headed myosin-VI move processively. *Biophysical Journal*, *90*(10), 3643–3652.

Jana, S. S., Kawamoto, S., & Adelstein, R. S. (2006). A Specific Isoform of Nonmuscle Myosin II-C Is Required for Cytokinesis in a Tumor Cell Line. *Journal of Biological Chemistry*, *281*(34), 24662–24670.

Jantsch-Plunger, V., Gönczy, P., Romano, A., Schnabel, H., Hamill, D., Schnabel, R., Hyman, A. A., & Glotzer, M. (2000). CYK-4: A Rho family GTPase activating protein

(GAP) required for central spindle formation and cytokinesis. *Journal of Cell Biology*, *149*(7), 1391–1404.

Jiao, M., Wu, D., & Wei, Q. (2018). Myosin II–interacting guanine nucleotide exchange factor promotes bleb retraction via stimulating cortex reassembly at the bleb membrane. *Molecular Biology of the Cell*, *29*(5), 643–656.

Jin, M., Li, S., Moghrabi, W. N., Sun, H., & Travis, G. H. (2005). Rpe65 is the retinoid isomerase in bovine retinal pigment epithelium. *Cell*, *122*(3), 449–459.

Jiu, Y., Kumari, R., Fenix, A. M., Schaible, N., Liu, X., Varjosalo, M., Krishnan, R., Burnette, D. T., & Lappalainen, P. (2019). Myosin-18B Promotes the Assembly of Myosin II Stacks for Maturation of Contractile Actomyosin Bundles. *Current Biology*, *29*(1), 81–92.e5.

Johnston, G. C., Prendergast, J. A., & Singer, R. A. (1991). The Saccharomyces cerevisiae MYO2 gene encodes an essential myosin for vectorial transport of vesicles. *The Journal of Cell Biology*, *113*(3), 539–551.

Jordan, P., & Karess, R. (1997). Myosin light chain-activating phosphorylation sites are required for oogenesis in Drosophila. *Journal of Cell Biology*, *139*(7), 1805–1819.

Joseph, J. D., & Means, A. R. (2002). Calcium binding is required for calmodulin function in Aspergillus nidulans. *Eukaryotic Cell*, *1*(1), 119–125.

Jung, G, Korn, E. D., & Hammer, J. A. (1987). The heavy chain of Acanthamoeba myosin IB is a fusion of myosin-like and non-myosin-like sequences. *Proceedings of the National Academy of Sciences of the United States of America*, *84*(19), 6720–6724.

Jung, G., & Hammer, J. A. (1994). The actin binding site in the tail domain of Dictyostelium myosin IC (myoC) resides within the glycine- and proline-rich sequence (tail homology region 2). *FEBS Letters*, *342*(2), 197–202.

Jung, Goeh, Schmidt, C. J., & Hammer, J. A. (1989). Myosin I heavy-chain genes of Acanthamoeba castellanii: Cloning of a second gene and evidence for the existence of a third isoform. *Gene*, *82*(2), 269–280.

Jung, Goeh, Titus, M. A., & Hammer, J. A. (2009). The Dictyostelium type V myosin MyoJ is responsible for the cortical association and motility of contractile vacuole membranes. *Journal of Cell Biology*, *186*(4), 555–570.

Kachur, T. M., Audhya, A., & Pilgrim, D. B. (2008). UNC-45 is required for NMY-2 contractile function in early embryonic polarity establishment and germline cellularization in C. elegans. *Developmental Biology*, *314*(2), 287–99.

Kaletta, T., & Hengartner, M. O. (2006). Finding function in novel targets: C. elegans as a model organism. *Nature Reviews Drug Discovery*, *5*(5), 387–399.

Kamasaki, T., Osumi, M., & Mabuchi, I. (2007). Three-dimensional arrangement of F-actin in the contractile ring of fission yeast. *The Journal of Cell Biology*, *178*(5), 765–771.

Kamath, R. (2003). Genome-wide RNAi screening in Caenorhabditis elegans. *Methods*, *30*(4), 313–321.

Kambara, T., & Ikebe, M. (2006). A unique ATP hydrolysis mechanism of single-headed processive myosin, myosin IX. *Journal of Biological Chemistry*, *281*(8), 4949–4957.

Kanada, M., Nagasaki, A., & Uyeda, T. Q. (2005). Adhesion-dependent and contractile ring-independent equatorial furrowing during cytokinesis in mammalian cells. *Molecular Biology of the Cell*, *16*(8), 3865–3872.

Karess, R. E., Chang, X., Edwards, K. A., Kulkarni, S., Aguilera, I., & Kiehartt, D. P. (1991). *The Regulatory Light Chain of Nonmuscle Myosin Is Encoded by spagheWsquash , a Gene Required for Cytokinesis in Drosophila*. *65*.

Kawano, Y., Fukata, Y., Oshiro, N., Amano, M., Nakamura, T., Ito, M., Matsumura, F., Inagaki, M., & Kaibuchi, K. (1999). Phosphorylation of Myosin-Binding Subunit (Mbs) of Myosin Phosphatase by Rho-Kinase in Vivo. *Journal of Cell Biology*, *147*(5), 1023–1038.

Kechad, A., Jananji, S., Ruella, Y., & Hickson, G. R. X. (2012). Anillin Acts as a Bifunctional Linker Coordinating Midbody Ring Biogenesis during Cytokinesis. *Current Biology*, *22*(3), 197–203.

Kelleher, J. F., Mandell, M. A., Moulder, G., Hill, K. L., L'Hernault, S. W., Barstead, R., & Titus, M. A. (2000). Myosin VI is required for asymmetric segregation of cellular

components during C. elegans spermatogenesis. *Current Biology*, *10*(23), 1489–1496.

Kellerman, K. A., & Miller, K. G. (1992). An unconventional myosin heavy chain gene from Drosophila melanogaster. *The Journal of Cell Biology*, *119*(4), 823–834.

Khaliullin, R. N., Green, R. A., Shi, L. Z., Gomez-Cavazos, J. S., Berns, M. W., Desai, A., & Oegema, K. (2018). A positive-feedback-based mechanism for constriction rate acceleration during cytokinesis in Caenorhabditis elegans. *Elife*, *7*, e36073.

Khandekar, S. S., Yi, T., Dul, E., Wrigh, L. L., Chen, S., Scott, G. F., Smith, G. K., Lee, D., Hu, E., & Kirkpatrick, R. B. (2006). Expression, purification, and characterization of an enzymatically active truncated human rho-kinase I (ROCK I) domain expressed in Sf-9 insect cells. *Protein and Peptide Letters*, *13*(4), 369–376.

Kiehart, D. P., Lutz, M. S., Chan, D., Ketchum, A. S., Laymon, R. A., Nguyen, B., & Goldstein, L. S. (1989). Identification of the gene for fly non-muscle myosin heavy chain: Drosophila myosin heavy chains are encoded by a gene family. *The EMBO Journal*, *8*(3), 913–922.

Kiehart, Daniel P., Franke, J. D., Chee, M. K., Montague, R. A., Chen, T. L., Roote, J., & Ashburner, M. (2004). Drosophila crinkled, mutations of which disrupt morphogenesis and cause lethality, encodes fly myosin VIIA. *Genetics*, *168*(3), 1337–1352.

Kim, H., Johnson, J. M., Lera, R. F., Brahma, S., & Burkard, M. E. (2017). Anillin Phosphorylation Controls Timely Membrane Association and Successful Cytokinesis. *PLoS Genetics*, *13*(1), 1–20.

Kim, S. V., Mehal, W. Z., Dong, X., Heinrich, V., Pypaert, M., Mellman, I., Dembo, M., Mooseker, M. S., Wu, D., & Flavell, R. A. (2006). Modulation of cell adhesion and motility in the immune system by Myo1f. *Science (New York, N.Y.)*, *314*(5796), 136–139.

Kim, S., Spike, C., & Greenstein, D. (2013). Control of oocyte growth and meiotic maturation in Caenorhabditis elegans. *Advances in Experimental Medicine and Biology*, *757*, 277–320.

Kim, W., Underwood, R. S., Greenwald, I., & Shaye, D. D. (2018). Ortholist 2: {A} new comparative genomic analysis of human and caenorhabditis elegans genes. *Genetics*, *210*(2), 445–461.

Kimura, K., Ito, M., Amano, M., Chihara, K., Fukata, Y., Nakafuku, M., Yamamori, B., Feng, J., Nakano, T., Okawa, K., Iwamatsu, A., & Kaibuchi, K. (1996). Regulation of Myosin Phosphatase by Rho and Rho-Associated Kinase (Rho-Kinase). *Science*, *273*(5272), 245–248.

Kimura, K., Tsuji, T., Takada, Y., Miki, T., & Narumiya, S. (2000). Accumulation of GTP-bound RhoA during cytokinesis and a critical role of ECT2 in this accumulation*. Journal of Biological Chemistry, 275*(23), 17233-17236.

Kinoshita, M., Kumar, S., Mizoguchi, A., Ide, C., Kinoshita, A., Haraguchi, T., Hiraoka, Y., & Noda, M. (1997). Nedd5, a mammalian septin, is a novel cytoskeletal component interacting with actin-based structures. *Genes & Development*, *11*(12), 1535–1547.

Kinoshita, Makoto, Field, C. M., Coughlin, M. L., Straight, A. F., & Mitchison, T. J. (2002). Self- and Actin-Templated Assembly of Mammalian Septins. *Developmental Cell*, *3*(6), 791–802.

Kirkham, M., Müller-Reichert, T., Oegema, K., Grill, S., & Hyman, A. A. (2003). SAS-4 is a C. elegans centriolar protein that controls centrosome size. *Cell*, *112*(4), 575–587.

Kitayama, C., Sugimoto, A., & Yamamoto, M. (1997). Type II myosin heavy chain encoded by the myo2 gene composes the contractile ring during cytokinesis in Schizosaccharomyces pombe. *The Journal of Cell Biology*, *137*(6), 1309–1319.

Kittelberger, N., Breunig, M., Martin, R., Knölker, H.-J., & Miklavc, P. (2016). The role of myosin 1c and myosin 1b in surfactant exocytosis. *Journal of Cell Science*, *129*(8), 1685–1696.

Kodera, N., & Ando, T. (2014). The path to visualization of walking myosin V by high-speed atomic force microscopy. *Biophysical Reviews*, *6*(3–4), 237–260.

Koe, C. T., Tan, Y. S., Lönnfors, M., Hur, S. K., Low, C. S. L., Zhang, Y., ... & Wang, H. (2018). Vibrator and PI4KIIIα govern neuroblast polarity by anchoring non-muscle myosin II. *Elife*, 7, e33555.

Köhler, D., Ruff, C., Meyhöfer, E., & Bähler, M. (2003). Different degrees of lever arm rotation control myosin step size. *The Journal of Cell Biology*, *161*(2), 237–241.

Kollmar, M. (2006). Thirteen is enough: the myosins of Dictyostelium discoideum and their light chains. *BMC genomics, 7*(1), 183.

Komaba, S., & Coluccio, L. M. (2015). Myosin 1b Regulates Amino Acid Transport by Associating Transporters with the Apical Plasma Membrane of Kidney Cells. *PloS One*, *10*(9), e0138012.

Kosako, H., Yoshida, T., Matsumura, F., Ishizaki, T., Narumiya, S., & Inagaki, M. (2000). Rho-kinase/ROCK is involved in cytokinesis through the phosphorylation of myosin light chain and not ezrin/radixin/moesin proteins at the cleavage furrow. *Oncogene*, *19*(52), 6059–6064.

Kovacevic, I., Orozco, J. M., & Cram, E. J. (2013). Filamin and phospholipase C-ε are required for calcium signaling in the Caenorhabditis elegans spermatheca. *PLoS Genetics*, *9*(5),

Kovács, M., Wang, F., Hu, A., Zhang, Y., & Sellers, J. R. (2003). Functional Divergence of Human Cytoplasmic Myosin II kinetic characterization of the non-muscle IIa isoform. *Journal of Biological Chemistry*, *278*(40), 38132–38140.

Kovar, D. R., Kuhn, J. R., Tichy, A. L., & Pollard, T. D. (2003). The fission yeast cytokinesis formin Cdc12p is a barbed end actin filament capping protein gated by profilin. *The Journal of Cell Biology*, *161*(5), 875–887.

Krendel, M., & Mooseker, M. S. (2005). Myosins: {Tails} (and {Heads}) of {Myosin} {Superfamily}: {Diversity} of. *Physiology*, *20*(20), 239–251.

Krendel, M., Osterweil, E. K., & Mooseker, M. S. (2007). Myosin 1E interacts with synaptojanin-1 and dynamin and is involved in endocytosis. *FEBS Letters*, *581*(4), 644–650.

Kühne, W. (1859). Untersuchungen über Bewegungen und Veränderung der contractilen Substanzen. *Archiv Für Anatomie, Physiologie Und Wissenschaftliche Medicin.*, 748–835.

Kurasawa, Y., Earnshaw, W. C., Mochizuki, Y., Dohmae, N., & Todokoro, K. (2004). Essential roles of KIF4 and its binding partner PRC1 in organized central spindle midzone formation. *The EMBO Journal*, *23*(16), 3237–3248.

Kussel-Andermann, P. (2000). Vezatin, a novel transmembrane protein, bridges myosin {VIIA} to the cadherin-catenins complex. *The EMBO Journal*, *19*(22), 6020–6029.

Kwon, T. J., Oh, S. K., Park, H. J., Sato, O., Venselaar, H., Choi, S. Y., Kim, S. H., Lee, K. Y., Bok, J., Lee, S. H., Vriend, G., Ikebe, M., Kim, U. K., & Choi, J. Y. (2014). The effect of novel mutations on the structure and enzymatic activity of unconventional myosins associated with autosomal dominant non-syndromic hearing loss. *Open Biology*, *4*(JULY).

Kyselá, K., Philimonenko, A. A., Philimonenko, V. V., Janácek, J., Kahle, M., & Hozák, P. (2005). Nuclear distribution of actin and myosin I depends on transcriptional activity of the cell. *Histochemistry and Cell Biology*, *124*(5), 347–358.

L'Hernault, S. W., Shakes, D. C., & Ward, S. (1988). Developmental genetics of chromosome I spermatogenesis-defective mutants in the nematode Caenorhabditis elegans. *Genetics*, *120*(2), 435–452.

Lalli, G., Gschmeissner, S., & Schiavo, G. (2003). Myosin Va and microtubule-based motors are required for fast axonal retrograde transport of tetanus toxin in motor neurons. *Journal of Cell Science*, *116*(22), 4639–4650.

Lapierre, L. A., Kumar, R., Hales, C. M., Navarre, J., Bhartur, S. G., Burnette, J. O., Provance Jr, D. W., Mercer, J. A., Bähler, M., & Goldenring, J. R. (2001). Myosin vb is associated with plasma membrane recycling systems. *Molecular Biology of the Cell*, *12*(6), 1843–1857.

Laplante, C., & Pollard, T. D. (2017). Response to Zambon et al. *Current Biology*, *27*(3), R101—-R102.

Laplante, C., Berro, J., Karatekin, E., Hernandez-Leyva, A., Lee, R., & Pollard, T. D. (2015). Three Myosins Contribute Uniquely to the Assembly and Constriction of the Fission Yeast Cytokinetic Contractile Ring. *Current Biology*, *25*(15), 1955–1965.

Laplante, C., Huang, F., Tebbs, I. R., Bewersdorf, J., & Pollard, T. D. (2016). Molecular organization of cytokinesis nodes and contractile rings by super-resolution

fluorescence microscopy of live fission yeast. *Proceedings of the National Academy of Sciences of the United States of America*, *113*(40), E5876—-E5885.

Laporte, D., Coffman, V. C., Lee, I. J., & Wu, J. Q. (2011). Assembly and architecture of precursor nodes during fission yeast cytokinesis. *Journal of Cell Biology*, *192*(6), 1005–1021.

Lappalainen, P., & Drubin, D. G. (1997). Cofilin promotes rapid actin filament turnover in vivo. *Nature*, *389*(6647), 211–211.

Lardennois, A., Pásti, G., Ferraro, T., Llense, F., Mahou, P., Pontabry, J., Rodriguez, D., Kim, S., Ono, S., & Beaurepaire, E. (2019). An actin-based viscoplastic lock ensures progressive body-axis elongation. *Nature*, *573*(7773), 266–270.

Larson, R. E., Espindola, F. S., & Espreafico, E. M. (1990). Calmodulin binding proteins and calcium/calmodulin regulated enzyme activities associated with brain actomyosin. *Journal of Neurochemistry*, *54*(4), 1288–1294.

Leal, A., Endele, S., Stengel, C., Huehne, K., Loetterle, J., Barrantes, R., Winterpacht, A., & Rautenstrauss, B. (2003). A novel myosin heavy chain gene in human chromosome 19q13.3. *Gene*, *312*(0), 165–171.

Lee, J., Spector, D., Godon, C., Labarre, J., & Toledano, M. B. (1999). A new antioxidant with alkyl hydroperoxide defense properties in yeast. *The Journal of Biological Chemistry*, *274*(8), 4537–4544.

Lee, S. F., & Côté, G. P. (1993). Isolation and characterization of three Dictyostelium myosin-I isozymes. *Journal of Biological Chemistry*, *268*(28), 20923–20929.

Lee, W. L., Ostap, E. M., Zot, H. G., & Pollard, T. D. (1999). Organization and ligand binding properties of the tail of Acanthamoeba myosin-IA. Identification of an actin-binding site in the basic (tail homology-1) domain. *The Journal of Biological Chemistry*, *274*(49), 35159–35171.

Lee, Y.-R. J., & Liu, B. (2004). Cytoskeletal motors in Arabidopsis. Sixty-one kinesins and seventeen myosins. *Plant Physiology*, *136*(4), 3877–3883.

Lemmon, M. A. (2008). Membrane recognition by phospholipid-binding domains. *Nature Reviews Molecular Cell Biology*, *9*(2), 99–111.

Lenz, M., Thoresen, T., Gardel, M. L., & Dinner, A. R. (2012). Contractile units in disordered actomyosin bundles arise from F-actin buckling. *Physical Review Letters*, *108*(23), 238107.

Levy, A. D., Yang, J., & Kramer, J. M. (1993). Molecular and genetic analyses of the Caenorhabditis elegans dpy-2 and dpy-10 collagen genes: A variety of molecular alterations affect organismal morphology. *Molecular Biology of the Cell*, *4*(8), 803–817.

Lewellyn, L., Dumont, J., Desai, A., & Oegema, K. (2010). Analyzing the effects of delaying aster separation on furrow formation during cytokinesis in the Caenorhabditis elegans embryo. *Molecular Biology of The Cell, 21*(1), 50-62.

Li, G., & Cui, Q. (2004). Mechanochemical coupling in myosin: A theoretical analysis with molecular dynamics and combined QM/MM reaction path calculations. *The Journal of Physical Chemistry B*, *108*(10), 3342–3357.

Li, X., Ikebe, R., & Ikebe, M. (2005). Activation of myosin Va function by melanophilin, a specific docking partner of myosin Va. *Journal of Biological Chemistry*, *280*(18), 17815–17822.

Li, X., Rhodes, T. E., Ikebe, R., Kambara, T., White, H. D., & Ikebe, M. (1998). Effects of mutations in the γ-phosphate binding site of myosin on its motor function. *Journal of Biological Chemistry*, *273*(42), 27404–27411.

Li, Y. R., & Yang, W. X. (2016). Myosins as fundamental components during tumorigenesis: {Diverse} and indispensable. *Oncotarget*, *7*(29), 46785–46812.

Liao, W., Elfrink, K., & Bähler, M. (2010). Head of myosin IX binds calmodulin and moves processively toward the plus-end of actin filaments. *Journal of Biological Chemistry*, *285*(32), 24933–24942.

Libby, R. T., & Steel, K. P. (2001). Electroretinographic anomalies in mice with mutations in Myo7a, the gene involved in human Usher syndrome type 1B. *Investigative Ophthalmology & Visual Science*, *42*(3), 770–778.

Lin, T., Tang, N., & Ostap, E. M. (2005). Biochemical and motile properties of Myo1b splice isoforms. *The Journal of Biological Chemistry*, *280*(50), 41562–41567.

Lindsay, A. J., & McCaffrey, M. W. (2009). Myosin Vb localises to nucleoli and associates with the RNA polymerase I transcription complex. *Cell Motility and the Cytoskeleton*, *66*(12), 1057–1072.

Lipatova, Z., Tokarev, A. A., Jin, Y., Mulholland, J., Weisman, L. S., & Segev, N. (2008). Direct interaction between a myosin V motor and the Rab GTPases Ypt31/32 is required for polarized secretion. *Molecular Biology of the Cell*, *19*(10), 4177–4187.

Liu, Ji, Maduzia, L. L., Shirayama, M., & Mello, C. C. (2010). NMY-2 maintains cellular asymmetry and cell boundaries, and promotes a SRC-dependent asymmetric cell division. *Developmental Biology*, *339*(2), 366–373.

Liu, Jinghe, Fairn, G. D., Ceccarelli, D. F., Sicheri, F., & Wilde, A. (2012). Cleavage furrow organization requires PIP 2-mediated recruitment of anillin. *Current Biology*, *22*(1), 64–69.

Liu, S. L., Fewkes, N., Ricketson, D., Penkert, R. R., & Prehoda, K. E. (2008). Filament-dependent and -independent localization modes of Drosophila non-muscle myosin II. *Journal of Biological Chemistry*, *283*(1), 380–387.

Liu, X., Shu, S., Billington, N., Williamson, C. D., Yu, S., Brzeska, H., Donaldson, J. G., Sellers, J. R., & Korn, E. D. (2016). Mammalian nonmuscle myosin II binds to anionic phospholipids with concomitant dissociation of the regulatory light chain. *Journal of Biological Chemistry*, *291*(48), 24828–24837.

Liu, X., Udovichenko, I. P., Brown, S. D., Steel, K. P., & Williams, D. S. (1999). Myosin VIIa participates in opsin transport through the photoreceptor cilium. *Journal of Neuroscience, 19*(15), 6267-6274.

Liu, Y.-J., Le Berre, M., Lautenschlaeger, F., Maiuri, P., Callan-Jones, A., Heuzé, M., Takaki, T., Voituriez, R., & Piel, M. (2015). Confinement and low adhesion induce fast amoeboid migration of slow mesenchymal cells. *Cell*, *160*(4), 659–672.

Loison, O., Weitkunat, M., Kaya-Çopur, A., Alves, C. N., Matzat, T., Spletter, M. L., Luschnig, S., Brasselet, S., Lenne, P.-F., & Schnorrer, F. (2018). Polarization-resolved microscopy reveals a muscle myosin motor-independent mechanism of molecular actin ordering during sarcomere maturation. *PLoS Biology*, *16*(4), e2004718.

López-Ortega, O., Ovalle-García, E., Ortega-Blake, I., Antillón, A., Chávez-Munguía, B., Patiño-López, G., Fragoso-Soriano, R., & Santos-Argumedo, L. (2016). Myo1g is an active player in maintaining cell stiffness in B-lymphocytes. *Cytoskeleton (Hoboken, N.J.)*, *73*(5), 258–268.

Lord, M., Laves, E., & Pollard, T. D. (2005). Cytokinesis depends on the motor domains of myosin-II in fission yeast but not in budding yeast. *Molecular Biology of the Cell*, *16*(11), 5346–5355.

Loria, A., Longhini, K. M., & Glotzer, M. (2012). The RhoGAP domain of CYK-4 has an essential role in RhoA activation. *Current Biology*, *22*(3), 213–219.

Lozanne, A. D., & Spudich, J. A. (1987). Disruption of the {Dictyostelium} myosin heavy chain gene by homologous recombination. *Science*, *236*(4805), 1086–1091.

Lu, H., Krementsova, E. B., & Trybus, K. M. (2006). Regulation of myosin V processivity by calcium at the single molecule level. *Journal of Biological Chemistry*, *281*(42), 31987–31994.

Lynch, T. J., Albanesi, J. P., Korn, E. D., Robinson, E. A., Bowers, B., & Fujisaki, H. (1986). ATPase activities and actin-binding properties of subfragments of Acanthamoeba myosin IA. *The Journal of Biological Chemistry*, *261*(36), 17156–17162.

Lynch, Thomas J, Brzeska, H., Miyata, H., & Korn, E. D. (1989). Purification and characterization of a third isoform of myosin {I} from {Acanthamoeba} castellanii. *Journal of Biological Chemistry*, *264*(32), 19333–19339.

Ma, X., Kovács, M., Conti, M. A., Wang, A., Zhang, Y., Sellers, J. R., & Adelstein, R. S. (2012). Nonmuscle myosin {II} exerts tension but does not translocate actin in vertebrate cytokinesis. *Proceedings of the National Academy of Sciences*, *109*(12), 4509–4514.

Mabuchi, I., & Okuno, M. (1977). The effect of myosin antibody on the division of starfish blastomeres. *The Journal of Cell Biology*, *74*(1), 251–263.

Madaule, P., Eda, M., Watanabe, N., Fujisawa, K., Matsuoka, T., Bito, H., Ishizaki, T., & Narumiya, S. (1998). Role of citron kinase as a target of the small GTPase Rho in cytokinesis. *Nature*, *394*(6692), 491–494.

Madaule, Pascal, Furuyashiki, T., Eda, M., Bito, H., Ishizaki, T., & Narumiya, S. (2000). Citron, a Rho target that affects contractility during cytokinesis. *Microscopy Research and Technique*, *49*(2), 123–126.

Maddox, A. S., & Oegema, K. (2003). Deconstructing cytokinesis. *Nature Cell Biology*, *5*(9), 773–776.

Maddox, A. S., Habermann, B., Desai, A., & Oegema, K. (2005). Distinct roles for two C. elegans anillins in the gonad and early embryo. *Development*, *132*(12), 2837–2848.

Maddox, A. S., Lewellyn, L., Desai, A., & Oegema, K. (2007). Anillin and the septins promote asymmetric ingression of the cytokinetic furrow. *Developmental Cell*, *12*(5), 827–835.

Maeda, I., Kohara, Y., Yamamoto, M., & Sugimoto, A. (2001). Large-scale analysis of gene function in Caenorhabditis elegans by high-throughput RNAi. *Current Biology*, *11*(3), 171–176.

Mangal, S., Sacher, J., Kim, T., Osório, D. S., Motegi, F., Carvalho, A. X., Oegema, K., & Zanin, E. (2018). TPXL-1 activates Aurora A to clear contractile ring components from the polar cortex during cytokinesis. *The Journal of Cell Biology*, *217*(3), 837–848.

Manstein, D. J., Ruppel, K. M., & Spudich, J. A. (1989). Expression and characterization of a functional myosin head fragment in Dictyostelium discoideum. *Science, 246*(4930), 656-658.

Manstein, D. J., Ruppel, K. M., & Spudich, J. A. (1989). Expression and characterization of a functional myosin head fragment in Dictyostelium discoideum. *Science*, *246*(4930), 656–658.

Manstein, D. J., Titus, M. A., De Lozanne, A., & Spudich, J. A. (1989). Gene replacement in Dictyostelium: Generation of myosin null mutants. *The EMBO Journal*, *8*(3), 923–932.

Maravillas-Montero, J. L., Gillespie, P. G., Patiño-López, G., Shaw, S., & Santos-Argumedo, L. (2011). Myosin 1c participates in B cell cytoskeleton rearrangements, is recruited to the immunologic synapse, and contributes to antigen presentation. *Journal of Immunology (Baltimore, Md.: 1950)*, *187*(6), 3053–3063.

Marston, D. J., & Goldstein, B. (2006). Symmetry Breaking in C. elegans: Another Gift from the Sperm. *Developmental Cell*, *11*(3), 273–274.

Marston, S. B., & Taylor, E. W. (1980). Comparison of the myosin and actomyosin ATPase mechanisms of the four types of vertebrate muscles. *Journal of Molecular Biology*, *139*(4), 573–600.

Martin, E., Laloux, H., Couette, G., Alvarez, T., Bessou, C., Hauser, O., Sookhareea, S., Labouesse, M., & Ségalat, L. (2002). Identification of 1088 new transposon insertions of {Caenorhabditis} elegans: A pilot study toward large-scale screens. *Genetics*, *162*(1), 521–524.

Matsudaira, P. T., & Burgess, D. R. (1979). Identification and organization of the components in the isolated microvillus cytoskeleton. *The Journal of Cell Biology*, *83*(3), 667–673.

Matsumura, F, Ono, S., Yamakita, Y., Totsukawa, G., & Yamashiro, S. (1998). Specific localization of serine 19 phosphorylated myosin II during cell locomotion and mitosis of cultured cells. *The Journal of Cell Biology*, *140*(1), 119–129.

Matsumura, Fumio, Yamakita, Y., & Yamashiro, S. (2011). Myosin light chain kinases and phosphatase in mitosis and cytokinesis. *Archives of Biochemistry and Biophysics*, *510*(2),

Matsumura, Fumio. (2005). Regulation of myosin II during cytokinesis in higher eukaryotes. *Trends in Cell Biology*, *15*(7), 371–377. https://doi.org/10.1016/j.tcb.2005.05.004

Maupin, P., & Pollard, T. D. (1986). Arrangement of actin filaments and myosin-like filaments in the contractile ring and of actin-like filaments in the mitotic spindle of dividing HeLa cells. *Journal of Ultrastructure and Molecular Structure Research*, *94*(1), 92–103.

Mavrakis, M., Azou-Gros, Y., Tsai, F.-C., Alvarado, J., Bertin, A., Iv, F., Kress, A., Brasselet, S., Koenderink, G. H., & Lecuit, T. (2014). Septins promote F-actin ring formation by crosslinking actin filaments into curved bundles. *Nature Cell Biology*, *16*(4), 322–334.

May, K. M., Watts, F. Z., Jones, N., & Hyams, J. S. (1997). Type II myosin involved in cytokinesis in the fission yeast, Schizosaccharomyces pombe. *Cell Motility and the Cytoskeleton*, *38*(4), 385–396.

Mayer, B. J. (2001). SH3 domains: Complexity in moderation. *Journal of Cell Science*, *114*(Pt 7), 1253–1263.

Mccarter, J., Bartlett, B., Dang, T., & Schedl, T. (1999). *On the Control of Oocyte Meiotic Maturation and Ovulation in Caenorhabditis elegans*. *128*, 111–128.

McGoldrick, C. A., Gruver, C., & May, G. S. (1995). myoA of Aspergillus nidulans encodes an essential myosin {I} required for secretion and polarized growth. *Journal of Cell Biology*, *128*(4), 577–

McKenzie, C., Bassi, Z. I., Debski, J., Gottardo, M., Callaini, G., Dadlez, M., & D'Avino, P. P. (2016). Cross-regulation between Aurora B and Citron kinase controls midbody architecture in cytokinesis. *Open Biology*, *6*(3), 160019.

Medeiros, N. A., Burnette, D. T., & Forscher, P. (2006). Myosin II functions in actin-bundle turnover in neuronal growth cones. *Nature Cell Biology*, *8*(3), 216–226.

Meissner, B., Warner, A., Wong, K., Dube, N., Lorch, A., McKay, S. J., Khattra, J., Rogalski, T., Somasiri, A., & Chaudhry, I. (2009). An integrated strategy to study muscle development and myofilament structure in Caenorhabditis elegans. *PLoS Genetics*, *5*(6).

Mele, C., Iatropoulos, P., Donadelli, R., Calabria, A., Maranta, R., Cassis, P., Buelli, S., Tomasoni, S., Piras, R., Krendel, M., Bettoni, S., Morigi, M., Delledonne, M., Pecoraro, C., Abbate, I., Capobianchi, M. R., Hildebrandt, F., Otto, E., Schaefer, F., Noris, M. (2011). MYO1E Mutations and Childhood Familial Focal Segmental Glomerulosclerosis. *New England Journal of Medicine*, *365*(4), 295–306.

Melli, L., Billington, N., Sun, S. A., Bird, J. E., Nagy, A., Friedman, T. B., Takagi, Y., & Sellers, J. R. (2018). Bipolar filaments of human nonmuscle myosin 2-A and 2-B have distinct motile and mechanical properties. *ELife*, *7*, 1–25.

Mendes Pinto, I., Rubinstein, B., Kucharavy, A., Unruh, J. R., & Li, R. (2012). Actin Depolymerization Drives Actomyosin Ring Contraction during Budding Yeast Cytokinesis. *Developmental Cell*, *22*(6), 1247–1260.

Ménétrey, J., Bahloul, A., Wells, A. L., Yengo, C. M., Morris, C. A., Sweeney, H. L., & Houdusse, A. (2005). The structure of the myosin {VI} motor reveals the mechanism of directionality reversal. *Nature*, *435*(7043), 779–785.

Mermall, V., & Miller, K. G. (1995). The 95F unconventional myosin is required for proper organization of the Drosophila syncytial blastoderm. *The Journal of Cell Biology*, *129*(6), 1575–1588.

Mermall, V., Bonafé, N., Jones, L., Sellers, J. R., Cooley, L., & Mooseker, M. S. (2005). Drosophila myosin $\backslash${{V}} is required for larval development and spermatid individualization. *Developmental Biology*, *286*(1), 238–255.

Mermall, V., McNally, J. G., & Miller, K. G. (1994). Transport of cytoplasmic particles catalysed by an unconventional myosin in living Drosophila embryos. *Nature*, *369*(6481), 560–562.

Mermall, V., Post, P. L., & Mooseker, M. S. (1998). Unconventional myosins in cell movement, membrane traffic, and signal transduction. *Science*, *279*(5350), 527–533.

Michalski, N., Michel, V., Bahloul, A., Lefevre, G., Barral, J., Yagi, H., Chardenoux, S., Weil, D., Martin, P., & Hardelin, J.-P. (2007). Molecular characterization of the ankle-link complex in cochlear hair cells and its role in the hair bundle functioning. *Journal of Neuroscience*, *27*(24), 6478–6488.

Mitsuhashi, M., Sakata, H., Kinjo, M., Yazawa, M., & Takahashi, M. (2011). Dynamic assembly properties of nonmuscle myosin II isoforms revealed by combination of fluorescence correlation spectroscopy and fluorescence cross-correlation spectroscopy. *The Journal of Biochemistry*, *149*(3), 253–263.

Moerman, D. G., Plurad, S., Waterston, R. H., & Baillie, D. L. (1982). Mutations in the unc-54 myosin heavy chain gene of Caenorhabditis elegans that alter contractility but not muscle structure. *Cell*, *29*(3), 773–781.

Mollinari, C., Kleman, J.-P., Jiang, W., Schoehn, G., Hunter, T., & Margolis, R. L. (2002). PRC1 is a microtubule binding and bundling protein essential to maintain the mitotic spindle midzone. *The Journal of Cell Biology*, *157*(7), 1175–1186.

Monsuur, A. J., de Bakker, P. I., Alizadeh, B. Z., Zhernakova, A., Bevova, M. R., Strengman, E., Franke, L., van't Slot, R., van Belzen, M. J., & Lavrijsen, I. C. (2005). Myosin IXB variant increases the risk of celiac disease and points toward a primary intestinal barrier defect. *Nature Genetics*, *37*(12), 1341–1344.

Mooseker, M. S., & Tilney, L. G. (1975). Organization of an actin filament-membrane complex. Filament polarity and membrane attachment in the microvilli of intestinal epithelial cells. *The Journal of Cell Biology*, *67*(3), 725–743.

Morgan, N. S., Heintzelman, M. B., & Mooseker, M. S. (1995). Characterization of myosin-IA and myosin-IB, two unconventional myosins associated with the Drosophila brush border cytoskeleton. *Developmental Biology*, *172*(1), 51–71.

Morgan, N. S., Skovronsky, D. M., Artavanis-Tsakonas, S., & Mooseker, M. S. (1994). The molecular cloning and characterization of Drosophila melanogaster myosin-IA and myosin-IB. *Journal of Molecular Biology*, *239*(3), 347–356.

Mori, K., Furusawa, T., Okubo, T., Inoue, T., Ikawa, S., Yanai, N., Mori, K. J., & Obinata, M. (2003). Genome structure and differential expression of two isoforms of a novel PDZ-containing myosin (MysPDZ)(Myo18A). *Journal of Biochemistry*, *133*(4), 405–413.

Mori, K., Matsuda, K., Furusawa, T., Kawata, M., Inoue, T., & Obinata, M. (2005). Subcellular localization and dynamics of MysPDZ (Myo18A) in live mammalian cells. *Biochemical and Biophysical Research Communications*, *326*(2), 491–498.

Morris, C. A., Wells, A. L., Yang, Z., Chen, L.-Q., Baldacchino, C. V., & Sweeney, H. L. (2003). Calcium functionally uncouples the heads of myosin VI. *Journal of Biological Chemistry*, *278*(26), 23324–23330.

Morris, L. B. (2002). *Integrated cassette for controlling fluid having an integral filter*. Google Patents.

Motegi, F., & Sugimoto, A. (2006). Sequential functioning of the ECT-2 RhoGEF, RHO-1 and CDC-42 establishes cell polarity in Caenorhabditis elegans embryos. *Nature Cell Biology*, *8*(9), 978–985.

Motegi, F., Nakano, K., Kitayama, C., Yamamoto, M., & Mabuchi, I. (1997). Identification of Myo3, a second type ǂI myosin heavy chain in the fission yeast Schizosaccharomyces pombe. *FEBS Letters*, *420*(2–3), 161–166.

Mukherjee, T. M., & Staehelin, L. A. (1971). The fine-structural organization of the brush border of intestinal epithelial cells. *Journal of Cell Science*, *8*(3), 573–599.

Muller, R. T., Honnert, U., Reinhard, J., & Bähler, M. (1997). The rat myosin myr 5 is a GTPase-activating protein for Rho in vivo: Essential role of arginine 1695. *Molecular Biology of the Cell*, *8*(10), 2039–2053.

Müller, T., Hess, M. W., Schiefermeier, N., Pfaller, K., Ebner, H. L., Heinz-Erian, P., Ponstingl, H., Partsch, J., Röllinghoff, B., Köhler, H., Berger, T., Lenhartz, H., Schlenck, B., Houwen, R. J., Taylor, C. J., Zoller, H., Lechner, S., Goulet, O., Utermann, G., … Janecke, A. R. (2008). MYO5B mutations cause microvillus inclusion disease and disrupt epithelial cell polarity. *Nature Genetics*, *40*(10), 1163–1165.

Munjal, A., & Lecuit, T. (2014). Actomyosin networks and tissue morphogenesis. *Development (Cambridge, England)*, *141*(9), 1789–93.

Munro, E., Nance, J., & Priess, J. R. (2004). Cortical flows powered by asymmetrical contraction transport PAR proteins to establish and maintain anterior-posterior polarity in the early C. elegans embryo. *Developmental Cell*, *7*(3), 413–424.

Murrell, M. P., & Gardel, M. L. (2012). F-actin buckling coordinates contractility and severing in a biomimetic actomyosin cortex. *Proceedings of the National Academy of Sciences*, *109*(51), 20820–20825.

Murthy, K., & Wadsworth, P. (2005). Myosin-II-dependent localization and dynamics of F-actin during cytokinesis. *Current Biology*, *15*(8), 724–731.

Naccache, S. N., & Hasson, T. (2006). Myosin VI altered at threonine 406 Stabilizes actin filaments in vivo. *Cell Motility and the Cytoskeleton*, *63*(10), 633–645.

Nagasaki, A., Kanada, M., & Uyeda, T. Q. (2009). Cell adhesion molecules regulate contractile ring-independent cytokinesis in Dictyostelium discoideum. *Cell Research*, *19*(2), 236–246.

Nagata, K., Kawajiri, A., Matsui, S., Takagishi, M., Shiromizu, T., Saitoh, N., Izawa, I., Kiyono, T., Itoh, T. J., & Hotani, H. (2003). Filament formation of MSF-A, a mammalian septin, in human mammary epithelial cells depends on interactions with microtubules. *Journal of Biological Chemistry*, *278*(20), 18538–18543.

Nakamori, Y., Emoto, M., Fukuda, N., Taguchi, A., Okuya, S., Tajiri, M., Miyagishi, M., Taira, K., Wada, Y., & Tanizawa, Y. (2006). Myosin motor Myo1c and its receptor

NEMO/IKK-gamma promote TNF-alpha-induced serine307 phosphorylation of IRS-1. *The Journal of Cell Biology*, *173*(5), 665–671.

Nalavadi, V., Nyitrai, M., Bertolini, C., Adamek, N., Geeves, M. A., & Bähler, M. (2005). Kinetic mechanism of myosin IXB and the contributions of two class IX-specific regions. *Journal of Biological Chemistry*, *280*(47), 38957–38968.

Nambiar, R., McConnell, R. E., & Tyska, M. J. (2009). Control of cell membrane tension by myosin-I. *Proceedings of the National Academy of Sciences of the United States of America*, *106*(29), 11972–11977.

Navinés-Ferrer, A., & Martín, M. (2020). Long-tailed unconventional class i myosins in health and disease. *International Journal of Molecular Sciences*, *21*(7).

Nedvetsky, P. I., Stefan, E., Frische, S., Santamaria, K., Wiesner, B., Valenti, G., Hammer III, J. A., Nielsen, S., Goldenring, J. R., & Rosenthal, W. (2007). A role of myosin Vb and Rab11-FIP2 in the aquaporin-2 shuttle. *Traffic*, *8*(2), 110–123.

Nelson, G. A., Roberts, T. M., & Ward, S. (1982). Caenorhabditis elegans spermatozoan locomotion: Amoeboid movement with almost no actin. *The Journal of Cell Biology*, *92*(1), 121–131.

Neufeld, T. P., & Rubin, G. M. (1994). The Drosophila peanut gene is required for cytokinesis and encodes a protein similar to yeast putative bud neck filament proteins. *Cell*, *77*(3), 371–379.

Neujahr, R., Heizer, C., & Gerisch, G. (1997). Myosin II-independent processes in mitotic cells of Dictyostelium discoideum: Redistribution of the nuclei, re-arrangement of the actin system and formation of the cleavage furrow. *Journal of Cell Science*, *110*(2), 123–137.

Newell-Litwa, K. A., Horwitz, R., & Lamers, M. L. (2015). Non-Muscle myosin II in disease: Mechanisms and therapeutic opportunities. *DMM Disease Models and Mechanisms*, *8*(12),

Nguyen, H., & Higuchi, H. (2005). Motility of myosin V regulated by the dissociation of single calmodulin. *Nature Structural & Molecular Biology*, *12*(2), 127–132.

Nguyen, L. T., Swulius, M. T., Aich, S., Mishra, M., & Jensen, G. J. (2018). Coarse-grained simulations of actomyosin rings point to a nodeless model involving both unipolar and bipolar myosins. *Molecular Biology of the Cell*, *29*(11), 1318–1331.

Nguyen, T. Q., Sawa, H., Okano, H., & White, J. G. (2000). The C. elegans septin genes, unc-59 and unc-61, are required for normal postembryonic cytokineses and morphogenesis but have no essential function in embryogenesis. *Journal of Cell Science*, *113*(21), 3825–3837.

Niederman, R., & Pollard, T. D. (1975). Human platelet myosin. II. In vitro assembly and structure of myosin filaments. *The Journal of Cell Biology, 67*(1), 72-92.

Niiya, F., Tatsumoto, T., Lee, K. S., & Miki, T. (2006). Phosphorylation of the cytokinesis regulator ECT2 at G2/M phase stimulates association of the mitotic kinase Plk1 and accumulation of GTP-bound RhoA. *Oncogene*, *25*(6), 827–837.

Nishikawa, M., Naganathan, S. R., Jülicher, F., & Grill, S. W. (2017). Controlling contractile instabilities in the actomyosin cortex. *ELife*, *6*, 1–21.

Niwayama, R., Shinohara, K., & Kimura, A. (2011). Hydrodynamic property of the cytoplasm is sufficient to mediate cytoplasmic streaming in the Caenorhabiditis elegans embryo. *Proceedings of the National Academy of Sciences*, *108*(29), 11900–11905.

Noguchi, T., Lenartowska, M., & Miller, K. G. (2006). Myosin VI stabilizes an actin network during Drosophila spermatid individualization. *Molecular Biology of the Cell*, *17*(6), 2559–2571.

Nussbaum-Krammer, C. I., Neto, M. F., Brielmann, R. M., Pedersen, J. S., & Morimoto, R. I. (2015). Investigating the spreading and toxicity of prion-like proteins using the metazoan model organism C. elegans. *JoVE (Journal of Visualized Experiments)*, *95*, e52321.

O'Connell, C. B., & Mooseker, M. S. (2003). Native Myosin-IXb is a plus-, not a minus-end-directed motor. *Nature Cell Biology*, *5*(2), 171–172.

O'Connell, C. B., Tyska, M. J., & Mooseker, M. S. (2007). Myosin at work: Motor adaptations for a variety of cellular functions. *Biochimica et Biophysica Acta (BBA)-Molecular Cell Research*, *1773*(5), 615–630.

O'Connell, C. B., Wheatley, S. P., Ahmed, S., & Wang, Y. (1999). The small GTP-binding protein rho regulates cortical activities in cultured cells during division. *The Journal of Cell Biology*, *144*(2), 305–313.

O'Neill, R. S., & Clark, D. V. (2016). Partial functional diversification of Drosophila melanogaster septin genes Sep2 and Sep5. *G3: Genes, Genomes, Genetics*, *6*(7), 1947–1957.

Oda, T., Iwasa, M., Aihara, T., Maéda, Y., & Narita, A. (2009). The nature of the globular-to fibrous-actin transition. *Nature, 457*(7228), 441-445.

Oda, T., Iwasa, M., Aihara, T., Maéda, Y., & Narita, A. (2009). The nature of the globular- to fibrous-actin transition. *Nature*, *457*(7228), 441–445.

Odronitz, F., & Kollmar, M. (2007). Drawing the tree of eukaryotic life based on the analysis of 2,269 manually annotated myosins from 328 species. *Genome Biology*, *8*(9), 1–23.

Oegema, K., Savoian, M. S., Mitchison, T. J., & Field, C. M. (2000). Functional analysis of a human homologue of the Drosophila actin binding protein anillin suggests a role in cytokinesis. *The Journal of Cell Biology*, *150*(3), 539–552.

Oelz, D. B., Rubinstein, B. Y., & Mogilner, A. (2015). A combination of actin treadmilling and cross-linking drives contraction of random actomyosin arrays. *Biophysical Journal*, *109*(9), 1818–1829.

Oh, H., Kim, H., Shin, B., Lee, K. H., Yeo, M. G., & Song, W. K. (2013). Interaction of Crk with myosin-1c participates in fibronectin-induced cell spreading. *International Journal of Biological Sciences*, *9*(8), 778.

Ökten, Z., Churchman, L. S., Rock, R. S., & Spudich, J. A. (2004). Myosin VI walks hand-over-hand along actin. *Nature Structural & Molecular Biology*, *11*(9), 884–887.

ollmar, M. (2006). Thirteen is enough: The myosins of Dictyostelium discoideum and their light chains. *BMC Genomics*, *7*, 1–15.

Olsen, J. V., Blagoev, B., Gnad, F., Macek, B., Kumar, C., Mortensen, P., & Mann, M. (2006). Global, in vivo, and site-specific phosphorylation dynamics in signaling networks. *Cell*, *127*(3), 635–648.

Omelchenko, T., & Hall, A. (2012). Myosin-IXA regulates collective epithelial cell migration by targeting RhoGAP activity to cell-cell junctions. *Current Biology*, *22*(4), 278–288.

Onishi, H., Kojima, S., Katoh, K., Fujiwara, K., Martinez, H. M., & Morales, M. F. (1998). Functional transitions in myosin: Formation of a critical salt-bridge and transmission of effect to the sensitive tryptophan. *Proceedings of the National Academy of Sciences*, *95*(12), 6653–6658.

Ono, K., & Ono, S. (2016). Two distinct myosin II populations coordinate ovulatory contraction of the myoepithelial sheath in the Caenorhabditis elegans somatic gonad. *Molecular Biology of the Cell*, *27*(7), 1131–1142.

Osório, D. S., Chan, F. Y., Saramago, J., Leite, J., Silva, A. M., Sobral, A. F., Gassmann, R., & Carvalho, A. X. (2019). Crosslinking activity of non-muscle myosin II is not sufficient for embryonic cytokinesis in C. elegans. In *Development (Cambridge, England)* (Vol. 146).

Ostap, E. M., & Pollard, T. D. (1996). Overlapping functions of myosin-I isoforms? *The Journal of Cell Biology*, *133*(2), 221–224.

Ou, G., Stuurman, N., D'Ambrosio, M., & Vale, R. D. (2010). Polarized Myosin Produces Unequal-Size Daughters During Asymmetric Cell Division. *Science*, *330*(6004), 677 LP – 680.

Ouderkirk, J. L., & Krendel, M. (2014). Non-muscle myosins in tumor progression, cancer cell invasion, and metastasis. *Cytoskeleton*, *71*(8), 447–463.

Padmanabhan, A., Ong, H. T., & Zaidel-Bar, R. (2017). Non-junctional E-Cadherin Clusters Regulate the Actomyosin Cortex in the C. elegans Zygote. *Current Biology*, *27*(1), 103–112.

Palani, S., Chew, T. G., Ramanujam, S., Kamnev, A., Harne, S., Chapa-y-Lazo, B., Hogg, R., Sevugan, M., Mishra, M., & Gayathri, P. (2017). Motor activity dependent and independent functions of myosin II contribute to actomyosin ring assembly and contraction in Schizosaccharomyces pombe. *Current Biology*, *27*(5), 751–757.

Pan, F., Malmberg, R. L., & Momany, M. (2007). Analysis of septins across kingdoms reveals orthology and new motifs. *BMC Evolutionary Biology*, *7*(1), 103.

Park, E.-C., & Horvitz, H. R. (1986). C. elegans unc-105 mutations affect muscle and are suppressed by other mutations that affect muscle. *Genetics*, *113*(4), 853–867.

Park, H., Li, A., Chen, L. Q., Houdusse, A., Selvin, P. R., & Sweeney, H. L. (2007). The unique insert at the end of the myosin {VI} motor is the sole determinant of directionality. *Proceedings of the National Academy of Sciences of the United States of America*, *104*(3), 778–783.

Pavicic-Kaltenbrunner, V., Mishima, M., & Glotzer, M. (2007). Cooperative Assembly of CYK-4/MgcRacGAP and ZEN-4/MKLP1 to Form the Centralspindlin Complex. *Molecular Biology of the Cell*, *18*(12), 4992–5003.

Pazdernik, N., & Schedl, T. (2013). Introduction to germ cell development in Caenorhabditis elegans. In *Germ cell development in C. elegans* (pp. 1–16). Springer.

Percipalle, P., & Farrants, A.-K. O. (2006). Chromatin remodelling and transcription: Be-WICHed by nuclear myosin 1. *Current Opinion in Cell Biology*, *18*(3), 267–274.

Pereira, G., & Schiebel, E. (2003). Separase regulates INCENP-Aurora B anaphase spindle function through Cdc14. *Science (New York, N.Y.)*, *302*(5653), 2120–2124.

Pestic-Dragovich, L., Stojiljkovic, L., Philimonenko, A. A., Nowak, G., Ke, Y., Settlage, R. E., Shabanowitz, J., Hunt, D. F., Hozak, P., & de Lanerolle, P. (2000). A myosin I isoform in the nucleus. *Science (New York, N.Y.)*, *290*(5490), 337–341.

Peterson, M. D., Urioste, A. S., & Titus, M. A. (1996). Dictyostelium discoideum myoJ: A member of a broadly defined myosin V class or a class XI unconventional myosin? *Journal of Muscle Research and Cell Motility*, *17*(4), 411–424.

Petritsch, C., Tavosanis, G., Turck, C. W., Jan, L. Y., & Jan, Y. N. (2003). The Drosophila myosin VI Jaguar is required for basal protein targeting and correct spindle orientation in mitotic neuroblasts. *Developmental Cell*, *4*(2), 273–281.

Petronczki, M., Glotzer, M., Kraut, N., & Peters, J.-M. (2007). Polo-like Kinase 1 Triggers the Initiation of Cytokinesis in Human Cells by Promoting Recruitment of the RhoGEF Ect2 to the Central Spindle. *Developmental Cell*, *12*(5), 713–725.

Petzoldt, A. G., Coutelis, J.-B., Géminard, C., Spéder, P., Suzanne, M., Cerezo, D., & Noselli, S. (2012). DE-Cadherin regulates unconventional Myosin ID and Myosin IC

in Drosophila left-right asymmetry establishment. *Development*, *139*(10), 1874–1884.

Philimonenko, V. V., Zhao, J., Iben, S., Dingová, H., Kyselá, K., Kahle, M., Zentgraf, H., Hofmann, W. A., de Lanerolle, P., Hozák, P., & Grummt, I. (2004). Nuclear actin and myosin I are required for RNA polymerase I transcription. *Nature Cell Biology*, *6*(12), 1165–1172.

Piano, F., Schetter, A. J., Morton, D. G., Gunsalus, K. C., Reinke, V., Kim, S. K., & Kemphues, K. J. (2002). Gene clustering based on RNAi phenotypes of ovary-enriched genes in C. elegans. *Current Biology*, *12*(22), 1959–1964.

Piekny, A J. (2003). The Caenorhabditis elegans nonmuscle myosin genes nmy-1 and nmy-2 function as redundant components of the let-502/Rho-binding kinase and mel-11/myosin phosphatase pathway during embryonic morphogenesis. *Development*, *130*(23), 5695–

Piekny, A., Werner, M., & Glotzer, M. (2005). Cytokinesis: Welcome to the Rho zone. *Trends in Cell Biology*, *15*(12), 651–658.

Piekny, Alisa J, & Mains, P. E. (2002). Rho-binding kinase (LET-502) and myosin phosphatase (MEL-11) regulate cytokinesis in the early Caenorhabditis elegans embryo. *Journal of Cell Science*, *115*(Pt 11), 2271–2282.

Piekny, Alisa J., & Glotzer, M. (2008). Anillin Is a Scaffold Protein That Links RhoA, Actin, and Myosin during Cytokinesis. *Current Biology*, *18*(1), 30–36.

Piekny, Alisa J., & Maddox, A. S. (2010). The myriad roles of Anillin during cytokinesis. *Seminars in Cell and Developmental Biology*, *21*(9), 881–891.

Pollard, T. D., & Wu, J. (2010). Understanding cytokinesis: Lessons from fission yeast. *Nature Reviews Molecular Cell Biology*, *11*(February), 149–155.

Poperechnaya, A., Varlamova, O., Lin, P., Stull, J. T., & Bresnick, A. R. (2000). Localization and activity of myosin light chain kinase isoforms during the cell cycle. *The Journal of Cell Biology*, *151*(3), 697–708.

Post, P. L., Bokoch, G. M., & Mooseker, M. S. (1998). Human myosin-IXb is a mechanochemically active motor and a GAP for RHO. *Journal of Cell Science*, *111*(7), 941–950.

Post, P. L., Tyska, M. J., O'Connell, C. B., Johung, K., Hayward, A., & Mooseker, M. S. (2002). Myosin-IXb is a single-headed and processive motor. *Journal of Biological Chemistry*, *277*(14), 11679–11683.

Poteryaev, D., Squirrell, J. M., Campbell, J. M., White, J. G., & Spang, A. (2005). Involvement of the actin cytoskeleton and homotypic membrane fusion in ER dynamics in Caenorhabditis elegans. *Molecular Biology of the Cell*, *16*(5), 2139–2153.

Praitis, V., Casey, E., Collar, D., & Austin, J. (2001). Creation of low-copy integrated transgenic lines in Caenorhabditis elegans. *Genetics*, *157*(3), 1217–1226.

Pranchevicius, M. C. S., Baqui, M. M., Ishikawa-Ankerhold, H. C., Lourenço, E. V., Leão, R. M., Banzi, S. R., dos Santos, C. T., Barreira, M. C. R., Espreafico, E. M., & Larson, R. E. (2008). Myosin Va phosphorylated on Ser1650 is found in nuclear speckles and redistributes to nucleoli upon inhibition of transcription. *Cell Motility and the Cytoskeleton*, *65*(6), 441–456.

Priti, A., Ong, H. T., Toyama, Y., Padmanabhan, A., Dasgupta, S., Krajnc, M., & Zaidel-Bar, R. (2018). Syncytial germline architecture is actively maintained by contraction of an internal actomyosin corset. *Nature Communications*, *9*(1), 1–15.

Raich, W. B., Moran, A. N., Rothman, J. H., & Hardin, J. (1998). Cytokinesis and Midzone Microtubule Organization in Caenorhabditis elegans Require the Kinesin-like Protein ZEN-4. *Molecular Biology of the Cell*, *9*(8), 2037–2049.

Rankin, C. H. (2002). From gene to identified neuron to behaviour in Caenorhabditis elegans. *Nat Rev Genet*, *3*(8), 622–630.

Rappaport, R. (1961). Experiments concerning the cleavage stimulus in sand dollar eggs. *Journal of Experimental Zoology*, *148*(1), 81–89.

Ratan, R. R., Maxfield, F. R., & Shelanski, M. L. (1988). Long-lasting and rapid calcium changes during mitosis. *The Journal of Cell Biology*, *107*(3), 993–999.

Rayment, I., Holden, H. M., Whittaker, M., Yohn, C. B., Lorenz, M., Holmes, K. C., & Milligan, R. A. (1993). Structure of the actin-myosin complex and its implications for muscle contraction. *Science*, *261*(5117), 58–65.

Reck-Peterson, S. L., Tyska, M. J., Novick, P. J., & Mooseker, M. S. (2001). The yeast class V myosins, Myo2p and Myo4p, are nonprocessive actin-based motors. *The Journal of Cell Biology*, *153*(5), 1121–1126.

Redemann, S., Pecreaux, J., Goehring, N. W., Khairy, K., Stelzer, E. H., Hyman, A. A., & Howard, J. (2010). Membrane invaginations reveal cortical sites that pull on mitotic spindles in one-cell C. elegans embryos. *PloS One*, *5*(8).

Reiners, J., Van Wijk, E., Märker, T., Zimmermann, U., Jürgens, K., te Brinke, H., Overlack, N., Roepman, R., Knipper, M., & Kremer, H. (2005). Scaffold protein harmonin (USH1C) provides molecular links between Usher syndrome type 1 and type 2. *Human Molecular Genetics*, *14*(24), 3933–3943.

Reinhard, J., Scheel, A. A., Diekmann, D., Hall, A., Ruppert, C., & Bähler, M. (1995). A novel type of myosin implicated in signalling by rho family {GTPases}. *The EMBO Journal*, *14*(4), 697–704.

Reymann, Anne-Cécile, Boujemaa-Paterski, R., Martiel, J.-L., Guérin, C., Cao, W., Chin, H. F., Enrique, M., Théry, M., & Blanchoin, L. (2012). Actin network architecture can determine myosin motor activity. *Science*, *336*(6086), 1310–1314.

Reymann, Anne-Cecile, Staniscia, F., Erzberger, A., Salbreux, G., & Grill, S. W. (2016). Cortical flow aligns actin filaments to form a furrow. *Elife*, *5*, e17807.

Rhee, D., Sanger, J. M., & Sanger, J. W. (1994). The premyofibril: Evidence for its role in myofibrillogenesis. *Cell Motility*, *28*(1), 1–24.

Richards, T. A., & Cavalier-Smith, T. (2005). Myosin domain evolution and the primary divergence of eukaryotes. *Nature*, *436*(7054), 1113–1118.

Robblee, J. P., Olivares, A. O., & Enrique, M. (2004). Mechanism of {Nucleotide} {Binding} to {Actomyosin} {VI} {Evidence} for {Allosteric} {Head}-{Head} {Communication}. *Journal of Biological Chemistry*, *279*(37), 38608–38617.

Roberts, K. L., & Baines, J. D. (2011). Actin in herpesvirus infection. *Viruses*, *3*(4), 336–346.

Robinson, D. N., & Spudich, J. A. (2000). Towards a molecular understanding of cytokinesis. *Trends in Cell Biology*, *10*(6), 228–237.

Rock, R. S., Rice, S. E., Wells, A. L., Purcell, T. J., Spudich, J. A., & Sweeney, H. L. (2001). Myosin {VI} is a processive motor with a large step size. *Proceedings of the National Academy of Sciences*, *98*(24), 13655–13659.

Rodriguez, O. C., & Cheney, R. E. (2002). Human myosin-Vc is a novel class V myosin expressed in epithelial cells. *Journal of Cell Science*, *115*(5), 991–1004.

Rodríguez-Palero, M. J., López-Díaz, A., Marsac, R., Gomes, J. E., Olmedo, M., & Artal-Sanz, M. (2018). An automated method for the analysis of food intake behaviour in Caenorhabditis elegans. *Scientific Reports*, *8*(1), 1–10.

Rogat, A. D., & Miller, K. G. (2002). A role for myosin {VI} in actin dynamics at sites of membrane remodeling during {Drosophila} spermatogenesis. *Journal of Cell Science*, *115*(24), 4855–4865.

Ronen, D., Rosenberg, M. M., Shalev, D. E., Rosenberg, M., Rotem, S., Friedler, A., & Ravid, S. (2010). The positively charged region of the myosin IIC non-helical tailpiece promotes filament assembly. *Journal of Biological Chemistry*, *285*(10), 7079–7086.

Rosé, S. D., Lejen, T., Casaletti, L., Larson, R. E., Pene, T. D., & Trifaró, J.-M. (2003). Myosins II and V in chromaffin cells: Myosin V is a chromaffin vesicle molecular motor involved in secretion. *Journal of Neurochemistry*, *85*(2), 287–298.

Rossanese, O. W., Reinke, C. A., Bevis, B. J., Hammond, A. T., Sears, I. B., O'Connor, J., & Glick, B. S. (2001). A role for actin, Cdc1p, and Myo2p in the inheritance of late Golgi elements in Saccharomyces cerevisiae. *The Journal of Cell Biology*, *153*(1), 47–62.

Rossman, K. L., Der, C. J., & Sondek, J. (2005). GEF means go: Turning on RHO GTPases with guanine nucleotide-exchange factors. *Nature Reviews Molecular Cell Biology*, *6*(2), 167–180.

Royou, A., Field, C., Sisson, J. C., Sullivan, W., & Karess, R. (2004). Reassessing the role and dynamics of nonmuscle myosin II during furrow formation in early Drosophila embryos. *Molecular Biology of the Cell*, *15*(2), 838–850.

Ruchaud, S., Carmena, M., & Earnshaw, W. C. (2007). The Chromosomal Passenger Complex: One for All and All for One. *Cell*, *131*(2), 230–231.

Ruppel, K. M., & Spudich, J. A. (1996). Structure-function studies of the myosin motor domain: Importance of the 50-kDa cleft. *Molecular Biology of the Cell*, *7*(7), 1123–1136.

Ruppert, C., Kroschewski, R., & Bähler, M. (1993). Identification, characterization and cloning of myr 1, a mammalian myosin-I. *The Journal of Cell Biology*, *120*(6), 1393–1403.

Ruprecht, V., Wieser, S., Callan-Jones, A., Smutny, M., Morita, H., Sako, K., Barone, V., Ritsch-Marte, M., Sixt, M., & Voituriez, R. (2015). Cortical contractility triggers a stochastic switch to fast amoeboid cell motility. *Cell*, *160*(4), 673–685.

Sabry, J. H., Moores, S. L., Ryan, S., Zang, J.-H., & Spudich, J. A. (1997). Myosin Heavy Chain Phosphorylation Sites Regulate Myosin Localization during Cytokinesis in Live Cells. *Molecular Biology of the Cell*, *8*(12), 2605–2615.

Sahlender, D. A., Roberts, R. C., Arden, S. D., Spudich, G., Taylor, M. J., Luzio, J. P., Kendrick-Jones, J., & Buss, F. (2005). Optineurin links myosin VI to the Golgi complex and is involved in Golgi organization and exocytosis. *The Journal of Cell Biology*, *169*(2), 285–295.

Sakai, T., Jung, H. S., Sato, O., Yamada, M. D., You, D.-J., Ikebe, R., & Ikebe, M. (2015). Structure and regulation of the movement of human myosin VIIA. *Journal of Biological Chemistry*, *290*(28), 17587–17598.

Salamon, M., Millino, C., Raffaello, A., Mongillo, M., Sandri, C., Bean, C., Negrisolo, E., Pallavicini, A., Valle, G., & Zaccolo, M. (2003). Human MYO18B, a novel unconventional myosin heavy chain expressed in striated muscles moves into the myonuclei upon differentiation. *Journal of Molecular Biology*, *326*(1), 137–149.

Salas-Cortes, L., Ye, F., Tenza, D., Wilhelm, C., Theos, A., Louvard, D., Raposo, G., & Coudrier, E. (2005). Myosin Ib modulates the morphology and the protein transport within multi-vesicular sorting endosomes. *Journal of Cell Science*, *118*(20), 4823–4832.

Salbreux, G., Prost, J., & Joanny, J.-F. (2009). Hydrodynamics of cellular cortical flows and the formation of contractile rings. *Physical Review Letters*, *103*(5), 058102.

Sanders, S. L., Gentzsch, M., Tanner, W., & Herskowitz, I. (1999). O-Glycosylation of Axl2/Bud10p by Pmt4p is required for its stability, localization, and function in daughter cells. *The Journal of Cell Biology*, *145*(6), 1177–1188.

Sanger, J. M., & Sanger, J. W. (1980). Banding and polarity of actin filaments in interphase and cleaving cells. *The Journal of Cell Biology*, *86*(2), 568–575.

Sapone, A., De Magistris, L., Pietzak, M., Clemente, M. G., Tripathi, A., Cucca, F., Lampis, R., Kryszak, D., Cartenì, M., & Generoso, M. (2006). Zonulin upregulation is associated with increased gut permeability in subjects with type 1 diabetes and their relatives. *Diabetes*, *55*(5), 1443–1449.

Sasaki, N., Shimada, T., & Sutoh, K. (1998). Mutational Analysis of the Switch II Loop ofDictyostelium Myosin II. *Journal of Biological Chemistry*, *273*(32), 20334–20340.

Sato, O., Komatsu, S., Sakai, T., Tsukasaki, Y., Tanaka, R., Mizutani, T., Watanabe, T. M., Ikebe, R., & Ikebe, M. (2017). Human myosin VIIa is a very slow processive motor protein on various cellular actin structures. *Journal of Biological Chemistry*, *292*(26), 10950–10960.

Schindelin, J., Arganda-Carreras, I., Frise, E., Kaynig, V., Longair, M., Pietzsch, T., Preibisch, S., Rueden, C., Saalfeld, S., & Schmid, B. (2012). Fiji: An open-source platform for biological-image analysis. *Nature Methods*, *9*(7), 676–682.

Schmidt, M., Bowers, B., Varma, A., Roh, D.-H., & Cabib, E. (2002). In budding yeast, contraction of the actomyosin ring and formation of the primary septum at cytokinesis depend on each other. *Journal of Cell Science*, *115*(2), 293–302.

Schmitz, C., Kinge, P., & Hutter, H. (2007). Axon guidance genes identified in a large-scale {RNAi} screen using the {RNAi}-hypersensitive {Caenorhabditis} elegans strain nre-1(hd20) lin-15b(hd126). *Proceedings of the National Academy of Sciences*, *104*(3), 834–839.

Scholze, M. J., Barbieux, K. S., De Simone, A., Boumasmoud, M., Süess, C. C. N., Wang, R., & Gönczy, P. (2018). PI(4,5)P2 forms dynamic cortical structures and directs

actin distribution as well as polarity in Caenorhabditis elegans embryos. *Development (Cambridge, England)*, *145*(11).

Schott, D. H., Collins, R. N., & Bretscher, A. (2002). Secretory vesicle transport velocity in living cells depends on the myosin-V lever arm length. *Journal of Cell Biology*, *156*(1), 35–39.

Schott, D., Ho, J., Pruyne, D., & Bretscher, A. (1999). The COOH-terminal domain of Myo2p, a yeast myosin V, has a direct role in secretory vesicle targeting. *The Journal of Cell Biology*, *147*(4), 791–808.

Schramm, A. C., Hocky, G. M., Voth, G. A., Blanchoin, L., Martiel, J.-L., & Enrique, M. (2017). Actin filament strain promotes severing and cofilin dissociation. *Biophysical Journal*, *112*(12), 2624–2633.

Schröder, R. R., Manstein, D. J., Jahn, W., Holden, H., Rayment, I., Holmes, K. C., & Spudich, J. A. (1993). Three-dimensional atomic model of F-actin decorated with Dictyostelium myosin S1. *Nature*, *364*(6433), 171–174.

Schroeder, T. E. (1968). Cytokinesis: Filaments in the cleavage furrow. *Experimental Cell Research*, *53*(1), 272–276.

Schroeder, T. E. (1972). THE CONTRACTILE RING: II. Determining its Brief Existence, Volumetric Changes, and Vital Role in Cleaving Arbacia Eggs. *The Journal of Cell Biology*, *53*(2), 419–434.

Schroeder, Thomas E. (1973). Actin in dividing cells: Contractile ring filaments bind heavy meromyosin. *Proceedings of the National Academy of Sciences*, *70*(6), 1688–1692.

Sellers, J. R. (1998). In vitro motility assay to study translocation of actin by myosin. *Current Protocols in Cell Biology*, (1), 13-2.

Sellers, J. R. (2000). Myosins: A diverse superfamily. *Biochimica et Biophysica Acta - Molecular Cell Research*, *1496*(1), 3–22.

Senften, M., Schwander, M., Kazmierczak, P., Lillo, C., Shin, J.-B., Hasson, T., Géléoc, G. S., Gillespie, P. G., Williams, D., & Holt, J. R. (2006). Physical and functional interaction between protocadherin 15 and myosin VIIa in mechanosensory hair cells. *Journal of Neuroscience*, *26*(7), 2060–2071.

Severson, A. F., Baillie, D. L., & Bowerman, B. (2002). A Formin Homology protein and a profilin are required for cytokinesis and Arp2/3-independent assembly of cortical microfilaments in C. elegans. *Current Biology : CB*, *12*(24), 2066–2075.

Shaye, D. D., & Greenwald, I. (2011). Ortholist: A compendium of C. Elegans genes with human orthologs. *PLoS ONE*, *6*(5).

Shelton, C. A., Carter, J. C., Ellis, G. C., & Bowerman, B. (1999). The Nonmuscle Myosin Regulatory Light Chain Gene mlc-4 Is Required. *Journal of Cell Biology*, *146*(2), 439–451.

Shepard, K. A., Gerber, A. P., Jambhekar, A., Takizawa, P. A., Brown, P. O., Herschlag, D., DeRisi, J. L., & Vale, R. D. (2003). Widespread cytoplasmic mRNA transport in yeast: Identification of 22 bud-localized transcripts using DNA microarray analysis. *Proceedings of the National Academy of Sciences*, *100*(20), 11429–11434.

Shimada, T., Sasaki, N., Ohkura, R., & Sutoh, K. (1997). Alanine scanning mutagenesis of the switch I region in the ATPase site of Dictyostelium discoideum myosin II. *Biochemistry*, *36*(46), 14037–14043.

Shutova, M. S., Spessott, W. A., Giraudo, C. G., & Svitkina, T. (2014). Endogenous species of mammalian nonmuscle myosin IIA and IIB include activated monomers and heteropolymers. *Current Biology*, *24*(17), 1958–1968.

Sieburth, D., Ch'ng, Q., Dybbs, M., Tavazoie, M., Kennedy, S., Wang, D., Dupuy, D., Rual, J. F., Hill, D. E., Vidal, M., Ruvkun, G., & Kaplan, J. M. (2005). Systematic analysis of genes required for synapse structure and function. *Nature*, *436*(7050), 510–516.

Silva, A. M., Osório, D. S., Pereira, A. J., Maiato, H., Pinto, I. M., Rubinstein, B., Gassmann, R., Telley, I. A., & Carvalho, A. X. (2016). Robust gap repair in the contractile ring ensures timely completion of cytokinesis. *Journal of Cell Biology*, *215*(6), 789–799.

Simmer, F., Moorman, C., Van Der Linden, A. M., Kuijk, E., Van Den Berghe, P. V. E., Kamath, R. S., Fraser, A. G., Ahringer, J., & Plasterk, R. H. A. (2003). Genome-wide RNAi of C. elegans using the hypersensitive rrf-3 strain reveals novel gene functions. *PLoS Biology*, *1*(1), 77–84.

Simons, M., Wang, M., McBride, O. W., Kawamoto, S., Yamakawa, K., Gdula, D., Adelstein, R. S., & Weir, L. (1991). Human nonmuscle myosin heavy chains are encoded by two genes located on different chromosomes. *Circulation Research*, *69*(2), 530–539.

Singh, D., Odedra, D., Dutta, P., & Pohl, C. (2019). Mechanical stress induces a scalable switch in cortical flow polarization during cytokinesis. *Journal of Cell Science*, *132*(19), jcs231357.

Sivaramakrishnan, S., Ashley, E., Leinwand, L., & Spudich, J. A. (2009). Insights into Human β-Cardiac Myosin Function from Single Molecule and Single Cell Studies. *Journal of Cardiovascular Translational Research*, *2*(4), 426–440.

Skop, A. R., Liu, H., Yates, J., Meyer, B. J., & Heald, R. (2004). Dissection of the mammalian midbody proteome reveals conserved cytokinesis mechanisms. *Science*, *305*(5680), 61–66.

Smith, S. J., & White, H. D. (1985). Kinetic mechanism of 1-N6-etheno-2-aza-ATP hydrolysis by bovine ventricular myosin subfragment 1 and actomyosin subfragment 1. *Journal of Biological Chemistry*, *260*(28), 15146–15155.

Soldati, T. (2003). Unconventional Myosins, Actin Dynamics and Endocytosis: A Ménage à Trois? *Traffic*, *4*(6), 358–366.

Sönnichsen, B., Koski, L. B., Walsh, A., Marschall, P., Neumann, B., Brehm, M., Alleaume, A.-M., Artelt, J., Bettencourt, P., Cassin, E., Hewitson, M., Holz, C., Khan, M., Lazik, S., Martin, C., Nitzsche, B., Ruer, M., Stamford, J., Winzi, M., … Echeverri, C. J. (2005). Full-genome {RNAi} profiling of early embryogenesis in {Caenorhabditis} elegans. *Nature*, *434*(7032), 462–469.

Spector, I., Shochet, N. R., Kashman, Y., & Groweiss, A. (1983). Latrunculins: Novel marine toxins that disrupt microfilament organization in cultured cells. *Science*, *219*(4584), 493–495.

Spéder, P., Ádám, G., & Noselli, S. (2006). Type ID unconventional myosin controls left–right asymmetry in Drosophila. *Nature*, *440*(7085), 803–807.

Spudich, G., Chibalina, M. V., Au, J. S.-Y., Arden, S. D., Buss, F., & Kendrick-Jones, J. (2007). Myosin VI targeting to clathrin-coated structures and dimerization is

mediated by binding to Disabled-2 and PtdIns (4, 5) P 2. *Nature Cell Biology*, *9*(2), 176–183.

Spudich, James A. (2001). The myosin swinging cross-bridge model. *Nature Reviews Molecular Cell Biology*, *2*(5), 387–392.

Stachowiak, M. R., Laplante, C., Chin, H. F., Guirao, B., Karatekin, E., Pollard, T. D., & O'Shaughnessy, B. (2014). Mechanism of cytokinetic contractile ring constriction in fission yeast. *Developmental Cell*, *29*(5), 547–561.

Stafford, W. F., Walker, M. L., Trinick, J. A., & Coluccio, L. M. (2005). Mammalian class I myosin, Myo1b, is monomeric and cross-links actin filaments as determined by hydrodynamic studies and electron microscopy. *Biophysical Journal*, *88*(1), 384–391.

Steigemann, P., Wurzenberger, C., Schmitz, M. H. A., Held, M., Guizetti, J., Maar, S., & Gerlich, D. W. (2009). Aurora B-Mediated Abscission Checkpoint Protects against Tetraploidization. *Cell*, *136*(3), 473–484.

Stein, L., Sternberg, P., Durbin, R., Thierry-Mieg, J., & Spieth, J. (2001). WormBase: Network access to the genome and biology of Caenorhabditis elegans. *Nucleic Acids Research*, *29*(1), 82–86.

Stiernagle, T. (2006). Maintenance of C. elegans. *WormBook : The Online Review of C. Elegans Biology*, *1999*, 1–11

Stöffler, H. E., Honnert, U., Bauer, C. A., Höfer, D., Schwarz, H., Müller, R. T., Drenckhahn, D., & Bähler, M. (1998). Targeting of the myosin-I myr 3 to intercellular adherens type junctions induced by dominant active Cdc42 in HeLa cells. *Journal of Cell Science*, *111 (Pt 18)*, 2779–2788.

Straight, A. F., Cheung, A., Limouze, J., Chen, I., Westwood, N. J., Sellers, J. R., & Mitchison, T. J. (2003). Dissecting temporal and spatial control of cytokinesis with a myosin II Inhibitor. *Science (New York, N.Y.)*, *299*(5613), 1743–7.

Straight, A. F., Field, C. M., & Mitchison, T. J. (2005). Anillin Binds Nonmuscle Myosin II and Regulates the Contractile Ring. *Molecular Biology of the Cell*, *16*(1), 193–201.

Straub, F. B. (1942). *Studies Int med Chem Univ Szeged*.

Su, K.-C., Takaki, T., & Petronczki, M. (2011). Targeting of the RhoGEF Ect2 to the Equatorial Membrane Controls Cleavage Furrow Formation during Cytokinesis. *Developmental Cell*, *21*(6), 1104–1115.

Suarez, C., Carroll, R. T., Burke, T. A., Christensen, J. R., Bestul, A. J., Sees, J. A., James, M. L., Sirotkin, V., & Kovar, D. R. (2015). Profilin regulates F-actin network homeostasis by favoring formin over Arp2/3 complex. *Developmental Cell*, *32*(1), 43–53.

Sun, L., Guan, R., Lee, I. J., Liu, Y., Chen, M., Wang, J., Wu, J. Q., & Chen, Z. (2015). Mechanistic Insights into the Anchorage of the Contractile Ring by Anillin and Mid1. *Developmental Cell*, *33*(4), 413–426.

Suzuki, H., Onishi, H., Takahashi, K., & Watanabe, S. (1978). Structure and function of chicken gizzard myosin. *The Journal of Biochemistry*, *84*(6), 1529–1542.

Swan, K. A., Severson, A. F., Carter, J. C., Martin, P. R., Schnabel, H., Schnabel, R., & Bowerman, B. (1998). cyk-1: A C. elegans FH gene required for a late step in embryonic cytokinesis. *Journal of Cell Science*, *111 (Pt 14)*, 2017–2027.

Swanson, J. A., Johnson, M. T., Beningo, K., Post, P., Mooseker, M., & Araki, N. (1999). A contractile activity that closes phagosomes in macrophages. *Journal of Cell Science*, *112 (Pt 3)*, 307–316.

Sweeney, H. L., & Houdusse, A. (2007). What can myosin VI do in cells? *Current Opinion in Cell Biology*, *19*(1), 57–66.

Swiatecka-Urban, A., Talebian, L., Kanno, E., Moreau-Marquis, S., Coutermarsh, B., Hansen, K., Karlson, K. H., Barnaby, R., Cheney, R. E., & Langford, G. M. (2007). Myosin Vb is required for trafficking of the cystic fibrosis transmembrane conductance regulator in Rab11a-specific apical recycling endosomes in polarized human airway epithelial cells. *Journal of Biological Chemistry*, *282*(32), 23725–23736.

Swulius, M. T., Nguyen, L. T., Ladinsky, M. S., Ortega, D. R., Aich, S., Mishra, M., & Jensen, G. J. (2018). Structure of the fission yeast actomyosin ring during constriction. *Proceedings of the National Academy of Sciences*, *115*(7), E1455–E1464.

Taheri-Talesh, N., Xiong, Y., & Oakley, B. R. (2012). The functions of myosin II and myosin V homologs in tip growth and septation in Aspergillus nidulans. *PLoS ONE*, *7*(2).

Takagishi, Y., Futaki, S., Itoh, K., Espreafico, E. M., Murakami, N., Murata, Y., & Mochida, S. (2005). Localization of myosin II and V isoforms in cultured rat sympathetic neurones and their potential involvement in presynaptic function. *The Journal of Physiology*, *569*(1), 195–208.

Takeda, K., Yu, Z.-X., Qian, S., Chin, T. K., Adelstein, R. S., & Ferrans, V. J. (2000). Nonmuscle myosin II localizes to the Z-lines and intercalated discs of cardiac muscle and to the Z-lines of skeletal muscle. *Cell Motility*, *46*(1), 59–68.

Taneja, N., Bersi, M. R., Baillargeon, S. M., Fenix, A. M., Cooper, J. A., Ohi, R., Gama, V., Merryman, W. D., & Burnette, D. T. (2020). Precise Tuning of Cortical Contractility Regulates Cell Shape during Cytokinesis. *Cell Reports*, *31*(1), 107477–107477.

Tang, N., Lin, T., & Ostap, E. M. (2002). Dynamics of myo1c (myosin-ibeta) lipid binding and dissociation. *The Journal of Biological Chemistry*, *277*(45), 42763–42768.

Taylor, R. S., & Weeds, A. G. (1976). The magnesium-ion-dependent adenosine triphosphatase of bovine cardiac Myosin and its subfragment-1. *Biochemical Journal*, *159*, 301–315.

Tcherkezian, J., & Lamarche-Vane, N. (2007). Current knowledge of the large RhoGAP family of proteins. *Biology of the Cell*, *99*(2), 67–86.

Timmons, L., Court, D. L., & Fire, A. (2001). Ingestion of bacterially expressed dsRNAs can produce specific and potent genetic interference in Caenorhabditis elegans. *Gene*, *263*(1–2), 103–112.

Tinevez, J.-Y., Schulze, U., Salbreux, G., Roensch, J., Joanny, J.-F., & Paluch, E. (2009). Role of cortical tension in bleb growth. *Proceedings of the National Academy of Sciences*, *106*(44), 18581–18586.

Tiwari, A., Jung, J.-J., Inamdar, S. M., Nihalani, D., & Choudhury, A. (2013). The myosin motor Myo1c is required for VEGFR2 delivery to the cell surface and for angiogenic signaling. *American Journal of Physiology. Heart and Circulatory Physiology*, *304*(5), H687-696.

Todi, S. V., Franke, J. D., Kiehart, D. P., & Eberl, D. F. (2005). Myosin VIIA defects, which underlie the Usher 1B syndrome in humans, lead to deafness in Drosophila. *Current Biology*, *15*(9), 862–868.

Todorov, P. T., Hardisty, R. E., & Brown, S. D. (2001). Myosin VIIA is specifically associated with calmodulin and microtubule-associated protein-2B (MAP-2B). *Biochemical Journal*, *354*(2), 267–274.

Tokuo, H., & Coluccio, L. M. (2013). Myosin-1c regulates the dynamic stability of E-cadherin–based cell–cell contacts in polarized Madin–Darby canine kidney cells. *Molecular Biology of the Cell*, *24*(18), 2820–2833.

Tóth, J., Kovács, M., Wang, F., Nyitray, L., & Sellers, J. R. (2005). Myosin V from Drosophila reveals diversity of motor mechanisms within the myosin V family. *Journal of Biological Chemistry*, *280*(34), 30594–30603.

Toth, M. J., Matthews, D. E., Tracy, R. P., & Previs, M. J. (2005). Age-related differences in skeletal muscle protein synthesis: Relation to markers of immune activation. *American Journal of Physiology-Endocrinology and Metabolism*, *288*(5), E883–E891.

Trent, C., Tsuing, N., & Horvitz, H. R. (1983). Egg-laying defective mutants of the nematode Caenorhabditis elegans. *Genetics*, *104*(4), 619–647.

Trichet, L., Sykes, C., & Plastino, J. (2008). Relaxing the actin cytoskeleton for adhesion and movement with Ena/VASP. *J Cell Biol*, *181*(1), 19–25.

Trivedi, D. V., David, C., Jacobs, D. J., & Yengo, C. M. (2012). Switch II mutants reveal coupling between the nucleotide-and actin-binding regions in myosin V. *Biophysical Journal*, *102*(11), 2545–2555.

Trybus, K M. (1989). Filamentous smooth muscle myosin is regulated by phosphorylation. *The Journal of Cell Biology*, *109*(6 Pt 1), 2887–94.

Trybus, K. M., & Lowey, S. (1984). Conformational states of smooth muscle myosin. Effects of light chain phosphorylation and ionic strength. *Journal of Biological Chemistry*, *259*(13), 8564–8571.

Trybus, Kathleen M. (2008). Myosin V from head to tail. *Cellular and Molecular Life Sciences*, *65*(9), 1378–1389.

Tyska, M. J., Mackey, A. T., Huang, J.-D., Copeland, N. G., Jenkins, N. A., & Mooseker, M. S. (2005). Myosin-1a Is Critical for Normal Brush Border Structure and Composition. *Molecular Biology of the Cell*, *16*(5), 2443–2457.

Tzolovsky, G., Millo, H., Pathirana, S., Wood, T., & Bownes, M. (2002). Identification and phylogenetic analysis of Drosophila melanogaster myosins. *Molecular Biology and Evolution*, *19*(7), 1041–1052.

Udovichenko, I. P., Gibbs, D., & Williams, D. S. (2002). Actin-based motor properties of native myosin VIIa. *Journal of Cell Science*, *115*(2), 445–450.

Uehara, R., Goshima, G., Mabuchi, I., Vale, R. D., Spudich, J. A., & Griffis, E. R. (2010). Determinants of myosin II cortical localization during cytokinesis. *Current Biology*, *20*(12), 1080–1085.

Uehara, R., Hosoya, H., & Mabuchi, I. (2008). In vivo phosphorylation of regulatory light chain of myosin II in sea urchin eggs and its role in controlling myosin localization and function during cytokinesis. *Cell Motility and the Cytoskeleton*, *65*(2), 100–115.

Umeki, N., Jung, H. S., Watanabe, S., Sakai, T., Li, X., Ikebe, R., Craig, R., & Ikebe, M. (2009). The tail binds to the head–neck domain, inhibiting ATPase activity of myosin VIIA. *Proceedings of the National Academy of Sciences*.

Umemoto, S., Bengur, A. R., & Sellers, J. R. (1989). Effect of multiple phosphorylations of smooth muscle and cytoplasmic myosins on movement in an in vitro motility assay. *The Journal of Biological Chemistry*, *264*(3), 1431–1436.

Uyeda, T Q, Abramson, P. D., & Spudich, J. a. (1996). The neck region of the myosin motor domain acts as a lever arm to generate movement. *Proceedings of the National Academy of Sciences of the United States of America*, *93*(9), 4459–4464.

Uyeda, Taro QP, Kron, S. J., & Spudich, J. A. (1990). Myosin step size: Estimation from slow sliding movement of actin over low densities of heavy meromyosin. *Journal of Molecular Biology*, *214*(3), 699–710.

van den Boom, F., Düssmann, H., Uhlenbrock, K., Abouhamed, M., & Bähler, M. (2007). The Myosin IXb motor activity targets the myosin IXb RhoGAP domain as cargo to sites of actin polymerization. *Molecular Biology of the Cell*, *18*(4), 1507–1518.

Van Gele, M., Dynoodt, P., & Lambert, J. (2009). Griscelli syndrome: A model system to study vesicular trafficking. *Pigment Cell & Melanoma Research*, *22*(3), 268–282.

van Haaften, G., Romeijn, R., Pothof, J., Koole, W., Mullenders, L. H., Pastink, A., Plasterk, R. H., & Tijsterman, M. (2006). Identification of conserved pathways of DNA-damage response and radiation protection by genome-wide RNAi. *Current Biology*, *16*(13), 1344–1350.

Varadi, A., Tsuboi, T., & Rutter, G. A. (2005). Myosin Va transports dense core secretory vesicles in pancreatic MIN6 β-cells. *Molecular Biology of the Cell*, *16*(6), 2670–2680.

Vasquez, C. G., Tworoger, M., & Martin, A. C. (2014). Dynamic myosin phosphorylation regulates contractile pulses and tissue integrity during epithelial morphogenesis. *Journal of Cell Biology*, *206*(3), 435–450.

Vavylonis, D., & Horan, B. G. (2017). Cell biology: Capturing formin's mechano-inhibition. *Current Biology*, *27*(19), R1078–R1080.

Vavylonis, D., Wu, J.-Q., Hao, S., O'Shaughnessy, B., & Pollard, T. D. (2008). Assembly mechanism of the contractile ring for cytokinesis by fission yeast. *Science*, *319*(5859), 97–100.

Veigel, C., Coluccio, L. M., Jontes, J. D., Sparrow, J. C., Milligan, R. A., & Molloy, J. E. (1999). The motor protein myosin-I produces its working stroke in two steps. *Nature*, *398*(6727), 530–533.

Velarde, N., Gunsalus, K. C., & Piano, F. (2007). Diverse roles of actin in C. elegansearly embryogenesis. *BMC Developmental Biology*, *7*(1), 142.

Velichkova, M., Guttman, J., Warren, C., Eng, L., Kline, K., Vogl, A. W., & Hasson, T. (2002). A human homologue of {Drosophila} kelch associates with myosin-{VIIa} in specialized adhesion junctions. *Cell Motility and the Cytoskeleton*, *51*(3), 147–164.

Verbrugghe, K. J. C., & White, J. G. (2004). SPD-1 Is Required for the Formation of the Spindle Midzone but Is Not Essential for the Completion of Cytokinesis in C. elegans Embryos. *Current Biology*, *14*(19), 1755–1760.

Verbrugghe, K. J. C., & White, J. G. (2007). Cortical centralspindlin and Gα have parallel roles in furrow initiation in early C. elegans embryos. *Journal of Cell Science*, *120*(10), 1772–1778.

Vernerey, F. J., & Akalp, U. (2016). Role of catch bonds in actomyosin mechanics and cell mechanosensitivity. *Physical Review E*, *94*(1), 012403.

Vernì, F., Somma, M. P., Gunsalus, K. C., Bonaccorsi, S., Belloni, G., Goldberg, M. L., & Gatti, M. (2004). Feo, the Drosophila Homolog of PRC1, Is Required for Central-Spindle Formation and Cytokinesis. *Current Biology*, *14*(17), 1569–1575.

Vicente-Manzanares, M., Ma, X., Adelstein, R. S., & Horwitz, A. R. (2009). Non-muscle myosin II takes centre stage in cell adhesion and migration. *Nature Reviews Molecular Cell Biology*, *10*, 778.

Vogel, S. K., Petrasek, Z., Heinemann, F., & Schwille, P. (2013). Myosin motors fragment and compact membrane-bound actin filaments. *Elife*, *2*, e00116.

von Dassow, G., Verbrugghe, K. J. C., Miller, A. L., Sider, J. R., & Bement, W. M. (2009). Action at a distance during cytokinesis. *Journal of Cell Biology*, *187*(6), 831–845.

Vreugde, S., Ferrai, C., Miluzio, A., Hauben, E., Marchisio, P. C., Crippa, M. P., Bussi, M., & Biffo, S. (2006). Nuclear myosin VI enhances RNA polymerase II-dependent transcription. *Molecular Cell*, *23*(5), 749–755.

Wakabayashi, Y., Dutt, P., Lippincott-Schwartz, J., & Arias, I. M. (2005). Rab11a and myosin Vb are required for bile canalicular formation in WIF-B9 cells. *Proceedings of the National Academy of Sciences*, *102*(42), 15087–15092.

Walker, D. S., Ly, S., Lockwood, K. C., & Baylis, H. A. (2002). A direct interaction between IP3 receptors and myosin II regulates IP3 signaling in C. elegans. *Current Biology*, *12*(11), 951–956.

Wallace, A. G., Raduwan, H., Carlet, J., & Soto, M. C. (2018). The {RhoGAP} {HUM}-7/myo9 integrates signals to modulate {RHO}-1/{RhoA} during embryonic morphogenesis in caenorhabditis elegans. *Development (Cambridge)*, *145*(23).

Wang, F.-S., Liu, C.-W., Diefenbach, T. J., & Jay, D. G. (2003). Modeling the role of myosin 1c in neuronal growth cone turning. *Biophysical Journal*, *85*(5), 3319–3328.

Wang, S.-C., Low, T. Y. F., Nishimura, Y., Gole, L., Yu, W., & Motegi, F. (2017). Cortical forces and CDC-42 control clustering of PAR proteins for Caenorhabditis elegans embryonic polarization. *Nature Cell Biology*, *19*(8), 988–995.

Wang, Z., & Pesacreta, T. C. (2004). A subclass of myosin XI is associated with mitochondria, plastids, and the molecular chaperone subunit TCP 1α in maize. *Cell Motility and the Cytoskeleton*, *57*(4), 218–232.

Warner, C. L., Stewart, A., Luzio, J. P., Steel, K. P., Libby, R. T., Kendrick Jones, J., & Buss, F. (2003). Loss of myosin VI reduces secretion and the size of the Golgi in fibroblasts from Snell's waltzer mice. *The EMBO Journal*, *22*(3), 569–579.

Warshaw, D. M., Kennedy, G. G., Work, S. S., Krementsova, E. B., Beck, S., & Trybus, K. M. (2005). Differential labeling of myosin V heads with quantum dots allows direct visualization of hand-over-hand processivity. *Biophysical Journal*, *88*(5), L30–L32.

Watanabe, N., Madaule, P., Reid, T., Ishizaki, T., Watanabe, G., Kakizuka, A., Saito, Y., Nakao, K., Jockusch, B. M., & Narumiya, S. (1997). P140mDia, a mammalian homolog of Drosophila diaphanous, is a target protein for Rho small GTPase and is a ligand for profilin. *The EMBO Journal*, *16*(11), 3044–3056.

Watanabe, S., Ando, Y., Yasuda, S., Hosoya, H., Watanabe, N., Ishizaki, T., & Narumiya, S. (2008). MDia2 induces the actin scaffold for the contractile ring and stabilizes its position during cytokinesis in NIH 3T3 cells. *Molecular Biology of the Cell*, *19*(5), 2328–2338.

Watanabe, S., De Zan, T., Ishizaki, T., & Narumiya, S. (2013). Citron kinase mediates transition from constriction to abscission through its coiled-coil domain. *Journal of Cell Science*, *126*(8), 1773–1784.

Watanabe, Takashi, Srichuwong, S., Arakane, M., Tamiya, S., Yoshinaga, M., Watanabe, I., Yamamoto, M., Ando, A., Tokuyasu, K., & Nakamura, T. (2010). Selection of

stress-tolerant yeasts for simultaneous saccharification and fermentation (SSF) of very high gravity (VHG) potato mash to ethanol. *Bioresource Technology*, *101*(24), 9710–9714.

Watanabe, Toshiyuki. (2007). Regulation of myosin {II} dynamics by phosphorylation and dephosphorylation of its light chain in epithelial cells. *\ldots Biology of the Cell*, *18*(February), 605–616.

Waterhouse, A. M., Procter, J. B., Martin, D. M., Clamp, M., & Barton, G. J. (2009). Jalview Version 2—A multiple sequence alignment editor and analysis workbench. *Bioinformatics*, *25*(9), 1189–1191.

Waterston, R. H. (1989). The minor myosin heavy chain, {mhcA}, of {Caenorhabditis} elegans is necessary for the initiation of thick filament assembly. *The EMBO Journal*, *8*(11), 3429–3436.

Webb, S. E., Lee, K. W., Karplus, E., & Miller, A. L. (1997). Localized calcium transients accompany furrow positioning, propagation, and deepening during the early cleavage period of zebrafish embryos. *Developmental Biology*, *192*(1), 78–92.

Weber, K. L., Sokac, A. M., Berg, J. S., Cheney, R. E., & Bement, W. M. (2004). A microtubule-binding myosin required for nuclear anchoring and spindle assembly. *Nature*, *431*(7006), 325–329.

Weck, M. L., Crawley, S. W., Stone, C. R., & Tyska, M. J. (2016). Myosin-7b promotes distal tip localization of the intermicrovillar adhesion complex. *Current Biology*, *26*(20), 2717–2728.

Weil, D., Küssel, P., Blanchard, S., Lévy, G., Levi-Acobas, F., Drira, M., Ayadi, H., & Petit, C. (1997). The autosomal recessive isolated deafness, DFNB2, and the Usher 1B syndrome are allelic defects of the myosin-VIIA gene. *Nature Genetics*, *16*(2), 191–193.

Weil, D., Levy, G., Sahly, I., Levi-Acobas, F., Blanchard, S., El-Amraoui, A., Crozet, F., Philippe, H., Abitbol, M., & Petit, C. (1996). Human myosin VIIA responsible for the Usher 1B syndrome: A predicted membrane-associated motor protein expressed in developing sensory epithelia. *Proceedings of the National Academy of Sciences*, *93*(8), 3232–3237.

Wells, A. L., Lin, A. W., Chen, L.-Q., Safer, D., Cain, S. M., Hasson, T., Carragher, B. O., Milligan, R. A., & Sweeney, H. L. (1999). Myosin VI is an actin-based motor that moves backwards. *Nature*, *401*(6752), 505–508.

Werner, M., Munro, E., & Glotzer, M. (2007). Astral signals spatially bias cortical myosin recruitment to break symmetry and promote cytokinesis. *Current Biology*, *17*(15), 1286–1297.

Whitman, C. O. (1887). *A contribution to the history of the germlayers in Clepsine*.

Whittaker, M., & Milligan, R. A. (1997). Conformational changes due to calcium-induced calmodulin dissociation in brush border MyosinI-decorated F-actin revealed by cryoelectron microscopy and image analysis. *Journal of Molecular Biology*, *269*(4), 548–557.

Whittaker, Michael, Wilson-Kubalek, E. M., Smith, J. E., Faust, L., Milligan, R. A., & Sweeney, H. L. (1995). A 35-Å movement of smooth muscle myosin on ADP release. *Nature*, *378*(6558), 748–751.

Wilkinson, S., Paterson, H. F., & Marshall, C. J. (2005). Cdc42-MRCK and Rho-ROCK signalling cooperate in myosin phosphorylation and cell invasion. *Nat Cell Biol*, *7*(3), 255–261.

Williams, B. D., & Waterston, R. H. (1994). Genes critical for muscle development and function in Caenorhabditis elegans identified through lethal mutations. *The Journal of Cell Biology*, *124*(4), 475–490.

Williams, D. S., & Lopes, V. S. (2011). The many different cellular functions of MYO7A in the retina. *Biochemical Society Transactions*, *39*(5), 1207–1210.

Williams, R., & Coluccio, L. M. (1994). Novel 130-kDa rat liver myosin-1 will translocate actin filaments. *Cell Motility and the Cytoskeleton*, *27*(1), 41–48.

Wilson, C. A., Tsuchida, M. A., Allen, G. M., Barnhart, E. L., Applegate, K. T., Yam, P. T., Ji, L., Keren, K., Danuser, G., & Theriot, J. A. (2010). Myosin II contributes to cell-scale actin network treadmilling through network disassembly. *Nature*, *465*(7296), 373–377.

Wirshing, A. C. E., & Cram, E. J. (2017). Myosin activity drives actomyosin bundle formation and organization in contractile cells of the Caenorhabditis elegans spermatheca. *Molecular Biology of the Cell*, *28*(14), 1937–1949.

Wirth, J. A., Jensen, K. A., Post, P. L., Bement, W. M., & Mooseker, M. S. (1996). Human myosin-IXb, an unconventional myosin with a chimerin-like rho/rac GTPase-activating protein domain in its tail. *Journal of Cell Science*, *109*(3), 653–661.

Wolfrum, U., Liu, X., Schmitt, A., Udovichenko, I. P., & Williams, D. S. (1998). Myosin VIIa as a common component of cilia and microvilli. *Cell Motility and the Cytoskeleton*, *40*(3), 261–271.

Wolke, U., Jezuit, E. A., & Priess, J. R. (2007). Actin-dependent cytoplasmic streaming in C. elegans oogenesis. *Development*, *134*(12), 2227–2236.

Wollrab, V., Thiagarajan, R., Wald, A., Kruse, K., & Riveline, D. (2016). Still and rotating myosin clusters determine cytokinetic ring constriction. *Nature Communications*, *7*, 11860.

Wu, J.-Q., Sirotkin, V., Kovar, D. R., Lord, M., Beltzner, C. C., Kuhn, J. R., & Pollard, T. D. (2006). Assembly of the cytokinetic contractile ring from a broad band of nodes in fission yeast. *The Journal of Cell Biology*, *174*(3), 391–402.

Wu, X. S., Tsan, G. L., & Hammer III, J. A. (2005). Melanophilin and myosin Va track the microtubule plus end on EB1. *The Journal of Cell Biology*, *171*(2), 201–207.

Wu, X., Bowers, B., Rao, K., Wei, Q., & Hammer III, J. A. (1998). Visualization of melanosome dynamics within wild-type and dilute melanocytes suggests a paradigm for myosin V function in vivo. *The Journal of Cell Biology*, *143*(7), 1899–1918.

Xie, P. (2010). A model for processive movement of single-headed myosin-IX. *Biophysical Chemistry*, *151*(1–2), 71–80.

Yamakita, Y., Yamashiro, S., & Matsumura, F. (1994). In vivo phosphorylation of regulatory light chain of myosin II during mitosis of cultured cells. *Journal of Cell Biology*, *124*(1–2), 129–137.

Yamashiro, S., Totsukawa, G., Yamakita, Y., Sasaki, Y., Madaule, P., Ishizaki, T., Narumiya, S., & Matsumura, F. (2003). Citron Kinase, a Rho-dependent Kinase, Induces Di-

phosphorylation of Regulatory Light Chain of Myosin II. *Molecular Biology of the Cell*, *14*(5), 1745–1756.

Yamashita, R. A., Sellers, J. R., & Anderson, J. B. (2000). Identification and analysis of the myosin superfamily in Drosophila: A database approach. *Journal of Muscle Research & Cell Motility*, *21*(6), 491–505.

Yang, C. X., Chen, H. Q., Chen, C., Yu, W. P., Zhang, W. C., Peng, Y. J., He, W. Q., Wei, D. M., Gao, X., & Zhu, M. S. (2006). Microfilament-binding properties of N-terminal extension of the isoform of smooth muscle long myosin light chain kinase. *Cell Research*, *16*(4), 367–376.

Yang, C.-H., Szeliga, J., Jordan, J., Faske, S., Sever-Chroneos, Z., Dorsett, B., Christian, R. E., Settlage, R. E., Shabanowitz, J., & Hunt, D. F. (2005). Identification of the surfactant protein A receptor 210 as the unconventional myosin 18A. *Journal of Biological Chemistry*, *280*(41), 34447–34457.

Yang, Y., Baboolal, T. G., Siththanandan, V., Chen, M., Walker, M. L., Knight, P. J., Peckham, M., & Sellers, J. R. (2009). A FERM domain autoregulates Drosophila myosin 7a activity. *Proceedings of the National Academy of Sciences*, *106*(11), 4189–4194.

Yengo, C. M., & Sweeney, H. L. (2004). Functional role of loop 2 in myosin V. *Biochemistry*, *43*(9), 2605–2612.

Yengo, C. M., Enrique, M., Chrin, L. R., Gaffney, D. P., & Berger, C. L. (2002). Actin-induced closure of the actin-binding cleft of smooth muscle myosin. *Journal of Biological Chemistry*, *277*(27), 24114–24119.

Yildiz, A., Forkey, J. N., McKinney, S. A., Ha, T., Goldman, Y. E., & Selvin, P. R. (2003). Myosin V walks hand-over-hand: Single fluorophore imaging with 1.5-nm localization. *Science*, *300*(5628), 2061–2065.

Yildiz, A., Park, H., Safer, D., Yang, Z., Chen, L.-Q., Selvin, P. R., & Sweeney, H. L. (2004). Myosin VI steps via a hand-over-hand mechanism with its lever arm undergoing fluctuations when attached to actin. *Journal of Biological Chemistry*, *279*(36), 37223–37226.

Yin, H. L., & Janmey, P. A. (2003). Phosphoinositide regulation of the actin cytoskeleton. *Annual Review of Physiology*, *65*, 761–789.

Yin, H., Pruyne, D., Huffaker, T. C., & Bretscher, A. (2000). Myosin V orientates the mitotic spindle in yeast. *Nature*, *406*(6799), 1013–1015.

Yonemura, S., & Pollard, T. D. (1992). The localization of myosin I and myosin II in Acanthamoeba by fluorescence microscopy. *Journal of Cell Science*, *102*(3), 629–642.

Yoshida, T., Kawai-Kowase, K., & Owens, G. K. (2004). Forced expression of myocardin is not sufficient for induction of smooth muscle differentiation in multipotential embryonic cells. *Arteriosclerosis, Thrombosis, and Vascular Biology*, *24*(9), 1596–1601.

Yoshimura, S., Takagi, Y., Harada, J., Teramoto, T., Thomas, S. S., Waeber, C., Bakowska, J. C., Breakefield, X. O., & Moskowitz, M. A. (2001). FGF-2 regulation of neurogenesis in adult hippocampus after brain injury. *Proceedings of the National Academy of Sciences*, *98*(10), 5874–5879.

Yoshizaki, H., Ohba, Y., Kurokawa, K., Itoh, R. E., Nakamura, T., Mochizuki, N., Nagashima, K., & Matsuda, M. (2003). Activity of Rho-family GTPases during cell division as visualized with FRET-based probes. *The Journal of Cell Biology*, *162*(2), 223–232.

Young, P. E., Pesacreta, T. C., & Kiehart, D. P. (1991). Dynamic changes in the distribution of cytoplasmic myosin during Drosophila embryogenesis. *Development (Cambridge, England)*, *111*(1), 1–14.

Young, P. E., Richman, a M., Ketchum, a S., & Kiehart, D. P. (1993). Morphogenesis in Drosophila requires nonmuscle myosin heavy chain function. *Genes & Development*, *7*(1), 29–41.

Yüce, Ö., Piekny, A., & Glotzer, M. (2005). An ECT2–centralspindlin complex regulates the localization and function of RhoA. *The Journal of Cell Biology*, *170*(4), 571–582.

Zadro, C., Alemanno, M. S., Bellacchio, E., Ficarella, R., Donaudy, F., Melchionda, S., Zelante, L., Rabionet, R., Hilgert, N., Estivill, X., Van Camp, G., Gasparini, P., & Carella, M. (2009). Are MYO1C and MYO1F associated with hearing loss? *Biochimica et Biophysica Acta - Molecular Basis of Disease*, *1792*(1), 27–32.

Zambon, P., Palani, S., Kamnev, A., & Balasubramanian, M. K. (2017). Myo2p is the major motor involved in actomyosin ring contraction in fission yeast. *Current Biology*, *27*(3), R99–R100.

Zhang, D., & Glotzer, M. (2015). The RhoGAP activity of CYK-4/MgcRacGAP functions non-canonically by promoting RhoA activation during cytokinesis. *ELife*, *4*.

Zhao, Z., & Manser, E. (2005). PAK and other Rho-associated kinases—Effectors with surprisingly diverse mechanisms of regulation. *Biochemical Journal*, *386*(2), 201–214.

Zhou, M., & Wang, Y.-L. (2008). Distinct Pathways for the Early Recruitment of Myosin II and Actin to the Cytokinetic Furrow. *Molecular Biology of the Cell*, *19*(1), 318–326.

Zhu, C., & Jiang, W. (2005). Cell cycle-dependent translocation of PRC1 on the spindle by Kif4 is essential for midzone formation and cytokinesis. *Proceedings of the National Academy of Sciences of the United States of America*, *102*(2), 343–348.

Zhu, Q., & Clarke, M. (1992). Association of calmodulin and an unconventional myosin with the contractile vacuole complex of Dictyostelium discoideum. *The Journal of Cell Biology*, *118*(2), 347–358.

Zhu, T., Beckingham, K., & Ikebe, M. (1998). High affinity Ca2+ binding sites of calmodulin are critical for the regulation of myosin Iβ motor function. *Journal of Biological Chemistry*, *273*(32), 20481–20486.

Zhu, T., Sata, M., & Ikebe, M. (1996). Functional expression of mammalian myosin Iβ: Analysis of its motor activity. *Biochemistry*, *35*(2), 513–522.

Zhuravlev, Y., Hirsch, S. M., Jordan, S. N., Dumont, J., Shirasu-Hiza, M., & Canman, J. C. (2017). CYK-4 regulates Rac, but not Rho, during cytokinesis. *Molecular Biology of the Cell*, *28*(9), 1258–

Zorca, C. E., Kim, L. K., Kim, Y. J., Krause, M. R., Zenklusen, D., Spilianakis, C. G., & Flavell, R. A. (2015). Myosin VI regulates gene pairing and transcriptional pause release in T cells. *Proceedings of the National Academy of Sciences*, *112*(13), E1587–E1593.

Zot, H. G., Doberstein, S. K., & Pollard, T. D. (1992). Myosin-I moves actin filaments on a phospholipid substrate: Implications for membrane targeting. *The Journal of Cell Biology*, *116*(2), 367–376.